UNIVERSITY OF CALIFORNIA SAN DIEGO

Copper Mediated Photochemical Cycloadditions for the Synthesis of Small Heterocycles

A dissertation submitted in partial satisfaction of the
requirements for the degree Doctor of Philosophy

in

Chemistry

by

Daniel Mark Flores

Committee in charge:

Professor Valerie A. Schmidt, Chair
Professor Carlo Ballatore
Professor Joshua Figueroa
Professor Kamil Godula
Professor Joseph O'Connor

2020

The dissertation of Daniel Mark Flores is approved, and it is acceptable in quality and form for publication on microfilm and electronically:

_____

_____

_____

_____

_____

Chair

University of California San Diego

2020

DEDICATION

For my grandparents,

Federico and Rosemary Flores

Roger and Margery Wood

EPIGRAPH

Nothing great was every achieved without enthusiasm.

Ralph Waldo Emerson

To improve is to change. To perfect is to change often.

Winston Churchill

Don’t give up. Don’t ever give up.

Jim Valvano

Just Do It.

Nike

Anchors up.

Pacifico

TABLE OF CONTENTS

LIST OF ABBREVIATIONS

The following list details common abbreviations used throughout this dissertation.

Abbreviation	Definition
2D	Two-dimensional
a, b, c	Unit cell lattice constants (Å)
Å	Angstrom
APCI	Atmospheric-Pressure Chemical Ionization
A.U.	Arbitrary Units
bISC	back intersystem crossing
bpy	2,2'-bipyridine
°C	degrees Celsius
calc.	calculated
CFL	Compact Fluorescence Light
c	centi (10^{-2})
COPC	Carbonyl-Olefin Photocycloaddition
COSY	homonuclear Correlation Spectroscopy
Cu	copper
d	doublet (NMR spectroscopy)
dd	doublet of doublets (NMR spectroscopy)
DCM	dichloromethane
DFT	density functional theory
DMAP	Dimethylamino Pyridine

DMF	dimethylformamide
dr	diastereomeric ratio
EA	Elemental Analysis
E_T	Triplet energy
ee	enantiomeric excess
equiv	equivalent
ESI	electrospray ionization
ET	energy transfer
Et	ethyl (*e.g.*, C_2H_5)
Et_2O	diethyl ether
F_0	observed structure factor
g	grams
GC-MS	gas chromatography-mass spectrometry
GOF	goodness of fit
GS	ground state
h	hour
h	Planck constant
HFS	Hartree-Fock-Slater
HMBC	Heteronuclear Multiple Bond Correlation
HOMO	Highest Occupied Molecular Orbital
HRMS	High Resolution Mass Spectrometry
HSQC	Heteronuclear Single Quantum Correlation

Hz	hertz (s^{-1}, cycles per second)
I^0_f	Intensity of fluorescence without a quencher
I_f	Intensity of fluorescence with a quencher
IC	interconversion
IOPC	Imine-Olefin Photocycloaddition
^{i}Pr	isopropyl
IR	infrared
ISC	Inter-System-Crossing
J	coupling constant through bonds
K	degrees Kelvin
k_q	quencher rate coefficient
L	charge neutral ligand
LMCT	Ligand to Metal Charge Transfer
LUMO	Lowest Unoccupied Molecular Orbital
M	Molar (moles/liter)
m	meter
	mili- (10^{-3})
	multiplet (NMR spectroscopy)
MA	Maleic Anhydride
Me	methyl (*e.g.*, CH_3)
MeCN	acetonitrile
Mes	mesityl (*i.e.*, 2,4,6-$Me_3C_6H_2$)

MHz	megahertz
min	minutes
mL	milliliter
MLCT	metal to ligand charge transfer
mm	millimeter
MO	molecular orbital
mol	moles
NB	Norbornene
nBu	n-butyl
neo	neocuproine
nm	nanometer
NMR	nuclear magnetic resonance
nOe	nuclear Overhaus effect
NOESY	Nuclear Overhause Effect SpectroscopY
ns	nanosecond
OLED	Organic Light Emitting Diode
OTf	triflate, trifluoromethylsulfonate
Ph	phenyl (*i.e.*, C_6H_5)
phosphor.	phosphorescence
PPh_3	triphenylphosphine
ppm	parts per million
PRE	persistent radical effect

PS	photosensitizer
[Q]	Quencher concentration
q	quartet (NMR spectroscopy)
R	organic moiety, alkyl group
R_1	residual value, claclulated from F_0-data
rt	room temperature
s	singlet (NMR spectroscopy)
SET	Single Electron Transfer
sept	septet (NMR spectroscopy)
t	triplet (NMR spectroscopy)
TADF	thermally activated delayed fluorescence
TBI	tris(2-oxobenzimidazolyl)borohydride
t-Bu	*tertiary*-butyl
Tc	tris(carbene)borates
THF	tetrahydrofuran
Tm	tris(thioimidazolyl)borates
TMS	trimethylsilane
Tmp	tris(2-mercaptopyridine)borates
TOFMS	Time Of Flight Mass Spectrometry
TP^{iPr}	tris(diisopropylphosphino)borate
Tp	tris(pyrazolyl)borate
Tp^*	tri-(3,5-dimethyl-1-pyrazolyl)borohydride

Tp^{cy}	tri-(3-cyclopropyl-1-pyrazolyl)borohydride
Tp^{Fur}	tri-(3-furan-1-pyrazolyl)borohydride
Tp^{Th}	tri-(3-thiophene-1-pyrazolyl)borohydride
TpCu	tris(pyrazolyl)borate copper(I)
TSe	tris(selenoimidazolyl)borate
Φ	quantum yield
UV	ultraviolet
UV-vis	ultraviolet-visible
V	unit cell volume
W	watt
WCA	Weakly Coordinating Anion
wR_2	weighted residual, calculated from F_0^2-data
Z	number of formula units per unit cell
Å	Angstrom (10^{-10} m)
a,b,g	unit cell angles (degrees)
d	NMR chemical shift relative to a standard (*e.g.*, TMS)
ε	extinction coefficient
h^n	hapticity of a coordinated ligand with *n* contiguous atoms coordinated to a metal center
q_{max}	Maximum diffraction angle in degrees
l	wavelength
l_{abs}	wavelength of absorbance

$l_{emission}$	wavelength of emission
l_{max}	wavelength of maximum absorbance
n	frequency (s^{-1})
t_0	excited state lifetime
m	micro (10^{-6})
r	calculated crystal density (g/cm^3)
F	quantum yield

LIST OF FIGURES

ACKNOWLEDGEMENTS

First and foremost, I have to thank Professor Valerie A. Schmidt. I have genuinely enjoyed my time here at UCSD and you are a huge reason for that. From day one you made it clear that this was a team effort, valuing my input and ideas. You have been motivating when chemistry did not work, encouraging when it did, and more than understanding when I had broken appendages. Thank you. I'm proud of the chemistry we were able to develop together and am eager to see how it grows. I know I will be the first of many PhDs to graduate under your guidance.

I would also like to thank my committee, Prof. Carlo Ballatore, Prof. Joshua Figueroa, Prof. Kamil Godula, and Prof. Joeseph OConnor, for the many discussions and insight shared that helped shape the direction of this work. I also have to thank all of the neighboring groups of Pac Hall for their extreme generosity in sharing their chemical inventory. I know I have pestered so many of you routinely and it does not go without great appreciation.

To my lab mates I hope I have been a positive mentor to you throughout graduate school. Pay it forward to the next group of students. Stay strong, if I get can get through this then you most definitely can. I'm proud of work ethic we've set as the bar for entry. Continue grinding and creating inspiring chemistry.

There are a number of people within the department whom I wish to thank. Neville you have been more than generous with your time in helping me trouble shoot glovebox problems, solving crystal structures, and supplying me with a couch when I was homeless. I owe you. Glen Junor thank you for guiding me in

setting up many of the DFT calculations seen in Chapters 4 & 5. Dr. Anthony Mrse for the countless discussions of both NMR experiments and the MLB season. The entire Tor group for their generosity with their UV-vis and Fluorometer and dealing with my incessant asking if the PTI was up and running (if it is let me know).

Prof. Christian Pester for mentoring me as a wide eyed undergraduate at UCSB, continual guidance throughout my professional development, and being a phenomenal friend. Prof. Susan Odom for providing me the opportunity to conduct research in her lab as an undergraduate at the University of Kentucky. Without that experience I would not have pursued this degree.

Troy where do I begin with you. We were in the trenches together and you've been a brother to me from day one. Whenever I've been down you have been there to pick me up and make me have a good time. I struggle to articulate what your friendship means to me; just know you are the most genuine and magical person I've ever encountered in my life. Don't ever change.

Sauntee you are the single most important person in me finishing this degree. You are the most loving and empathetic person I know. I would not have made it through without your love and support. Your resilience and passion inspired me to push through. I only hope that I can return the favor in the future. I will forever cherish our memories made because they're so intertwined with this degree.

To the climbing squad, Logan, Angus, Michael, Katia, and Sho thank you for showing me the ropes and filling my weekends with gnarly adventures. I can't wait to see the crags we hit in the future. Remember just don't fall and go up.

To all of my friends, Ben, Sarah, Michael, Katia, Dan, Nicole, Neville, Adri, Adam, Evan, Troy, Melissa, Sam, Warren, Kevin, Jackson, Joey, and the rest of Bohr's Models it has been one hell of a ride and I couldn't think of a rowdier bunch of fools I'd rather experience grad school with. We worked and partied hard and have been there for each other in ways that are hard to fully describe. I cannot wait for each of you to experience the feeling of finally finishing this degree and sharing in that joy with you. I look forward to roasting all of you.

To my family, thank you for putting up with me. I would not be where I am today without your endless love and support. Dad I wouldn't be able to do what I love without your sacrifice. Mom whenever I am exhausted and frustrated, I hear you in my head saying, "The world looks better on a full stomach and good night's sleep." Jackie and T I couldn't ask for better mentors in life. I've leaned heavily on you two these past few years. Uncle Freddy and Auntie Linda your spontaneous generosity always made life just a little bit easier.

To everyone once again thank you. If I've forgotten you, I am sorry, but know I deeply appreciate the help you have given me. Stay stoked.

Chapter 3: This chapter is adapted with permission from **D. M. Flores**; V. A. Schmidt. “Intermolecular 2+2 Carbonyl-Olefin Photocycloadditions Enabled by Cu(I)-Norbornene MLCT.” *Journal of the American Chemical Society* **2019**, 141, 8741. Copyright 2019, American Chemical Society. The dissertation author is the first author on this paper.

Material presented in **Chapter 4** will appear in an upcoming publication by Flores, D. M., Neville, M. L., Schmidt, V. A. The dissertation author is the primary author of this manuscript.

VITA

2015 Bachelor of Science, University of Kentucky

2017 Master of Science, University of California San Diego

2020 Doctor of Philosophy, University of California San Diego

PUBLICATIONS

"**Flores, D. M.;** Schmidt, V. A. *J. Am. Chem. Soc.* **2019,** *141*, 22, 8741. "Substrate Dependent MLCT Enabled Intermolecular 2+2 Carbonyl-Olefin Photocycloadditions Catalyzed by Tris(pyrazolyl)borate Copper"

FIELDS OF STUDY

Major Field: Organic Chemistry

ABSTRACT OF THE DISSERTATION

Copper Mediated Photochemical Cycloadditions for the Synthesis of Small Heterocycles

by

Daniel Mark Flores

Doctor of Philosophy in Chemistry

University of California San Diego, 2020

Professor Valerie A. Schmidt, Chair

The 2+2 photocycloaddition of two pi components is advantageous for the synthesis of 4-membered rings due to the ability to rapidly generate molecular complexity from an atom-economical approach. However, these theoretically simple transformations are synthetically challenging due to mechanistic constraints. Despite the prevalence of these small carbo- and heterocycle rings there is a dearth of practical synthetic methodology for their synthesis

Drawing inspiration from the fields of Lewis Acid catalysis, photoredox catalysis, and the prevalence of copper in photocatalytic reactions we set out to develop new methodologies to fill the void. Early work focused on attempts at using various photosensitizers or preformed substrate-catalyst complexes to facilitate the desired cycloaddition. While these did not produce the desired cycloadduct

these experiments offered valuable insight into the photochemistry of copper and our experimental setup.

Utilizing the tridentate scorpionate ligand trispyrazolylborohydride led to the successful development of a 2+2 carbonyl-olefin photocycloaddition (COPC) for the synthesis of oxetanes. Notably, this method engages alkyl ketones, which are more challenging to engage via direct irradiation pathways. The optimized system was also seen to work for the analogous Analogously, this method works for 2+2 imine-olefin photocycloadditions (IOPC) to generate azetidines with diverse functional group tolerance. Mechanistic investigations and single X-ray crystallography support the in-situ formation of a Cu-olefin resting state. Full molecule density functional theory (DFT) calculations indicate that upon irradiation this complex undergoes a MLCT that ultimately leads to oxetane or azetidine formation.

To further expand the scope of the 2+2 COPC and IOPC, we sought to utilize DFT calculations to rationally design ligands. A computational high through put screening method has been developed for evaluating the photophysical properties of various tridentate ligands bound to copper. While there are discrepancies with experimental data this enables a quick evaluation of the electronic transitions and an approximation of where they will occur. This has led to the rational design of several Tp derivatives as well as identifying Tm, Tmp, Tc, and trisphosphino as promising ligands. Moving forward these scorpionates will be

synthesized and their corresponding Cu complexes evaluated as catalysts for the 2+2 COPC and 2+2 IOPC.

Chapter 1

Overview of Organometallic Photocatalysts

1.1 Synthetic Organic Photochemistry

In 1965 Woodward and Hoffman's seminal report on the conservation of orbital symmetry heavily influenced molecular orbital theory and fundamentally changed the way chemists think about chemical reactivity, particularly through photochemical excitation.[1–4] Photoexcitation enables access to molecular excited states, which enables remarkably different reactivity than the ground state. This has led to extensive mechanistic studies on various processes as well as the photophysical properties of the reactants. For organic molecules the most relevant excited states to consider are the first excited singlet and triplet states. These states are accessible through two main pathways: 1) direct excitation of the substrate through irradiation or 2) sensitization through a bimolecular energy transfer.[5]

Excitation through sensitization requires the use of a photosensitizer (PS); a molecule or complex whereupon excitation to the triplet excited state can undergo an energy transfer to a substrate. Although this process can occur as the result of emission from the PS and subsequent absorption of that emitted light by the acceptor, energy transfer more commonly occurs through non-radiative processes. The two most common mechanisms of non-radiative energy transfer are known as Forster and Dexter energy transfer. Forster energy transfer is a dipolar mechanism that takes place through space. The transition moment dipole

of the donor couples nonradiatively with the transition moment dipole of the acceptor. The Dexter mechanism is the simultaneous electron transfer between the donor acceptor molecules, requiring orbital overlap (**Figure 1.1**).[6–9] Both Forster and Dexter energy transfer yield the same products, but the physical origin of the reaction are fundamentally different.

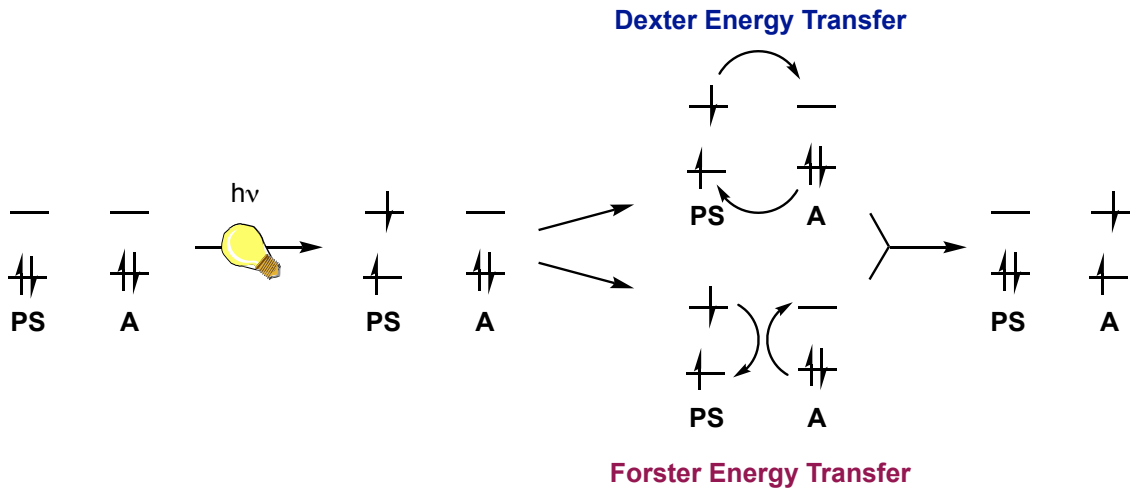

Figure 1.1 Excitation by sensitization through a bimolecluar energy transfer between a photosensitizer **PS** and an acceptor molecule **A**.

In determining which mode of excitation is more likely to succeed there are several inherent properties of each substrate that should be identified. Absorption maximas (λ_{max}) can easily be obtained from an electromagnetic absorption spectrum and are crucial in selecting an appropriate light source for irradiation. From UV-vis spectra recorded with varying compound concentrations the extinction coefficients (ε) of all bands can be obtained. The extinction coefficient is the most convenient way to express the efficiency of light absorption with larger

coefficients corresponding to efficient processes. Nevertheless, even weak absorptions can be of significant importance to a photochemical process. Assigning a specific electronic transition to an absorption band is of even greater significance. Quantum yield (Φ) is the number of times a specific process occurs per photon absorbed by the system, ranging from 0 to 10^5. Typical quantum yields associated with traditional photocycloadditions range from 0.1 – 1.0. Low quantum yields can still lead to excellent chemical yields but are wasteful in energy and often are sensitive to competing reactions. Another key piece of information is the excited state lifetime of a molecule or complex. This gives indication of the spin state the reaction is proceeding through, with singlet excited state lifetimes on the scale of pico- to nanoseconds and triplet excited state lifetimes on the scale of microseconds. Generally, reactions proceeding through triplet states are more efficient processes due the long-lived excited states. The last photophysical property to consider is the triplet energy (E_T) of a substrate or photosensitizer. If the E_T of a photosensitizer is higher than that of the substrate then excitation through sensitization is possible.[5] However, just because this pathway is possible does not mean it will always occur and should be determined experimentally through Stern-Volmer Luminescence quenching experiments.

The Stern-Volmer relationship allows the kinetics of a photophysical intermolecular deactivation process, or sensitization, to be quantified.[10] Fluorescence and phosphorescence are two modes of intramolecular deactivation. An intermolecular deactivation (a sensitization) is where a different substrate

A

$$\frac{I^0_f}{I_f} = 1 + k_q \tau_0 [Q]$$

B

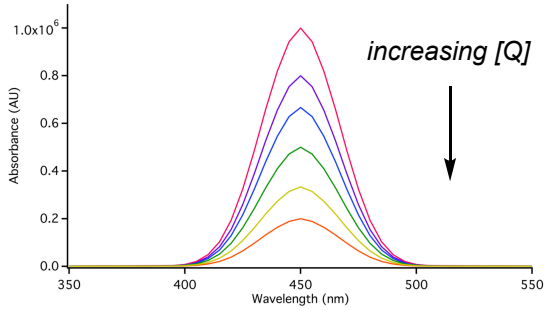

C

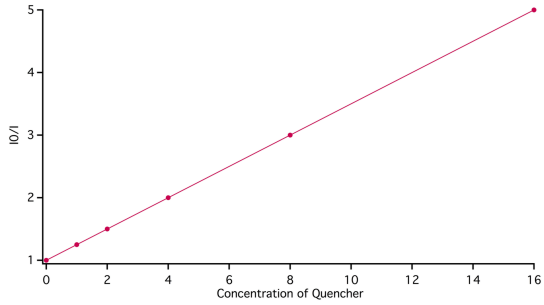

Figure 1.2 **A** Equation for the kinetics of the Stern-Volmer relationship. **B** Theoretical fluorescence spectrum of an acceptor molecule with increasing concentration of a quencher. **C** Linear relationship between the concentration of the quencher and the intensity of fluorescence.

accelerates the decay rate of a molecular excited state and is represented by the equation above (**Figure 1.2**). Where I^0_f is the intensity of fluorescence without a photosensitizer, I_f is the rate of fluorescence with a quencher, k_q is the quencher rate coefficient, τ_0 is the lifetime of the emissive excited state without a quencher present, and [Q] is the concentration of the quencher.[11–13] Simply put, if a sensitization occurs there will be a clear linear decline in fluorescence as the concentration of the quencher increases. Distinguishing between direct excitation or an energy transfer is of great significance due to the implications it has on the mechanism of the overall transformation.

1.2 Lewis Acid Catalysis

Based on Woodward and Hoffman's reasoning it is expected that photochemical cycloadditions should be, and are, typified by a 2+2 reaction; in which two pi-components exchange pi bonds for sigma bonds forming cyclic compounds. For synthetic chemists these are powerful reactions that offer atom-economical approaches to rapidly construct molecular complexity. The most well-known examples of such a transformation include olefin dimerizations (see chapter 2), the Paternò-Büchi reaction (see chapter 3), and the Aza-Paternò-Büchi reaction (see chapter 4), but each suffers from various inherent drawbacks. The underlying limitation is the mechanistic requirement for direct excitation of substrates requiring the use of high energy UV light, which and can lead to various side reactions that are difficult to outcompete.[6,14–18]

A clever way to circumnavigate this challenge is to utilize Lewis acids to induce a bathochromic absorption shift in substrates. The use of Lewis acid coordination can also enhance the excited state lifetimes of certain substrates, enabling access to the desired excited triplet state that may otherwise difficult to populate. Although conceptually simple, this idea was not exploited until 2013 when Bach utilized a chiral boron-based Lewis acid for an enantioselective intramolecular enone [2+2] photocycloaddition (**Figure 1.3**).[19] This work demonstrated that 5,6-dihydro-4-pyridones underwent a >50 nm bathochromic shift upon Lewis acid coordination. It is this coordination complex that is then irradiated to populate a triplet excited state, which ultimately cyclizes to produce

cyclobutane containing product. This seminal work opened the door for enantioselective photocycloadditions to become viable synthetic transformations for chemists as this approach was shown to work on several enones and has been extended to intermolecular examples.[20–23]

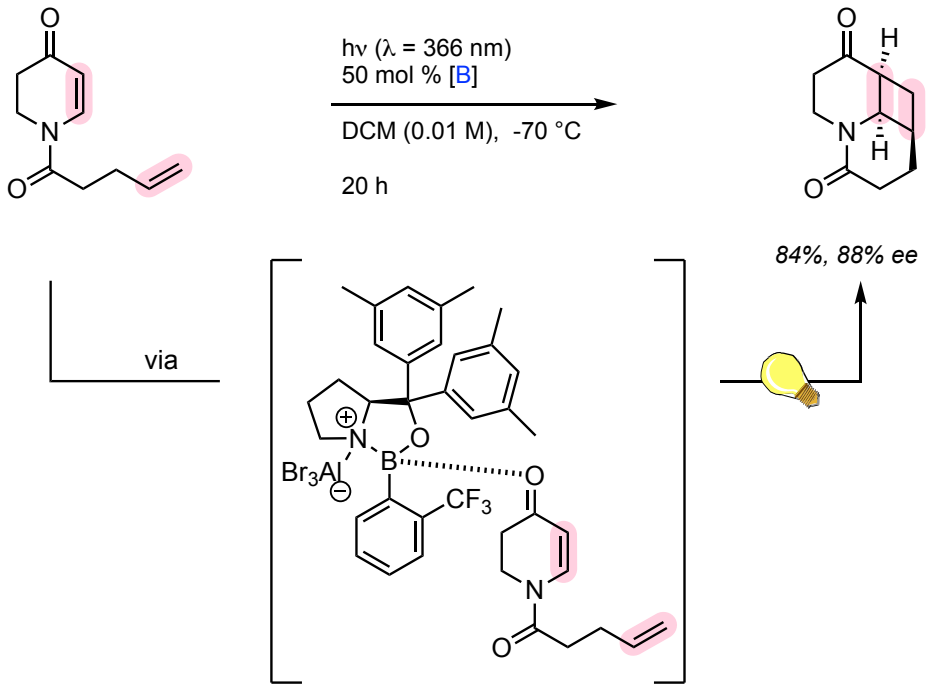

Figure 1.3 Chiral Lewis acid catalysis activated by UV-light.

In 2017, Meggers and coworkers extended this approach using a rhodium catalyst that facilitates an enantioselective intermolecular [2+2] photocycloaddition.[24] Upon substrate coordination to the Lewis acid catalyst this complex absorbs visible light to generate an excited state that directly reacts with activated alkenes to form cyclobutanes (**Figure 1.4**). This unique approach uses achiral starting materials, but upon substrate coordination the complex becomes

chiral at the metal center, enabling this transformation to occur with high enantio- and diastereoselectivity. The main limitation to this chemistry is the requirement of an N-heterocycle being present to induce the desired photoactive complex.[25,26]

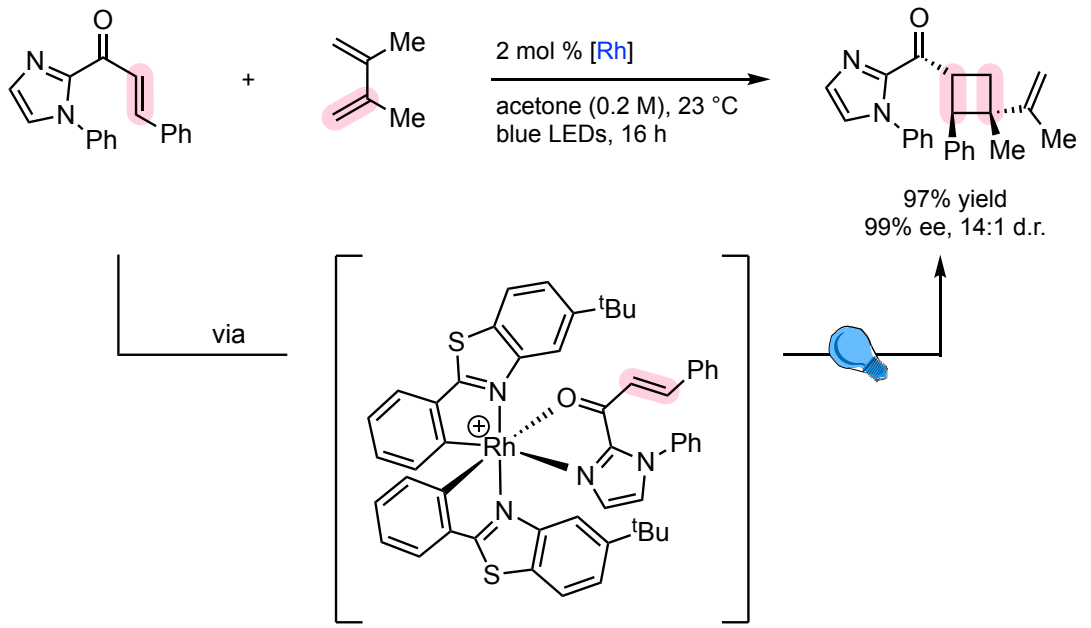

Figure 1.4 Chiral Lewis acid catalysis activated by visible light.

Yoon and coworkers contributed to this field with the development of an asymmetric [2+2] photocycloaddition of 2-hydroxychalcones using a combination of chiral Lewis acid and an additional photosensitizer. Complexation of the carbonyl substrate with Sc(III) was shown to dramatically decrease the triplet energy of the substrate. This enabled a Ru based photosensitizer to excite the complex to its triplet state through an energy transfer process. This excited state can then react with dimethylbutadiene to produce the corresponding cyclobutane. High enantioselectivity was observed upon the addition of a chiral ligand, such as 2,6-Bis[(4S)-4-tert-butyloxazolin-2-yl]pyridine, which Sc can simultaneously

coordinate to, producing a chiral excited state (**Figure 1.5**).[27] While a huge step in the right direction the utility of this reaction by the broader scientific community is hindered by the limited substrate scope with respect to the enone and the alkene.[28–31]

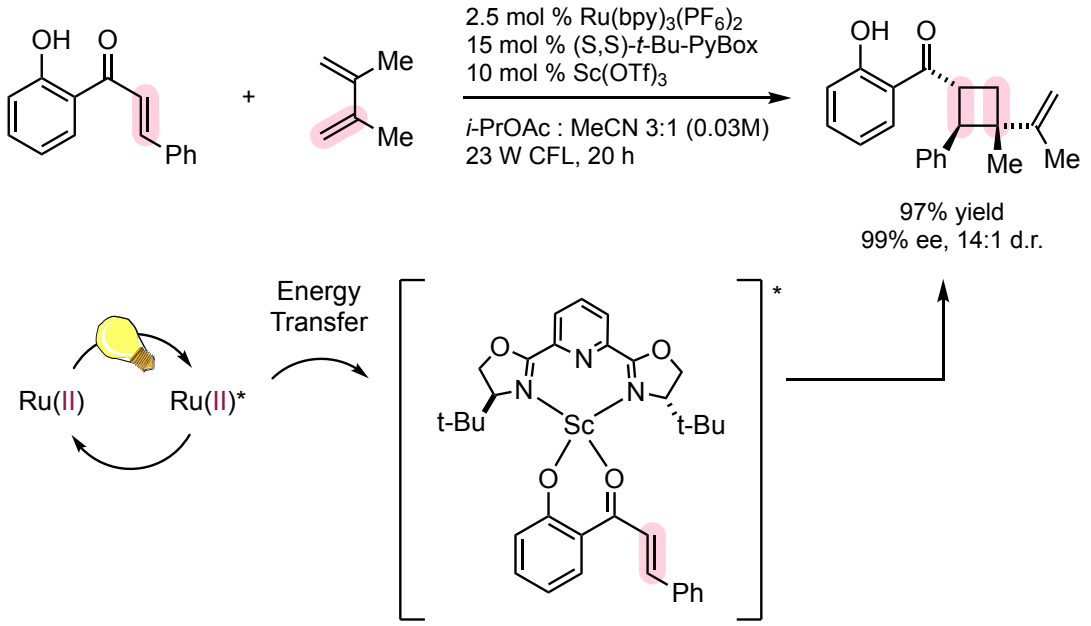

Figure 1.5 Chiral Lewis acid catalysis activated by UV-light.

Each of these examples displayed the ability of Lewis acid catalysis to either red-shift the absorption maxima of coordinated enones or lower the E_T of the substrate. Both cases enable the corresponding excited states more readily accessible, and reactivity can be controlled through a chiral environment. Expanding these approaches beyond conjugated enones that require multipoint coordination to the catalyst is highly desirable. Even more sought after is the ability to engage a broader range of nonconjugated/minimally activated alkenes.

1.3 Photoredox Catalysis

The photophysical properties of Ru(II) and Ir(III) polypyridyl complexes, such as $Ru(bpy)_3^{2+}$, have been well studied since the 1970's.[12] These luminescent complexes were originally intended for synthetic inorganic applications in carbon dioxide reductions,[32,33] water splitting,[34–36] and solar cell materials.[37–41] The effectiveness of a complex in these roles was determined by its excited state properties. As such, catalysts were designed with precise control over their redox potentials, excited state lifetimes, and quantum yields. This has been achieved by focusing on three fundamental aspects of the catalyst structure; ligand design and the coordination environment, manipulation of available oxidation states at the metal center, and electronic excitation.[42]

This class of complexes typically display/possess two distinct absorption features, the first around 290 nm representing a ligand centered $\pi - \pi^*$ transition. The second is in the visible region (400-480 nm) corresponding to a metal to ligand charge transfer (MLCT). As the name suggests, this type of transition is the excitation of an electron from a primarily metal-based orbital to an unoccupied orbital that is predominately ligand in character. This results in a formally oxidized metal center and a ligand framework that has undergone a single electron reduction. Rapid ISC to the lowest-energy triplet state produces a long-lived photoexcited species that can engage in single electron transfer (SET) with organic substrates to produce radicals (**Figure 1.6**).[43–45] In this photoexcited state this

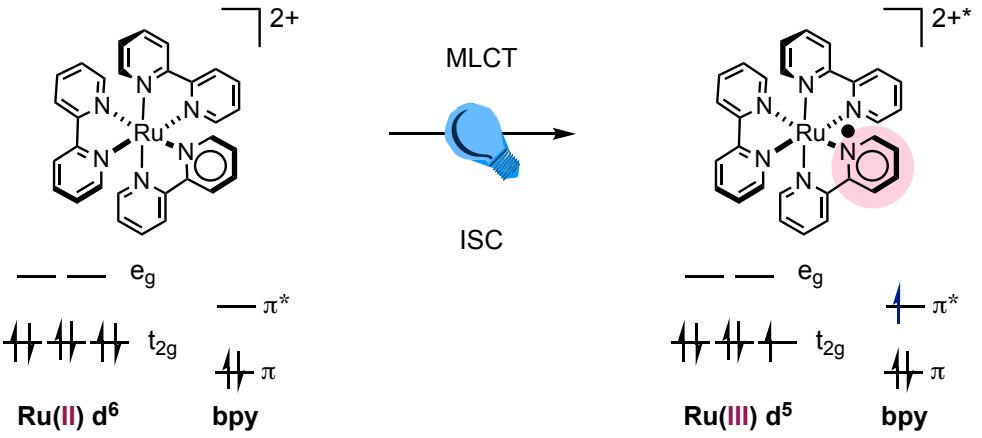

Figure 1.6 Excitation of $Ru(bpy)_3$ with visible light induces a MLCT, producing an excited state that can behave as an oxidant or a reductant.

species has the remarkable property of being both more oxidizing and reducing than the ground state.[46,47]

It was not until 2008 that organic chemists began exploiting these excited state properties to forge organic bonds, and the field of photoredox catalysis within synthetic organic chemistry was born. The near-simultaneous reports by the MacMillan, Yoon, and Stephenson groups spurred intense interest in using Ru(II) and Ir(III) photocatalysts to facilitate challenging organic transformations (**Figure 1.7**).[48–50]

Stephenson and co-workers developed a general reductive dehalogenation protocol utilizing $Ru(II)(bpy)_3$. Reaction conditions require a stoichiometric reductant such as a tertiary amine, formic acid, or Hantzsch ester. Photoexcitation of $Ru(II)(bpy)_3$ leads to $Ru(II)(bpy)_3$* which can undergo a SET with the amine generating an aminium radical cation and $Ru(I)(bpy)_3$. This Ru(I) species can reduce an α-chloroester to the α-carbonyl radical, ultimately producing the ester

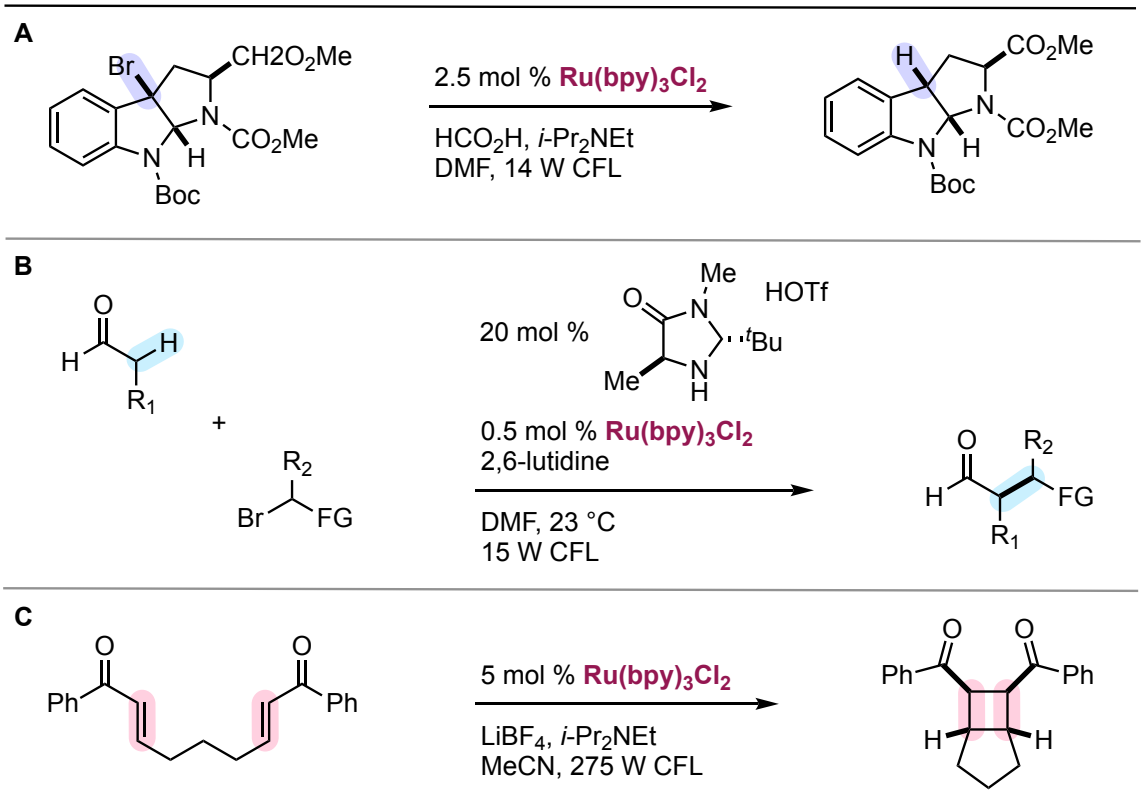

Figure 1.7 Seminal reactions in the field of photoredox catalysis. **A.** Reductive dehalogenation **B.** Asymmetric α-alkylation of aldehydes. **C**. Redox neutral enone photocycloaddition.

after proton abstraction (**Figure 1.8**).[49] MacMillan and Nicewicz established a dual photoredox organocatalytic method for long standing challenge of enantioselective a-alkylation of aldehydes.[50] This transformation exploited the ability of photoredox catalysts to generate organic radicals that combine with catalytically generated enamines enantioselectively. Yoon and coworkers disclosed a photoredox catalyzed intramolecular [2+2] enone cycloaddition that utilized a Lewis acid to control the reactivity of the enone.[48]

The use of these complexes in the development of novel synthetic transformations has enabled significant gains in the field of chemical synthesis.[51–53] Notwithstanding, the use of these catalysts suffers from several drawbacks.

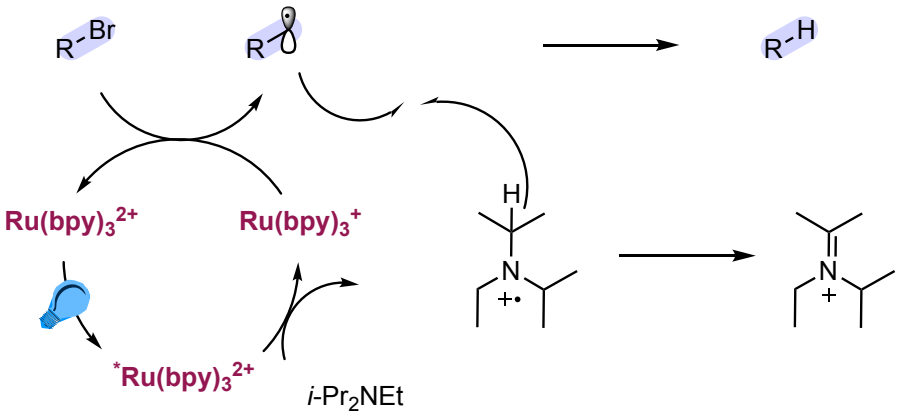

Figure 1.8 Mechanism of reductive dehalogenation using $Ru(bpy)_3^{2+}$ as a photocatalyst

First, ruthenium and iridium are two of the rarest elements on Earth, are expensive, and not ideal in terms of sustainability. The toxicity of these metals is also a concern, limiting their use pharmaceutical research. Chemically, they are hampered by the defined redox potentials chemists have to work within. This disables them from activating minimally functionalized substrates, such as electronically unactivated olefins, to forge new bonds. Due to these constraints it is desirable to find an abundant transition metal that displays comparable electronic transitions to catalyze organic reactions.

To this end significant effort has been put into the design of organic photocatalysts and dyes.[54–57] These organic chromophores have been well established to participate in photoinduced electron transfer processes, but until recently they have not been applied to organic synthesis.[58,59] These catalysts offer

significantly more than a metal-free alternative as they enable access to unique chemistries to a wide range of substrates that are challenging to engage.

1.4 Copper Complexes in Photochemistry

The ability to circumnavigate efficient non-radiative decay pathways common in first row transition metal ions with d^1-d^9 electronic configurations, enables these d^{10} Cu(I) complexes to be versatile in their use.[52] Utilizing pyridine or polypyridyl ligands, excitation and interconversion (IC) leads to the population of a low lying ^{1}MLCT state. Rapid ISC produces a ^{3}MLCT state that has a lifetime on the nano- to microsecond timescale, and at low temperatures displays phosphorescence.[60] If the energy gap between the ^{1}MLCT and ^{3}MLCT is sufficiently small (<1000cm^{-1}) and sufficient thermal energy is available, thermally activated back intersystem crossing (bISC) can be achieved.[60,61] This leads to a Boltzmann distribution for the emissive $^{1/3}$MLCT state. At higher temperatures a

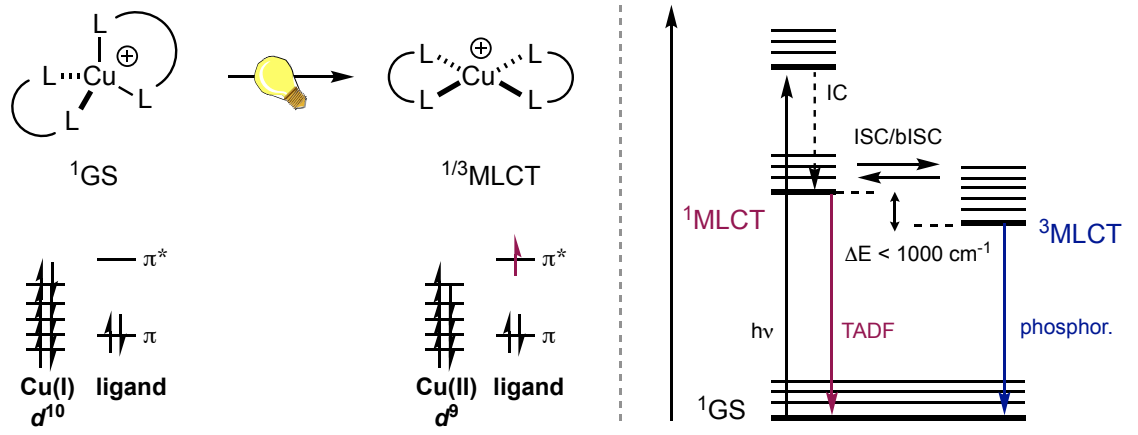

Figure 1.9 Electronic transition of a MLCT in a four coordinate pseudotetrahedral Cu(I) complex and geometrical distortion of the excited state.

radiative process called thermally activated delayed fluorescence (TADF) is dominant (**Figure 1.9**).[62,63,64]

Further study of these excited states has demonstrated a formally reduced ligand and a Cu(II) ion is produced. In contrast to the pseudotetrahedral geometry of the ground state Cu(I) complex, the new d^9 Cu(II) center prefers a square planar geometry and leads to a Jahn-Teller Distortion.[61,65] This translates to a structural distortion via flattening and enables efficient non radiative processes to occur, therefore reducing luminescence quantum yields (**Figure 1.9**). Furthermore, this flattened geometry enables solvent molecules or counter ions to coordinate to the cationic metal center forming exciplexes, which are non-luminescent. Due to these undesired quenching pathways ligands should be designed to minimize the flattening of the excited state.

These observations have led to the widespread development of mononuclear luminescent Cu(I) complexes with applications for solar cells,[66,67] organic light emitting diodes (OLEDs),[68–72,73–76] and photocatalytic reactions. Particularly noteworthy is the exploitation of TDAF to design such complexes to harvest singlet and triplet excitons and have a specific fluorescence emission, which is desirable for OLEDs.

With respect to photocatalytic reactions, a rapidly emerging class of photocatalyst are copper based as they are a low-cost alternative to Ru and Ir and offer inaccessible inner-sphere mechanisms. Numerous photochemical reactions including olefin difunctionalization and cross-couplings that generate C-C, C-N, C-

O, and C-S bonds have been developed.[24-46] Furthermore, Cu can serve as a Lewis acid to activate C-C pi bond functionalities or be used in tandem with

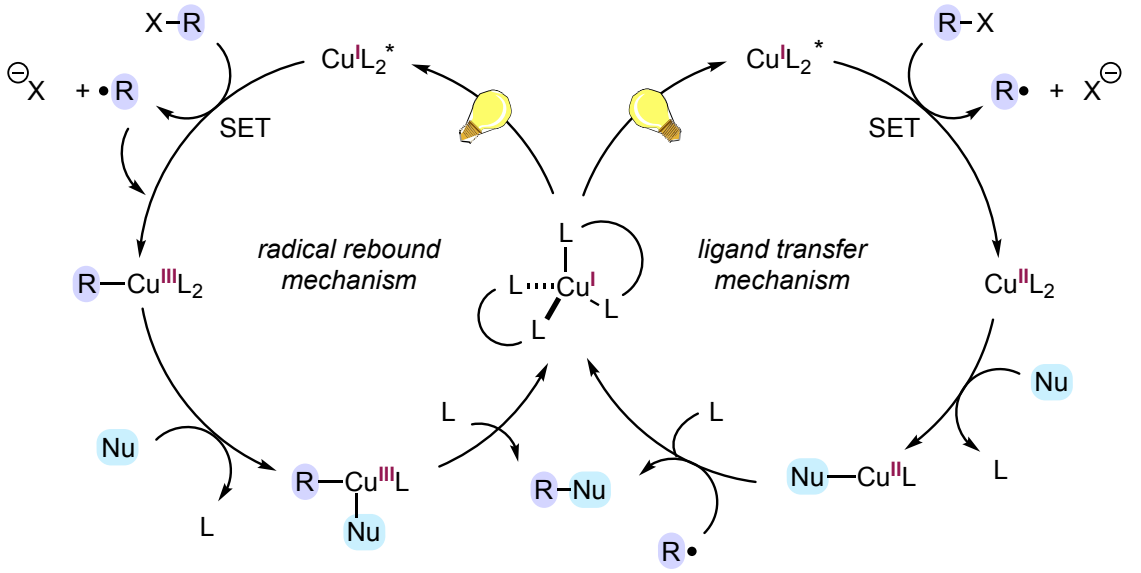

Figure 1.10 Cu(I) photocatalysts follow one of two mechanistic paradigms, either radical rebound or ligand transfer mechansim.

conventional photocatalysts for efficient dual catalytic systems.[100–108] This versatility is owed/due to the ability of copper to stabilize organic radical intermediates that are generated in photocatalytic cycles, also known as the persistent radical effect (PRE).[109]

Photocatalysts that are Cu-based follow one of two mechanistic paradigms; a rebound mechanism or a ligand transfer mechanism (**Figure 1.10**). In a rebound mechanism photoexcitation of the catalyst generates an excited state that can undergo SET with organic substrates, generating a radical species and formally a Cu(II) intermediate. This radical can rebind with the Cu(II) intermediate to generate a high valent Cu(III)-R intermediate that undergoes ligand exchange with a

nucleophile. Subsequent reductive elimination produces the desired cross coupled product and regenerates the initial Cu(I) complex. Alternatively, the transient Cu(II) intermediate can undergo ligand exchange with a nucleophile, ultimately transferring this group to the persistent radical to yield the cross-coupled product and the original Cu(I) catalyst.[109,110]

Within the last several years Cu(II) complexes have found their way into visible light photoredox catalysis. The utility of these complexes is based on the seminal work Kochi did, demonstrating that upon UV irradiation $Cu(II)Cl_2$ homolyzes to Cu(I)Cl and a chlorine radical.[111] Activation of Cu(II) with suitable ligands enables this homolysis to occur using visible light, generating a radical (Z) and a formal Cu(I) species.[112,113] This radical can react with a coupling partner, to produce a radical intermediate that is ultimately reduced by Cu(I), producing an anion and the original Cu(II) complex (**Figure 1.11**).[109,114]

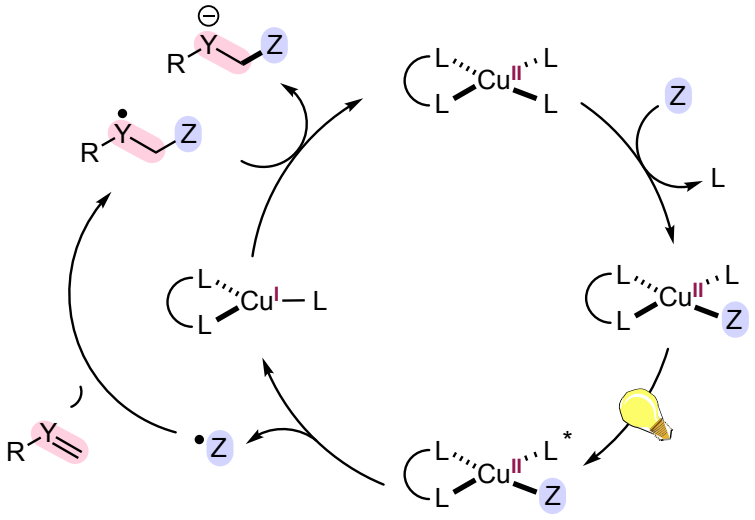

Figure 1.11 Cu(I) photocatalysts follow one of two mechanistic paradigms, either radical rebound or ligand transfer mechansim.

In addition to serving as catalysts through inner sphere mechanisms, Cu complexes can act as photosensitizers. Due to the possibility of heteroleptic coordination environments these catalysts can be finely tuned for such a purpose.

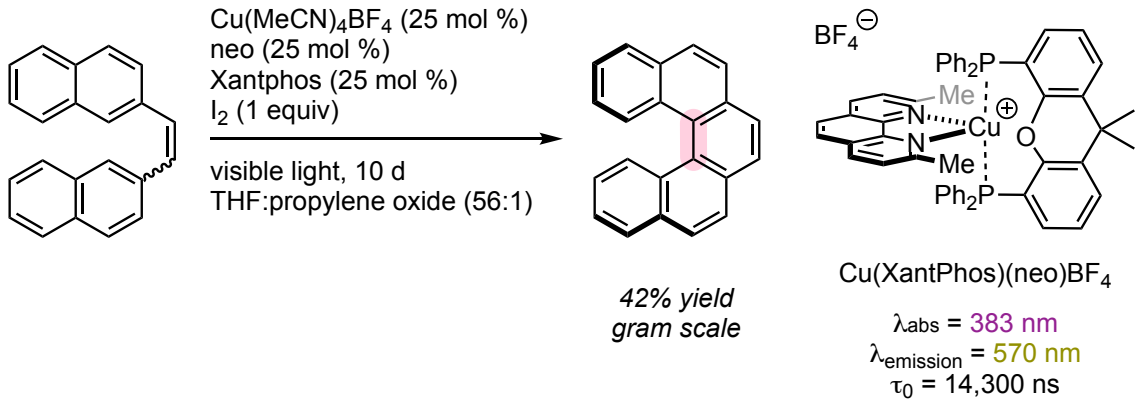

Figure 1.12 Use of bisphosphine and diamine ligands form a Cu(I) photosensitizer in-situ for the synthesis of polyaromatic carbocycles.

A perfect example of this is use of Cu(Xantphos)(neo)BF_4 for the synthesis of polyaromatic carbocycles (**Figure 1.12**).[115,116] Using rigidified and sterically congested bisphosphines enforces a pseudotetrahedral geometry at the metal center. Incorporation of a diamine ligand can offer control over the optical absorbances and redox potentials of the excited state.[117–120]

Photochemistry within synthetic organic chemistry has seen a boom due to these recent advances. No longer are photochemical reactions thought to produce a complex mixture of products but are capable of facilitating some of the most sought-after transformations in organic chemistry. Significant effort has been put into understanding the photophysical properties of the substrates and catalysts, leading to a clear understanding of the mechanisms through which they proceed.

This has enabled the rational design of organometallic complexes to undergo specific electronic transitions at anticipated wavelengths. It is under these pretexts that this dissertation attempts to expand on the synthetic utility of Cu mediated photocycloadditions for the synthesis of small heterocycles through alkene activation.

1.5 References

(1) Woodward, R. B.; Hoffmann, R. The Conservation of Orbital Symmetry. *Angew. Chemie Int. Ed. English* **1969**, *8* (11), 781–853. https://doi.org/10.1002/anie.196907811.

(2) Woodward, R. B.; Hoffmann, R. Stereochemistry of Electrocyclic Reactions. *J. Am. Chem. Soc.* **1965**, *87* (2), 395–397. https://doi.org/10.1021/ja01080a054.

(3) Hoffmann, R.; Woodward, R. B. Selection Rules for Concerted Cycloaddition Reactions. *J. Am. Chem. Soc.* **1965**, *87* (9), 2046–2048. https://doi.org/10.1021/ja01087a034.

(4) Woodward, R. B.; Hoffmann, R. Selection Rules for Sigmatropic Reactions. *J. Am. Chem. Soc.* **1965**, *87* (11), 2511–2513. https://doi.org/10.1021/ja01089a050.

(5) Horspool, W. M. Organic Photochemistry. *Annu. Reports Prog. Chem. - Sect. C* **1983**, *80*, 87–105. https://doi.org/10.1039/PC9838000087.

(6) Braslavsky, S. E. Glossary of Terms Used in Photochemistry 3rd Edition: (IUPAC Recommendations 2006). *Pure Appl. Chem.* **2007**, *79* (3), 293–465. https://doi.org/10.1351/pac200779030293.

(7) Dexter, D. L. A Theory of Sensitized Luminescence in Solids. *J. Chem. Phys.* **1953**, *21* (5), 836–850. https://doi.org/10.1063/1.1699044.

(8) Cheng, P.-C. The Contrast Formation in Optical Microscopy. In *Handbook Of Biological Confocal Microscopy*; Pawley, J. B., Ed.; Springer US: Boston, MA, 2006; pp 162–206. https://doi.org/10.1007/978-0-387-45524-2_8.

(9) Fret, T.; Fret, T. Förster Resonance Energy Transfer. *Encycl. Astrobiol.*

2015, 884–884. https://doi.org/10.1007/978-3-662-44185-5_100411.

(10) Schöpf, H.-G. Mehra, J. / Rechenberg, H., The Historical Development of Quantum Theory. Vol. 1, Part 1 & 2: The Quantum Theory of Planck, Einstein, Bohr and Sommerfeld: Its Foundation and the Rise of Its Difficulties, 1900–1925. Berlin-Heidelberg-New York, Springer-Verlag 1982. Part 1: XLVII, 372 S., DM 75, —. US $ 31.30. ISBN 3-540-90642-8, Part 2: VI, 506 S., DM 85, —. US $ 34.00. ISBN 3-540-90667-3. *ZAMM - J. Appl. Math. Mech. / Zeitschrift für Angew. Math. und Mech.* **1983**, *63* (10), 522. https://doi.org/doi:10.1002/zamm.19830631018.

(11) Green, N. J. B.; Pimblott, S. M.; Tachiya, M. Generalizations of the Stern-Volmer Relation. *J. Phys. Chem.* **1993**, *97* (1), 196–202. https://doi.org/10.1021/j100103a034.

(12) Lytle, F. E.; Hercules, D. M. The Luminescence of Tris (2,2′-Bipyridine) Ruthenium (II) Dichloride. *J. Am. Chem. Soc.* **1969**, *91* (2), 253–257. https://doi.org/10.1021/ja01030a006.

(13) Laws, W. R.; Contino, P. B. B. T.-M. in E. [21] Fluorescence Quenching Studies: Analysis of Nonlinear Stern-Volmer Data. In *Numerical Computer Methods*; Academic Press, 1992; Vol. 210, pp 448–463. https://doi.org/https://doi.org/10.1016/0076-6879(92)10023-7.

(14) Turro, N. J.; Dalton, J. C.; Dawes, K.; Farrington, G.; Hautala, R.; Morton, D.; Niemczyk, M.; Schore, N. Molecular Photochemistry of Alkanones in Solution: α-Cleavage, Hydrogen Abstraction, Cycloaddition, and Sensitization Reactions. *Acc. Chem. Res.* **1972**, *5* (3), 92–101. https://doi.org/10.1021/ar50051a002.

(15) Padwa, A. Photochemistry of the Carbon–Nitrogen Double Bond. *Chem. Rev.* **1977**, *77* (1), 37–68. https://doi.org/10.1021/cr60305a004.

(16) D'Auria, M.; Racioppi, R. Oxetane Synthesis through the Paternò-Büchi Reaction. *Molecules* **2013**, *18* (9), 11384–11428. https://doi.org/10.3390/molecules180911384.

(17) NORRISH, R. G. W.; BAMFORD, C. H. Photo-Decomposition of Aldehydes and Ketones. *Nature* **1937**, *140* (3535), 195–196. https://doi.org/10.1038/140195b0.

(18) Pitts, J. N.; Blacet, F. E. Methyl Ethyl Ketone Photochemical Processes. *J. Am. Chem. Soc.* **1950**, *72* (6), 2810–2811. https://doi.org/10.1021/ja01162a544.

(19) Brimioulle, R.; Bach, T. Enantioselective Lewis Acid Catalysis of Intramolecular Enone [2+2] Photocycloaddition Reactions. *Science (80-.).* **2013**, *342* (6160), 840–843. https://doi.org/10.1126/science.1244809.

(20) Stegbauer, S.; Jandl, C.; Bach, T. Enantioselective Lewis Acid Catalyzed Ortho Photocycloaddition of Olefins to Phenanthrene-9-Carboxaldehydes. *Angew. Chemie Int. Ed.* **2018**, *57* (44), 14593–14596. https://doi.org/doi:10.1002/anie.201808919.

(21) Hörmann, F. M.; Chung, T. S.; Rodriguez, E.; Jakob, M.; Bach, T. Evidence for Triplet Sensitization in the Visible-Light-Induced [2+2] Photocycloaddition of Eniminium Ions. *Angew. Chemie Int. Ed.* **2018**, *57* (3), 827–831. https://doi.org/doi:10.1002/anie.201710441.

(22) Poplata, S.; Bach, T. Enantioselective Intermolecular [2+2] Photocycloaddition Reaction of Cyclic Enones and Its Application in a Synthesis of (-)-Grandisol. *J. Am. Chem. Soc.* **2018**, *140* (9), 3228–3231. https://doi.org/10.1021/jacs.8b01011.

(23) Poplata, S.; Tröster, A.; Zou, Y. Q.; Bach, T. Recent Advances in the Synthesis of Cyclobutanes by Olefin [2 +2] Photocycloaddition Reactions. *Chem. Rev.* **2016**, *116* (17), 9748–9815. https://doi.org/10.1021/acs.chemrev.5b00723.

(24) Huang, X.; Quinn, T. R.; Harms, K.; Webster, R. D.; Zhang, L.; Wiest, O.; Meggers, E. Direct Visible-Light-Excited Asymmetric Lewis Acid Catalysis of Intermolecular [2+2] Photocycloadditions. *J. Am. Chem. Soc.* **2017**, *139* (27), 9120–9123. https://doi.org/10.1021/jacs.7b04363.

(25) Ma, J.; Rosales, A. R.; Huang, X.; Harms, K.; Riedel, R.; Wiest, O.; Meggers, E. Visible-Light-Activated Asymmetric β-C-H Functionalization of Acceptor-Substituted Ketones with 1,2-Dicarbonyl Compounds. *J. Am. Chem. Soc.* **2017**, *139* (48), 17245–17248. https://doi.org/10.1021/jacs.7b09152.

(26) Huo, H.; Fu, C.; Harms, K.; Meggers, E. Asymmetric Catalysis with Substitutionally Labile yet Stereochemically Stable Chiral-at-Metal Iridium(III) Complex. *J. Am. Chem. Soc.* **2014**, *136* (8), 2990–2993. https://doi.org/10.1021/ja4132505.

(27) Kalisky, Y. Energy Transfer. *Phys. Eng. Solid State Lasers* **2009**, *354* (6318), 93–104. https://doi.org/10.1117/3.660249.ch7.

(28) Daub, M. E.; Jung, H.; Lee, B. J.; Won, J.; Baik, M. H.; Yoon, T. P.

Enantioselective [2+2] Cycloadditions of Cinnamate Esters: Generalizing Lewis Acid Catalysis of Triplet Energy Transfer. *J. Am. Chem. Soc.* **2019**, *141* (24), 9543–9547. https://doi.org/10.1021/jacs.9b04643.

(29) Zheng, J.; Swords, W. B.; Jung, H.; Skubi, K. L.; Kidd, J. B.; Meyer, G. J.; Baik, M. H.; Yoon, T. P. Enantioselective Intermolecular Excited-State Photoreactions Using a Chiral Ir Triplet Sensitizer: Separating Association from Energy Transfer in Asymmetric Photocatalysis. *J. Am. Chem. Soc.* **2019**, *141* (34), 13625–13634. https://doi.org/10.1021/jacs.9b06244.

(30) Skubi, K. L.; Kidd, J. B.; Jung, H.; Guzei, I. A.; Baik, M. H.; Yoon, T. P. Enantioselective Excited-State Photoreactions Controlled by a Chiral Hydrogen-Bonding Iridium Sensitizer. *J. Am. Chem. Soc.* **2017**, *139* (47), 17186–17192. https://doi.org/10.1021/jacs.7b10586.

(31) Miller, Z. D.; Lee, B. J.; Yoon, T. P. Enantioselective Crossed Photocycloadditions of Styrenic Olefins by Lewis Acid Catalyzed Triplet Sensitization. *Angew. Chemie Int. Ed.* **2017**, *56* (39), 11891–11895. https://doi.org/doi:10.1002/anie.201706975.

(32) Morimoto, T.; Nakajima, T.; Sawa, S.; Nakanishi, R.; Imori, D.; Ishitani, O. CO2 Capture by a Rhenium(I) Complex with the Aid of Triethanolamine. *J. Am. Chem. Soc.* **2013**, *135* (45), 16825–16828. https://doi.org/10.1021/ja409271s.

(33) Takeda, H.; Ishitani, O. Development of Efficient Photocatalytic Systems for CO2 Reduction Using Mononuclear and Multinuclear Metal Complexes Based on Mechanistic Studies. *Coord. Chem. Rev.* **2010**, *254* (3), 346–354. https://doi.org/https://doi.org/10.1016/j.ccr.2009.09.030.

(34) Lowry, M. S.; Bernhard, S. Synthetically Tailored Excited States: Phosphorescent, Cyclometalated Iridium(III) Complexes and Their Applications. *Chem. - A Eur. J.* **2006**, *12* (31), 7970–7977. https://doi.org/10.1002/chem.200600618.

(35) Meyer, T. J. Chemical Approaches to Artificial Photosynthesis. *Acc. Chem. Res.* **1989**, *22* (5), 163–170. https://doi.org/10.1021/ar00161a001.

(36) NREL. Proceedings of the 1999 U.S. DOE Hydrogen Program Review. *Doe Osti.Gov* **2000**, No. October.

(37) Reger, D. L.; Grattan, T. C.; Brown, K. J.; Little, C. A.; Lamba, J. J. S.; Rheingold, A. L.; Sommer, R. D. Syntheses of Tris(Pyrazolyl)Methane Ligands and {[Tris(Pyrazolyl)Methane]Mn(CO)3} SO3CF3 Complexes:

Comparison of Ligand Donor Properties. *J. Organomet. Chem.* **2000**, *607* (1–2), 120–128. https://doi.org/10.1016/S0022-328X(00)00290-4.

(38) Flamigni, L.; Barbieri, A.; Sabatini, C.; Ventura, B.; Barigelletti, F. Photochemistry and Photophysics of Coordination Compounds: Iridium. In *Photochemistry and Photophysics of Coordination Compounds II*; Balzani, V., Campagna, S., Eds.; Springer Berlin Heidelberg: Berlin, Heidelberg, 2007; pp 143–203. https://doi.org/10.1007/128_2007_131.

(39) Balzani, V.; Bergamini, G.; Campagna, S.; Puntoriero, F. Photochemistry and Photophysics of Coordination Compounds: Overview and GeneralConcepts. In *Photochemistry and Photophysics of Coordination Compounds I*; Balzani, V., Campagna, S., Eds.; Springer Berlin Heidelberg: Berlin, Heidelberg, 2007; pp 1–36. https://doi.org/10.1007/128_2007_132.

(40) Dixon, I. M.; Collin, J.-P.; Sauvage, J.-P.; Flamigni, L.; Encinas, S.; Barigelletti, F. A Family of Luminescent Coordination Compounds: Iridium() Polyimine Complexes. *Chem. Soc. Rev.* **2000**, *29* (6), 385–391. https://doi.org/10.1039/B000704H.

(41) Rensmo, H.; Lunell, S.; Siegbahn, H. Absorption and Electrochemical Properties of Ruthenium(II) Dyes, Studied by Semiempirical Quantum Chemical Calculations. *J. Photochem. Photobiol. A Chem.* **1998**, *114* (2), 117–124. https://doi.org/https://doi.org/10.1016/S1010-6030(98)00217-2.

(42) Zysman-colman, E. *Iridium (III) in Optoelectronic and Photonics Applications Edited By*.

(43) Baba, A. I.; Shaw, J. R.; Simon, J. A.; Thummel, R. P.; Schmehl, R. H. The Photophysical Behavior of D6 Complexes Having Nearly Isoenergetic MLCT and Ligand Localized Excited States. *Coord. Chem. Rev.* **1998**, *171*, 43–59. https://doi.org/https://doi.org/10.1016/S0010-8545(98)90009-1.

(44) Kalyanasundaram, K. Photophysics, Photochemistry and Solar Energy Conversion with Tris(Bipyridyl)Ruthenium(II) and Its Analogues. *Coord. Chem. Rev.* **1982**, *46*, 159–244. https://doi.org/https://doi.org/10.1016/0010-8545(82)85003-0.

(45) Juris, A.; Balzani, V.; Belser, P.; von Zelewsky, A. Characterization of the Excited State Properties of Some New Photosensitizers of the Ruthenium (Polypyridine) Family. *Helv. Chim. Acta* **1981**, *64* (7), 2175–2182. https://doi.org/doi:10.1002/hlca.19810640723.

(46) Tucker, J. W.; Stephenson, C. R. J. Shining Light on Photoredox Catalysis:

Theory and Synthetic Applications. *J. Org. Chem.* **2012**, *77* (4), 1617–1622. https://doi.org/10.1021/jo202538x.

(47) Prier, C. K.; Rankic, D. A.; MacMillan, D. W. C. Visible Light Photoredox Catalysis with Transition Metal Complexes: Applications in Organic Synthesis. *Chem. Rev.* **2013**, *113* (7), 5322–5363. https://doi.org/10.1021/cr300503r.

(48) Ischay, M. A.; Anzovino, M. E.; Du, J.; Yoon, T. P. Efficient Visible Light Photocatalysis of [2+2] Enone Cycloadditions. *J. Am. Chem. Soc.* **2008**, *130* (39), 12886–12887. https://doi.org/10.1021/ja805387f.

(49) Narayanam, J. M. R.; Tucker, J. W.; Stephenson, C. R. J. Electron-Transfer Photoredox Catalysis: Development of a Tin-Free Reductive Dehalogenation Reaction. *J. Am. Chem. Soc.* **2009**, *131* (25), 8756–8757. https://doi.org/10.1021/ja9033582.

(50) Nicewicz, D. A.; MacMillan, D. W. C. Merging Photoredox Catalysis with Organocatalysis: The Direct Asymmetric Alkylation of Aldehydes. *Chemtracts* **2010**, *23* (2), 73–76.

(51) Twilton, J.; Le, C. C.; Zhang, P.; Shaw, M. H.; Evans, R. W.; MacMillan, D. W. C. The Merger of Transition Metal and Photocatalysis. *Nat. Rev. Chem.* **2017**, *1*. https://doi.org/10.1038/s41570-017-0052.

(52) Arias-Rotondo, D. M.; McCusker, J. K. The Photophysics of Photoredox Catalysis: A Roadmap for Catalyst Design. *Chem. Soc. Rev.* **2016**, *45* (21), 5803–5820. https://doi.org/10.1039/c6cs00526h.

(53) Reckenthäler, M.; Griesbeck, A. G. Photoredox Catalysis for Organic Syntheses. *Adv. Synth. Catal.* **2013**, *355* (14–15), 2727–2744. https://doi.org/10.1002/adsc.201300751.

(54) Fagnoni, M.; Dondi, D.; Ravelli, D.; Albini, A. Photocatalysis for the Formation of the C-C Bond. *Chem. Rev.* **2007**, *107* (6), 2725–2756. https://doi.org/10.1021/cr068352x.

(55) Pandey, G. Photoinduced Electron Transfer (PET) in Organic Synthesis. In *Photoinduced Electron Transfer V*; Mattay, J., Ed.; Springer Berlin Heidelberg: Berlin, Heidelberg, 1993; pp 175–221. https://doi.org/10.1007/3-540-56746-1_11.

(56) Fukuzumi, S.; Ohkubo, K. Selective Photocatalytic Reactions with Organic Photocatalysts. *Chem. Sci.* **2013**, *4* (2), 561–574.

https://doi.org/10.1039/C2SC21449K.

(57) Wang, Y.; Wang, X.; Antonietti, M. Polymeric Graphitic Carbon Nitride as a Heterogeneous Organocatalyst: From Photochemistry to Multipurpose Catalysis to Sustainable Chemistry. *Angew. Chemie Int. Ed.* **2012**, *51* (1), 68–89. https://doi.org/doi:10.1002/anie.201101182.

(58) Miranda, M. A.; García, H. 2,4,6-Triphenylpyrylium Tetrafluoroborate as an Electron-Transfer Photosensitizer. *Chem. Rev.* **1994**, *94* (4), 1063–1089. https://doi.org/10.1021/cr00028a009.

(59) Romero, N. A.; Nicewicz, D. A. Organic Photoredox Catalysis. *Chem. Rev.* **2016**, *116* (17), 10075–10166. https://doi.org/10.1021/acs.chemrev.6b00057.

(60) Mara, M. W.; Fransted, K. A.; Chen, L. X. Interplays of Excited State Structures and Dynamics in Copper(I) Diimine Complexes: Implications and Perspectives. *Coord. Chem. Rev.* **2015**, *282–283*, 2–18. https://doi.org/https://doi.org/10.1016/j.ccr.2014.06.013.

(61) Iwamura, M.; Takeuchi, S.; Tahara, T. Ultrafast Excited-State Dynamics of Copper(I) Complexes. *Acc. Chem. Res.* **2015**, *48* (3), 782–791. https://doi.org/10.1021/ar500353h.

(62) Yersin, H.; Czerwieniec, R.; Shafikov, M. Z.; Suleymanova, A. F. TADF Material Design: Photophysical Background and Case Studies Focusing on Cu(I) and Ag(I) Complexes. *Chemphyschem* **2017**, *18* (24), 3508–3535. https://doi.org/10.1002/cphc.201700872.

(63) Leitl, M. J.; Zink, D. M.; Schinabeck, A.; Baumann, T.; Volz, D.; Yersin, H. Copper(I) Complexes for Thermally Activated Delayed Fluorescence: From Photophysical to Device Properties. *Top. Curr. Chem.* **2016**, *374* (3), 25. https://doi.org/10.1007/s41061-016-0019-1.

(64) Reviews, C. S. Photochemistry with Earth-Abundant Metals – Fundamentals, Concepts, and Case Studies. **2019**.

(65) Cunningham, C. T.; Moore, J. J.; Cunningham, K. L. H.; Fanwick, P. E.; McMillin, D. R. Structural and Photophysical Studies of Cu(NN)2+ Systems in the Solid State. Emission at Last from Complexes with Simple 1,10-Phenanthroline Ligands. *Inorg. Chem.* **2000**, *39* (16), 3638–3644. https://doi.org/10.1021/ic000082s.

(66) Hattori, S.; Wada, Y.; Yanagida, S.; Fukuzumi, S. Blue Copper Model

Complexes with Distorted Tetragonal Geometry Acting as Effective Electron-Transfer Mediators in Dye-Sensitized Solar Cells. *J. Am. Chem. Soc.* **2005**, *127* (26), 9648–9654. https://doi.org/10.1021/ja0506814.

(67) Magni, M.; Giannuzzi, R.; Colombo, A.; Cipolla, M. P.; Dragonetti, C.; Caramori, S.; Carli, S.; Grisorio, R.; Suranna, G. P.; Bignozzi, C. A.; et al. Tetracoordinated Bis-Phenanthroline Copper-Complex Couple as Efficient Redox Mediators for Dye Solar Cells. *Inorg. Chem.* **2016**, *55* (11), 5245—5253. https://doi.org/10.1021/acs.inorgchem.6b00204.

(68) Hashimoto, M.; Igawa, S.; Yashima, M.; Kawata, I.; Hoshino, M.; Osawa, M. Highly Efficient Green Organic Light-Emitting Diodes Containing Luminescent Three-Coordinate Copper(I) Complexes. *J. Am. Chem. Soc.* **2011**, *133* (27), 10348–10351. https://doi.org/10.1021/ja202965y.

(69) Chen, W.-C.; Lee, C.-S.; Tong, Q.-X. Blue-Emitting Organic Electrofluorescence Materials: Progress and Prospective. *J. Mater. Chem. C* **2015**, *3* (42), 10957–10963. https://doi.org/10.1039/C5TC02420J.

(70) Wang, Z.; Zhu, J.; Liu, Z.; Wu, P.; Wang, H.; Zhang, Z.; Wei, B. Thermally Activated Delayed Fluorescence of Co-Deposited Copper(i) Complexes: Cost-Effective Emitters for Highly Efficient Organic Light-Emitting Diodes. *J. Mater. Chem. C* **2017**, *5* (28), 6982–6988. https://doi.org/10.1039/C7TC01531C.

(71) Paquin, F.; Rivnay, J.; Salleo, A.; Stingelin, N.; Silva, C. Multi-Phase Semicrystalline Microstructures Drive Exciton Dissociation in Neat Plastic Semiconductors. *J. Mater. Chem. C* **2015**, *3* (I), 10715–10722. https://doi.org/10.1039/b000000x.

(72) Volz, D.; Chen, Y.; Wallesch, M.; Liu, R.; Fléchon, C.; Zink, D. M.; Friedrichs, J.; Flügge, H.; Steininger, R.; Göttlicher, J.; et al. Bridging the Efficiency Gap: Fully Bridged Dinuclear Cu(I)-Complexes for Singlet Harvesting in High-Efficiency OLEDs. *Adv. Mater.* **2015**, *27* (15), 2538–2543. https://doi.org/10.1002/adma.201405897.

(73) Reineke, S.; Thomschke, M.; Lüssem, B.; Leo, K. White Organic Light-Emitting Diodes: Status and Perspective. *Rev. Mod. Phys.* **2013**, *85* (3), 1245–1293. https://doi.org/10.1103/RevModPhys.85.1245.

(74) Chou, P.-T.; Chi, Y. Phosphorescent Dyes for Organic Light-Emitting Diodes. *Chem. - A Eur. J.* **2007**, *13* (2), 380–395. https://doi.org/10.1002/chem.200601272.

(75) Wallesch, M.; Volz, D.; Zink, D. M.; Schepers, U.; Nieger, M.; Baumann, T.; Bräse, S. Bright Coppertunities: Multinuclear Cu(I) Complexes with N-P Ligands and Their Applications. *Chemistry* **2014**, *20* (22), 6578–6590. https://doi.org/10.1002/chem.201402060.

(76) Hu, T.; He, L.; Duan, L.; Qiu, Y. Solid-State Light-Emitting Electrochemical Cells Based on Ionic Iridium(Iii) Complexes. *J. Mater. Chem.* **2012**, *22* (10), 4206–4215. https://doi.org/10.1039/C2JM16185K.

(77) Pirtsch, M.; Paria, S.; Matsuno, T.; Isobe, H.; Reiser, O. [Cu(Dap)2Cl] As an Efficient Visible-Light-Driven Photoredox Catalyst in Carbon–Carbon Bond-Forming Reactions. *Chem. – A Eur. J.* **2012**, *18* (24), 7336–7340. https://doi.org/doi:10.1002/chem.201200967.

(78) Bagal, D. B.; Kachkovskyi, G.; Knorn, M.; Rawner, T.; Bhanage, B. M.; Reiser, O. Trifluoromethylchlorosulfonylation of Alkenes: Evidence for an Inner-Sphere Mechanism by a Copper Phenanthroline Photoredox Catalyst. *Angew. Chemie Int. Ed.* **2015**, *54* (24), 6999–7002. https://doi.org/doi:10.1002/anie.201501880.

(79) Hazra, A.; Lee, M. T.; Chiu, J. F.; Lalic, G. Photoinduced Copper-Catalyzed Coupling of Terminal Alkynes and Alkyl Iodides. *Angew. Chemie Int. Ed.* **2018**, *57* (19), 5492–5496. https://doi.org/doi:10.1002/anie.201801085.

(80) Das, D. K.; Kumar Pampana, V. K.; Hwang, K. C. Copper Catalyzed Photoredox Synthesis of α-Keto Esters{,} Quinoxaline{,} and Naphthoquinone: Controlled Oxidation of Terminal Alkynes to Glyoxals. *Chem. Sci.* **2018**, *9* (37), 7318–7326. https://doi.org/10.1039/C8SC03447H.

(81) Xiao, P.; Li, C. X.; Fang, W. H.; Cui, G.; Thiel, W. Mechanism of the Visible-Light-Mediated Copper-Catalyzed Coupling Reaction of Phenols and Alkynes. *J. Am. Chem. Soc.* **2018**, *140* (44), 15099–15113. https://doi.org/10.1021/jacs.8b10387.

(82) Ragupathi, A.; Sagadevan, A.; Lin, C.-C.; Hwu, J.-R.; Hwang, K. C. Copper(i)-Catalysed Oxidative C–N Coupling of 2-Aminopyridine with Terminal Alkynes Featuring a C□C Bond Cleavage Promoted by Visible Light. *Chem. Commun.* **2016**, *52* (79), 11756–11759. https://doi.org/10.1039/C6CC05506K.

(83) Charpe, V. P.; Hande, A. A.; Sagadevan, A.; Hwang, K. C. Visible-Light Induced Copper(i)-Catalysed Denitrogenative Oxidative Coupling of Hydrazinylpyridines with Terminal Alkynes. *Green Chem.* **2018**, *20* (21), 4859–4864. https://doi.org/10.1039/C8GC01180J.

(84) Matier, C. D.; Schwaben, J.; Peters, J. C.; Fu, G. C. Copper-Catalyzed Alkylation of Aliphatic Amines Induced by Visible Light. *J. Am. Chem. Soc.* **2017**, *139* (49), 17707–17710. https://doi.org/10.1021/jacs.7b09582.

(85) Murarka, S. N-(Acyloxy)Phthalimides as Redox-Active Esters in Cross-Coupling Reactions. *Adv. Synth. Catal.* **2018**, *360* (9), 1735–1753. https://doi.org/doi:10.1002/adsc.201701615.

(86) Sagadevan, A.; Hwang, K. C. Photo-Induced Sonogashira C□C Coupling Reaction Catalyzed by Simple Copper(I) Chloride Salt at Room Temperature. *Adv. Synth. Catal.* **2012**, *354* (18), 3421–3427. https://doi.org/doi:10.1002/adsc.201200683.

(87) Sagadevan, A.; Charpe, V. P.; Ragupathi, A.; Hwang, K. C. Visible Light Copper Photoredox-Catalyzed Aerobic Oxidative Coupling of Phenols and Terminal Alkynes: Regioselective Synthesis of Functionalized Ketones via C□C Triple Bond Cleavage. *J. Am. Chem. Soc.* **2017**, *139* (8), 2896–2899. https://doi.org/10.1021/jacs.6b13113.

(88) Sagadevan, A.; Charpe, V. P.; Hwang, K. C. Copper(i) Chloride Catalysed Room Temperature Csp–Csp Homocoupling of Terminal Alkynes Mediated by Visible Light. *Catal. Sci. Technol.* **2016**, *6* (21), 7688–7692. https://doi.org/10.1039/C6CY01400C.

(89) Liu, Z.; Chen, H.; Lv, Y.; Tan, X.; Shen, H.; Yu, H. Z.; Li, C. Radical Carbofluorination of Unactivated Alkenes with Fluoride Ions. *J. Am. Chem. Soc.* **2018**, *140* (19), 6169–6175. https://doi.org/10.1021/jacs.8b03077.

(90) Sagadevan, A.; Lyu, P.-C.; Hwang, K. C. Visible-Light-Activated Copper(i) Catalyzed Oxidative Csp–Csp Cross-Coupling Reaction: Efficient Synthesis of Unsymmetrical Conjugated Diynes without Ligands and Base. *Green Chem.* **2016**, *18* (16), 4526–4530. https://doi.org/10.1039/C6GC01463A.

(91) Sagadevan, A.; Ragupathi, A.; Lin, C.-C.; Hwu, J. R.; Hwang, K. C. Visible-Light Initiated Copper(i)-Catalysed Oxidative C–N Coupling of Anilines with Terminal Alkynes: One-Step Synthesis of α-Ketoamides. *Green Chem.* **2015**, *17* (2), 1113–1119. https://doi.org/10.1039/C4GC01623H.

(92) Sagadevan, A.; Ragupathi, A.; Hwang, K. C. Photoinduced Copper-Catalyzed Regioselective Synthesis of Indoles: Three-Component Coupling of Arylamines, Terminal Alkynes, and Quinones. *Angew. Chemie Int. Ed.* **2015**, *54* (47), 13896–13901. https://doi.org/doi:10.1002/anie.201506579.

(93) He, J.; Chen, C.; Fu, G. C.; Peters, J. C. Visible-Light-Induced, Copper-Catalyzed Three-Component Coupling of Alkyl Halides, Olefins, and Trifluoromethylthiolate to Generate Trifluoromethyl Thioethers. *ACS Catal.* **2018**, *8* (12), 11741–11748. https://doi.org/10.1021/acscatal.8b04094.

(94) Creutz, S. E.; Lotito, K. J.; Fu, G. C.; Peters, J. C. Photoinduced Ullmann C-N Coupling: Demonstrating the Viability of a Radical Pathway. *Science (80-.).* **2012**, *338* (6107), 647–651. https://doi.org/10.1126/science.1226458.

(95) Bissember, A. C.; Lundgren, R. J.; Creutz, S. E.; Peters, J. C.; Fu, G. C. Transition-Metal-Catalyzed Alkylations of Amines with Alkyl Halides: Photoinduced, Copper-Catalyzed Couplings of Carbazoles. *Angew. Chemie Int. Ed.* **2013**, *52* (19), 5129–5133. https://doi.org/doi:10.1002/anie.201301202.

(96) Uyeda, C.; Tan, Y.; Fu, G. C.; Peters, J. C. A New Family of Nucleophiles for Photoinduced, Copper-Catalyzed Cross-Couplings via Single-Electron Transfer: Reactions of Thiols with Aryl Halides under Mild Conditions (O C). *J. Am. Chem. Soc.* **2013**, *135* (25), 9548–9552. https://doi.org/10.1021/ja404050f.

(97) Greaney, M. F. Copper Catalysis in a Blue Light. *Science (80-.).* **2016**, *351* (6274), 666. https://doi.org/10.1126/science.aaf1071.

(98) Lei, W. L.; Wang, T.; Feng, K. W.; Wu, L. Z.; Liu, Q. Visible-Light-Driven Synthesis of 4-Alkyl/Aryl-2-Aminothiazoles Promoted by in Situ Generated Copper Photocatalyst. *ACS Catal.* **2017**, *7* (11), 7941–7945. https://doi.org/10.1021/acscatal.7b02818.

(99) Meng, Q. Y.; Gao, X. W.; Lei, T.; Liu, Z.; Zhan, F.; Li, Z. J.; Zhong, J. J.; Xiao, H.; Feng, K.; Chen, B.; et al. Identifying Key Intermediates Generated in Situ from Cu(II) Salt-Catalyzed C-H Functionalization of Aromatic Amines under Illumination. *Sci. Adv.* **2017**, *3* (8). https://doi.org/10.1126/sciadv.1700666.

(100) Ye, Y.; Sanford, M. S. Merging Visible-Light Photocatalysis and Transition-Metal Catalysis in the Copper-Catalyzed Trifluoromethylation of Boronic Acids with CF 3I. *J. Am. Chem. Soc.* **2012**, *134* (22), 9034–9037. https://doi.org/10.1021/ja301553c.

(101) Le, C.; Chen, T. Q.; Liang, T.; Zhang, P.; MacMillan, D. W. C. A Radical Approach to the Copper Oxidative Addition Problem: Trifluoromethylation of Bromoarenes. *Science (80-.).* **2018**, *360* (6392), 1010–1014. https://doi.org/10.1126/science.aat4133.

(102) Tlahuext-Aca, A.; Candish, L.; Garza-Sanchez, R. A.; Glorius, F. Decarboxylative Olefination of Activated Aliphatic Acids Enabled by Dual Organophotoredox/Copper Catalysis. *ACS Catal.* **2018**, *8* (3), 1715–1719. https://doi.org/10.1021/acscatal.7b04281.

(103) Mao, R.; Balon, J.; Hu, X. Cross-Coupling of Alkyl Redox-Active Esters with Benzophenone Imines: Tandem Photoredox and Copper Catalysis. *Angew. Chemie Int. Ed.* **2018**, *57* (30), 9501–9504. https://doi.org/doi:10.1002/anie.201804873.

(104) Mao, R.; Frey, A.; Balon, J.; Hu, X. Decarboxylative C(Sp 3)-N Cross-Coupling via Synergetic Photoredox and Copper Catalysis. *Nat. Catal.* **2018**, *1* (2), 120–126. https://doi.org/10.1038/s41929-017-0023-z.

(105) Wang, D.; Zhu, N.; Chen, P.; Lin, Z.; Liu, G. Enantioselective Decarboxylative Cyanation Employing Cooperative Photoredox Catalysis and Copper Catalysis. *J. Am. Chem. Soc.* **2017**, *139* (44), 15632–15635. https://doi.org/10.1021/jacs.7b09802.

(106) Sha, W.; Deng, L.; Ni, S.; Mei, H.; Han, J.; Pan, Y. Merging Photoredox and Copper Catalysis: Enantioselective Radical Cyanoalkylation of Styrenes. *ACS Catal.* **2018**, *8* (8), 7489–7494. https://doi.org/10.1021/acscatal.8b01863.

(107) Zhang, Y.; Traber, P.; Zedler, L.; Kupfer, S.; Gräfe, S.; Schulz, M.; Frey, W.; Karnahl, M.; Dietzek, B. Cu(i) vs. Ru(Ii) Photosensitizers: Elucidation of Electron Transfer Processes within a Series of Structurally Related Complexes Containing an Extended π-System. *Phys. Chem. Chem. Phys.* **2018**, *20* (38), 24843–24857. https://doi.org/10.1039/C8CP04595J.

(108) Kautzky, J. A.; Wang, T.; Evans, R. W.; Macmillan, D. W. C. Decarboxylative Trifluoromethylation of Aliphatic Carboxylic Acids. *J. Am. Chem. Soc.* **2018**, *140* (21), 6522–6526. https://doi.org/10.1021/jacs.8b02650.

(109) Hossain, A.; Bhattacharyya, A.; Reiser, O. Copper's Rapid Ascent in Visible-Light Photoredox Catalysis. *Science (80-.).* **2019**, *364* (6439). https://doi.org/10.1126/science.aav9713.

(110) Mitani, M.; Kato, I.; Koyama, K. Photoaddition of Alkyl Halides to Olefins Catalyzed by Copper(I) Complexes. *J. Am. Chem. Soc.* **1983**, *105* (22), 6719–6721. https://doi.org/10.1021/ja00360a033.

(111) Kochi, J. K. Photolyses of Metal Compounds: Cupric Chloride in Organic Media. *J. Am. Chem. Soc.* **1962**, *84* (11), 2121–2127.

https://doi.org/10.1021/ja00870a025.

(112) Guo, J.-J.; Hu, A.; Chen, Y.; Sun, J.; Tang, H.; Zuo, Z. Photocatalytic C−C Bond Cleavage and Amination of Cycloalkanols by Cerium(III) Chloride Complex. *Angew. Chemie Int. Ed.* **2016**, *55* (49), 15319–15322. https://doi.org/doi:10.1002/anie.201609035.

(113) Hu, A.; Guo, J. J.; Pan, H.; Zuo, Z. Selective Functionalization of Methane, Ethane, and Higher Alkanes by Cerium Photocatalysis. *Science (80-.).* **2018**, *361* (6403), 668–672. https://doi.org/10.1126/science.aat9750.

(114) Li, Y.; Zhou, K.; Wen, Z.; Cao, S.; Shen, X.; Lei, M.; Gong, L. Copper(II)-Catalyzed Asymmetric Photoredox Reactions: Enantioselective Alkylation of Imines Driven by Visible Light. *J. Am. Chem. Soc.* **2018**, *140* (46), 15850–15858. https://doi.org/10.1021/jacs.8b09251.

(115) Liu, L.; Katz, T. J. Bromine Auxiliaries in Photosyntheses of [5]Helicenes. *Tetrahedron Lett.* **1991**, *32* (47), 6831–6834. https://doi.org/https://doi.org/10.1016/0040-4039(91)80418-6.

(116) Hernandez-Perez, A. C.; Collins, S. K. Heteroleptic Cu-Based Sensitizers in Photoredox Catalysis. *Acc. Chem. Res.* **2016**, *49* (8), 1557–1565. https://doi.org/10.1021/acs.accounts.6b00250.

(117) Cuttell, D. G.; Kuang, S. M.; Fanwick, P. E.; McMillin, D. R.; Walton, R. A. Simple Cu(I) Complexes with Unprecedented Excited-State Lifetimes. *J. Am. Chem. Soc.* **2002**, *124* (1), 6–7. https://doi.org/10.1021/ja012247h.

(118) McCormick, T.; Jia, W. L.; Wang, S. Phosphorescent Cu(I) Complexes of 2-(2′-Pyridylbenzimidazolyl) Benzene: Impact of Phosphine Ancillary Ligands on Electronic and Photophysical Properties of the Cu(I) Complexes. *Inorg. Chem.* **2006**, *45* (1), 147–155. https://doi.org/10.1021/ic051412h.

(119) Armaroli, N.; Accorsi, G.; Holler, M.; Moudam, O.; Nierengarten, J.-F.; Zhou, Z.; Wegh, R. T.; Welter, R. Highly Luminescent CuI Complexes for Light-Emitting Electrochemical Cells. *Adv. Mater.* **2006**, *18* (10), 1313–1316. https://doi.org/doi:10.1002/adma.200502365.

(120) Zhang, Q.; Zhou, Q.; Cheng, Y.; Wang, L.; Ma, D.; Jing, X.; Wang, F. Highly Efficient Green Phosphorescent Organic Light-Emitting Diodes Based on CuI Complexes. *Adv. Mater.* **2004**, *16* (5), 432–436. https://doi.org/doi:10.1002/adma.200306414.

Chapter 2

The Photochemistry of Cu(I)-Olefin Complexes: Lessons Learned

2.1 Introduction

The first example of Cu(I) catalysis in organic photochemistry was reported in 1967 by Srinivasan for the photolysis of 1,5-cyclooctadiene in the presence of Cu(I)Cl. X-ray studies determined the preferential formation of a dimeric Cu-olefin complex.[1] Following this seminal report, Cu(I) coordination has been used as a tether to pre-organize alkenes to undergo intramolecular 2+2 photocycloadditions (**Figure 2.1**). This approach has been utilized for the synthesis for various terpenoid natural products,[2–4] cubane like structures,[5–7] and caged structures.[8,9] Replacing the Cu(I) source for one with a weakly coordinating anion, such as

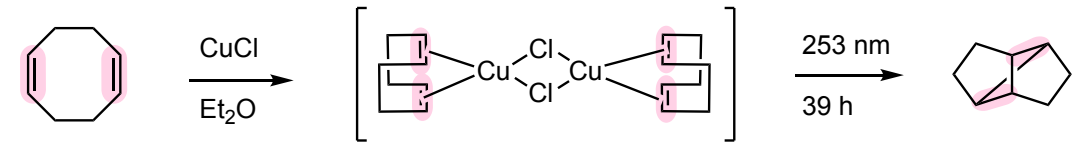

Srinivasan *J. Am. Chem. Soc.* **1964**, *86*, 3318

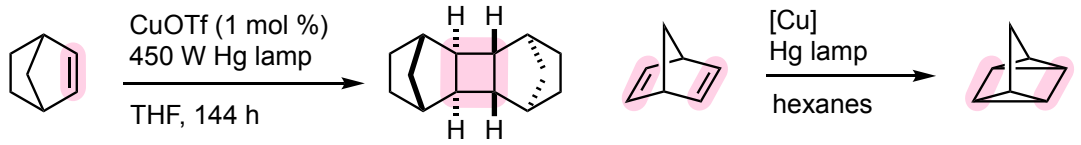

Kochi *Tet. Lett.* **1973**, *14*, 2529 *88% yield* Kutal *Adv. Chem. Ser.* **1978**, *168*, 158

Figure 2.1 Use of Cu(I) salts as catalysts for olefin dimerizations

triflate, appreciably increases the yield of these reactions, particularly for the intermolecular dimerization of cyclic olefins such as norbornene,[10] and has been utilized in the synthesis of ladderanes (**Figure 2.2**).[11] In contrast to the above-mentioned dimerization of norbornene, norbornadiene selectively undergoes

valence isomerization to quadricyclane in the presence of Cu(I) catalysts. This process has been shown to be insensitive to the identity of ligands coordinating to the metal center.

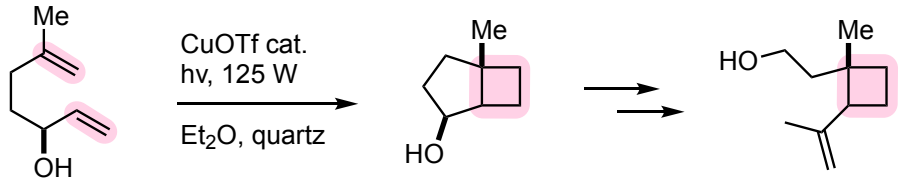

Mattay *J. Org. Chem.* **1995**, *60* (22), 7256–7266.

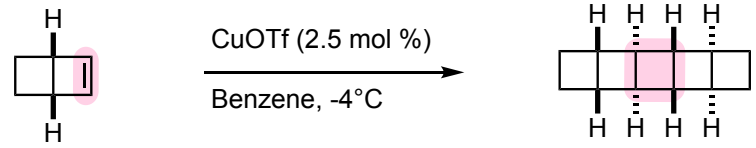

Burns, J. Am. Chem. Soc. 2016, 138, 15845 42% yield

Figure 2.2 Selected use of Cu(I) salts for the dimerization of simple alkenes in the total synthesis of natural products.

Initially, the mechanism for these reactions was not well understood and widely speculated on. Subsequent work supported the hypothesis of a Cu(I)-olefin complex readily forming in solution as evident by nuclear magnetic resonance (NMR) and infrared (IR) spectroscopy.[12,13] This complexation produces two strong electronic transitions in the UV region around 236 nm and 272 nm, neither of which are present in the absence of Cu(I).[14] The nature of these transitions was proposed to be a MLCT and a ligand to metal charge transfer (LMCT) respectively, however which excitation process lead to productive photochemistry/cycloaddition was unclear. It was not until Budzelar utilized the Hartree-Fock-Slater (HFS) method to unambiguously determine the lowest energy excitation is a Cu 3d – alkene π^* MLCT. This results in the formation of a formal Cu(II) atom with a localized metal-

carbon sigma-bond, producing a 1,3-biradical species.[15] This excited state can then combine with another olefin and ultimately cyclize to produce a cyclobutane (**Figure 2.3**). It is under these pretexts that attempts were made to expand on the

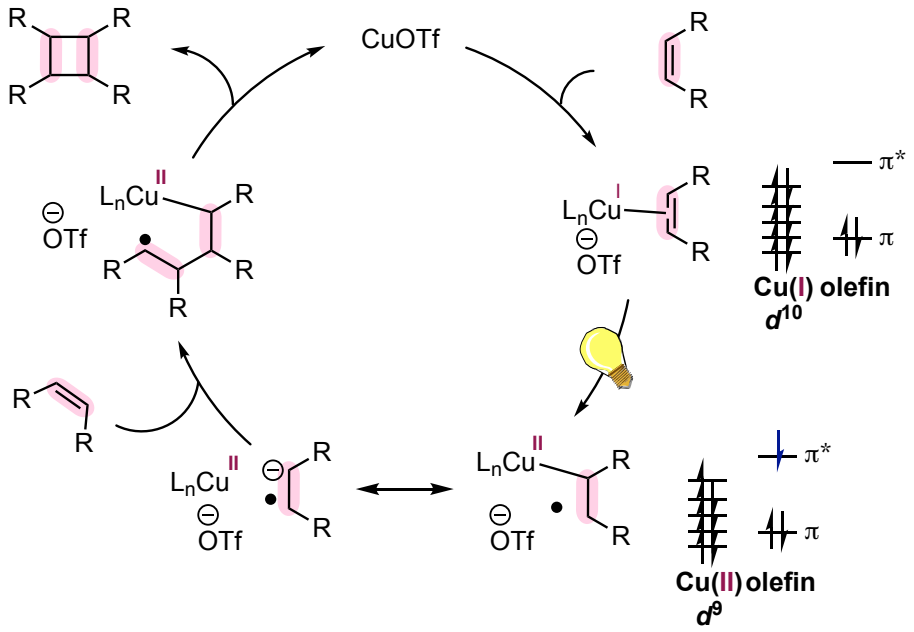

Figure 2.3 Mechanism for Cu(I) facilitating the 2+2 photocycloaddition of simple alkenes.

photochemical transformations facilitated by Cu(I) through use of an appropriate supporting ligand and control of the coordination environment to divert the alkyl radical to new modes of reactivity.

2.2 Efforts Toward an Intramolecular Alkene Trimerization

The diallylation of *cis*-2-butene-1,4-diol with allyl bromide provided substrate **1** in excellent yield on multigram scale. The atom tethering the alkenes together could be changed to S, $SiMe_2$, or N-*t*Bu through a slight modification of

the starting materials (**Figure 2.4**). Preparation of these substrates provided a small library for which attempts at an intramolecular trimerization were attempted.

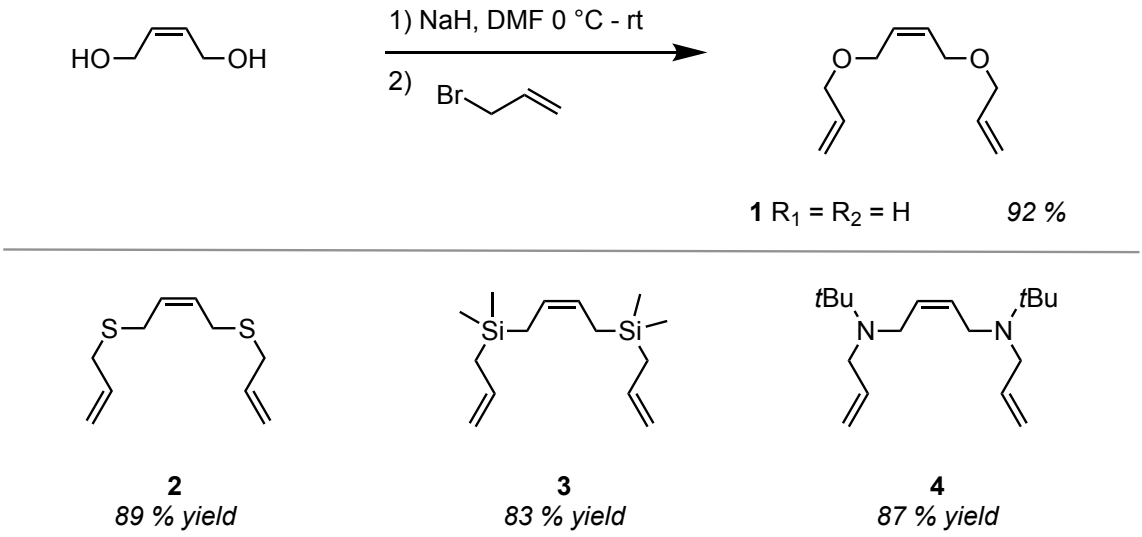

Figure 2.4 Synthesis of tri-ene substrates. For full synthetic procedures see Chapter 2.5 .

Our investigation began by irradiating an ethereal solution of **1** with 20 mol % CuBr with 8W UVC lights (**Figure 2.5**, entry 1). Even after prolonged reaction time the starting material was cleanly recovered with no detection of new products via ^{1}H-NMR or GC-MS. Altering the copper source to various Cu(I) salts with weakly coordinating anions had no effect on the reaction outcome (entries 2-8). Changing the irradiation source to a 36W UVC germicidal lamp resulted in the isomerization of the internal olefin. This result remained consistent regardless of the copper salt used (entries 9-15). Interestingly, irradiation with the germicidal lamp and using CuOTf resulted in the formation of cyclobutane **5** (entry 16). This inspired us to pursue the use of a weakly coordinating anion (WCA) developed by

the Krossing group however, this also resulted in the formation of compound **5** (entry 17).[16–18]

entry	deviation from standard conditions	reaction time (h)	outcome
1	None	36	no rxn
2	20 mol % $Cu(MeCN)_4OTf$	36	no rxn
3	20 mol % $Cu(MeCN)_4PF_6$	36	no rxn
4	20 mol % $Cu(MeCN)_4BF_4$	36	no rxn
5	20 mol % CuCl	36	no rxn
6	20 mol % CuI	36	no rxn
7	20 mol % $CuSbF_6$	36	no rxn
8	20 mol % CuOTf C_6H_6	36	no rxn
9	36 W UVC lamp, 20 mol % $Cu(MeCN)_4OTf$	36	**6,** >95*% yield*
10	36 W UVC lamp, 20 mol % $Cu(MeCN)_4PF_6$	36	**6,** >95*% yield*
11	36 W UVC lamp, 20 mol % $Cu(MeCN)_4BF_4$	36	**6,** >95*% yield*
12	36 W UVC lamp, 20 mol % $Cu(MeCN)_4BF_4$	36	**6,** >95*% yield*
13	36 W UVC lamp, 20 mol % CuCl	36	**6,** >95*% yield*
14	36 W UVC lamp, 20 mol % CuI	36	**6,** >95*% yield*
15	36 W UVC lamp, 20 mol % $CuSbF_6$	36	**6,** >95*% yield*
16	36 W UVC lamp, 20 mol % $(CuOTf)_2\,C_6H_6$	36	**5**,42*% yield*
17	20 mol % $Cu[Al(OC(CF_3)_3)_4]$	36	**5**, 31% yield

Figure 2.5 Reaction screening for the attempts at a [2+2+2] photocycloaddition of alkenes. No rxn = no reaction.

Taking the most successful reaction conditions and screening our library of substrates yielded varying outcomes. Oxygen tethered substrates resulted in analogous cyclobutane formation (**Figure 2.5**), while the sulfur and nitrogen analogs lead to isomerization of the internal alkene, and silicon containing substrates lead to decomposition.

It was postulated that only two of the olefins were coordinating to the metal center and thus preventing the desired [2+2+2] photocycloaddition to occur. To enforce coordination of all three alkenes attempts were made to prepare the macrocyclic substrate **12** but the desired cyclization was never observed to take

place. While unsuccessful in facilitating a [2+2+2] photocycloaddition of alkenes these results illustrate the importance of using a WCA the irradiation source.

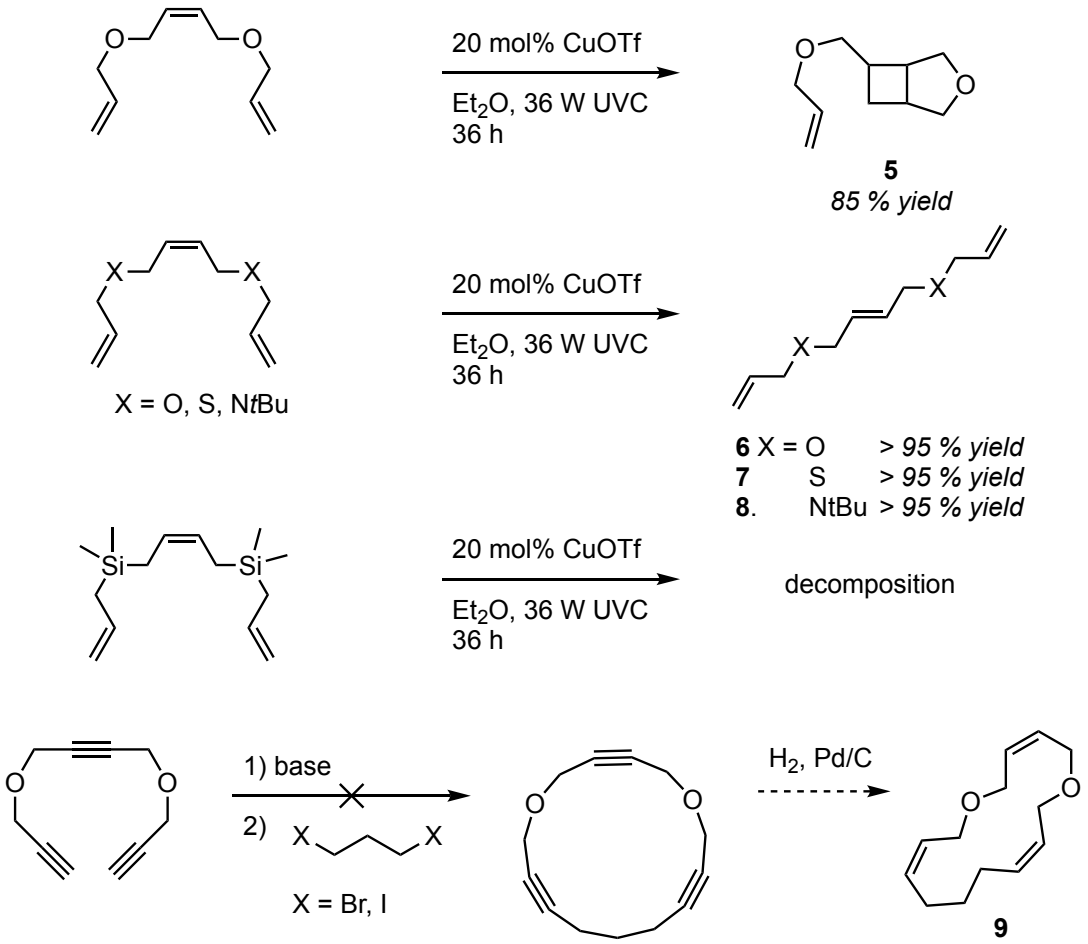

Figure 2.6 Reaction outcomes for the photochemical reactions of various tri-ene substrates. Attempts at the preparation of a cyclic triene substrate were unsuccessful.

We were also interested if changing the one of the alkenes to a carbonyl or imine would result in the analogous intramolecular 2+2 photocycloaddition. Unfortunately, this was not the case as using **10** or **11** resulted in no reaction of the starting material (**Figure 2.7**). It is clear this type of activation is unique to olefins.

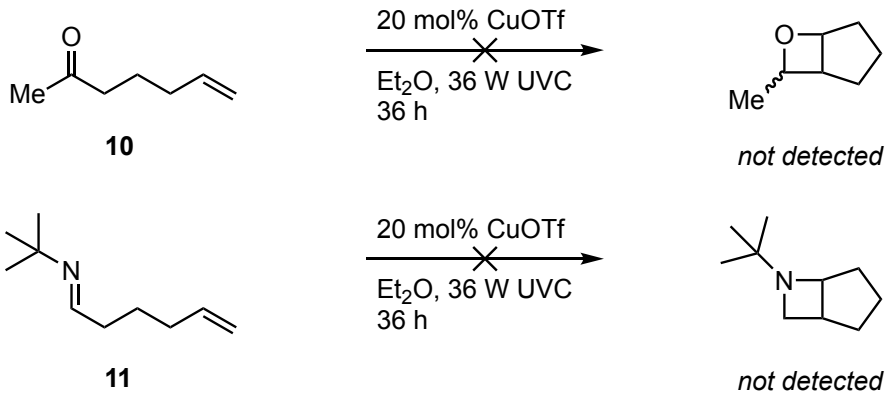

Figure 2.7 Attempts at using copper salts to facilitate the intramolecular photocycloaddition to produce an oxetane or azetidine.

2.3 Photochemistry of a-Imino Ester Copper complexes

With the previous observation that simple Cu salts could bring together two olefins in both an intra- and intermolecular reaction we sought to prepare a variety of Cu complexes with both of our substrates coordinated to the metal center. It was postulated that having the desired pi components precoordinated to the metal center would facilitate the desired photocycloaddition.

Condensation of various primary amines with ethyl glyoxylate provided a small library of a-imino esters (**Figure 2.8**). Attempts were made at coordinating these substrates to Cu with an additional olefin, but crystals suitable for single x-ray diffraction were not obtained. Photochemical reactions were carried out with the hypothesis that premixing the substrates and the Cu catalyst would pre-form the desired complex and irradiation would produce the desired cycloadduct.

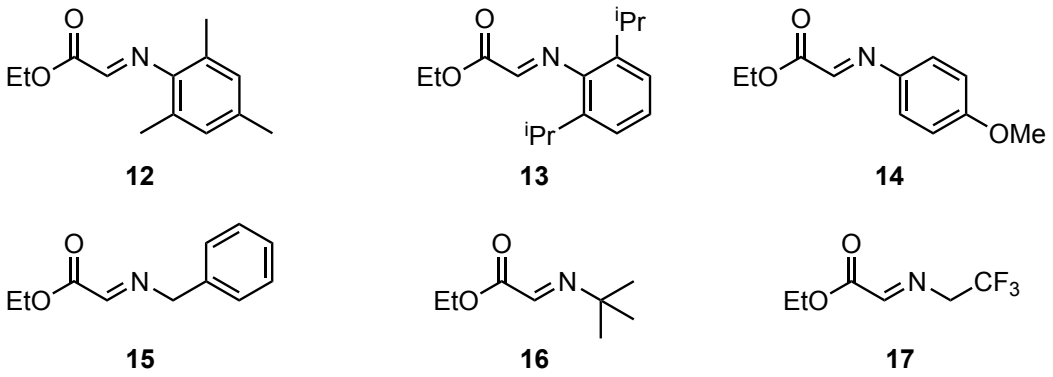

Figure 2.8 Library of α-imino ester comounds prepared

Altering the substituent on the imine did not result in any new species being detected by NMR or GC-MS (**Figure 2.9**, entries 1-6). Similarly, changing the steric or electronic properties of the alkene did not produce the desired cycloadduct (entries 7-10). Additionally, the source of Cu did not affect the reaction as starting material was cleanly recovered (entries 11-13). Changing the light source from the 32 W UVC germicidal lamp to a 13 W CFL did provide trace amounts of a new species being formed, however this result was not reproduceable and the product was not able to be isolated and fully characterized (entry 14).

It was possible that the carbonyl of the ester was not Lewis basic enough to coordinate to the metal center. Therefore, we changed our substrates to α-diimines or a-imino pyridines with the idea that the incorporation of a second nitrogen atom would facilitate better coordination. The same outcome of no reaction was routinely observed regardless of the alkene (**Figure 2.10**, entries 1-10), Cu salt (entries 11-13), or irradiation source (entries 14-15) used. Xantphos

was added in order to enforce the desired tetrahedral geometry at Cu, but again no reaction took place (entry 16).

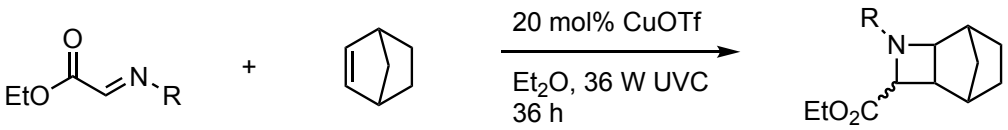

entry	deviation from standard conditions	outcome
1	**12**	no rxn
2	**13**	no rxn
3	**14**	no rxn
4	**15**	no rxn
5	**16**	no rxn
6	**17**	no rxn
7	**12**, *n*-butyl vinyl ether	no rxn
8	**12**, *tert*-butyl ethylene	no rxn
9	**12**, cyclohexene	no rxn
10	**12**, O-boc allyl alcohol	no rxn
11	**12**, CuBr	no rxn
12	**12**, CuI	no rxn
13	**12**, $Cu(MeCN)_4PF_6$	no rxn
14	**16**, 32 W UVC lamp	trace product

Figure 2.9 Reaction screening for the intermolecular 2+2 cycloaddition of α-imino esters with varying olefins.

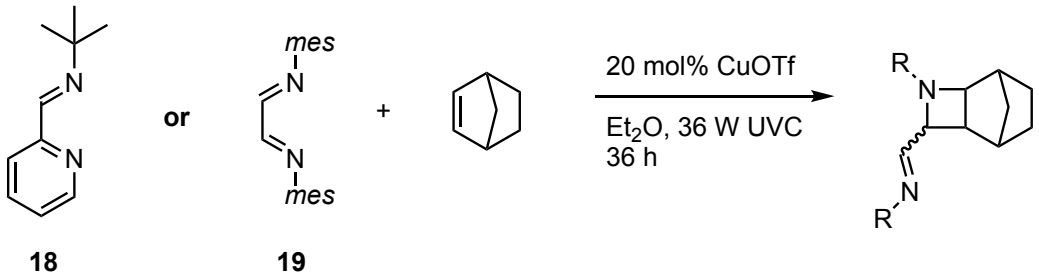

18 **19**

entry	deviation from standard conditions	outcome
1	**18**	no rxn
2	**18**, *n*-butyl vinyl ether	no rxn
3	**18**, cyclohexene	no rxn
4	**18**, *tert*-butyl ethylene	no rxn
5	**18**, O-boc allyl alcohol	no rxn
6	**19**, *n*-butyl vinyl ether	no rxn
7	**19**, cyclohexene	no rxn
8	**19**, *tert*-butyl ethylene	no rxn
9	**19**, O-boc allyl alcohol	no rxn
10	**19**, *n*-butyl vinyl ether	no rxn
11	**18**, CuBr	no rxn
12	**19**, CuI	no rxn
13	**18**, $Cu(MeCN)_4PF_6$	no rxn
14	**18**, 32 W UVC lamp	no rxn
15	**19**, 32 W UVC lamp	no rxn
16	**18**, Xantphos	no rxn

Figure 2.10 Reaction screening for the intermolecular 2+2 cycloaddition of α-diimes or α-imino pyridines with varying olefins.

2.4 Conclusions

Although these experiments did not yield the desired outcome they offer a great deal of insight into the system and various factors to consider when designing our experimental setup. It was evident that the wattage of the light source played an important factor as no reactivity was seen to occur with anything less than 32 W. Additionally, limiting deep UVC light (< 250 nm) is necessary as it can lead to

undesirable electronic transition and decomposition of the starting material. The importance of having a weakly coordinating anion, such as triflate, was crucial to seeing any reactivity of the starting material. Lastly, a tetrahedral geometry of the metal center should be enforced throughout the entire reaction.

2.5 Synthetic Procedures and Characterization Data

General Considerations. All air- and moisture-sensitive manipulations were carried out using standard high vacuum line, Schlenk or cannula techniques or in an M. Braun inert atmosphere drybox containing an atmosphere of purified nitrogen. Solvents for air- and moisture-sensitive manipulations were dried and deoxygenated using literature procedures.

^{1}H and ^{13}C NMR were recorded on Bruker 300 MHz or Varian 500 MHz spectrometers at 300 and 126 MHz, respectively. All chemical shifts are reported relative to $SiMe_4$ using ^{1}H (residual) chemical shifts of the solvent as a secondary standard. GC analyses were performed using an Agilent Technologies 7890B gas chromatograph equipped with an Agilent 7693 autosampler and Agilent HP-5 capillary column (30 m x 0.320mm x 250μm). Standard method parameters: 1.2 mL/min flow rate with oven program 80 – 250 °C with a ramp rate of 25 °C/min and hold time of 8.7 minutes at 250 °C. High-resolution mass spectra were measured using a Thermo LCQdeca APCI-MS.

Photochemical Reactions. Photochemical reactions were prepared in a dry nitrogen filled glovebox and were carried out with either 8 W UVA lamps in a modified light box or a 32 W germicidal lamp in fume hood. The light source was placed approximately 20 cm from the sample and the reaction mixture was stirred vigorously using a magnetic stir bar. All reactions were performed in quartz tubes that were capped and sealed with electrical tape.

Preparation of Substrates

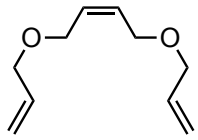

1 was synthesized by a known procedure. Physical and spectral data was in accordance with literature data.[19]

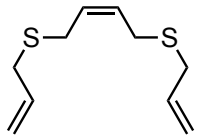

2 was synthesized by a known procedure. Physical and spectral data was in accordance with literature data. [20]

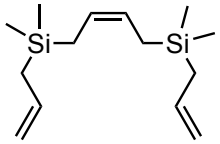

3 was synthesized by a known procedure. Physical and spectral data was in accordance with literature data.[21]

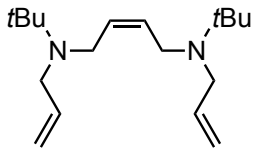

4 was synthesized by a known procedure. Physical and spectral data was in accordance with literature data.[22]

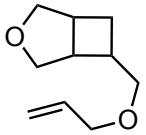

5 was synthesized by irradiation of **1** with a 32 W UVC germicidal lamp in the presence of CuOTf (20 mol%) in diethyl ether. Analytical data for **5**:

^{1}H-NMR (300 MHz; $CDCl_3$): δ 5.97-5.88 (m, 1H), 5.31-5.17 (m, 2H), 4.10 (d, *J* = 10.0 Hz, 1H), 4.00-3.95 (m, 3H), 3.74 (d, *J* = 9.1 Hz, 1H), 3.54-3.36 (m, 4H), 3.00-2.87 (m, 1H), 2.72-2.66 (m, 1H), 2.29-2.22 (m, 1H), 1.82 (m, 1H), 1.37-1.26 (m, 1H), 1.24-1.20 (m, 1H)

^{13}C-NMR (126 MHz; $CDCl_3$): δ 133.9, 117.1, 78.4, 76.9, 73.8, 72.5, 43.0, 40.1, 31.8, 28.1

HRMS (APCI-TOFMS) Calc. for $[C_{10}H_{16}O_2+H^+]^+$ = 169.1228, Found =169.1227

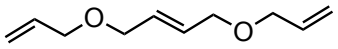

6 was synthesized from **1** by irradiation with a 32 W UVC germicidal lamp in the presence of CuOTf (20 mol%) in diethyl ether. Physical and spectral data was in accordance with literature data.[23]

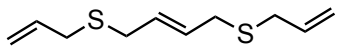

7 was synthesized from **2** by irradiation with a 32 W UVC germicidal lamp in the presence of CuOTf (20 mol%) in diethyl ether. Physical and spectral data was in accordance with literature data.[20]

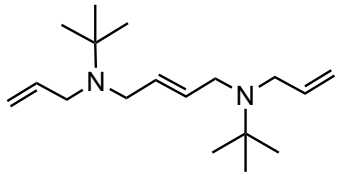

8 was synthesized from **4** by irradiation with a 32 W UVC germicidal lamp in the presence of CuOTf (20 mol%) in diethyl ether.. Physical and spectral data was in accordance with literature data. [21]

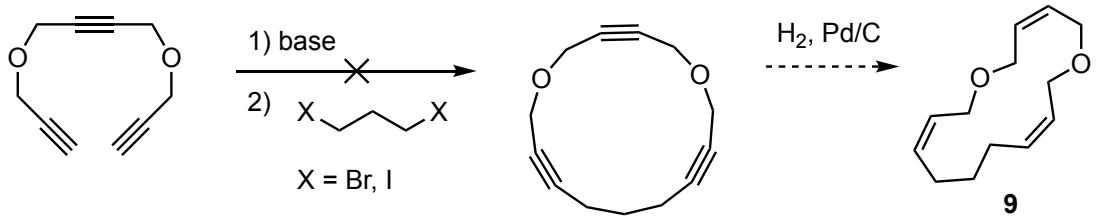

9 was planned to be made via the hydrogenation of the tri-yne macrocycle. The tri-yne was to be made via deprotonation and alkylation of the terminal alkynes, but desired cyclized product was never observed. Attempted reaction conditions can be seen below.

Temperature (°C)	Eq. nBuLi	Alkylating Agent	Solvent	Outcome
-78	2.2	2,3-dibromopropane	THF	No Rxn
-78	1.1	2,3-dibromopropane	THF	No Rxn
0	2.2	2,3-dibromopropane	THF	No Rxn
0	1.1	2,3-dibromopropane	THF	No Rxn
0	2.2	ICH_3	THF	Alkylation
-78	2.2	2,3-dibromopropane	THF	No Rxn
0	2.2	2,3-dibromopropane	THF	No Rxn
-78	2.2	2,3-dibromopropane	Ether	No Rxn

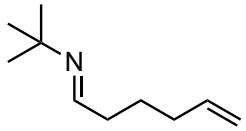

11 was synthesized by a known procedure. Physical and spectral data was in accordance with literature data.[24]

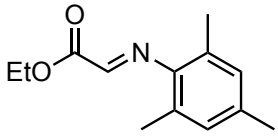

12 was synthesized by a known procedure. Physical and spectral data was in accordance with literature data.[25]

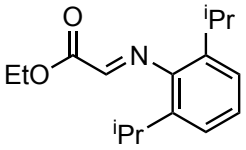

13 was synthesized by a known procedure. Physical and spectral data was in accordance with literature data.

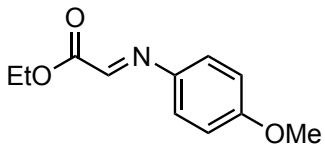

14 was synthesized by a known procedure. Physical and spectral data was in accordance with literature data.[26]

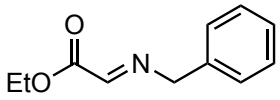

15 was synthesized by a known procedure. Physical and spectral data was in accordance with literature data.[26]

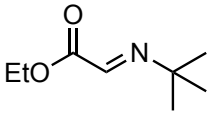

16 was synthesized by a known procedure. Physical and spectral data was in accordance with literature data.[27]

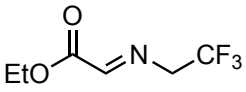

17 was synthesized by a known procedure. Physical and spectral data was in accordance with literature data.[28]

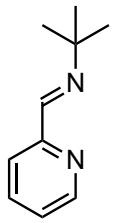

18 was synthesized by a known procedure. Physical and spectral data was in accordance with literature data.[29]

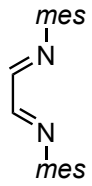

19 was synthesized by a known procedure. Physical and spectral data was in accordance with literature data.[30]

2.6 References

(1) Srinivasan, R. Photochemical Transformations of 1,5-Cyclooctadiene. *J. Am. Chem. Soc.* **1964**, *86* (16), 3318–3321. https://doi.org/10.1021/ja01070a023.

(2) Barbero, A.; García, C.; Pulido, F. J. Allylsilane-Vinylcopper Reagents: Palladium-Mediated Coupling with Alkenyl Halides. Synthesis and Photochemical [2+2] Cyclization of (±)-Ipsdienol. *Synlett* **2001**, No. 6, 824–826. https://doi.org/10.1055/s-2001-14589.

(3) Langer, K.; Mattay, J. Stereoselective Intramolecular Copper(I)-Catalyzed [2 + 2]-Photocycloadditions. Enantioselective Synthesis of (+)- and (-)-Grandiso. *J. Org. Chem.* **1995**, *60* (22), 7256–7266. https://doi.org/10.1021/jo00127a034.

(4) Panda, J.; Ghosh, S. Intramolecular [2+2] Photocycloaddition for the Direct Stereoselective Synthesis of Cyclobutane Fused γ-Lactols. *Tetrahedron Lett.* **1999**, *40* (36), 6693–6694. https://doi.org/10.1016/S0040-4039(99)01379-9.

(5) Chou, T. C.; Yeh, Y. L.; Lin, G. H. A Fragmentation-Photocyclization Approach towards Homosecohexaprismane Skeleton. *Tetrahedron Lett.* **1996**, *37* (48), 8779–8782. https://doi.org/10.1016/S0040-4039(96)02030-8.

(6) 川筋道雄; 寺中正昭; 般木芳則; 大平政人; 細川治; 三崎拓郎; 岩喬. 5. 小児発作性心房性頻拍症に対する高周波誘導型ペースメーカー植え込み(第 6 回日本小児外科学会北陸地方会). *J. Japanese Soc. Pediatr. Surg.* **1978**, *14* (3), 478. https://doi.org/10.11164/jjsps.14.3_478_1.

(7) Brand Organisch-Chemisches Institut Der Universitat Neidelberg, Fm Neuenheimer. **1994**, *35* (28).

(8) Fischer, J. W.; Hollins, R. A.; Lowe-Ma, C. K.; Nissan, R. A.; Chapman, R. D. Synthesis and Characterization of 1,2,3,4-Cyclobutanetetranitramine Derivatives. *J. Org. Chem.* **1996**, *61* (26), 9340–9343. https://doi.org/10.1021/jo9613040.

(9) Chebolu, R.; Zhang, W.; Galoppini, E.; Gilardi, R. Copper(I)-Catalyzed Intramolecular Photocycloadditions of Dicyclopentadiene Derivatives Linked by Removable Tethers. *Tetrahedron Lett.* **2000**, *41* (16), 2831–2834. https://doi.org/10.1016/S0040-4039(00)00273-2.

(10) Salomon, R. G.; Kochi, J. K. Copper(I) Catalysis in Photocycloadditions. I. **1973**, *81* (1), 1137–1144.

(11) Mercer, J. A. M.; Cohen, C. M.; Shuken, S. R.; Wagner, A. M.; Smith, M. W.; Moss, F. R.; Smith, M. D.; Vahala, R.; Gonzalez-Martinez, A.; Boxer, S. G.; et al. Chemical Synthesis and Self-Assembly of a Ladderane Phospholipid. *J. Am. Chem. Soc.* **2016**, *138* (49), 15845–15848. https://doi.org/10.1021/jacs.6b10706.

(12) Solomon, R. G.; Kochi, J. K. Cationic Benzene and Olefin Complexes of Copper(I) Trifluoromethanesulphonate. *J. Chem. Soc. Chem. Commun.* **1972**, *0* (9), 559–560. https://doi.org/10.1039/C39720000559.

(13) Salomon, R. G.; Kochi, J. K. Cationic Olefin Complexes of Copper(I). Structure and Bonding in Group Ib Metal-Olefin Complexes. *J. Am. Chem. Soc.* **1973**, *95* (6), 1889–1897. https://doi.org/10.1021/ja00787a031.

(14) Salomon, R. G. Homogeneous Metal-Catalysis in Organic Photochemistry. *Tetrahedron* **1983**, *39* (4), 485–575. https://doi.org/10.1016/S0040-4020(01)91830-7.

(15) Budzellar, P. H. M.; Timmermans, P. J. J. A.; Mackor, A.; Baerends, E. J. Bonding in the Ground State and Excited States of Copper-Alkene Complexes. *J. Organomet. Chem.* **1987**, *331* (3), 397–407. https://doi.org/10.1016/0022-328X(87)80011-6.

(16) Santiso-quiñones, G.; Reisinger, A.; Slattery, J.; Krossing, I. Homoleptic Cu-Phosphorus and Cu-Ethene Complexes . **2007**, No. c.

(17) Krossing, I. The Facile Preparation of Weakly Coordinating Anions: Structure and Characterisation of Silverpolyfluoroalkoxyaluminates AgAl(ORF)4, Calculation of the Alkoxide Ion Affinity. *Chem. - A Eur. J.* **2001**, *7* (2), 490–502. https://doi.org/10.1002/1521-3765(20010119)7:2<490::AID-CHEM490>3.0.CO;2-I.

(18) Krossing, I.; Bihlmeier, A.; Raabe, I.; Trapp, N. Structure and Characterization of CI3+[Al{OC(CF3)3}4]−; Lewis Acidities of CX3+ and BX3. *Angew. Chemie Int. Ed.* **2003**, *42* (13), 1531–1534. https://doi.org/10.1002/anie.200250172.

(19) Ding, L.; Xie, M.; Yang, D.; Song, C. Efficient Synthesis of Long-Chain Highly Branched Polymers via One-Pot Tandem Ring-Opening Metathesis Polymerization and Acyclic Diene Metathesis Polymerization. *Macromolecules* **2010**, *43* (24), 10336–10342. https://doi.org/10.1021/ma1020903.

(20) Zhong, C.; Wang, Y.; Hung, A. W.; Schreiber, S. L.; Young, D. W. Diastereoselective Control of Intramolecular Aza-Michael Reactions Using Achiral Catalysts. *Org. Lett.* **2011**, *13* (20), 5556–5559. https://doi.org/10.1021/ol202276h.

(21) Richter, W. J.; Neugebauer, B. Synthesis of Trans-1,4-Bis[Dimethylorganylsilyl]-2-Butenes. *Synthesis (Stuttg).* **1985**, *1985* (11), 1059–1060. https://doi.org/10.1055/s-1985-31428.

(22) Clayden, J.; Watson, D. W.; Helliwell, M.; Chambers, M. β-Lactams or γ-Lactams by 4-Exo-Trig or 5-Endo-Trig Anionic Cyclisation of Lithiated Acrylamide Derivatives. *Chem. Commun.* **2003**, No. 20, 2582–2583. https://doi.org/10.1039/B308029C.

(23) Jayaprakash, S. H.; Krishna, B. S.; Prasad, S. S.; Sudha, S. S.; Reddy, C. S. Sodium Perborate: A Facile Catalyst for Allylation of Active Centers. *Synth. Commun.* **2015**, *45* (3), 355–362.

https://doi.org/10.1080/00397911.2014.963874.

(24) Harrington, P. E.; Tius, M. A. A Formal Total Synthesis of Roseophilin: Cyclopentannelation Approach to the Macrocyclic Core. *Org. Lett.* **1999**, *1* (4), 649–652. https://doi.org/10.1021/ol990124k.

(25) Garrido-Castro, A. F.; Gini, A.; Maestro, M. C.; Alemán, J. Unlocking the Direct Photocatalytic Difluoromethylation of C□N Bonds. *Chem. Commun.* **2020**, *56* (26), 3769–3772. https://doi.org/10.1039/D0CC01353F.

(26) Žabka, M.; Kocian, A.; Bilka, S.; Andrejčák, S.; Šebesta, R. Transformation of Racemic Azlactones into Enantioenriched Dihydropyrroles and Lactones Enabled by Hydrogen-Bond Organocatalysis. *European J. Org. Chem.* **2019**, *2019* (35), 6077–6087. https://doi.org/10.1002/ejoc.201901052.

(27) Peng, X.; Zhu, Y.; Ramirez, T. A.; Zhao, B.; Shi, Y. New Reactivity of Oxaziridine: Pd(II)-Catalyzed Aromatic C–H Ethoxycarbonylation via C–C Bond Cleavage. *Org. Lett.* **2011**, *13* (19), 5244–5247. https://doi.org/10.1021/ol2021252.

(28) Ponce, A.; Alonso, I.; Adrio, J.; Carretero, J. C. Stereoselective Ag-Catalyzed 1,3-Dipolar Cycloaddition of Activated Trifluoromethyl-Substituted Azomethine Ylides. *Chem. – A Eur. J.* **2016**, *22* (14), 4952–4959. https://doi.org/10.1002/chem.201504869.

(29) Su, B.; Bunescu, A.; Qiu, Y.; Zuend, S. J.; Ernst, M.; Hartwig, J. F. Palladium-Catalyzed Oxidation of β-C(Sp3)–H Bonds of Primary Alkylamines through a Rare Four-Membered Palladacycle Intermediate. *J. Am. Chem. Soc.* **2020**, *142* (17), 7912–7919. https://doi.org/10.1021/jacs.0c01629.

(30) Papadaki, E.; Magrioti, V. Synthesis of Pentafluorobenzene-Based NHC Adducts and Their Catalytic Activity in the Microwave-Assisted Reactions of Aldehydes. *Tetrahedron Lett.* **2020**, *61* (4), 151419. https://doi.org/https://doi.org/10.1016/j.tetlet.2019.151419.

Chapter 3

Intermolecular 2+2 Carbonyl-Olefin Photocycloadditions Enabled by a Cu(I)-Norbornene MLCT

3.1 Introduction

Oxetanes are four membered heterocycles containing an oxygen atom[1]. Although less common than their 3, 5, and 6 membered analogs oxetanes are valuable synthetic intermediates[2,3], bioisosteres in medicinal chemistry[4], and are prevalent in numerous biologically active molecules.[5–10] At first glance it is reasonable to assume these cyclic ethers are less common due to the inherent ring strain they possess; however, this instability is comparable to readily accessible epoxides (**Figure 3.1**).[11] Despite these facts, there is a dearth of practical synthetic methodologies for the construction of oxetanes.

Traditional methods for the synthesis of oxetanes relies heavily on intramolecular S_N2 type chemistry. This can be synthetically challenging due to the inherent ring strain making the kinetics of cyclization slow, necessitating anionic nucleophiles and good leaving groups to be utilized. These constraints limit the scope and functional group compatibility of such transformations, while also generating stoichiometric waste.

Alternatively, oxetanes can be synthesized through a [2+2] photochemical cycloaddition of a C=O double bond and a C=C double bond, known as the Paternò-Büchi reaction.[12,13] Despite being a named reaction the utility of this atom economical approach for the synthesis of oxetanes is hindered due to various drawbacks. Mechanistically this reaction proceeds via the photoexcitation of a

carbonyl to the singlet excited state followed by inter-system-crossing (ISC) to the excited triplet state.[14] Subsequent nucleophilic attack of the alkene towards the carbonyl half-filled n-orbital forms a new C-O bond first and generates a 1,4-biradical.[15,16] Upon ISC back to the singlet state and radical recombination the corresponding oxetane is produced (**Figure 3.2 A**). Reaction of the singlet state carbonyl is known however, it is far less common and mechanistically more complex.[12]

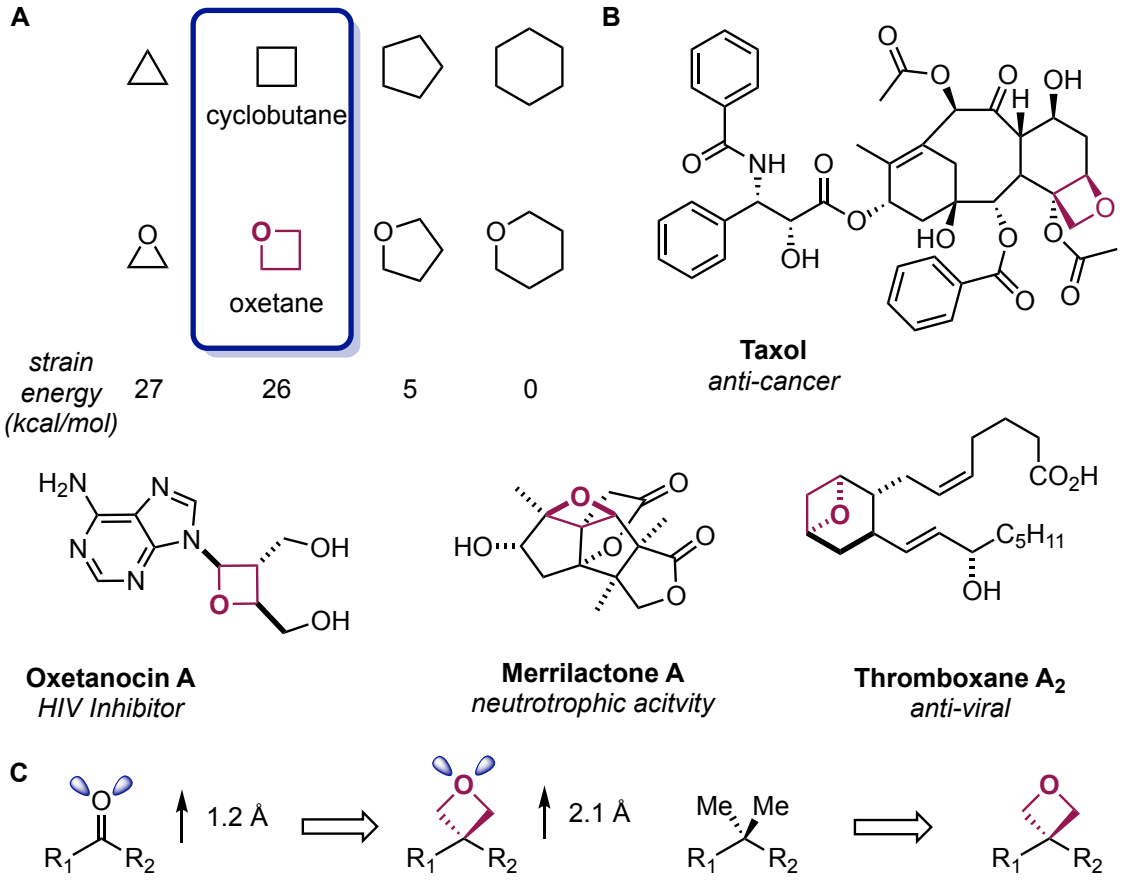

Figure 3.1 A. Relative ring strain between cyclic hydrocarbons and cylcic ethers. **B.** Notable biologically active compounds that contain an oxetane. **C**. Utility of oxetanes as replacement groups for carbonyls and gem-dimethyl groups.

The mechanistic requirement for direct excitation limits the scope of carbonyl compounds to those that can access an n-π^* singlet or triplet state. Due to their high lying n-π^* transitions esters, amides, and carboxylic acids rarely partake in a Paternò-Büchi reaction. Aryl ketones and aldehydes are the prototypical carbonyl partners for this transformation, while their aliphatic counterparts are more challenging to engage due to competing Norrish fragmentation pathways. With respect to the alkene electron rich, electron poor, and unactivated olefins work as addition partners, although yields can vary significantly.[10,17–19] Increasing the scope of this transformation to include alkyl ketones and unactivated olefins would greatly expand the chemical space available to synthetic chemists. Catalyst controlled approaches to address this issue have not been widely developed.

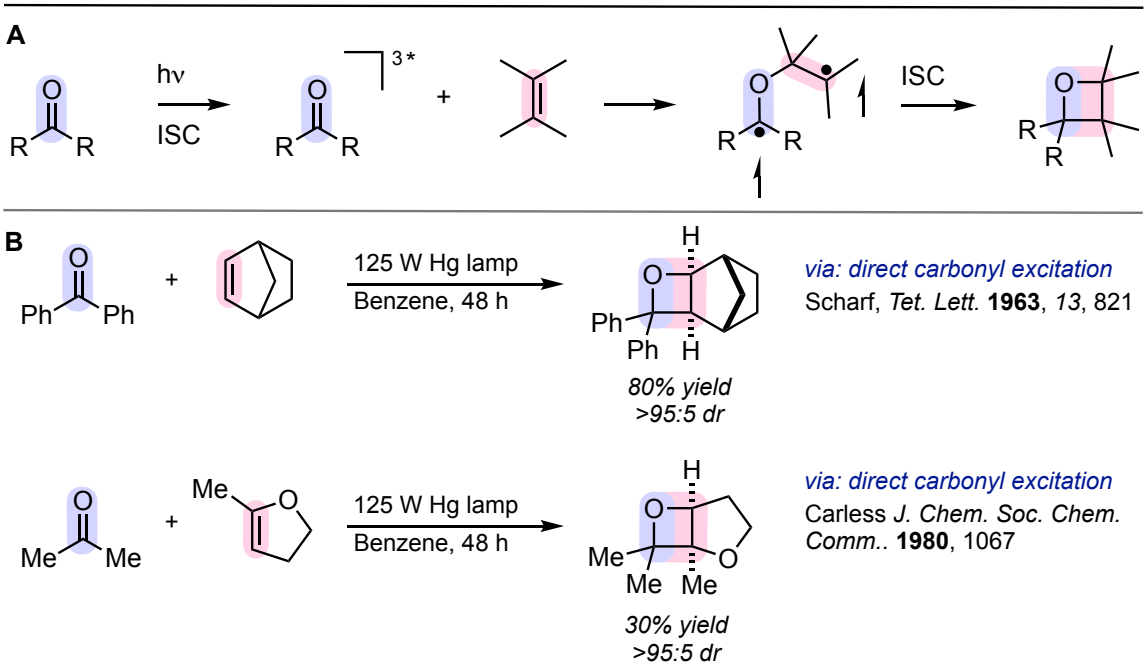

Figure 3.2 A. General mechanism for the Paternò-Büchi reaction. **B**. Selected examples of the Paterno Buchi reaction proceeding through direct carbonyl excitation.

The ability of polypyridyl Rh and Ir transition metal compounds to undergo metal to ligand charge transfer (MLCT) upon irradiation is the fundamental photophysical property that spurred the field of photoredox catalysis.[20,21] The coordination environment, manipulation of oxidation states, and electronic excitation of these complexes were design features selected to promote MLCT and generate relatively long-lived excited states capable of intermolecular electron or energy transfer.[22,23] Within photoredox catalysis radical-type reactivity occurring at the highly conjugated ligands is rare. Instead the excited states of these complexes have been used as excellent single electron donors or acceptors, as well as photosensitizers (see Chapter 1). However, recent examples have emerged where the active species that undergoes excitation is a substrate-metal complex.[24–28] We anticipated that upending many of the properties that make photoredox catalysts successful could unlock the potential for new mechanistic pathways featuring MLCT and access new reactivity modes.

Makor and Kochi were among the first to report that catalytic copper(I) triflate significantly improved the efficiency of simple alkene photodimerizations via excitation of an in situ formed Cu(I)-olefin complex.[29–34] These examples required prolonged reaction times (~days) and high wattage (450 W) immersion-well photoreactor setups to achieve even moderate reaction efficiencies. Salomon and co-workers initially proposed that excitation of an in situ formed Cu(I)-olefin complex resulted in a charge transfer event between the metal center and the

alkene ligand leading to cyclobutane formation.[34] Budzelaar and coworkers later computationally confirmed that the directionality of the charge transfer event was metal (Cu) to ligand (olefin) (MLCT).[32] Analogously, the valence isomerization of norbornadiene to quadricyclane was reported using a range of pre-catalysts including Cu(I)-halides[35,36] and other Cu(I) compounds bearing neutral mono- and bi-dentate phosphines[26,37–40], mono-anionic oxoquinolinato[41] and tris(pyrazolyl)borate[42] chelates. Spectroscopic studies by Kutal and coworkers also confirmed that Cu(I) mediated norbornadiene to quadricyclane valence isomerization occurred by excitation of an in situ generated Cu-η^2-norbornadiene complex and proceeds via a MLCT.[42]

It was envisioned that with an appropriate supporting ligand, excitation of a Cu(I)-olefin compound in the presence of a carbonyl could form an oxetane – inverting the conventional 2+2 photocycloadditive oxetane forming pathway of the Paternò-Büchi reaction. By activation of a metal-olefin complex rather than direct excitation of either substrate, this approach could alter the reactivity of the excited state and allow a more diverse range of carbonyls to participate in 2+2 carbonyl-olefin photocycloadditions (2+2 COPC). We selected tris(pyrazolyl)borate (Tp)[43] for our investigations as we anticipated that the monoanionic state could mimic the electronic influences of the weakly coordinating triflate anion commonly used, and the tridentate facial coordination mode could simultaneously allow for olefin coordination[23] and inhibit non-productive quenching via flattening (see Chapter 1).[44–46]

3.2 Reaction Screening and Optimization

Irradiation of a 1:3 mixture of methyl isobutyl ketone and norbornene in the presence of 10 mol % hydrotris(pyrazolyl)borate copper(I) (**TpCu**) in diethyl ether with a 100 W Hg lamp for 12 h resulted in 49% yield of oxetane **1** as a 55:45 mixture of diastereomers at C2 with exclusive *cis-exo* disposition at the ring junction (see below). In the absence of **TpCu** or light **1** was not detected (entries 2 and 3). Omission of either the ketone, alkene, or copper(I) source did not result in any productive chemistry with the starting materials cleanly recovered (entries 4-6). Exclusion of a Tp source and using only CuOTf results in the formation of **1** in 13% yield and 11% yield of norbornene dimer (entry 7). In place of using preformed **TpCu**, it can be made in-situ by equimolar mixing of CuOTf and KTp but results in diminished efficiency (31 vs 49% yield, entry 8 vs 1). Switching the reaction vessel from a borosilicate culture tube to a quartz test tube led to the formation of **1** in 16% yield (entry 9). Solvent screening was conducted, and diethyl ether was found be optimal with other common organic solvents leading to lower yields or incomplete conversion after 12 h of irradiation (entries 10-14).

Decreasing the loading of **TpCu** led to prolonged reaction times and lower yielding reactions (entries 15 and 16). Increasing the **TpCu** content past 20 mol % had little improvement on the yield likely due to solubility issues at these higher concentrations (entries 17 and 18). Varying the equivalents of norbornene past 3 equivalents had a marginal increase on the reaction yield (entries 19-21). Making norbornene the limiting reagent and having the carbonyl in excess led to significant

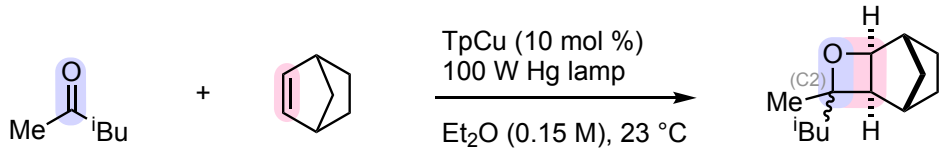

1

entry	deviation from standard conditions	reaction time (h)	yield of 1
1	None	12	z49%
2	No **TpCu**	12	*n.d.*
3	No light	12	*n.d.*
4	No carbonyl	12	*n.d.*
5	No norbornene	12	*n.d.*
6	No Cu source, KTp	12	*n.d.*
7	No Tp source, CuOTf	12	13% + 11% NBD
8	CuOTf +KTp (10 mol % each)	12	31%
9	Quartz test tube	12	16%
10	Tetrahydrofuran solvent	12	35%
11	Dichloromethane solvent	12	*n.d.*
12	Toluene solvent	12	52% conv.
13	Benzene solvent	12	50% conv.
14	Pentane solvent	12	*n.d.*
15	2.5 mol % **TpCu**	48	21%
16	5 mol % **TpCu**	24	36%
17	20 mol % **TpCu**	12	56%
18	40 mol % **TpCu**	12	59%
19	1 equiv. Norbornene	36	33%
20	2 equiv. Norbornene	24	42%
21	5 equiv. Norbornene	12	56%
22	1.1 equiv ketone (+ 1 equiv norbornene)	36	32%
23	3 equiv ketone (+ 1 equiv norbornene)	12	<10%
24	5 equiv ketone (+ 1 equiv norbornene)	12	*n.d.*
25	0.01 M	48	<10%
26	0.05 M	36	21%
27	0.30 M	24	35%
28	0.50 M	60	24%
29	$Cu(OTf)_2$ + KTp (10 mol% each)	12	<10%
30	AgOTf + KTp (10 mol% each)	12	n.d.
31	$Zn(OTf)_2$ + KTp (10 mol% each)	12	n.d.
32	$Sc(OTf)_3$ + KTp(10 mol% each)	12	n.d.
33	1 mol% Triflic acid	12	n.d.

Figure 3.3 2+2 COPC reaction optimization. n.d. = not detected.

inhibition of productive chemistry (entries 22-24). Altering the concentration with respect to the limiting reagent drastically diminishes the yield of the reaction and

requires prolonged irradiation (entries 25-28). Combing $Cu(OTf)_2$ and KTp in an equimolar ratio produced the desired product in only 15% yield (entry 30). Substituting $Cu(OTf)_2$ with various triflate salts or triflic acid did not lead to product formation (entries 30-33).

Throughout these optimizations a deep blue coloring of the products was routinely observed. Recrystallization via slow evaporation provided single crystals suitable for X-ray diffraction identifying bis(hydrotris(pyrazolyl)borate) copper(II) as the source of the discoloration. This NMR silent byproduct results from the degradation of **TpCu** when exposed to molecular oxygen. Removal of this material necessitated purification via silica gel chromatography. The requirement for chromatography resulted in the degradation of oxetane products and isolated yields being lower than the calculated NMR yields.

3.3 Scope of 2+2 COPC Reactivity

Various alkyl ketones were investigated using this copper catalyzed 2+2 COPC conditions. Irradiation of acetone, a common organic photosensitizer, reacted with norbornene to form oxetane **2** in 51% yield. 5-Hexen-2-one, which contains a terminal alkene, was converted to **3** in 45% yield as a 55:45 mixture of diastereomers at C2 (**Figure 3.4**). No intra- or intermolecular reactivity was observed as a result of the α-olefin. Cyclic ketones proved to be outstanding carbonyl substrates generating oxetanes **4-10** in good to excellent yields and in each case, exclusively as the cis-exo diastereomers (assigned by analogy to

compound **2**). These examples showcase the tolerance of acid sensitive acetal, ether, basic tertiary amine, and thioether functionality during 2+2 COPC.

Assorted other aliphatic ketones and aldehydes were screened with oxetane formation observed via GC-MS and NMR spectroscopy. Particularly noteworthy was the ability of paraformaldehyde to be converted to the corresponding oxetane in 22% NMR yield. However, product isolation and full characterization proved to be challenging. Attempts at purification by chromatography on acidic silica gel, neutral silica gel or basic alumina resulted in

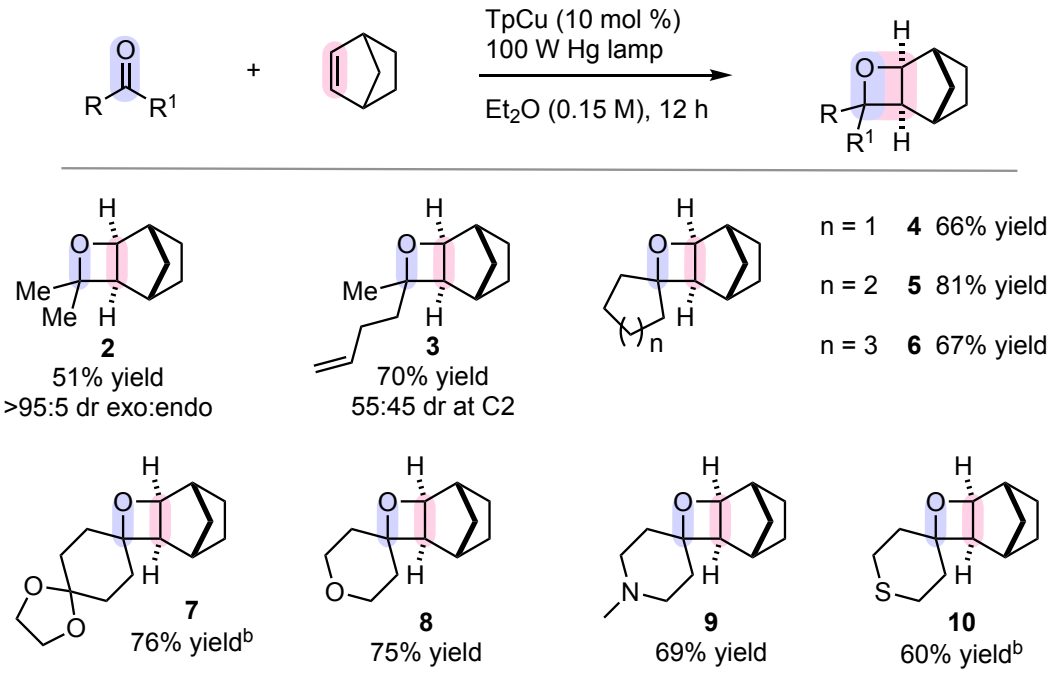

Figure 3.4 [a]Yields determined by ^{1}H NMR of crude reaction mixtures using durene as an internal standard; diastereomeric ratios were determined via ^{1}H NMR of the crude reaction mixtures with the structure of the major diastereomer show. [b]Isolated yields following purification via silica gel chromatography

significant degradation of material as observed by NMR. Performing this

purification under a nitrogen atmosphere or with cold solvents did not prevent the destruction of the oxetane products.

Oxetane formation was not detected in substrates containing 1,3-dicarbonyl functionalities. This is likely due to tautomers being present which preferentially coordinate to **TpCu** over norbornene and shunting productive photochemistry. The introduction of additional chromophores, such as aryl groups, significantly inhibited oxetane formation likely due to the high extinction coefficients they possess. Additionally, other carbonyl units such as esters, amides, and $\alpha-\beta$ unsaturated ketones remained unreacted under these conditions[47].

Aryl ketones such as benzophenone, are prototypical carbonyls in Paternò-Büchi reactions. When subjected to our standard conditions, benzophenone produced benzopinacol formation in 42% yield without detection of the corresponding oxetane. A control experiment without added **TpCu** resulted in similar reaction efficiency and selectivity for ketone dimerization (see Chapter 3.4.1 for further discussion).

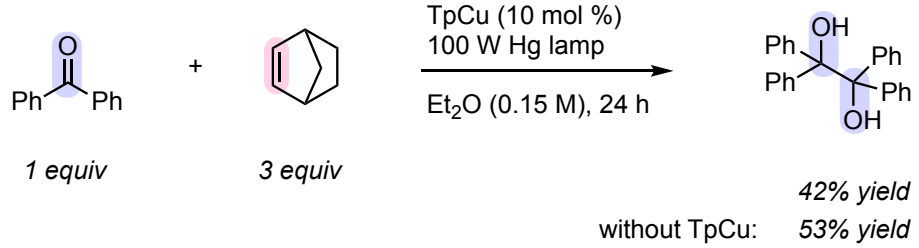

Figure 3.5 [a]Yields determined by ^{1}H NMR of crude reaction mixtures using durene as an internal standard

With respect to the olefin this reactivity remained unique to norbornene. A wide range of simple olefins were screened under the optimized conditions (**Figure**

3.6). Altering the alkene to being electron rich, electron deficient, or unactivated alkenes did not affect reactivity as no oxetane formation was observed. Sterics similarly did not have an impact on an alkenes ability to produce the desired oxetane. Functionalized norbornenes displayed trace oxetane formation (<10 % yield) when reacted with methyl isobutyl ketone. The reason for this limited reactivity will be discussed in the following section (section **3.4.2**).

The relative stereochemistry of the oxetane products was determined through a series of two-dimensional NMR experiments for compound **2**. Chemical shifts and integrations identify protons A, H, and G. Proton A is bonded to the carbon at 80 ppm. The lack of any signals by HSQC for the carbon at 83.5 ppm suggest this is the quaternary carbon. Strong HMBC correlation between protons G and H with ^{13}C at 50 ppm suggests this carbon is part of the oxetane, and is bonded to proton F. COSY cross peak of A confirms the identity of F. Proton F should only couple with A, and not E, due to the torsional angle of ~90°. The nOe between G and I_1, and absence of cross peaks between G and I_2 suggests exo ring configuration. Literature precedent also agrees I_1 is oriented towards the oxetane ring.

Ketones

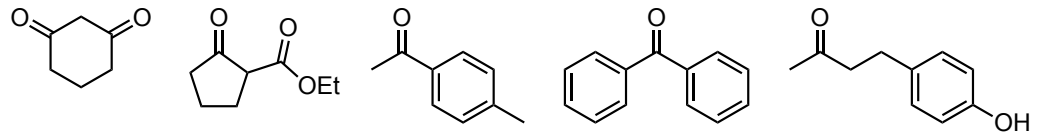

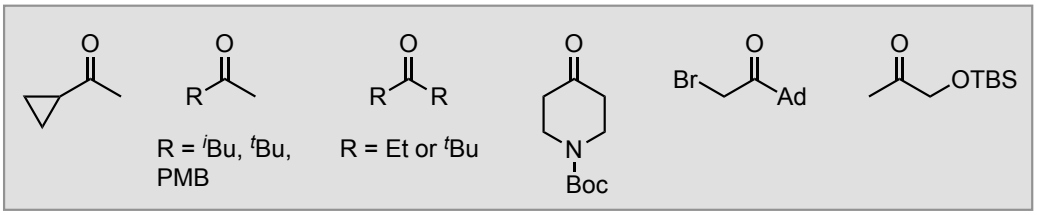

Aldehydes

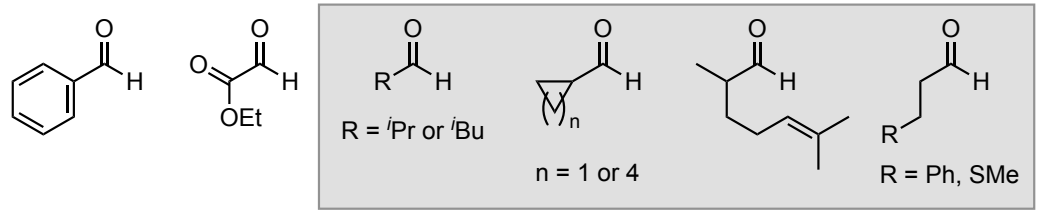

Other carbonyls

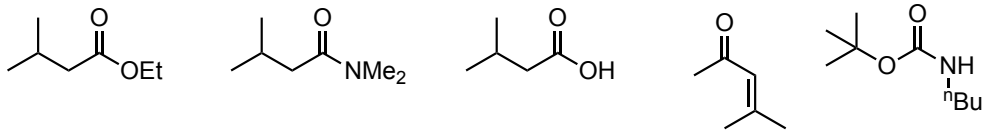

Olefines

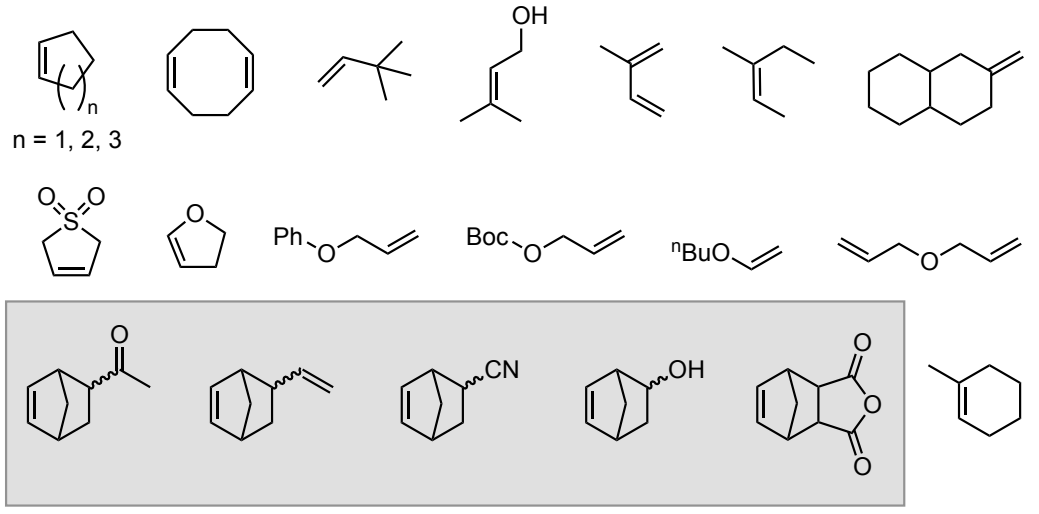

Figure 3.6 Unsuccessful substrates screened in the 2+2 COPC optimized conditions. Compounds in grey showed product formation as observed via ^{1}H NMR and GC-MS, but were unable to be isolate as pure material.

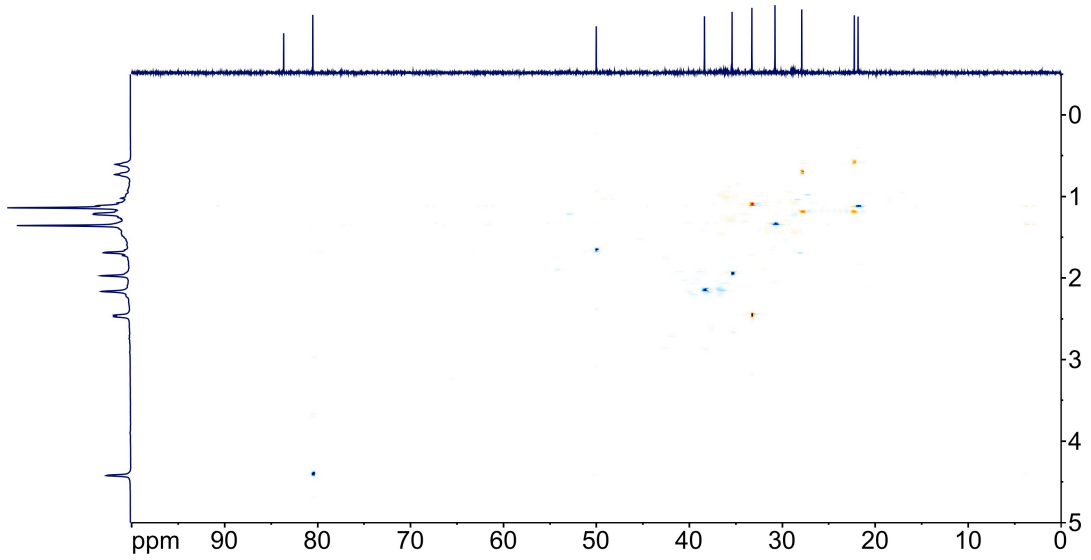

Figure 3.7 ^{1}H-^{13}C HSQC of compound **2**

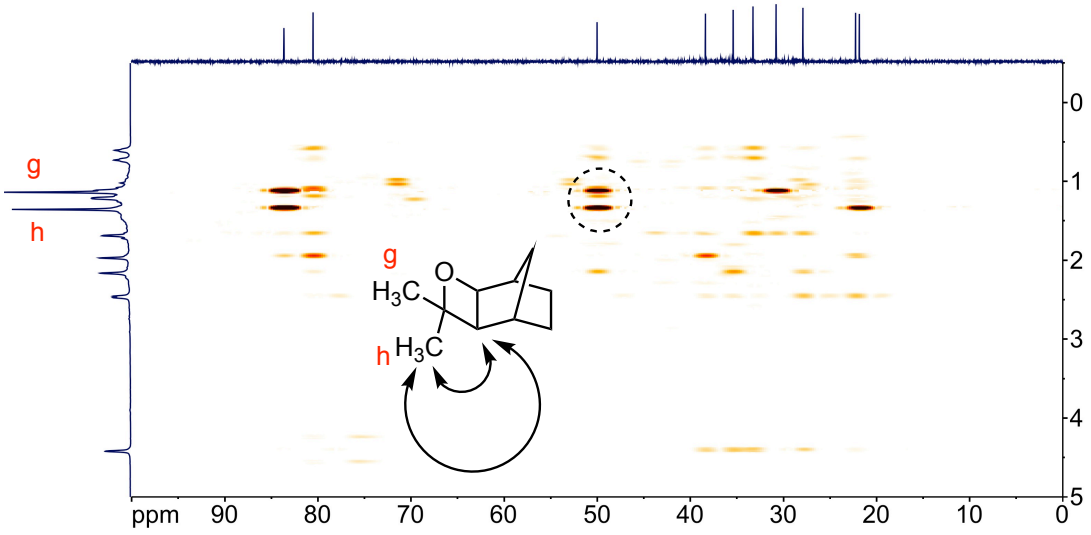

Figure 3.8 ^{1}H-^{13}C HMBC of compound **2**. Cross peaks show nO between protons g and i_1.

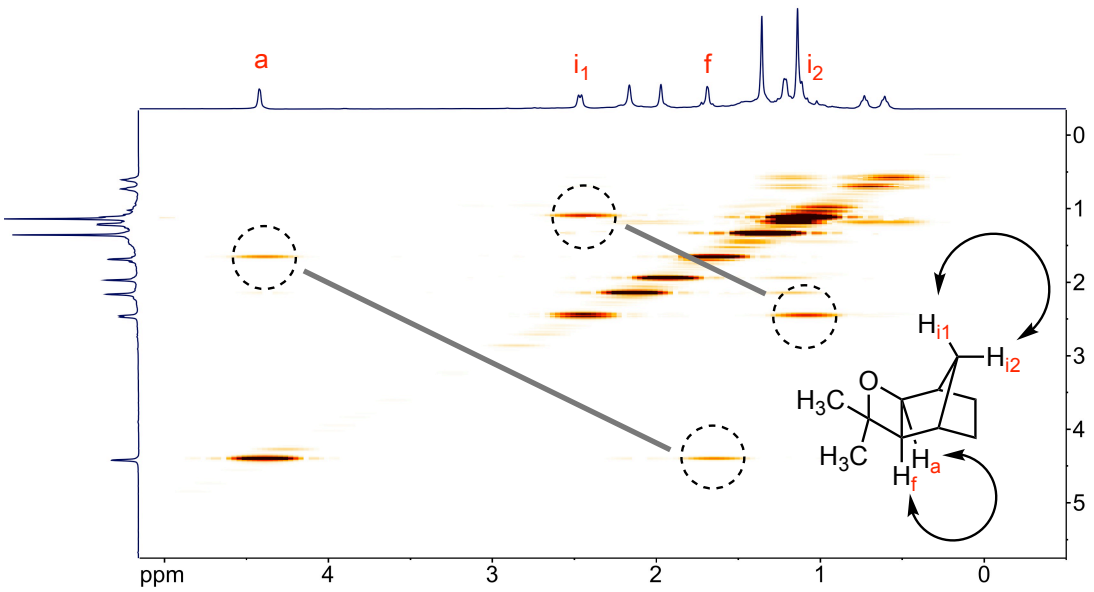

Figure 3.9 ^{1}H-^{1}H COSY of compound **2**. Cross peaks show coupling between protons a and f, and between i_1 and i_2.

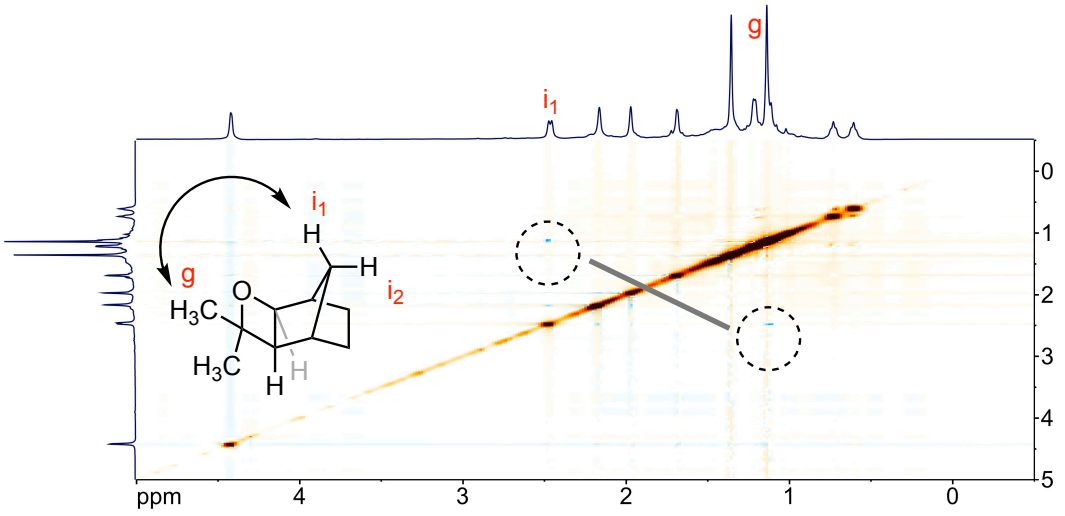

Figure 3.10 ^{1}H-^{1}H NOSEY of compound **2**. Cross peaks show nOe between protons g and i_1.

3.4 Mechanistic Investigation of the Carbonyl-Olefin Photocycloaddition

3.4.1 UV-vis Spectroscopy

To interrogate the mechanism by which this copper catalyzed 2+2 COPC reaction proceeds we collected the electronic absorption spectra of diethyl ether solutions of **TpCu** (green line, **Figure 3.11**) and an equimolar mixture of **TpCu** and methyl isobutyl ketone (gold line). Both spectra are nearly identical and lack any distinct absorption features between 200-400 nm. Conversely, an ethereal solution of **TpCu** and norbornene (1:1 molar ratio, pink line) has a broad absorption feature

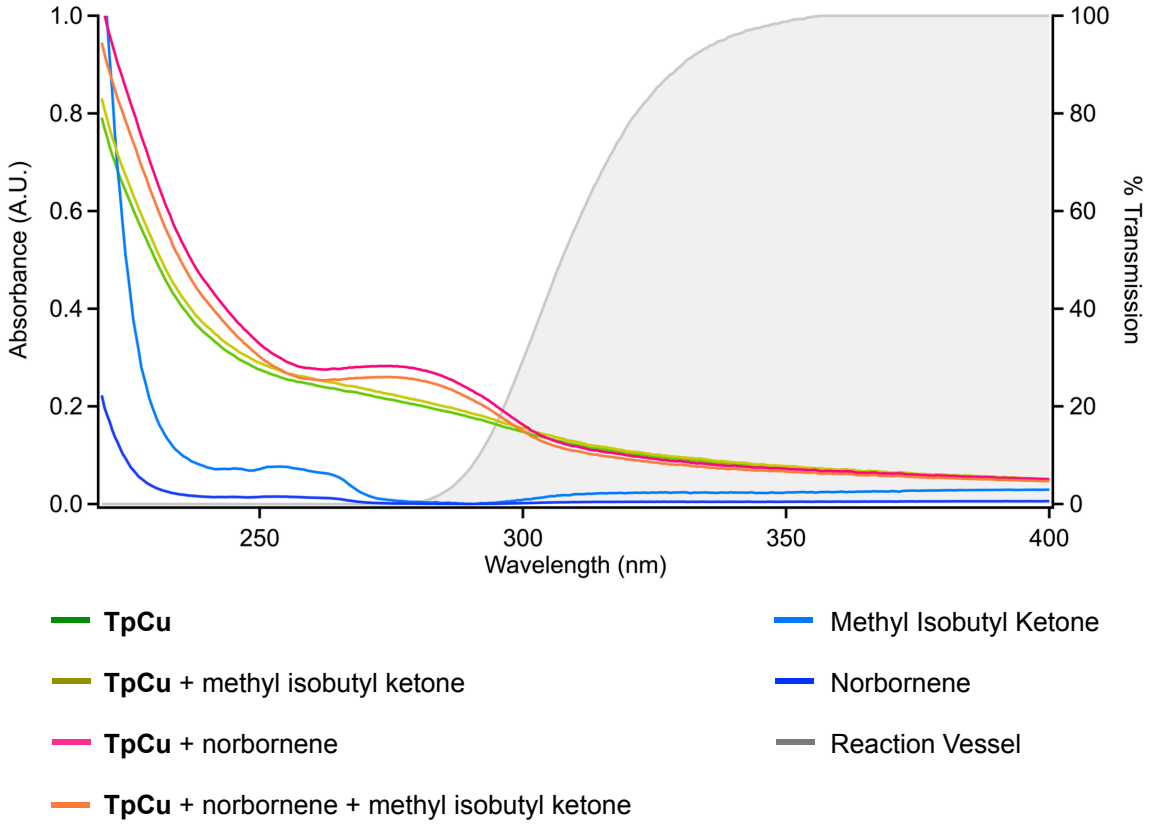

Figure 3.11 Electronic absorption spectra. All samples were collected at 0.5 mM in diethyl ether and as equimolar mixtures of the compounds indicated with each component being 0.5 mM. The transmission spectrum of the reaction vessels used in this study is overlaid for reference (right vertical axis).

with a maximum at 272 nm, suggesting the formation of a new species in solution. A 1:1:1 mixture of TpCu, norbornene, and methyl isobutyl ketone (orange line) displays the same absorption features as without added ketone, suggesting that this new species is the resting-state species.

The borosilicate reaction vessels used transmit very little light at <280 nm (**Figure 3.11**, grey line), indicating that oxetane formation is the result of absorption at >280 nm. Oxetane **1** was detected in only 60% conversion after 12 h of irradiation when a long pass 300 nm cut-on filter was applied compared to >98% conversion without the filter. Transmission through the cut-on filter ranges from <1% below 295 nm to >22% above 300 nm. The correlation between the decreased amount of light that reaches the reaction mixture between 280 and 300 nm and the decreased conversion to **1** suggest that oxetane forming excitation occurs in this region.

To investigate the lack of 2+2 COPC reactivity with aryl carbonyls an analogous set of spectroscopic experiments were conducted using 4-methyl acetophenone. The electronic absorption spectra of 4-methyl acetophenone shows a λ_{max} at 250 nm and 282 nm and has a smaller extinction coefficient than **TpCuNB** at all wavelengths above 267 nm, indicating a lack of reactivity is not attributed to the preferential excitation of aryl carbonyl over **TpCuNB**. Selectivity for benzophenone dimerization in ethereal solvents rather than oxetane formation with norbornene in benzene solutions has been previously reported. [48,49] The lack of background Paternò-Büchi reactivity can be attributed to the diethyl ether

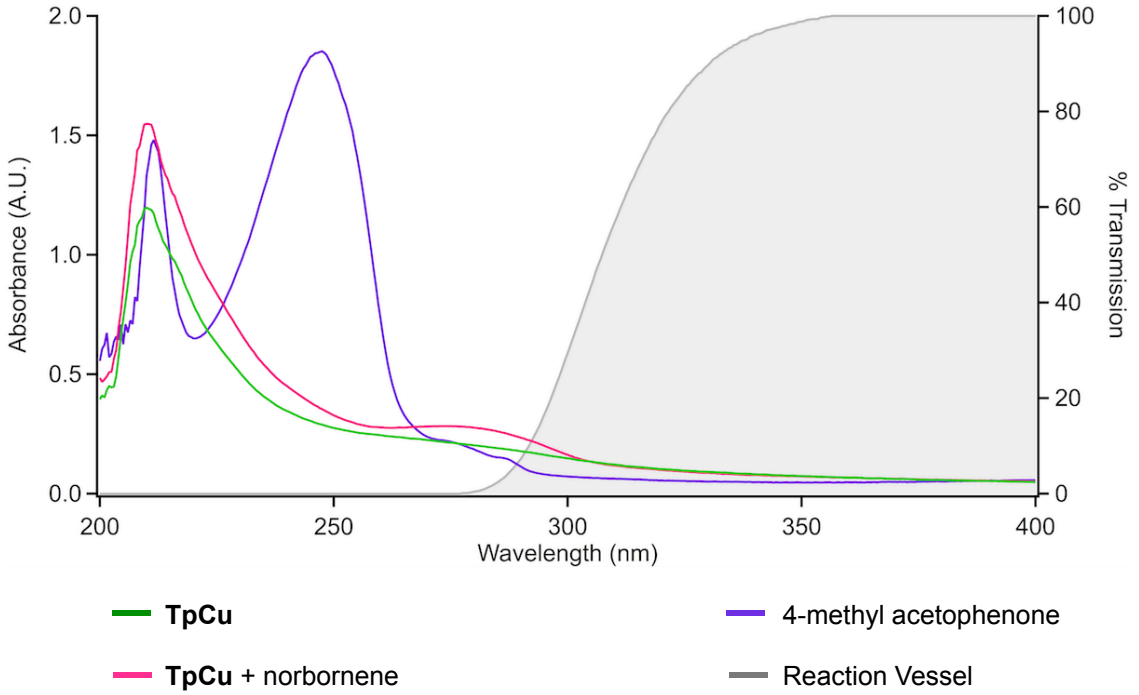

Figure 3.12 Electronic absorption spectra. All samples were collected at 0.5 mM in diethyl ether and as equimolar mixtures of the compounds indicated with each component being 0.5 mM. The transmission spectrum of the reaction vessels used in this study is overlaid for reference (right vertical axis).

solvent used and the failure of aryl ketones to produce oxetanes in our study to the inability of the Cu-mediated pathway to outcompete ketone dimerization.

3.4.2 NMR Spectroscopy

Another spectroscopic tool to investigate the species formed in solution, and their relatie rates of formation, is ^{1}H NMR. A series of NMR coordination experiments were in line with the electronic absorption data. **TpCu** displays three distinct proton signals (**Figure 3.13**, spectrum C). A mixture of **TpCu** and methyl isobutyl ketone does not result in the appearance of a new compound as the spectra is identical to the pure starting materials (spectrum D). However, in the

presence of norbornene a Cu-olefin complex is formed as evidenced by the downfield chemical shift change from 7.10 to 7.43 ppm of the proton at the C3 pyrazole position and a broadening of the signals corresponding to norbornene (spectrum E). The ^{1}H NMR spectrum of a 1:10:30 ratio of **TpCu**, methyl isobutyl ketone, and norbornene (spectrum F) showed the same characteristic C5 pyrazole proton chemical shift that was observed from stoichiometric mixing of **TpCu** and

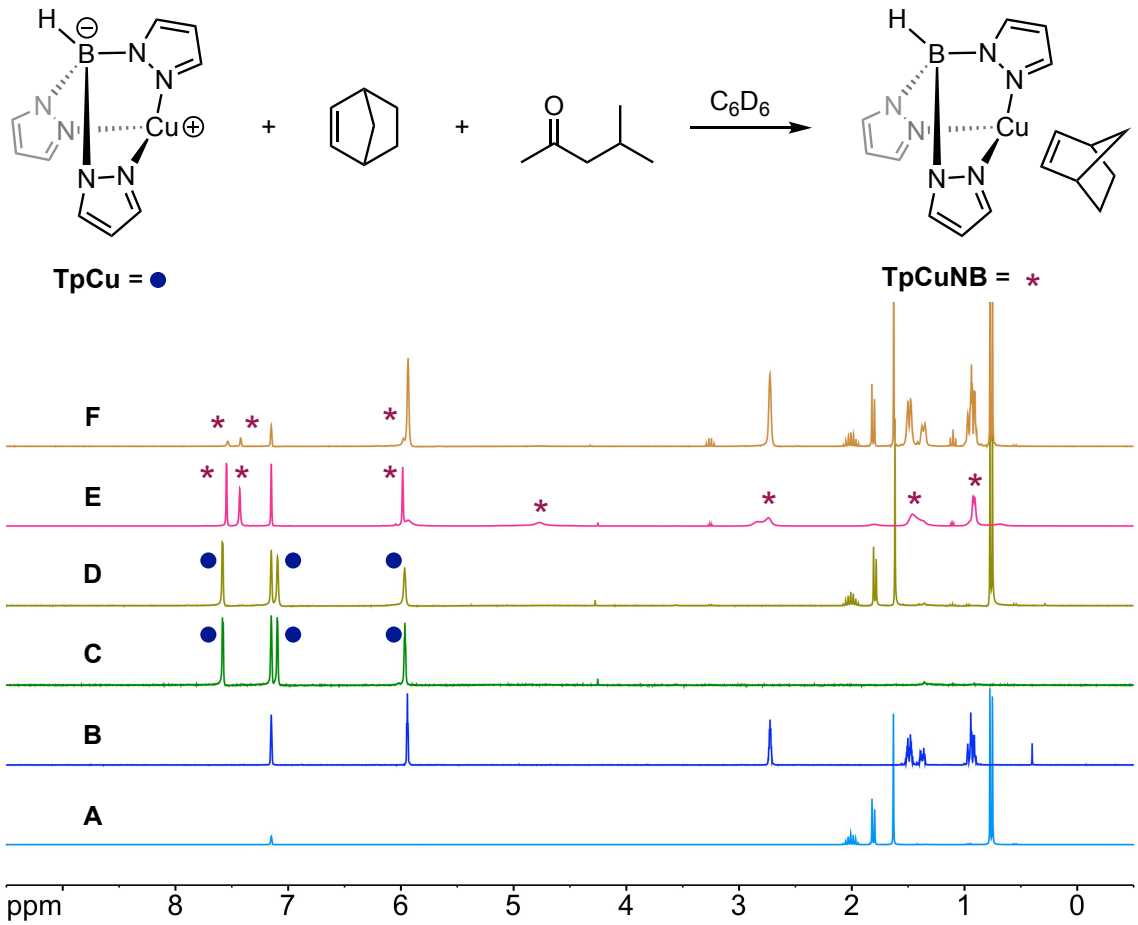

Figure 3.13 ^{1}H-NMR spectrum of reaction components. All samples were prepared in benzene-d_6. Spectrum A is methyl isobutyl ketone. Spectrum B is norbornene. Spectrum C is **TpCu**. Spectrum D is **TpCu** + 1 equiv methyl isobutyl ketone. Spectrum E is **TpCuNB**. Spectrum F is 1:10:30 mixture of **TpCu**/methyl isobutyl ketone/norbornene.

norbornene, suggesting that **TpCuNB** is form under the reaction conditions and is the resting state species.

We were curious how readily this Cu-olefin complex formed in solution. To experimentally determine this norbornene was sequentially added to a solution of **TpCu** in deuterated benzene. With as little as 0.25 equivalents norbornene in solution the formation **TpCuNB** can be observed by ^{1}H NMR (**Figure 3.14**).

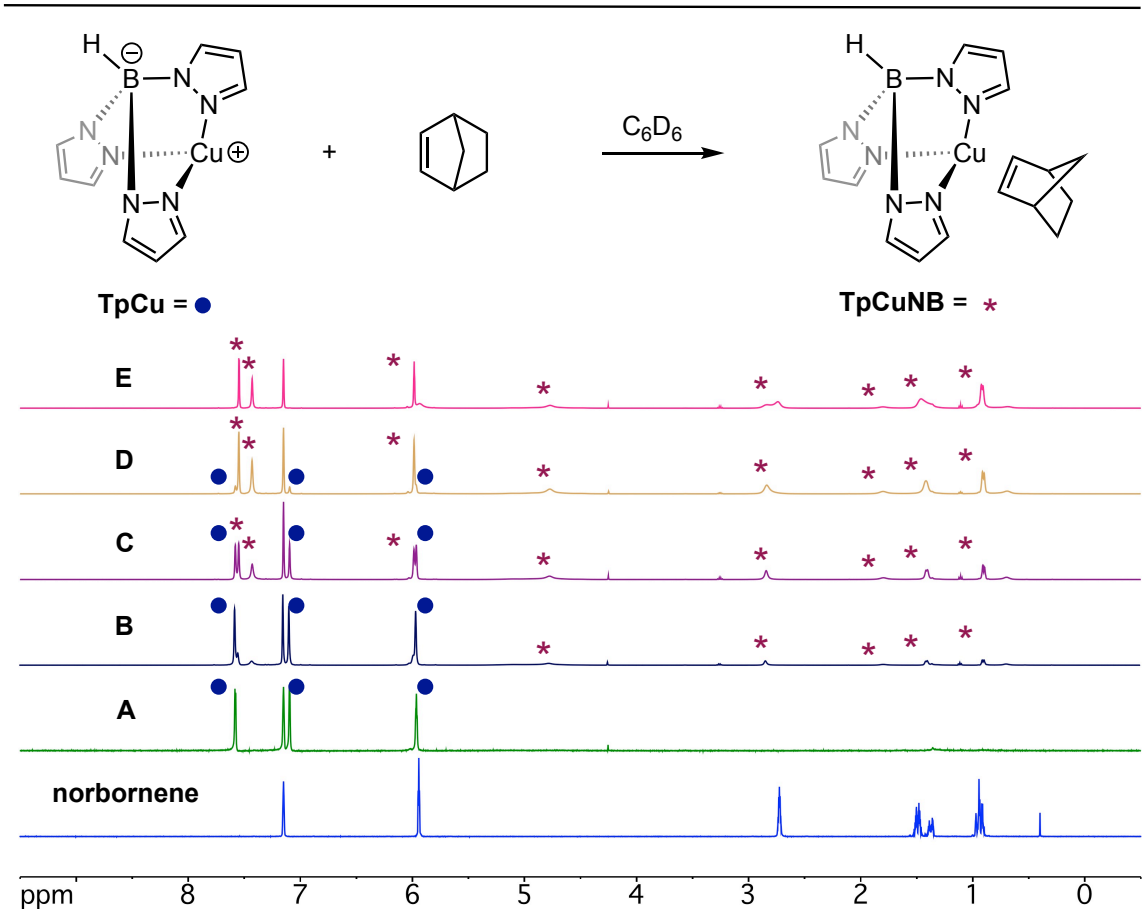

Figure 3.14 ^{1}H-NMR spectrum of **TpCu** with varying equivalents of norbornene. Spectrum A is **TpCu** only. Spectrum B is 1 equiv **TpCu** + 0.25 equiv norbornene. Spectrum C is 1 equiv **TpCu** + 0.5 equiv norbornene. Spectrum D is 1 equiv **TpCu** + 0.75 equiv norbornene. Spectrum E is 1 equiv **TpCu** + 1.0 equiv norbornene.

Addition up to one equivalent of norbornene shows the conversion of **TpCu** to

TpCuNB. Contrarily, the sub-stoichiometric addition of an alkyl ketone did not indicate coordination between the Cu catalyst and the carbonyl (**Figure 3.15**). Surprisingly, this coordination appeared limited to norbornene as ligation to a diverse range of olefins was not observed spectroscopically. This lack of coordination to other olefins accounts for their lack of reactivity in the 2+2 COPC.

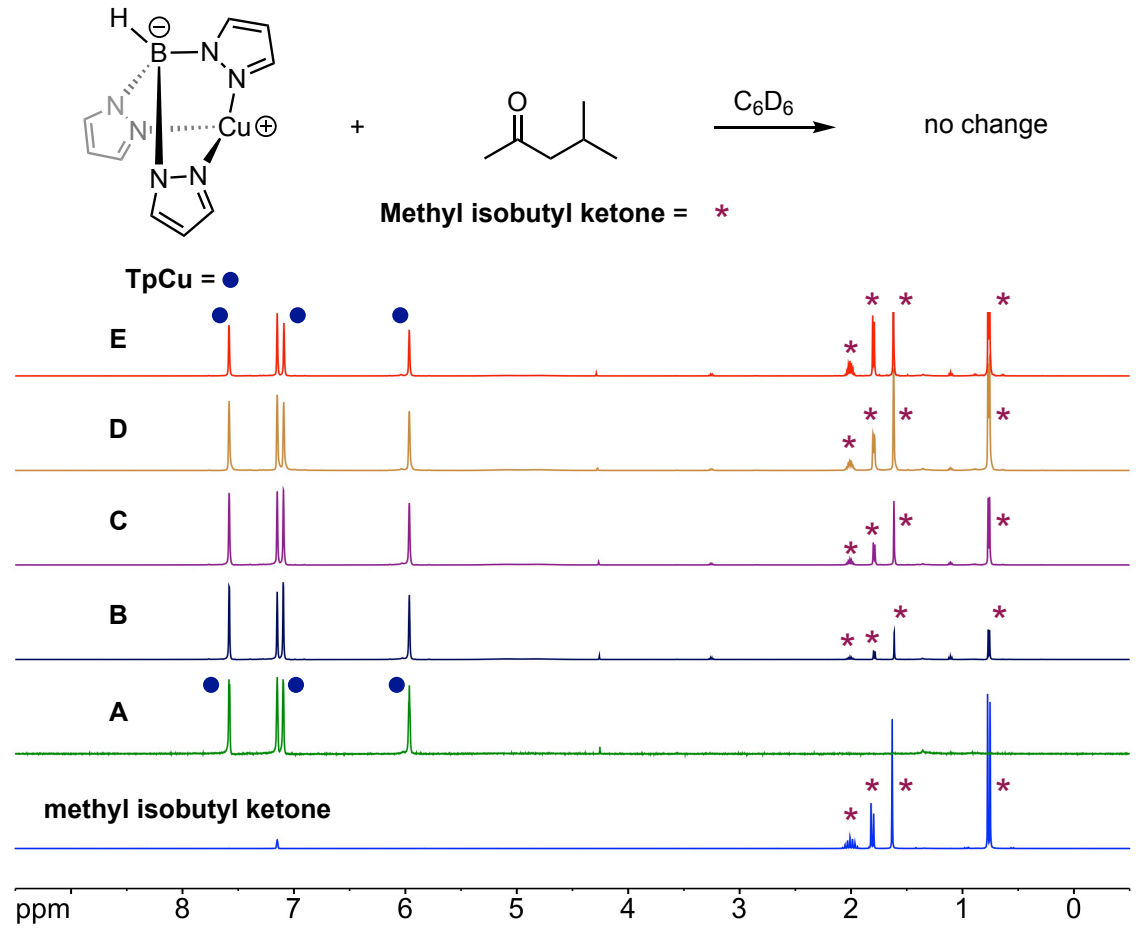

Figure 3.15 ^{1}H-NMR spectrum of **TpCu** with varying equivalents of methyl isobutyl ketone. Spectrum A is **TpCu** only. Spectrum B is 1 equiv **TpCu** + 0.25 equiv methyl isobutyl ketone. Spectrum C is 1 equiv **TpCu** + 0.5 equiv methyl isobutyl ketone. Spectrum D is 1 equiv **TpCu** + 0.75 equiv methyl isobutyl ketone. Spectrum E is 1 equiv **TpCu** + 1.0 equiv methyl isobutyl ketone.

An equimolar mixture of **TpCu** and 4-methyl acetophenone produced a ^{1}H NMR spectrum identical to pure starting material (**Figure 3.16**). Addition of one equivalent of norbornene to the sample resulted in the diagnostic downfield shift of the C5 pyrazole proton of **TpCu**. This indicates the formation of the Cu-olefin complex is not inhibited by the presence of aryl carbonyls.

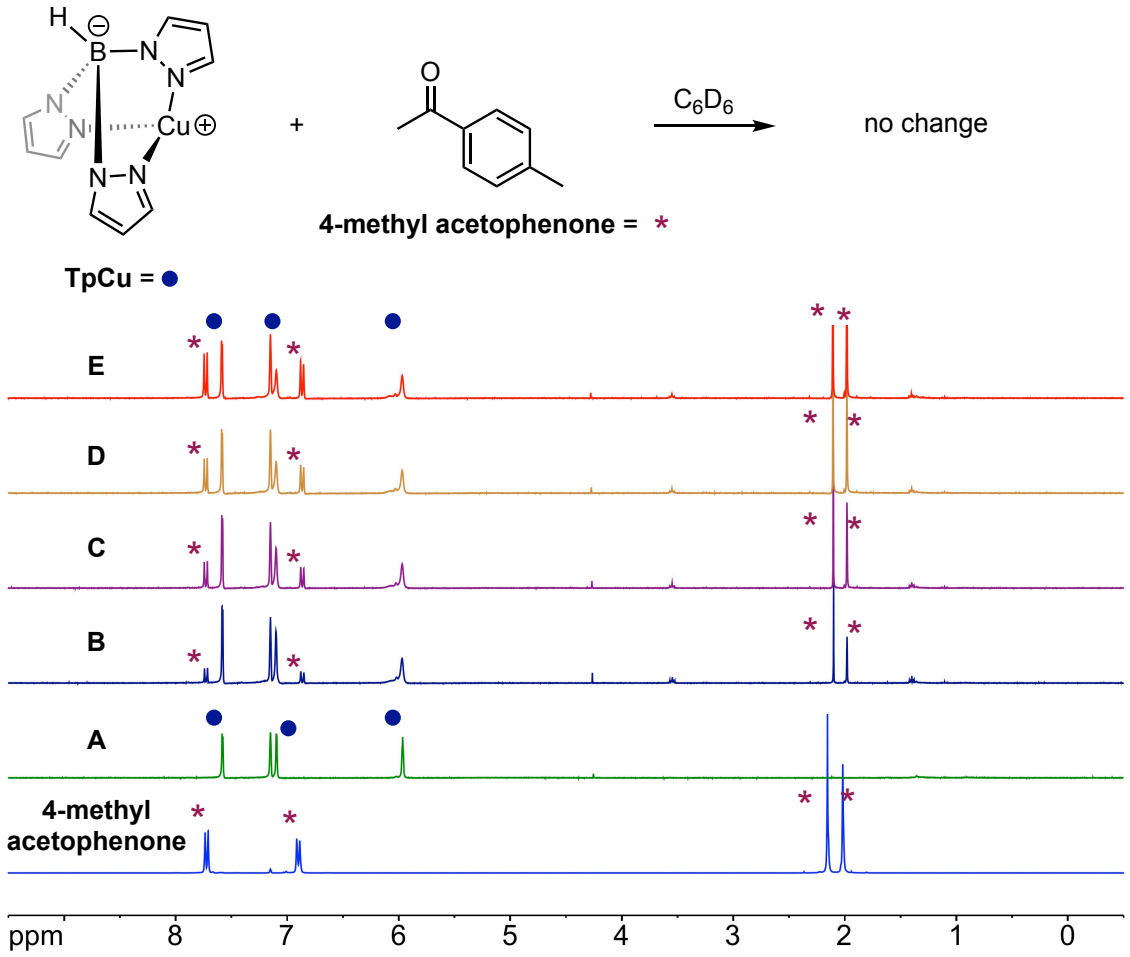

Figure 3.16 ^{1}H-NMR spectrum of **TpCu** with varying equivalents of 4-methyl acetophenone. Spectrum A is **TpCu** only. Spectrum B is 1 equiv **TpCu** + 0.25 equiv 4-methyl acetophenone. Spectrum C is 1 equiv **TpCu** + 0.5 equiv 4-methyl acetophenone. Spectrum D is 1 equiv **TpCu** + 0.75 equiv 4-methyl acetophenone. Spectrum E is 1 equiv **TpCu** + 1.0 equiv 4-methyl acetophenone.

3.4.3 Luminescence Quenching

As with any photochemical process there is the possibility of excitation through sensitization. To examine this possibility a series of Stern-Volmer luminescence quenching studies were conducted (see Chapter 1.1). Because we are not irradiating in the region where the substrates themselves absorb light they can be ruled out as sensitizers. This leaves two possible sensitizers in our system: **TpCu** or the in-situ formed **TpCuNB**. The data did not exhibit a positive linear relationship between the concentration of additional norbornene or methyl isobutyl ketone in the presence of **TpCu**. The same lack of correlation in the presence of **TpCuNB** was also observed. This suggests the 2+2 COPC does not proceed through sensitization, however the absence of an

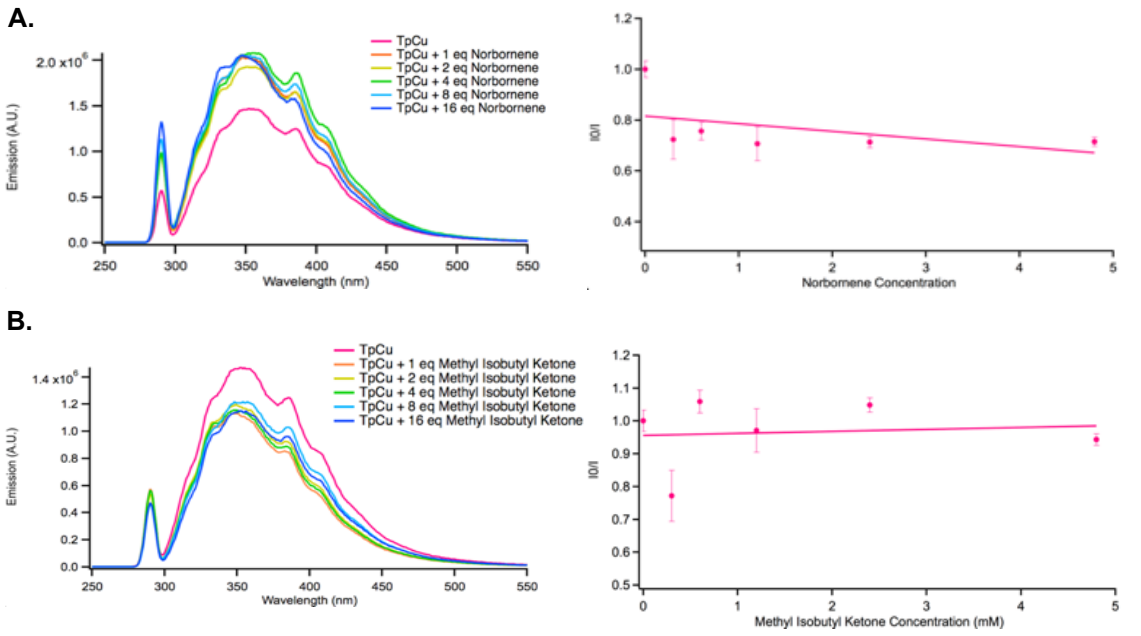

Figure 3.17 A. Emission plot and Stern-Volmer plot of **TpCu** with varying concentration of norbornene. **B.** Emission plot and Stern-Volmer plot of **TpCu** with varying concentration of methyl isobutyl ketone

observed quenching relationship does not definitely exclude the possibility that an additional sensitization process may contribute to oxetane formation.

3.4.4 Mechanistic Proposal

In alignment with the previously reported mechanisms of Cu-mediated alkene photodimerization and valence isomerization and our collected data, we propose the Cu-catalyzed COPC proceeds through initial olefin coordination to **TpCu** to form **TpCuNB**. Excitation between 280 – 300 nm results in MLCT to formally generate a Cu(II) metal center and an alkene radical anion. The absence of reactivity for other alkenes in this 2+2 COPC suggests that norbornene interaction with **TpCu** is preferred and is the source of observed reactivity. Trapping of this polarized intermediate by the carbonyl unit of the alkyl ketone can result in oxetane formation. The exact nature of the penultimate intermediate is highly speculated on. It is reasonable to envision a sigma bonded Cu(II)-carbon species with a pendent oxygen radical. However, it is possible that a Cu(III)-metallacycle could also be present. At this time, we do not have evidence that conclusively supports either scenario.

The spin state of the 2+2 photocycloadditions is commonly inferred based on the stereochemistry of the products detected. However, the use of norbornene in our present work precludes an analogous interpretation, because geometric constraints would result in identical products irrespective of spin state.

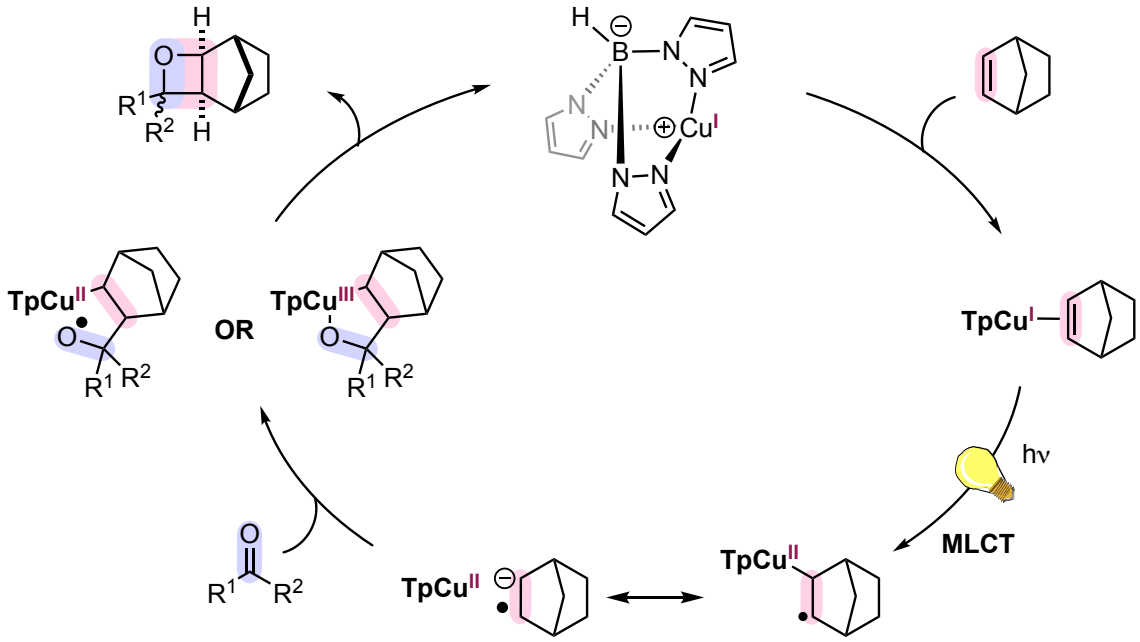

Figure 3.18 Proposed mechanism for the 2+2 COPC

3.5 Conclusions

The development of a Cu-catalyzed 2+2 carbonyl-olefin photocycloaddition of alkyl ketones and norbornene that accesses the corresponding oxetanes via a mechanistically distinct pathway from the conventional Paternò-Büchi reactions has been disclosed. This approach enables traditionally challenging alkyl ketones to engage in four membered ring formation, because direct carbonyl excitation is avoided. Mechanistic investigations support the in situ formed **TpCuNB** is the photoactive species that upon excitation leads to oxetane formation. This intermolecular 2+2 COPC process disrupts the traditional paradigm of carbonyl direct excitation for oxetane formation and was achieved using a MLCT enabled through alkene substrate coordination. This distinct approach towards substrate

activation has the potential to engage unactivated olefins that are challenging to engage photochemically, such as ethylene, and transform them into high value products. The theoretical limitation of this platform is solely the ability of the substrate to coordinate to the Cu catalyst and thus through catalyst design is subject to further development.

3.6 Synthetic Procedures and Characterization Data

General Considerations. All air- and moisture-sensitive manipulations were carried out using standard high vacuum line, Schlenk or cannula techniques or in an M. Braun inert atmosphere drybox containing an atmosphere of purified nitrogen. Solvents for air- and moisture-sensitive manipulations were dried and deoxygenated using literature procedures.

^{1}H and ^{13}C NMR were recorded on Bruker 300 MHz or Varian 500 MHz spectrometers at 300 and 126 MHz, respectively. All chemical shifts are reported relative to $SiMe_4$ using ^{1}H (residual) chemical shifts of the solvent as a secondary standard. GC analyses were performed using an Agilent Technologies 7890B gas chromatograph equipped with an Agilent 7693 autosampler and Agilent HP-5 capillary column (30 m x 0.320mm x 250μm). Standard method parameters: 1.2 mL/min flow rate with oven program 80 – 250 °C with a ramp rate of 25 °C/min and hold time of 8.7 minutes at 250 °C. High-resolution mass spectra were measured using a Thermo LCQdeca APCI-MS.

Photophysical Methods. Electronic absorption and fluorescence experiments were conducted using sealable 1-cm path length fused quartz cuvettes (Starna Cells, catalog number 3-Q-10-GL14-C, 3.5 mL volume) using a Shimadzu UV-2450 UV-Vis spectrometer and a HORIBA Scientific Fluoromax-4 fluorometer. Samples were prepared in a dry nitrogen glove box. Filter experiments were conducted using a long pass UV filter with a cut-on wavelength of 300 nm (Asahi Spectra XUL0300).

Stern-Volmer Quenching Studies. Stern-Volmer luminescence quenching experiments were run with freshly prepared solutions of 3.0 x 10^{-4} M **TpCu** or **TpCuNB** as indicated in diethyl ether at room temperature under an inert atmosphere. The solutions were irradiated at 294 nm and luminescence was measured at 350 nm. Each sample was prepared three times, the luminescence was acquired and averaged. The average of the results was used for the graphical representation and determination of K_{SV}. The data show that norbornene and methyl isobutyl ketone are shown to be unable to quench the excited state of **TpCu** or **TpCuNB**. For all tabular and graphical data, see **Tables S2- S4** and **Figures S2-S7** below.

Photochemical Reactions. Photochemical reactions were carried out using two 100-W Blak-Ray Long Wave Ultraviolet Lamps (Hg) in a fume hood. The light sources was placed approximately 20 cm from the sample and the reaction mixture

was stirred vigorously using a magnetic stir bar. All reactions were performed in VWR 13 x 100 mm borosilicate culture tubes that were capped and sealed with electrical tape.

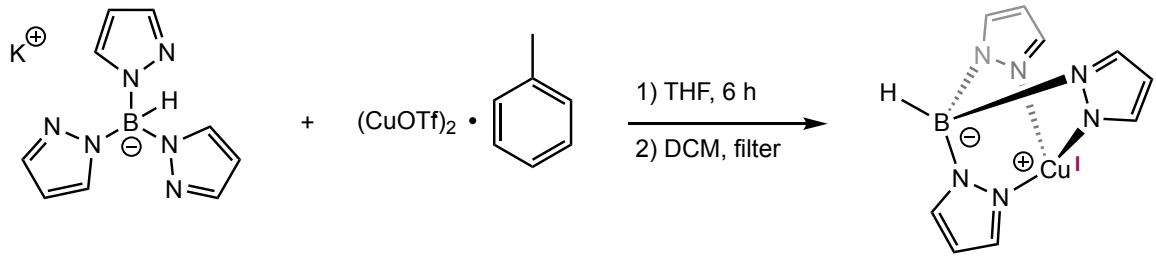

Preparation of TpCu. In a nitrogen filled glovebox, a 20 mL vial was charged with CuCl (0.125g, 1 equiv), potassium trispyrazolylborate (0.318 g, 1 equiv) and a magnetic stir bar. A mixture of THF (4 mL) and dried, degassed acetone (4 mL) was added and the mixture was stirred vigorously for 6 h. The solvent was removed under reduced pressure, the resultant solid extracted with dichloromethane (5 mL), and the suspension filtered through a thin pad of celite on a fritted funnel. Removal of the solvent under reduced pressure provided **TpCu** (0.349 g, 98% yield) as a faint blue solid. Analytical data for **TpCu**: ^{1}H-NMR (500 MHz; C_6D_6): δ 7.58 (d, J=1.8 Hz, 3H), 7.09 (d, J=1.2 Hz 3H), 5.96 (t, J=1.8 Hz, 3H). ^{13}C-NMR (126 MHz; C_6D_6): δ 141.8, 135.9, 104.9. HRMS (ESI-TOFMS): Calc. for $[C_9H_{10}BCuN_6]^+$ =276.0352, Found = 276.0354.

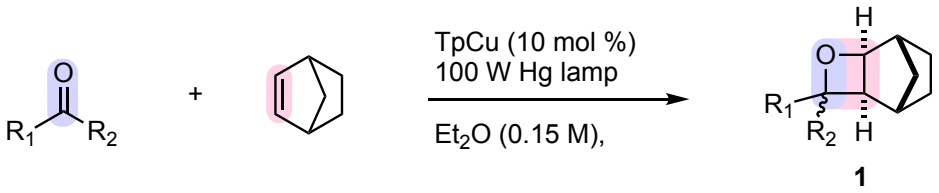

1

General 2+2 COPC Reaction Procedures. In a glovebox to a borosilicate culture tube charged with a magnetic stir bar was added ketone (30 mg, 1.0 equiv), **TpCu** (0.1 equiv), norbornene (3.0 equiv), and diethyl ether (0.15M). The vial was capped, sealed with electrical tape, and irradiated with a UVP Blak-Ray B-100A UV lamp in an assembled photoreactor fitted with an exhaust fan and 20" box fan. After 12 h, or otherwise indicated, the reaction mixture was filtered through a glass filter, rinsed with an additional 1 mL Et_2O, and solvent removed under reduced pressure. A 0.6M solution of durene in C_6D_6 added (100 μL) before diluting with additional C_6D_6 for ^{1}H-NMR analysis. The sample was then concentrated under reduced pressure and purified by flash chromatography.

Characterization of Oxetane Products.

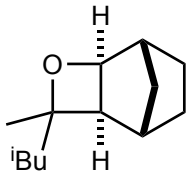

1 was synthesized via general COPC procedure in 49% NMR yield determined using durene as an internal standard as an average of 3 independent trials (51%, 49% and 46% yield each) and 24% isolated yield (55:45 diastereomeric mixture at C2, > 95:5 *exo:endo*) as a white solid. Analytical data for **1**:

^{1}H-NMR (300 MHz; C_6D_6): δ 4.42 (d, J=4.5 Hz, 1H), 2.50 (m, 1H), 2.15 (s, 1H), 2.09 (s, 1H), 2.01 (s, 1H), 1.77 (d, *J* = 4.7 Hz, 1H), 1.72-1.63 (m, 2H), 1.51-1.34 (m, 3H), 1.22 (d, *J* = 6.0 Hz, 2H), 1.15 (s, 2H), 1.04 (d, J=6.0 Hz, 2H), 0.97 (d, J=6.0 Hz, 1H), 0.91 (d, J=6.0 Hz, 2H), 0.81 (d, J=6.0 Hz, 1H), 0.74 (m, 1H), 0.62 (m, 1H).

^{13}C-NMR (126 MHz; C_6D_6): δ 86.16, 86.09, 81.2, 51.8, 51.3, 50.4, 43.1, 38.5, 35.46, 35.30, 33.7, 33.4, 28.0, 27.4, 24.61, 24.48, 23.93, 23.81, 23.4, 22.33, 22.19, 19.2.

HRMS (APCI-TOFMS) Calc. for $[C_{13}H_{22}O+H^+]^+$ = 195.1744, Found = 195.1744.

R_f (silica gel, 5% Acetone in Pentane): 0.5.

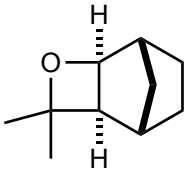

2 was synthesized via general COPC procedure in 51% NMR yield determined using durene as an internal standard and 21% isolated yield (>95:5 *exo:endo* as determined by a series of multidimensional NMR experiments) as a white solid. Analytical data for **2**:

^{1}H-NMR (300 MHz; C_6D_6): δ 4.42 (d, J=2.4 Hz, 1H), 2.47 (d, J=5.7 Hz, 1H), 2.16 (s, 1H), 1.97 (s, 1H), 1.66 (d, J= 3.6 Hz, 1H), 1.36 (m, 4H), 1.21 (d, J=4.0 Hz, 2H), 1.13 (m, 4H), 0.67 (m, 2H).

^{13}C-NMR (126 MHz; C_6D_6): δ 84.1, 80.9, 50.4, 38.8, 35.8, 33.6, 31.2, 28.3, 22.6, 22.2.

HRMS (ESI-TOFMS) Calc. for $[C_{10}H_{16}O+H^+]^+$ = 153.1275 Found = 153.1275.

R_f (silica gel, 5% Acetone in Pentane): 0.5.

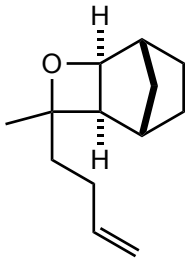

3 was synthesized via general COPC procedure in 45% NMR yield determined using durene as an internal standard and 25% isolated yield (55:45 diastereomeric mixture at C2, > 95:5 *exo:endo* as determined by analogy to **1** and **2** above) as a white solid. Analytical data for **3**:

^{1}H-NMR (300 MHz; $CDCl_3$): δ 5.84 (m, 1H), 5.07-4.92 (m, 2H), 4.53 (d, J=4.2 Hz, 1 H), 2.33 (s, 1H), 2.23 (s, 2H), 2.17-2.07 (m, 1H), 2.01 (dd, J=4.8 Hz, J=11.6 Hz, 1H), 1.94-1.60 (m, 3H), 1.43 (m, 3H), 1.28 (m, 1H), 1.20 (s, 2H), 0.97 (m, 1H), 0.83 (m, 1H).

^{13}C-NMR (126 MHz; $CDCl_3$): δ 138.92, 138.74, 114.50, 114.43, 86.96, 86.88, 82.2, 81.7, 50.4, 49.4, 42.9, 38.56, 38.45, 35.56, 35.36, 34.1, 33.7, 28.21, 28.09, 28.01, 27.96, 27.7, 22.5, 22.3, 19.6.

HRMS (APCI-TOFMS) Calc. for $[C_{13}H_{20}O+H^+]^+$ = 193.1586, Found = 193.1587.

R_f (silica gel, 5% Acetone in Pentane): 0.6.

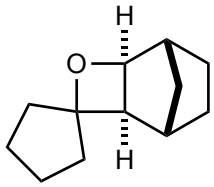

4 was synthesized via general COPC procedure in 66% NMR yield determined using durene as an internal standard and 33% isolated yield (> 95:5 *exo:endo* as determined by analogy to **2**) as a white solid. Analytical data for **4**:

^{1}H-NMR (300 MHz; $CDCl_3$): δ 4.51 (d, J=4.5 Hz, 1H), 2.21 (m, 4H), 2.08 (m, 1H), 1.88-1.22 (m, 10H), 0.96 (m, 1H), 0.84 (m, 1H).

^{13}C-NMR (126 MHz; $CDCl_3$): δ 95.45, 82.06, 49.89, 42.43, 39.30, 35.95, 33.22, 32.94, 27.60, 23.86, 23.07, 22.46.

HRMS (APCI-TOFMS) Calc. for $[C_{12}H_{18}O+H^+]^+$ = 179.1430, Found = 179.1429.

R_f (silica gel, 5% Acetone in Pentane): 0.6.

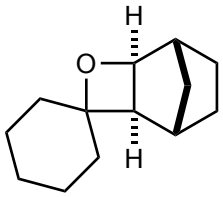

5 was synthesized via general COPC procedure in 81% NMR yield determined using durene as an internal standard and 33% isolated yield (> 95:5 *exo:endo* as determined by analogy to **2**) as a white solid. Analytical data for **5**:

^{1}H-NMR (300 MHz; $CDCl_3$): δ 4.53 (d, J=4.5 Hz, 1H), 2.33 (d, J=9.9 Hz, 1H), 2.19 (m, 3H), 1.96 (m, 1H), 1.83 (m, 2H), 1.67-0.81 (m, 13).

^{13}C-NMR (126 MHz; $CDCl_3$): δ 86.99, 82.01, 48.85, 39.85, 38.60, 34.90, 33.78, 31.83, 28.23, 25.57, 23.14, 22.88, 22.34.

HRMS (APCI-TOFMS) Calc. for $[C_{13}H_{20}O+H^+]^+$ = 193.1586, Found = 193.1587.

R_f (silica gel, 5% Acetone in Pentane): 0.6.

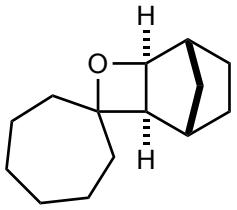

6 was synthesized via general COPC procedure in 67% NMR yield determined using durene as an internal standard and 32% isolated yield (> 95:5 *exo:endo* as determined by analogy to **2**) as a white solid. Analytical data for **6**:

^{1}H-NMR (300 MHz; $CDCl_3$): δ 4.47 (d, J=4.8 Hz, 1H), 2.21-1.79 (m, 7 H), 1.47-0.97 (m, 15H).

^{13}C-NMR (126 MHz; $CDCl_3$): δ 90.1, 81.7, 51.0, 42.4, 38.6, 35.6, 34.2, 33.7, 29.3, 28.8, 28.1, 22.5, 22.04, 21.94.

HRMS (APCI-TOFMS) Calc. for $[C_{14}H_{22}O+H^+]^+$ = 207.1743, Found = 207.1743.

R_f (silica gel, 5% Acetone in Pentane): 0.6.

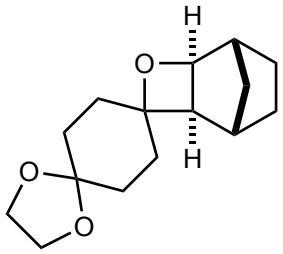

7 was synthesized via general COPC procedure in 96% NMR yield determined using durene as an internal standard and 76% isolated yield (> 95:5 *exo:endo* as determined by analogy to **2**) as a white solid. Analytical data for **7**:

^{1}H-NMR (300 MHz; $CDCl_3$): δ 4.57 (d, J=4.2 Hz, 1H), 3.92 (s, 4H), 2.33 (d, J=9.9 Hz, 1H), 2.25 (m, 2H), 2.02 (m, 2H), 1.92-1.72 (m, 5H), 1.71-1.56 (m, 2H), 1.53-1.43 (m, 4H), 1.32-1.24 (m, 3H), 1.11 (d, J=12.3 Hz, 1H), 0.98 (m, 1H), 0.87-0.84 (m, 1H).

^{13}C-NMR (126 MHz; $CDCl_3$): δ 108.3, 85.7, 82.3, 64.53, 64.44, 48.5, 38.6, 36.7, 35.2, 33.8, 31.01, 30.94, 28.6, 28.3, 22.4.

HRMS (ESI-TOFMS) Calc. for $[C_{15}H_{22}O_3+H^+]^+$ = 251.1642 Found = 251.1642.

R_f (5 % Acetone in Pentane): 0.75.

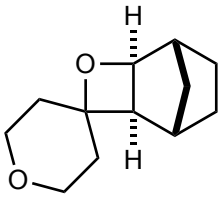

8 was synthesized via general COPC procedure, irradiating for 24 h, in 75% NMR yield determined using durene as an internal standard and 22% isolated yield (> 95:5 *exo:endo* as determined by analogy to **2**) as a white solid. Analytical data for **8**:

^{1}H-NMR (300 MHz; $CDCl_3$): δ 4.63 (d, J=4.8 Hz, 1H), 3.85 (m, 1H), 3.72 (m, 1H), 3.61 (m, 1H), 3.49 (m, 1H), 2.32 (m, 3H), 2.08 (d, J=4.8 Hz, 1H), 1.89 (m, 4H), 1.70 (m, 1H), 1.51-1.48 (m, 3H), 1.35 (m, 2H), 1.06-0.99 (m, 1H), 0.89 (m, 1H).

^{13}C-NMR (126 MHz; $CDCl_3$): δ 83.8, 82.4, 64.52, 64.48, 49.0, 40.0, 38.7, 34.8, 33.7, 32.7, 28.1, 22.3.

HRMS (APCI-TOFMS) Calc. for $[C_{12}H_{18}O_2+H^+]^+$ = 195.1380 Found = 195.1379.

R_f (silica gel, 5 % Acetone in Pentane): 0.5.

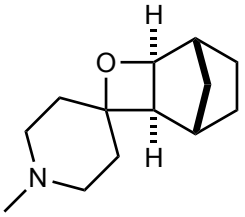

9 was synthesized via general COPC procedure, irradiating for 24 h, in 69% NMR yield determined using durene as an internal standard and 14% isolated yield (> 95:5 *exo:endo* as determined by analogy to **2**) as a white solid. Analytical data for **9**:

^{1}H-NMR (300 MHz; $CDCl_3$): δ 4.42 (s, 1H – apparent singlet due to broadening), 2.52-2.36 (m, 4H), 2.19-1.68 (m, 8H), 1.21-1.08 (m, 4H), 0.75-0.70 (m, 1H), 0.61-0.57 (m, 1H).

^{13}C-NMR (126 MHz; $CDCl_3$): δ 83.4, 81.3, 54.9, 52.1, 48.4, 45.9, 39.1, 38.6, 34.6, 33.6, 31.5, 28.0, 22.1.

HRMS (APCI-TOFMS) Calc. for $[C_{13}H_{21}NO]^+$ = 217.1199 Found = 217.1197.

R_f (silica gel, 5 % Acetone in Pentane): 0.25.

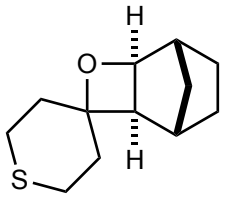

10 was synthesized via general COPC procedure, irradiating for 24 h, in 89% NMR yield determined using durene as an internal standard and 60% isolated yield (> 95:5 *exo:endo* as determined by analogy to **2**) as a white solid. Analytical data for **10**:

^{1}H-NMR (300 MHz; $CDCl_3$): δ 4.55 (d, J=3.0 Hz, 1H), 2.94-2.39 (m, 5H), 2.26 (s, 3H), 2.14 (m, 1H), 2.05 (m, 2H), 1.96 (m, 2H), 1.45 (m, 2H), 1.30 (d, J=9.9 Hz, 1H), 1.13 (m, 1H) 0.97-0.94 (m, 1H), 0.86-0.82 (m, 1H).

^{13}C-NMR (126 MHz; $CDCl_3$): δ 85.1, 82.5, 49.2, 40.3, 38.5, 34.7, 34.1, 33.0, 28.2, 25.3, 25.0, 22.0.

HRMS (APCI-TOFMS) Calc. for $[C_{12}H_{18}OS+H^+]^+$ = 211.1151 Found = 211.1151.

R_f (silica gel, 5 % Acetone in Pentane): 0.4.

3.7 Acknowledgements

Chapter 3 is adapted in part from Flores, D. M.; Schmidt, V. A. *J. Am. Chem. Soc.* **2019**, *141*, 8741-8745. Copyright 2019, American Chemical Society. Permission to include published material in this dissertation has been obtained from all coauthors. The dissertation author is the first author of this paper.

3.8 References

(1) *Nomenclature of Organic Chemistry: IUPAC Recommendations and Preferred Names 2013*; The Royal Society of Chemistry, 2014; pp P001–P004. https://doi.org/10.1039/9781849733069-FP001.

(2) Ahmad, S.; Yousaf, M.; Mansha, A.; Rasool, N.; Zahoor, A. F.; Hafeez, F.; Rizvi, S. M. A. Ring-Opening Reactions of Oxetanes: A Review of Methodology Development and Synthetic Applications. *Synth. Commun.* **2016**, *46* (17), 1397–1416. https://doi.org/10.1080/00397911.2016.1208245.

(3) Malapit, C. A.; Howell, A. R. Recent Applications of Oxetanes in the Synthesis of Heterocyclic Compounds. *J. Org. Chem.* **2015**, *80* (17), 8489–8495. https://doi.org/10.1021/acs.joc.5b01255.

(4) Burkhard, J. A.; Wuitschik, G.; Rogers-Evans, M.; Müller, K.; Carreira, E. M. Oxetanes as Versatile Elements in Drug Discovery and Synthesis. *Angew. Chemie - Int. Ed.* **2010**, *49* (48), 9052–9067. https://doi.org/10.1002/anie.200907155.

(5) Wani, M. C.; Taylor, H. L.; Wall, M. E.; Coggon, P.; Mcphail, A. T. Plant Antitumor Agents.VI.The Isolation and Structure of Taxol, a Novel Antileukemic and Antitumor Agent from Taxus Brevifolia2. *J. Am. Chem. Soc.* **1971**, *93* (9), 2325–2327. https://doi.org/10.1021/ja00738a045.

(6) Kingston, D. G. I. THE CHEMISTRY OF TAXOL P ~ Ph ~ OCHs PhCOO. *Paharmac. Ther.* **1991**, *52*, 1–34.

(7) Huang, J. M.; Yokoyama, R.; Yang, C. S.; Fukuyama, Y. Merrilactone A, a Novel Neurotrophic Sesquiterpene Dilactone from Illicium Merrillianum. *Tetrahedron Lett.* **2000**, *41* (32), 6111–6114. https://doi.org/10.1016/S0040-4039(00)01023-6.

(8) Wang, Y.; Fleet, G. W. J.; Storer, R.; Myers, P. L.; Wallis, C. J.; Doherty, O.; Watkin, D. J.; Vogt, K.; Witty, D. R.; Wilson, F. X.; et al. Synthesis of the Potent Antiviral Oxetane Nucleoside Epinoroxetanocin from D-Lyxonolactone. *Tetrahedron: Asymmetry* **1990**, *1* (8), 527–530. https://doi.org/10.1016/S0957-4166(00)80541-8.

(9) Murakami, A. NII-Electronic Library Service. *Chem. Pharm. Bull.* **1970**, No. 43, 2091.

(10) D'Auria, M.; Racioppi, R. Oxetane Synthesis through the Paternò-Büchi Reaction. *Molecules* **2013**, *18* (9), 11384–11428. https://doi.org/10.3390/molecules180911384.

(11) Tanaka, Y. Contribution of Ring Strain and Basicity to Reactivity of Cyclic Ethers in Cationic Copolymerization. *J. Macromol. Sci. Part A - Chem.* **1967**, *1* (6), 1059–1068. https://doi.org/10.1080/10601326708053757.

(12) Fréneau, M.; Hoffmann, N. The Paternò-Büchi Reaction—Mechanisms and Application to Organic Synthesis. *J. Photochem. Photobiol. C Photochem. Rev.* **2017**, *33*, 83–108. https://doi.org/10.1016/j.jphotochemrev.2017.10.002.

(13) Büchi, G.; Inman, C. G.; Lipinsky, E. S. Light-Catalyzed Organic Reactions. I. The Reaction of Carbonyl Compounds with 2-Methyl-2-Butene in the Presence of Ultraviolet Light. *J. Am. Chem. Soc.* **1954**, *76* (17), 4327–4331. https://doi.org/10.1021/ja01646a024.

(14) Collier, M. The Sting of the Scorpion. *Mummies, magic Med. Anc. Egypt* **2016**, 102–114. https://doi.org/10.7765/9781784997502.00021.

(15) Dauben, W. G.; Salem, L.; Turro, N. J. A Classification of Photochemical Reactions. *Acc. Chem. Res.* **1975**, *8* (2), 41–54. https://doi.org/10.1021/ar50086a001.

(16) Turro, N. J.; Dalton, J. C.; Dawes, K.; Farrington, G.; Hautala, R.; Morton, D.; Niemczyk, M.; Schore, N. Molecular Photochemistry of Alkanones in Solution: α-Cleavage, Hydrogen Abstraction, Cycloaddition, and Sensitization Reactions. *Acc. Chem. Res.* **1972**, *5* (3), 92–101. https://doi.org/10.1021/ar50051a002.

(17) Bull, J. A.; Croft, R. A.; Davis, O. A.; Doran, R.; Morgan, K. F. Oxetanes: Recent Advances in Synthesis, Reactivity, and Medicinal Chemistry. *Chem. Rev.* **2016**, *116* (19), 12150–12233. https://doi.org/10.1021/acs.chemrev.6b00274.

(18) Hoffmann, N. Photochemical Reactions as Key Steps in Organic Synthesis. *Chem. Rev.* **2008**, *108* (3), 1052–1103. https://doi.org/10.1021/cr0680336.

(19) Odom, S. a.; Ergun, S.; Poudel, P. P.; Parkin, S. R. A Fast, Inexpensive Method for Predicting Overcharge Performance in Lithium-Ion Batteries. *Energy Environ. Sci.* **2014**, *7* (2), 760. https://doi.org/10.1039/c3ee42305k.

(20) Prier, C. K.; Rankic, D. A.; MacMillan, D. W. C. Visible Light Photoredox Catalysis with Transition Metal Complexes: Applications in Organic Synthesis. *Chem. Rev.* **2013**, *113* (7), 5322–5363. https://doi.org/10.1021/cr300503r.

(21) Shaw, M. H.; Twilton, J.; MacMillan, D. W. C. Photoredox Catalysis in Organic Chemistry. *J. Org. Chem.* **2016**, *81* (16), 6898–6926. https://doi.org/10.1021/acs.joc.6b01449.

(22) Michelet, B.; Deldaele, C.; Kajouj, S.; Moucheron, C.; Evano, G. A General Copper Catalyst for Photoredox Transformations of Organic Halides. *Org. Lett.* **2017**, *19* (13), 3576–3579. https://doi.org/10.1021/acs.orglett.7b01518.

(23) Reiser, O. Shining Light on Copper: Unique Opportunities for Visible-Light-Catalyzed Atom Transfer Radical Addition Reactions and Related Processes. *Acc. Chem. Res.* **2016**, *49* (9), 1990–1996. https://doi.org/10.1021/acs.accounts.6b00296.

(24) Skubi, K. L.; Kidd, J. B.; Jung, H.; Guzei, I. A.; Baik, M. H.; Yoon, T. P. Enantioselective Excited-State Photoreactions Controlled by a Chiral Hydrogen-Bonding Iridium Sensitizer. *J. Am. Chem. Soc.* **2017**, *139* (47), 17186–17192. https://doi.org/10.1021/jacs.7b10586.

(25) Shields, B. J.; Kudisch, B.; Scholes, G. D.; Doyle, A. G. Long-Lived Charge-Transfer States of Nickel(II) Aryl Halide Complexes Facilitate Bimolecular Photoinduced Electron Transfer. *J. Am. Chem. Soc.* **2018**, *140* (8), 3035–3039. https://doi.org/10.1021/jacs.7b13281.

(26) Lim, C. H.; Kudisch, M.; Liu, B.; Miyake, G. M. C-N Cross-Coupling via Photoexcitation of Nickel-Amine Complexes. *J. Am. Chem. Soc.* **2018**, *140* (24), 7667–7673. https://doi.org/10.1021/jacs.8b03744.

(27) Ravetz, B. D.; Wang, J. Y.; Ruhl, K. E.; Rovis, T. Photoinduced Ligand-to-Metal Charge Transfer Enables Photocatalyst-Independent Light-Gated Activation of Co(II). *ACS Catal.* **2019**, *9* (1), 200–204. https://doi.org/10.1021/acscatal.8b04326.

(28) Huang, X.; Quinn, T. R.; Harms, K.; Webster, R. D.; Zhang, L.; Wiest, O.; Meggers, E. Direct Visible-Light-Excited Asymmetric Lewis Acid Catalysis of Intermolecular [2+2] Photocycloadditions. *J. Am. Chem. Soc.* **2017**, *139* (27), 9120–9123. https://doi.org/10.1021/jacs.7b04363.

(29) Trecker, D. J.; Foote, R. S.; Henry, J. P.; McKeon, J. E. Photochemical Reactions of Metal-Complexed Olefins. II. Dimerization of Norbornene and Derivatives. *J. Am. Chem. Soc.* **1966**, *88* (13), 3021–3026. https://doi.org/10.1021/ja00965a024.

(30) Salomon, R. G. Homogeneous Metal-Catalysis in Organic Photochemistry. *Tetrahedron* **1983**, *39* (4), 485–575. https://doi.org/10.1016/S0040-4020(01)91830-7.

(31) Salomon, R. G.; Folting, K.; Streib, W. E.; Kochi, J. K. Copper(I) Catalysis in Photocycloadditions. 11. Cyclopen Tene, Cyclohexene, and Cyclohep Tene. *Perspective* **1973**, No. I, 1145–1152.

(32) Budzellar, P. H. M.; Timmermans, P. J. J. A.; Mackor, A.; Baerends, E. J. Bonding in the Ground State and Excited States of Copper-Alkene Complexes. *J. Organomet. Chem.* **1987**, *331* (3), 397–407. https://doi.org/10.1016/0022-328X(87)80011-6.

(33) Sarkar, N.; Nayek, A.; Ghosh, S. Copper(I)-Catalyzed Intramolecular Asymmetric [2 + 2] Photocycloaddition. Synthesis of Both Enantiomers of Cyclobutane Derivatives. *Org. Lett.* **2004**, *6* (12), 1903–1905. https://doi.org/10.1021/ol049696h.

(34) Salomon, R. G.; Kochi, J. K. Cationic Olefin Complexes of Cop per(I). Structure and Bonding in Group Ib Metal-Olefin Complexes. *J. Am. Chem. Soc.* **1973**, *95* (6), 1889–1897. https://doi.org/10.1021/ja00787a031.

(35) Schwendiman, D. P.; Kutal, C. Catalytic Role of Copper(I) in the Photoassisted Valence Isomerization of Norbornadiene. *J. Am. Chem. Soc.* **1977**, *99* (17), 5677–5682. https://doi.org/10.1021/ja00459a025.

(36) Schwendiman, D. P.; Kutal, C. Transition Metal Photoassisted Valence Isomerization of Norbornadiene. An Attractive Energy-Storage Reaction.

Inorg. Chem. **1977**, *16* (3), 719–721. https://doi.org/10.1021/ic50169a047.

(37) Borsub, N.; Chang, S. C.; Kutal, C. Ligand Control of the Mechanism of Photosensitization by Copper(I) Compounds. *Inorg. Chem.* **1982**, *21* (2), 538–543. https://doi.org/10.1021/ic00132a015.

(38) Fife, D. J.; Moore, W. M.; Morse, karen W. Photosensitized Isomerization of Norbornadiene to Quadricyclane with (Arylphosphine)Copper(I) Halides. *J. Am. Chem. Soc.* **1985**, *107* (24), 7077–7083. https://doi.org/10.1021/ja00310a053.

(39) Grutsch, P. A.; Kutal, C. Photobehavior of Copper(I) Compounds. Role of Copper(I)-Phosphine Compounds in the Photosensitized Valence Isomerization of Norbornadiene. *J. Am. Chem. Soc.* **1979**, *101* (15), 4228–4233. https://doi.org/10.1021/ja00509a031.

(40) Grutsch, P. A.; Kutal, C. Use of Copper(I) Phosphine Compounds to Photosensitize the Valence Isomerization of Norbornadiene. *J. Am. Chem. Soc.* **1977**, *99* (19), 6460–6463. https://doi.org/10.1021/ja00461a059.

(41) Franceschi, F.; Guardigli, M.; Solari, E.; Floriani, C.; Chiesi-Villa, A.; Rizzoli, C. Designing Copper(I) Photosensitizers for the Norbornadiene-Quadricyclane Transformation Using Visible Light: An Improved Solar Energy Storage System. *Inorg. Chem.* **1997**, *36* (18), 4099–4107. https://doi.org/10.1021/ic9706156.

(42) Sterling, R. F.; Kutal, C. Photoconversion of Norbornadiene to Quadricyclene in the Presence of a Copper(I) Carbonyl Compound. *Inorg. Chem.* **1980**, *19* (6), 1502–1505. https://doi.org/10.1021/ic50208a016.

(43) Trofimenko, S. Recent Advances in Poly(Pyrazolyl)Borate (Scorpionate) Chemistry. *Chem. Rev.* **1993**, *93* (3), 943–980. https://doi.org/10.1021/cr00019a006.

(44) Eggleston, M. K.; McMillin, D. R.; Koenig, K. S.; Pallenberg, A. J. Steric Effects in the Ground and Excited States of Cu(NN)2+ Systems. *Inorg. Chem.* **1997**, *36* (2), 172–176. https://doi.org/10.1021/ic960698a.

(45) Shaw, G. B.; Grant, C. D.; Shirota, H.; Castner, E. W.; Meyer, G. J.; Chen, L. X. Ultrafast Structural Rearrangements in the MLCT Excited State for Copper(I) Bis-Phenanthrolines in Solution. *J. Am. Chem. Soc.* **2007**, *129* (7), 2147–2160. https://doi.org/10.1021/ja067271f.

(46) Gothard, N. A.; Mara, M. W.; Huang, J.; Szarko, J. M.; Rolczynski, B.;

Lockard, J. V.; Chen, L. X. Strong Steric Hindrance Effect on Excited State Structural Dynamics of Cu(I) Diimine Complexes. *J. Phys. Chem. A* **2012**, *116* (9), 1984–1992. https://doi.org/10.1021/jp211646p.

(47) LeCloux, D. D.; Tokar, C. J.; Osawa, M.; Houser, R. P.; Keyes, M. C.; Tolman, W. B. Optically Active and C3-Symmetric Tris(Pyrazolyl)Hydroborate and Tris(Pyrazolyl)Phosphine Oxide Ligands: Synthesis and Structural Characterization. *Organometallics* **1994**, *13* (7), 2855–2866. https://doi.org/10.1021/om00019a048.

(48) Scharf, D.; Korte, F. Photosensibilisierte Cyclodimerisierung von Norbornen. *Tetrahedron Lett.* **1963**, *4* (13), 821–823. https://doi.org/https://doi.org/10.1016/S0040-4039(01)90722-1.

(49) Arnold, D. R.; Hinman, R. L.; Glick, A. H. Chemical Properties of the Carbonyl n, π State. The Photochemical Preparation of Oxetanes. *Tetrahedron Lett.* **1964**, *5* (22), 1425–1430. https://doi.org/https://doi.org/10.1016/S0040-4039(00)90493-3.

Chapter 4

Intermolecular 2+2 Carbonyl-Olefin Photocycloadditions Enabled by a Cu(I)-Norbornene MLCT

4.1 Introduction

Nitrogen heterocycles are prevalent motifs in small molecule pharmaceuticals and their rapid construction continues to drive new reaction development.[1] While 3-, 5- and 6-membered N-heterocycles are exceptionally common with a variety of synthetically accessible routes for their construction, 4-membered heterocycles are scarce by comparison though azetidines display promising biological activity (**Figure 4.1**).[1–7] Additionally, azetidines are versatile synthetic intermediates readily undergoing ring-opening, ring-expansion, and ring-contraction reactions. Furthermore, enantiomerically pure azetidines have been implemented as either, ligands for metal catalyzed reactions or chiral auxiliaries.

Azetidines are one of the most challenging of the azaheterocycles to synthesize due to the inherent ring strain making ring closure significantly uphill energetically. Conventional methods rely on S_N2 displacement of a leaving group by nitrogen, limiting the scope of this approach as well as the generation of stoichiometric waste. Alternatively, these small heterocycles can be constructed through the cycloaddition of ketenes and imines to form β-lactams and subsequent reduction. However, this approach suffers from low *ee*'s and there can be problems associated with the reduction of other functional groups present in the molecule.

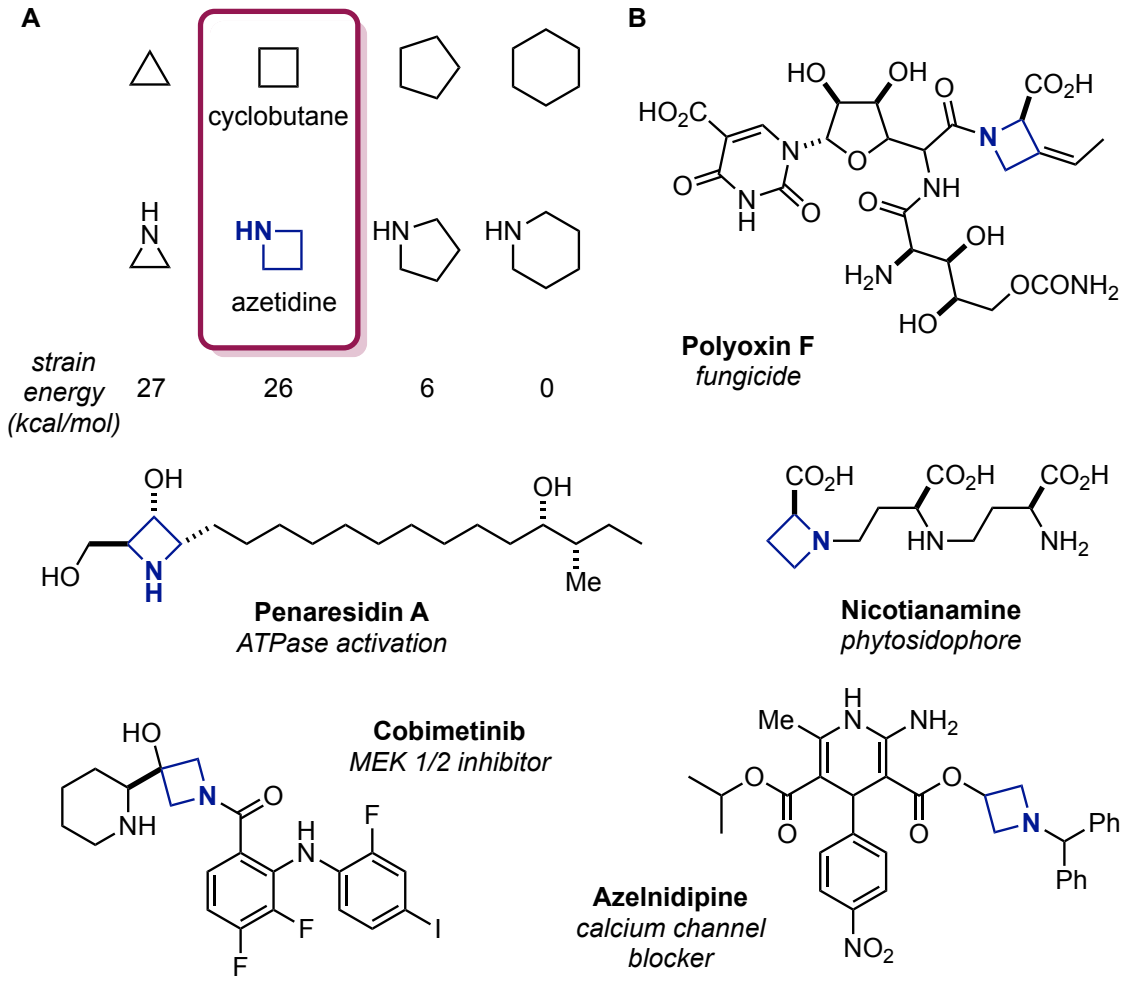

Figure 4.1 A. Relative ring strain between cyclic hydrocarbons and cylcic amines. **B.** Notable biologically active compounds that contain an azetidine.

The 2+2 photocycloaddition of two π-components a prototypical example of 4-membered ring construction. While limited, the Paternò-Büchi reaction forms oxetanes through direct irradiation of a carbonyl C=O double bond to access an excited state which is intercepted by a C=C double bond.[8–11] Analogously the Aza-Paternò-Büchi produces azetidines by replacement of the carbonyl unit with an

imine. Examples of such a transformation are exceptionally rare due to the excited state of imines preferentially undergoing radiationless decay upon rotation about the C=N π-bond. This low barrier E/Z isomerization leads to a loss of electronic energy and lack of reactivity in 2+2 photocycloadditions (**Figure 4.2**).[12] Successful

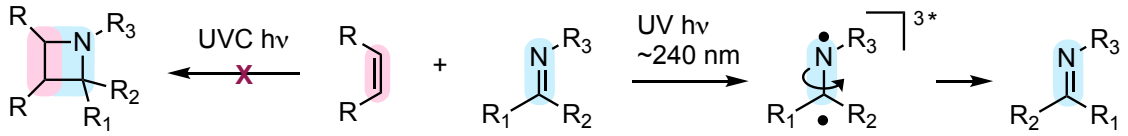

Figure 4.2 Direct imine excitation results in isomerization rather than new bond formation.

reports of an Aza- Paternò-Büchi reaction utilize cyclic imines or are limited to unique substrate pairings (**Figure 4.3**). Previous strategies to overcome this nonproductive pathway have used cyclic imines, preferential excitation of the C=C bond partner in an intramolecular setting, or both. Despite these advances, catalyst-controlled approaches to a 2+2 imine-olefin photocycloaddition (IOPC) remain limited as general strategies to azetidine synthesis. Based on the success of our COPC approach (see chapter 3) we hypothesized that a 2+2 IOPC may be achieved to access azetidines by coordination and MLCT through coordination of either the alkene or imine pi-component.

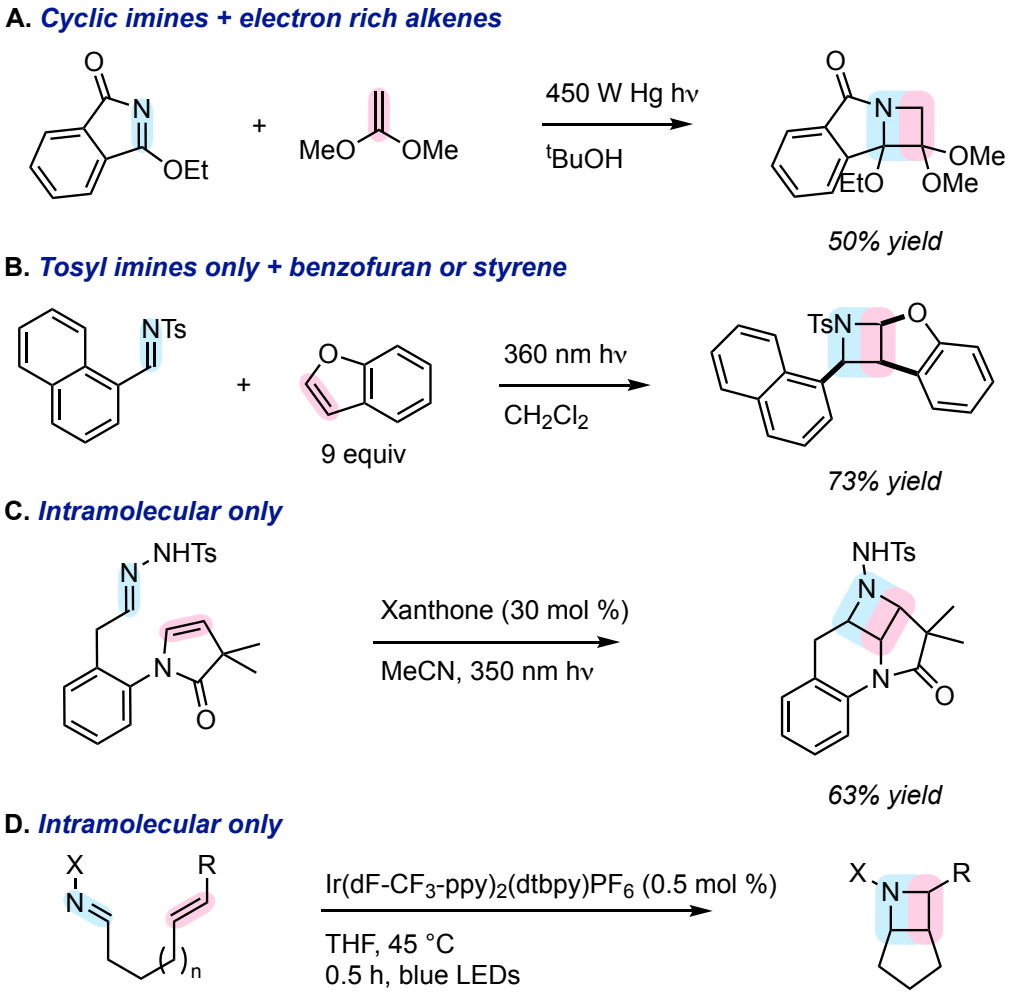

Figure 4.3 Previous examples of an Aza-Paternò-Büchi and stategries to overcome that overcome the nonproductive pathway of imine isomerization.

4.2 Reaction Screening and Optimization

To assess the validity of this hypothesis we irradiated a mixture of *N*-butyl-2-methylporpan-1-imine (1 equiv), norbornene (3 equiv), and **TpCu** (0.2 equiv) in diethyl ether using a 100 W Hg lamp for 8 h. This resulted in formation of the corresponding azetidine **1** in 31% yield as a 52:48 diastereomeric mixture at the C2 position. Removing **TpCu** or conducting the reaction in the dark both resulted

in no appreciable formation of azetidine 1. Similar control experiment for the selective removal of either the imine, norbornene, or a Cu source also resulted in azetidine formation not being detected. Lowering the catalyst loading below 20 mol % resulted in diminished yields, while increasing it to 40 mol % lead to a modest increase in reaction yield. Making the imine the limiting reagent and increasing the equivalencies of norbornene significantly reduced reaction efficiency. Increasing the equivalencies of the imine to three resulted in 79% isolated yield of azetidine **1**. Decreasing the concentration of the reaction below 0.15 M lead to longer reaction times and lower yields. Increasing the concentration above 0.15 M did not result in shorter reaction times, but moderately lower overall yields. Combining $Cu(OTf)_2$ and KTp in an equimolar ratio produced the desired product in <10% yield (entry 21). Exchanging CuOTf with various isoelectronic triflate salts or triflic acid did not lead to product formation (entries 22-25).

Throughout these optimizations a deep blue coloring of the products was routinely observed, attributed to the presence of Tp_2Cu as a byproduct. This NMR silent byproduct results from the degradation of **TpCu** when exposed to molecular oxygen. Removal of this material was achieved through concentration of the reaction mixture, and extracting the azetidine product with methanol, eliminating the need for purification by chromatography.

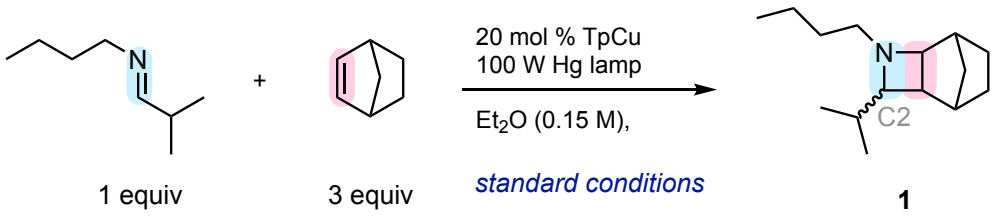

entry	deviation from standard conditions	reaction time (h)	yield of 1
1	None	24	55%
2	No **TpCu**	24	*n.d.*
3	No light	24	*n.d.*
4	No imine	24	*n.d.*
5	No norbornene	24	*n.d.*
6	No Cu source, KTp	24	*n.d.*
7	No Tp source, CuOTf	24	*n.d.*
8	CuOTf +KTp (20 mol % each)	24	28%
9	2.5 mol % **TpCu**	32	33%
10	5 mol % **TpCu**	24	36%
11	10 mol % **TpCu**	24	51%
12	40 mol % **TpCu**	24	80%
13	2 equiv. Norbornene (+ 1 equiv imine)	24	64%
14	3 equiv. Norbornene (+ 1 equiv imine)	24	31%
15	3 equiv imine	24	79%
16	5 equiv imine	24	85%
17	0.01 M	48	10 % conversion
18	0.05 M	36	39%
19	0.30 M	24	40%
20	0.50 M	24	32%
21	$Cu(OTf)_2$ + KTp (10 mol% each)	24	<10%
22	AgOTf + KTp (10 mol% each)	24	n.d.
23	$Zn(OTf)_2$ + KTp (10 mol% each)	24	n.d.
24	$Sc(OTf)_3$ + KTp(10 mol% each)	24	n.d.
25	1 mol% Triflic acid	24	n.d.

Figure 4.4 Reaction optimization for the 2+2 IOPC

4.3 Scope of Imine-Olefin Photocycloaddition

In exploration of imines that similarly undergo Cu-catalyzed 2+2 IOPC with norbornene, we found that aldimines from *N*-allyl amine and isobutyraldehyde, 3-

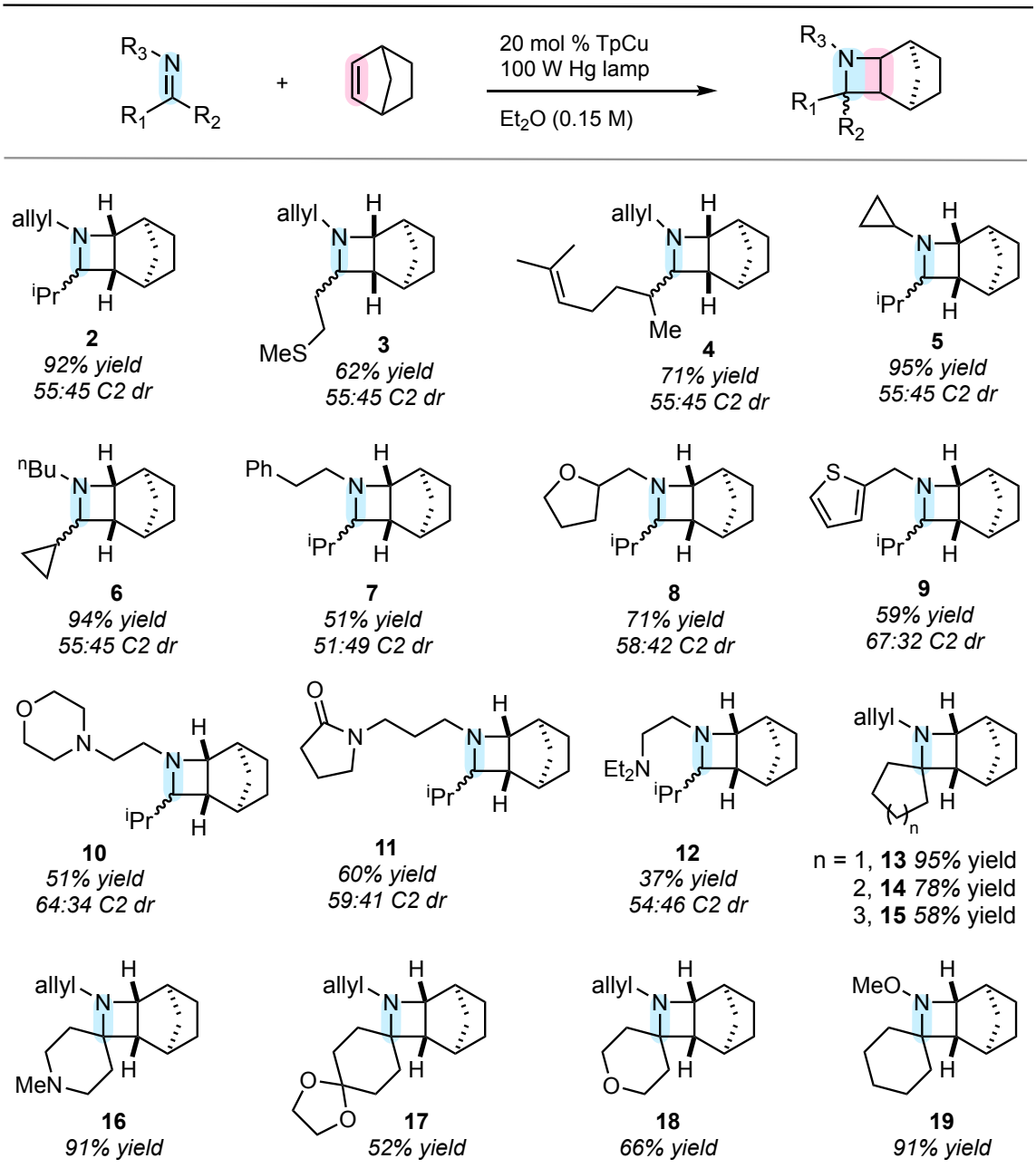

Figure 4.5 Scope of the 2+2 IOPC. For specific reaction conditions see section 4.6

(methylthio)propanal, and melonal all successfully were converted to their

corresponding azetidines, **2**, **3**, and **4**, respectively, in good to excellent yields (**Figure 4.5**). We also prepared and subjected both *N*-cyclopropyl isopropyl imine and *N*-butyl cyclopropyl imine, to our 2+2 IOPC conditions and exclusively observed the formation of corresponding azetidines, **5** and **6** in 95% and 94% yield, respectively. Cyclopropyl ring-opened products were not detected in either case, suggesting that if localized C- or N-centered radicals were formed, their lifetimes were shorter than the rate of cyclopropyl aminyl radical (8×10^7 s^{-1} at 50 °C)[13] or cyclopropyl C-centered radical (1.3×10^8 s^{-1} at 25 °C) openings.[12]

While imines derived from acetophenone, benzaldehyde, or anilines did not participate in this 2+2 IOPC, a phenethylamine derived isobutyraldimine, produced azetidine **7** in 51% yield as a 51:49 mixture of diastereomers at C2, suggesting that arene groups are tolerated when not conjugated to the imine. Altering the identity of the N-substituent of the imine demonstrated that tetrahydrofuran (**8**, 71% yield), thiophene (**9**, 59% yield), morpholine (**10**, 51% yield), and γ-lactam (**11**, 60% yield) groups were tolerated. Productive 2+2 IOPC was particularly notable in the presence of an amide remaining intact in azetidine **11**, showcasing the chemoselectivity of olefin activation even in the presence of other π-components capable of absorbing UV light. An acyclic, 3° amine was similarly carried through the 2+2 IOPC process, producing **12** in 51% yield. Imines derived from ketones also reacted efficiently to produce the corresponding azetidines even when the imine also contained a Lewis-basic 3° amine, acetal, or ether functionalities (compounds **13**-**18** in 52-95% yield). Cyclohexanone *O*-methyl oxime also

performed well as an imine component, delivering the corresponding *N*-methoxy azetidine **19** in 92% yield.

Biologically active azetidines such as penaresidin A, nicotianamine,

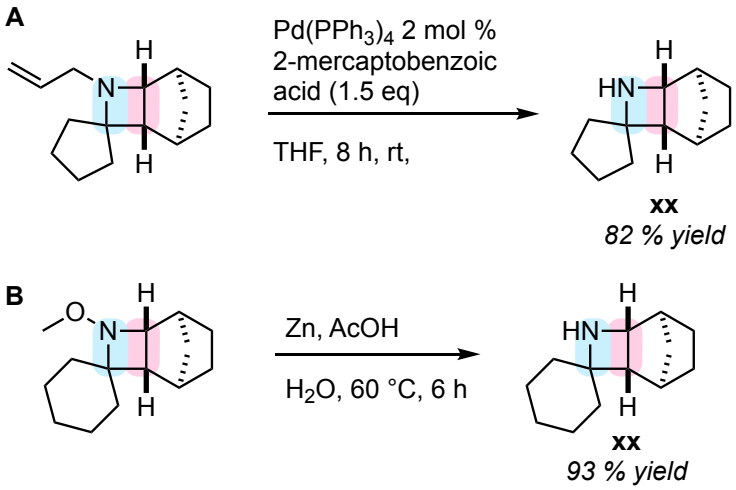

Figure 4.6 A Deallylation to reveal secondary azetidine. **B** Reductive N-O bond cleavage to reveal secondary azetidine.

medicanine, and mugineic acid feature *N*-alkyl groups or are unsubstituted at nitrogen, but access to these 2° azetidines can be challenging using existing cyclization methods that require the removal of stubborn protecting groups or require *N*-substituents that are not amenable to cleavage. However, this Cu-catalyzed 2+2 IOPC is uniquely capable of engaging *N*-alkyl imines. *N*-Allyl azetidine **13** underwent deallylation to reveal the corresponding 2° azetidine in 82% yield using 2 mol % $Pd(PPh_3)_4$ and 2-mercaptobenzoic acid. Similarly, *N*-methoxy azetidine **19** underwent reductive N-O bond cleavage using activated Zn dust in aqueous acetic acid to provide the corresponding unsubstituted azetidine in 93% yield (**Figure 4.6**).

The olefin component can also be diversified in this Cu-catalyzed 2+2 IOPC process (Scheme 3). Norbornenes containing acetyl (**20**, 95% yield), vinyl (**21**, 85% yield and **22**, 82% yield), cyano (**23**, 47% yield), and *tert*-butyldimethyl silyl ether (**24**, 91% yield) groups were successfully coupled with *N*-allyl cyclopentanimine. The identity of azetidine **22** was additionally confirmed through determination of the solid-state structure of its hydroiodic salt using X-ray diffraction (**Figure 4.8**).

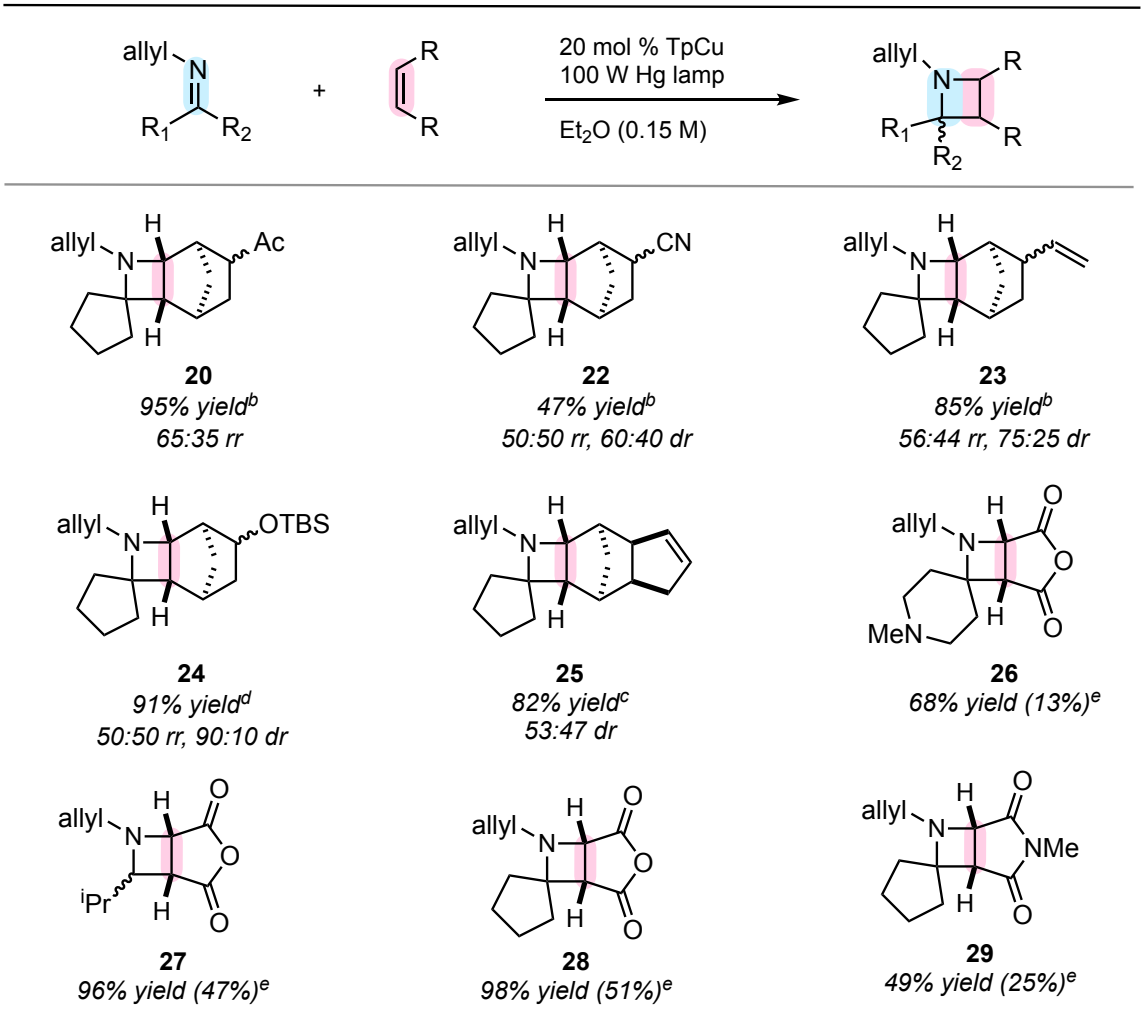

Figure 4.7 Scope of the 2+2 IOPC. For specific reaction conditions see section 4.6

Maleic anhydride is known to undergo selective cyclobutene forming 2+2 photocycloaddition with ethylene using acetophenone as a photosensitizer.[14] Direct excitation of maleic anhydride with *N*-allyl cyclopentanimine resulted in the formation of azetidine **25** in 51% yield along with numerous other unidentified byproducts. Subjecting the same reactant pair to irradiation in the presence of 20 mol % **TpCu** resulted in the formation of **25** in 98% yield without the previously observed byproducts as determined by GC-MS analysis. Similarly, *N*-allyl cyclohexanimine, *N*-allyl-1-methylpiperidin-4-imine, and *N*-allyl-2-methylpropan-1-imine were converted to their corresponding azetidines with maleic anhydride but the use of **TpCu** dramatically increased reaction efficiencies (**26**, 84% vs. 43%; **27**, 68% vs. 13%; and **28**, 96% vs. 47% yield, respectively). *N*-Methyl maleimide was also successfully converted to the corresponding azetidine **29** with *N*-allyl cyclopentanimine in 49% yield (**Figure 4.7**).

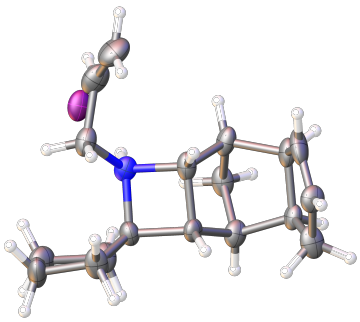

Figure 4.8 Solid state structure of azetidine **25-HI**

A specific subclass of substrates containing N-heterocycles as well as α-imino esters were found to be incompatible with this 2+2 IOPC chemistry. A wide range of simple olefins were screened under the optimized conditions (see chapter 3.3) but this reactivity remained unique to norbornene and its derivatives, maleic anhydride, and maleimide. Particularly noteworthy was the lack of reactivity observed with ethylene, 4-cyclopentene-1,3-dione, and 1,4-benzoquinone (**Figure 4.9**). The reasons for the lack of reactivity for each of these cases will be discussed in the following section.

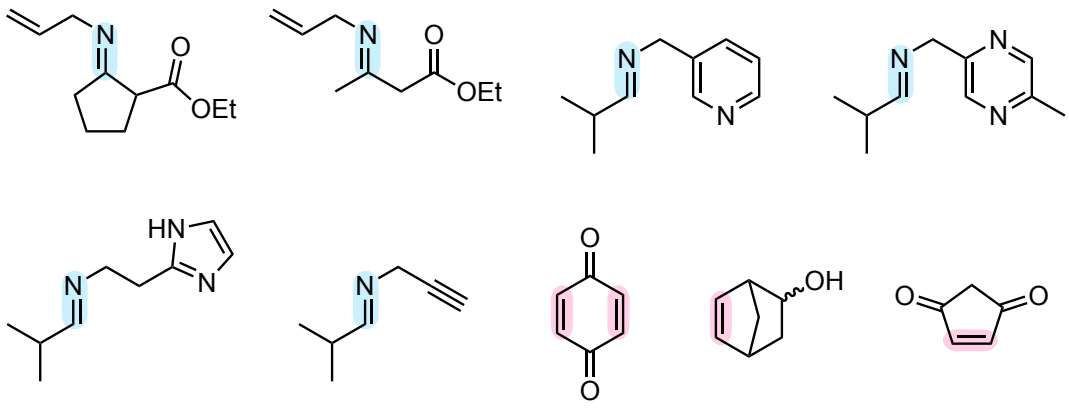

Figure 4.9 Unsuccesfull substrates screened in the 2+2 IOPC optimized conditions

4.4 Mechanistic Investigation

4.4.1 UV-vis Spectroscopy

In our Cu-mediated 2+2 carbonyl-olefin photocycloaddition studies we observed that norbornene coordination to **TpCu** was necessary for oxetane formation. We initially hypothesized that this 2+2 IOPC could occur through activation of either the imine or alkene and set out to assess this using a

combination of electronic absorption and NMR spectroscopies. We collected the electronic absorption spectra of diethyl ether solutions of **TpCu** (green line, **Figure 4.10**) and an equimolar mixture of **TpCu** and imine **1**. Addition of the imine produces a broad absorption feature with a maximum at 274 nm, suggesting the formation of a new species in solution. Similarly, an ethereal solution of **TpCu** and norbornene (1:1 molar ratio, pink line) has a broad absorption feature with a maximum at 272 nm, suggesting coordination in solution. A 1:1:1 mixture of **TpCu**,

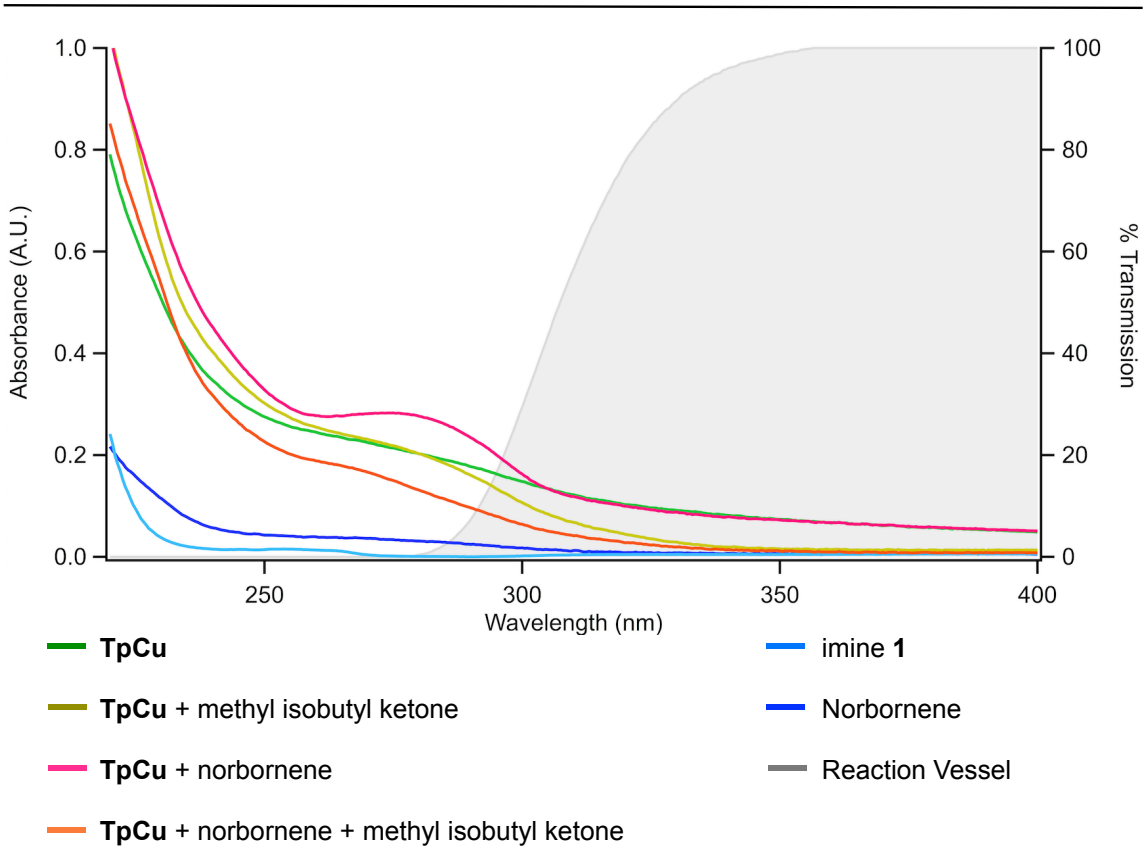

Figure 4.10 Electronic absorption spectra. All samples were collected at 0.5 mM in diethyl ether and as equimolar mixtures of the compounds indicated with each component being 0.5 mM. The transmission spectrum of the reaction vessels used in this study is overlaid for reference (right vertical axis).

norbornene, and imine **1** (orange line) does not resemble any one species, but a mixture of the two.

The analogous spectroscopic experiments were conducted by replacing norbornene with maleic anhydride (**Figure 4.11)**. A solution of a stoichiometric mixture of **TpCu** and maleic anhydride (pink line) results in an electronic absorption spectrum displaying a new broad feature with a maximum at 263 nm, which is very similar to the spectrum observed of **TpCuNB**, and is nearly identical to the spectrum of a stoichiometric mixture of **TpCu**, maleic anhydride and *N*-butyl

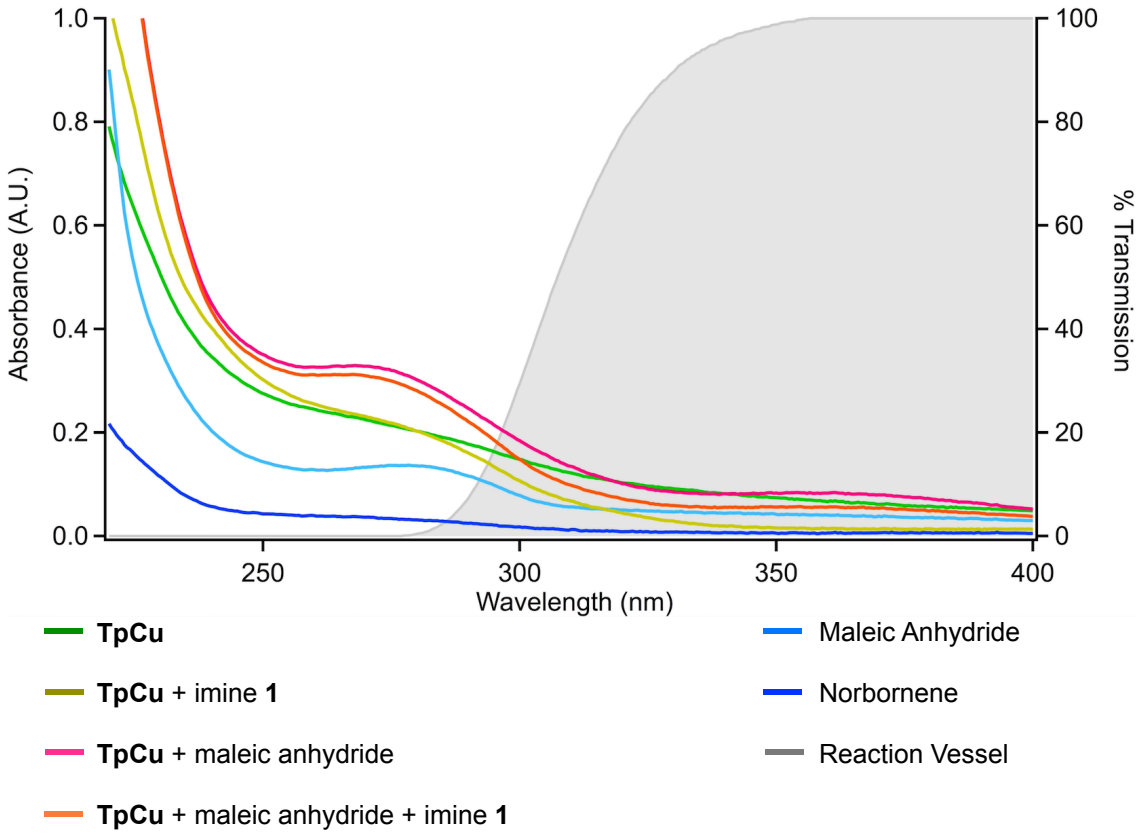

Figure 4.11 Electronic absorption spectra. All samples were collected at 0.5 mM in diethyl ether and as equimolar mixtures of the compounds indicated with each component being 0.5 mM. The transmission spectrum of the reaction vessels used in this study is overlaid for reference (right vertical axis).

isobutylimine (orange line). While neither *N*-butyl isobutylimine (dark blue line) or norbornene has significant absorptions above 250 nm, maleic anhydride (light blue line) does, which explains why a small amount of background photochemistry was observed with this alkene. The transmission spectrum of the borosilicate glass reaction vessels used in this study (grey shading) shows that light below 280 nm is effectively filtered from reaching the reaction mixture and suggests that azetidine forming absorptions occur at wavelengths longer than 280 nm. Combined with the 300 nm cut-on filter results (Table 1, entry 6), this supports that azetidine formation predominately occurs from excitation between 280-300 nm.

4.4.2 NMR Spectroscopy

The corresponding NMR coordination experiments were in line with the electronic absorption data. **TpCu** displays three distinct proton signals (**Figure 4.12**, spectrum C). A mixture of **TpCu** and imine **1** results in the downfield shift from 7.10 to 7.20 ppm of the proton at the C3 pyrazole position as well as an upfield shift from 7.33 to 6.93 ppm of the vinyl imine proton, suggesting imine coordination to **TpCu**. In the presence of norbornene a Cu-olefin complex is formed as evidenced by the downfield chemical shift change from 7.10 to 7.43 ppm of the proton at the C3 pyrazole position and a broadening of the signals of norbornene. The ^{1}H NMR spectrum of a 1:1:1 ratio of **TpCu**, imine 1, and norbornene shows the averaging of these, suggesting that norbornene and imine 1 readily exchange

in solution. From this data it is inconclusive to say which species leads to azetidine formation upon excitation.

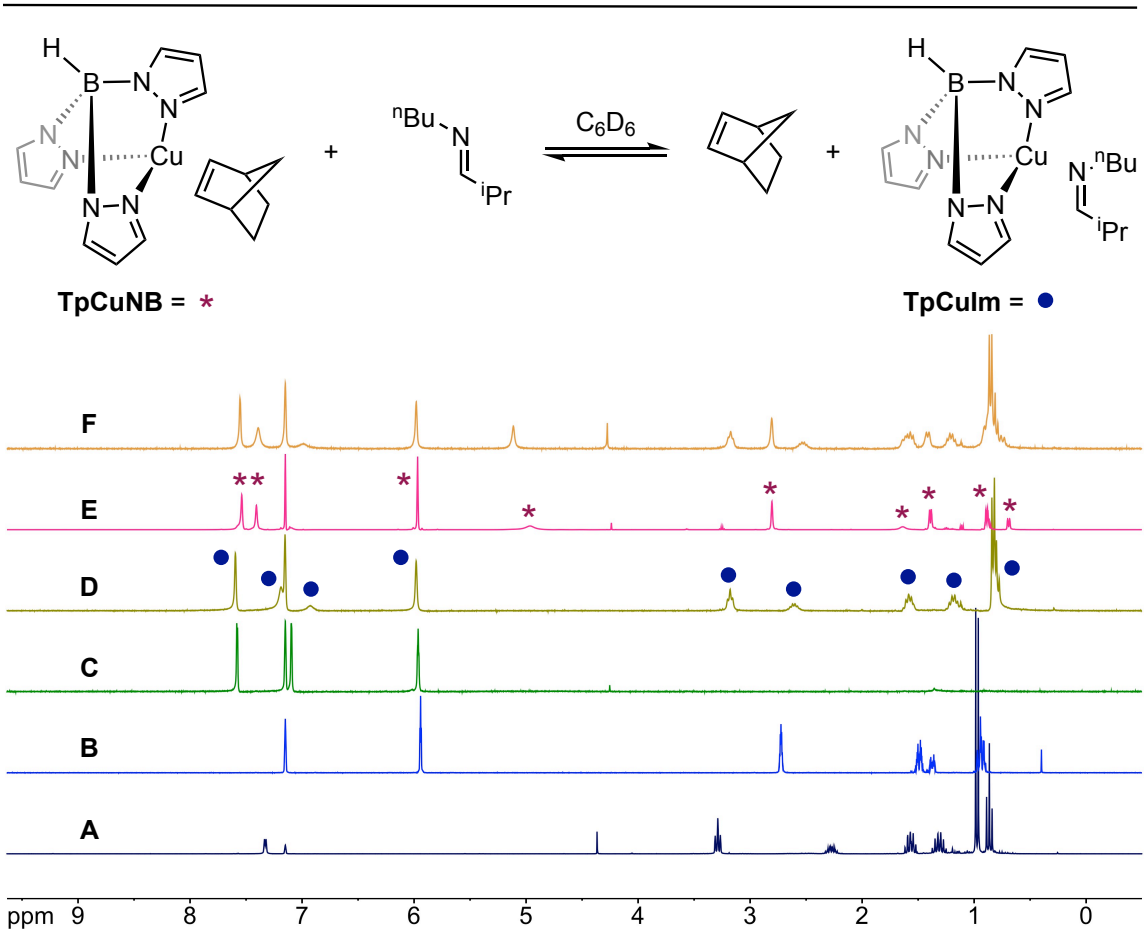

Figure 4.12 ^{1}H-NMR spectrum of reaction components. All samples were prepared in benzene-d_6. All mixing experiments were done in equimolar ratios. Spectrum A = imine **1**. Spectrum B = norbornene. Spectrum C = **TpCu**. Spectrum D = **TpCu** + imine 1. Spectrum E = **TpCu** + norbornene. Spectrum F = **TpCu** + imine 1 + norbornene.

When observed by ^{1}H-NMR a stoichiometric mixing experiment of maleic anhydride and **TpCu** (**Figure 4.13**) resulted in a downfield shift of the proton on the C5 position of the pyrazole of **TpCu**, from 7.10 ppm to 7.33 ppm, as well as the broadening and upfield shift of the vinylic protons of maleic anhydride from 5.59 to 4.89 ppm, suggesting the formation of a **TpCuMA** olefin adduct**.** The

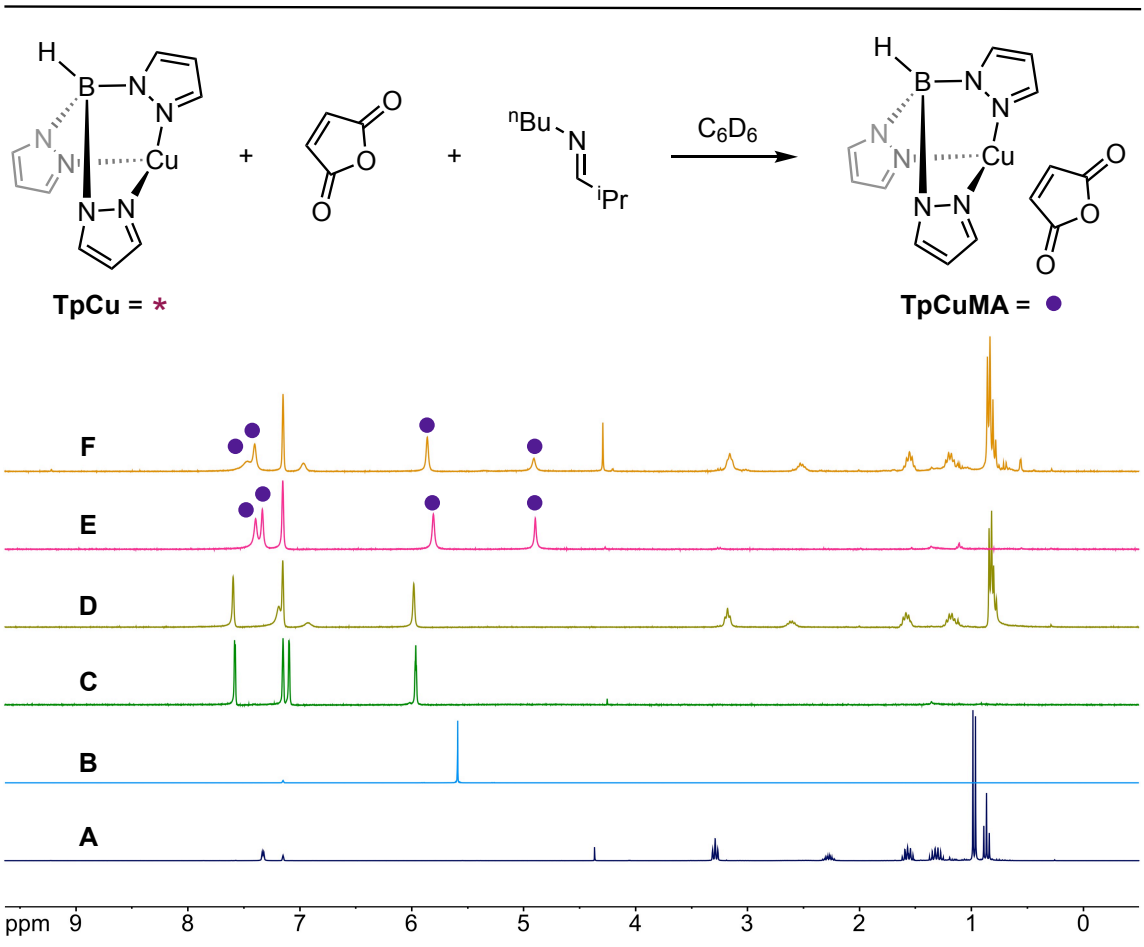

Figure 4.13 ^{1}H-NMR spectrum of reaction components. All samples were prepared in benzene-d_6. All mixing experiments were done in equimolar ratios unless otherwise noted. Spectrum A = imine **1**. Spectrum B = maleic anhydride. Spectrum C = **TpCu**. Spectrum D = **TpCu** + imine **1**. Spectrum E = **TpCuMA**. Spectrum F = **TpCu** (0.1 equiv) + maleic anhydride (1.0 equiv) + imine **1** (3.0 equiv).

addition of one equivalent of imine **1** does not result in the shifting of proton signals associated with **TpCuMA** or the imine itself. This suggests that **TpCuMA** is formed in solution and is the resting state species of the system.

4.4.3 X-ray Crystallography

Significant effort was spent attempting to isolate and characterize **TpCuNB** and **TpCuMA**. An equimolar mixture of **TpCu** and norbornene in THF afforded **TpCu-NB** as a white crystalline solid in 87% yield and report herein the solid-state structure of **TpCu-NB** as determined by single crystal X-ray diffraction. The coordination geometry of the complex is best described as pseudo-tetrahedral about the Cu-ion. The carbon-carbon bond distance of the coordinated olefin of 1.387 Å is similar to that found in other Cu(I)-norbornene compounds (1.36-1.39 Å).[12,15–17] These relatively short carbon-carbon bond distances of Cu(I)-olefin complexes suggest that σ-bonding, rather than π-back-bonding, is the predominant metal-olefin coordination interaction. Examination of the Cu-N(pyrazolyl) bond distances reveal that while two were nearly equivalent (Cu-N(2) = 1.999(2), Cu-N(4) = 2.010(2)), the third was significantly longer (Cu-N(6) = 2.274(2)), breaking the C_3 symmetry axis of the hydrotris(pyrazolyl)borate chelate.

The solid-state structure of **TpCuMA** was determined by single crystal X-ray diffraction (**Figure 4.14**), which confirmed its identity. The coordination geometry of the complex is analogous to that of **TpCuNB**. While the 1.390 Å carbon-carbon bond length of the coordinated maleic anhydride is elongated

compared to the free olefin (1.3032 Å),[18] compared to the only one other reported, structurally characterized Cu(I)-maleic anhydride compound supported by an iminophosphanamide chelate with an 1.49 Å olefin C-C bond distance,[19] it still suggests that the bonding in **TpCuMA** is analogous to that observed in **TpCuNB**.

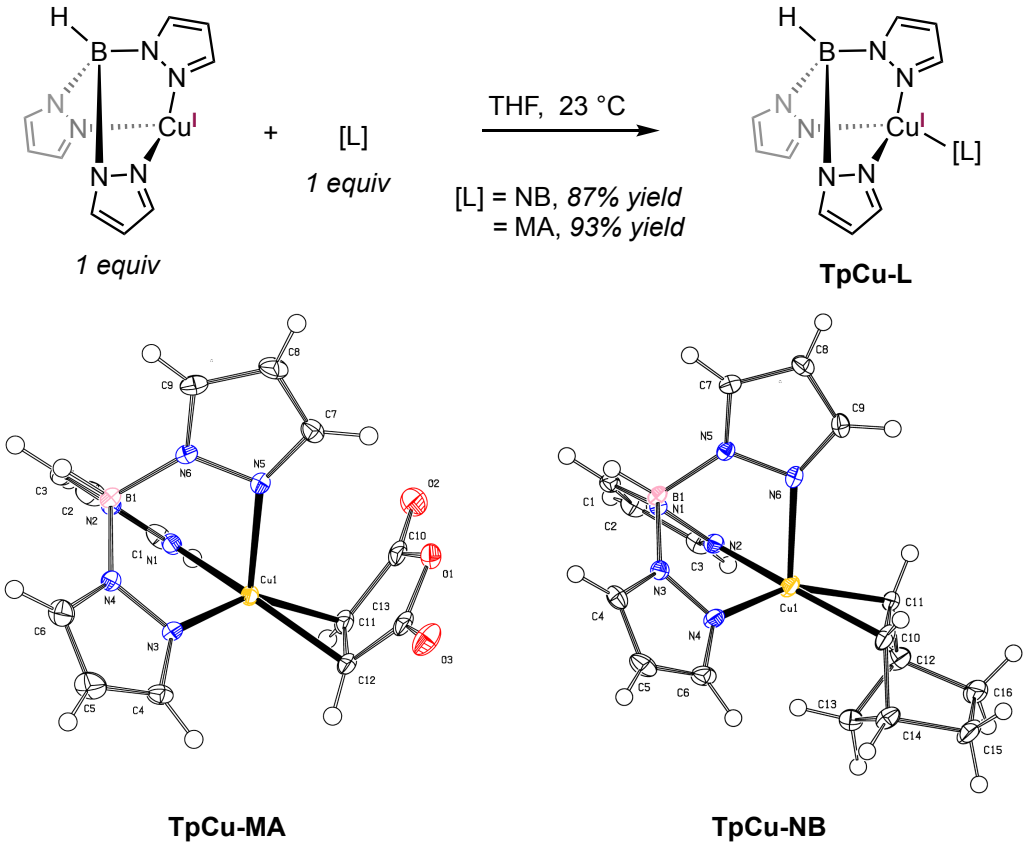

Figure 4.14 Preparation of **TpCuMA** and **TpCuNB** with their respective ORTEP plots.

4.4.4 Stern-Volmer Luminescence Quenching

Stern-Volmer luminescence quenching studies were carried out to determine if there is an intermolecular deactivation pathway within this system.

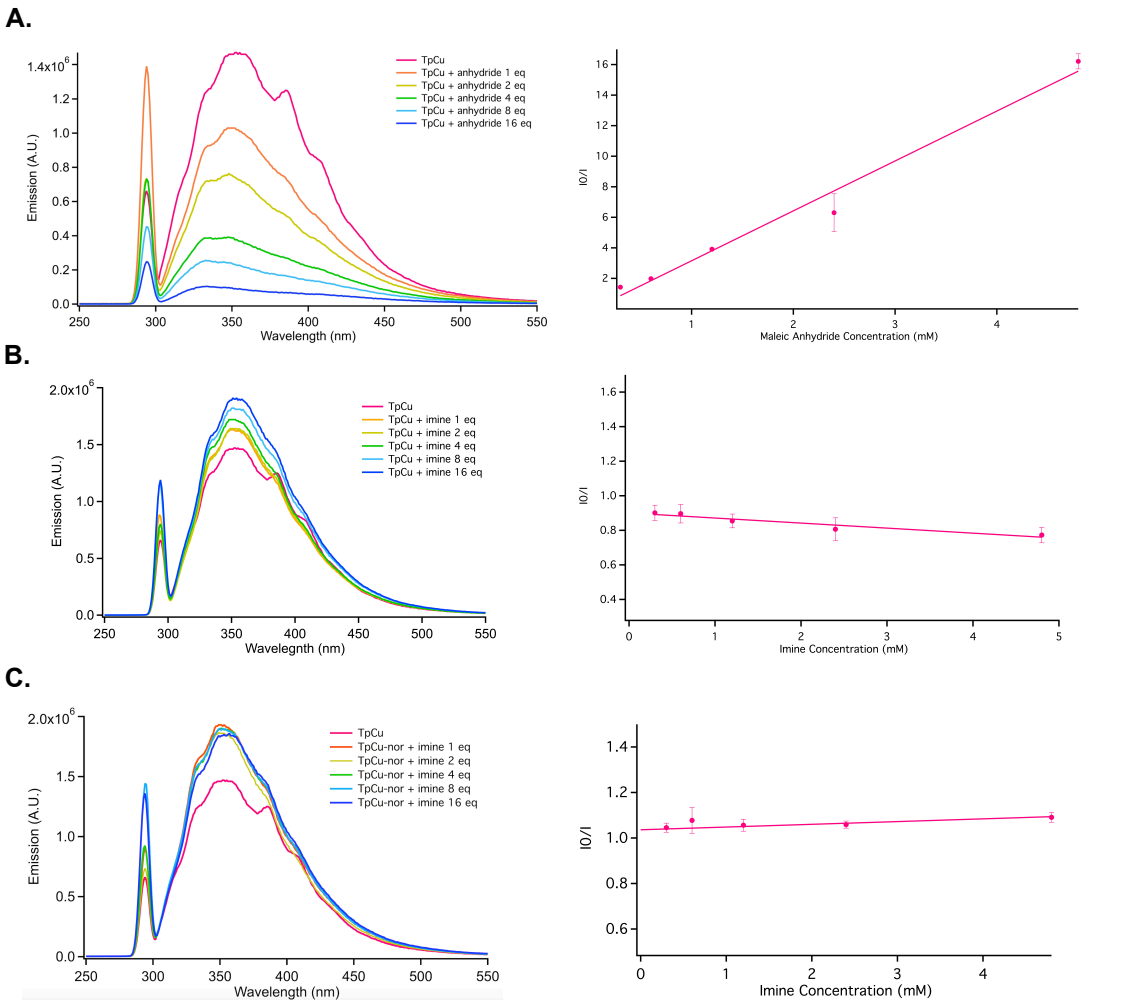

Figure 4.15 A. Emission plot and Stern-Volmer plot of **TpCu** with varying concentration of maleic anhydride. **B.** Emission plot and Stern-Volmer plot of **TpCu** with varying concentration of N-isobutylidenebutylamine **C.** Emission plot and Stern-Volmer plot of **TpCuNB** with varying concentration of N-isobutylidenebutylamine

The data did not exhibit a linear relationship between the concentration of additional norbornene or imine in the presence of **TpCu** (**Figure 4.15**). This suggests the 2+2 IOPC does not proceed through sensitization; however, the absence of a linear quenching relationship does not definitively exclude the possibility that an additional sensitization process may contribute to azetidine formation. Conversely, when the olefin is maleic anhydride there is a clear linear

relationship between maleic anhydride concentration and luminescence quenching. This indicates that the catalyst **TpCu** can act as a photosensitizer for maleic anhydride (**Figure 4.15 A**).

4.4.5 Mechanistic Proposal

A mechanistic proposal in-line with the spectroscopic data involves alkene coordination to the Cu(I)-center followed by MLCT (**Figure 4.16**). Full-molecule density functional theory (DFT) calculations of **TpCuNB** were conducted at the M11 level of theory as it most accurately matched the experimentally obtained electronic absorption spectrum of **TpCuNB**, (see Chapter 4.4.1) and was used to construct qualitative molecular orbital diagrams for **TpCuNB**. As shown in **Figure 4.16 A** the highest occupied molecular orbital (HOMO) and the lowest unoccupied molecular orbital (LUMO) of **TpCuNB** are predominately **TpCu**-based and olefin(π^*)-based orbitals, respectively. This supports prior DFT calculations that concluded that MLCT of idealized cationic Cu(I)-ethylene compounds is responsible for the observed cyclobutane forming 2+2 photocycloadditions.[20] This excited state selectively captures the imine C=N group affording the azetidine product analogously to our previously reported 2+2 COPC process.[21] We attribute the chemoselectivity of azetidine formation over alkene dimerization pathways to the known rapid rates of C-centered radical addition to C=N double bonds (6×10^6 – 1×10^8 s^{-1} at 80 °C)[22] and preference over alkene addition.[23] The exact nature of the penultimate intermediate is not well known and highly speculated on. It is

reasonable to think that after addition into the imine there is a pendent N-centered radical that can cyclize to produce the final azetidine product. Alternatively, back electron transfer from Cu could produce a 1,4-biradical that could recombine to form the corresponding azetidine. A second possibility is that instead of a pendent radical, a Cu(III) metallocycle is generated and reductive elimination affords the

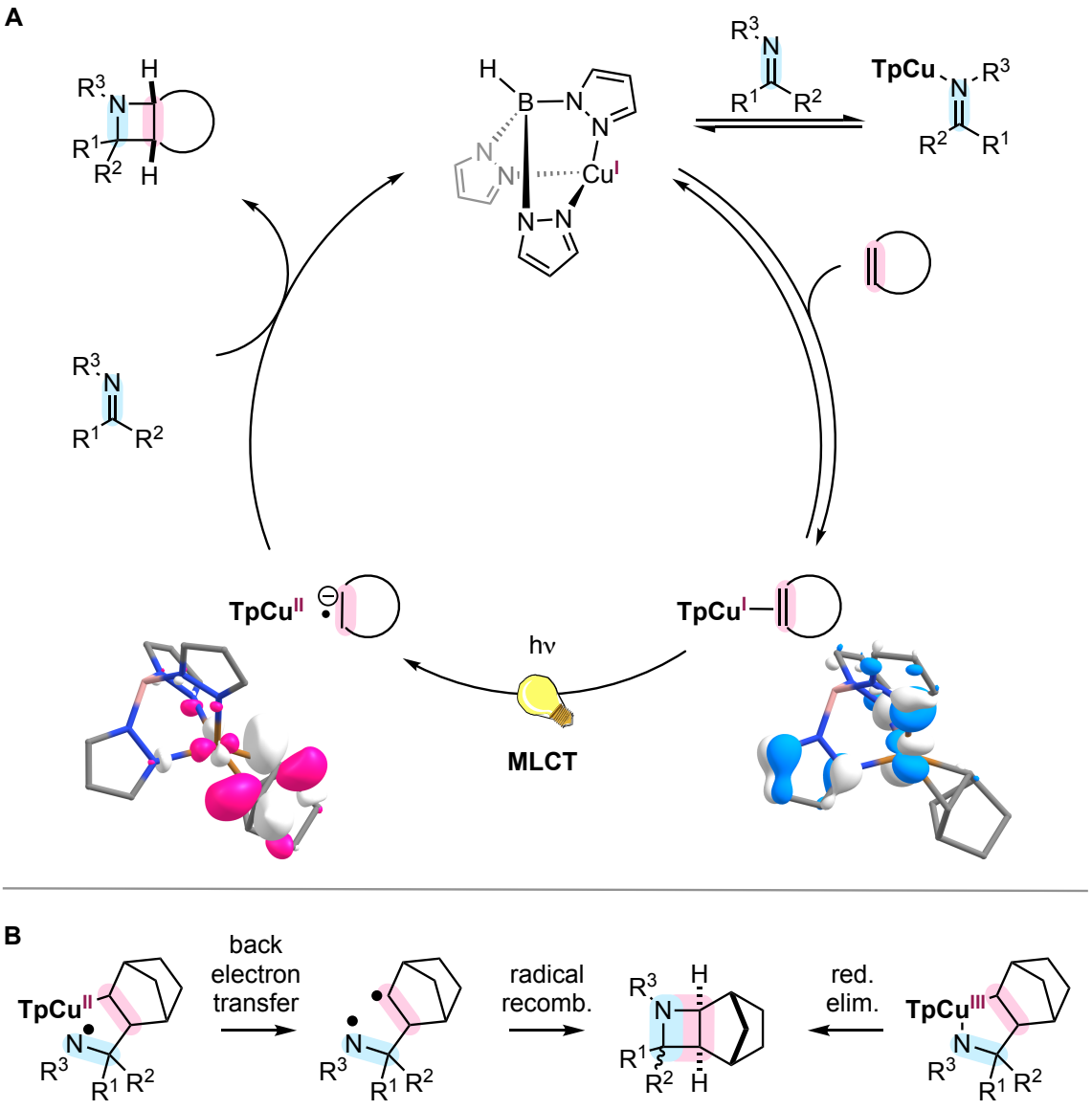

Figure 4.16 A. Proposed mechanism for the 2+2 IOPC. **B.** Possible pathways for cyclization.

azetidine (**Figure 4.16 B**). We have no data to support or disprove any of these possibilities.

4.5 Exchange Studies

During our mechanistic studies it was evident multiple substrates have the capability of coordinating to **TpCu**. We were interested in determining the spectrochemical series for this system and if other common ligands would coordinate. As previously described, through ^{1}H-NMR it was observed that when imine 1 was added to solution of **TpCuMA** the alkene was not displaced. Conversely, when imine 1 was added to a solution of **TpCuNB** an averaging of

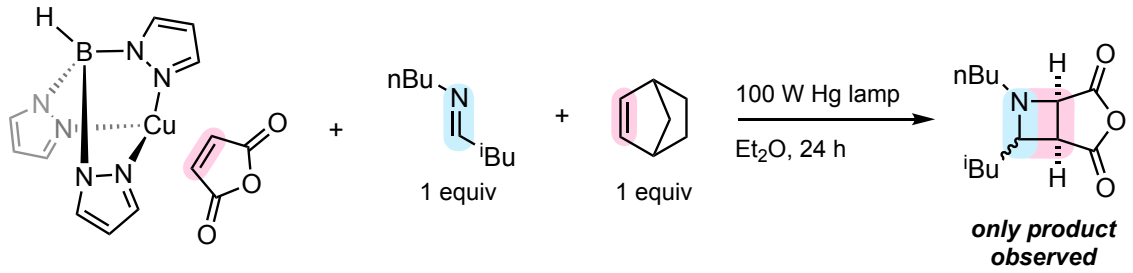

Figure 4.17 Cross-over experiment using 1.0 equivalents of **TpCuMA**, N-isobutylidene butylamine, and norbornene.

signals was observed, suggesting rapid ligand exchange. Due to this observed trend a cross-over experiment was conducted where an equimolar mixture of **TpCuMA**, norbornene, and imine **1** was irradiated for 24 h. Only azetidine **27** was detected by GC-MS and ^{1}H-NMR and not the corresponding product containing norbornene (**1**) (**Figure 4.17**). Initially, this supported the hypothesis that olefin coordination to the metal center is required for productive photochemistry to occur.

However, subsequent ^{1}H-NMR dosing experiments revealed norbornene has the capability of displacing maleic anhydride even when starting from **TpCuMA.**

We conducted several displacement reactions by subjecting **TpCuMA** to a variety of different ligands. Triphenylphosphine and N,N-dimethylaminopyridine (DMAP) readily displace the olefin to provide the corresponding adducts which were confirmed by single X-ray diffraction.

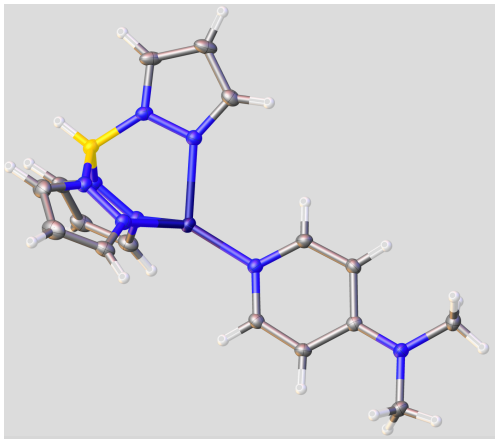

TpCuDMAP

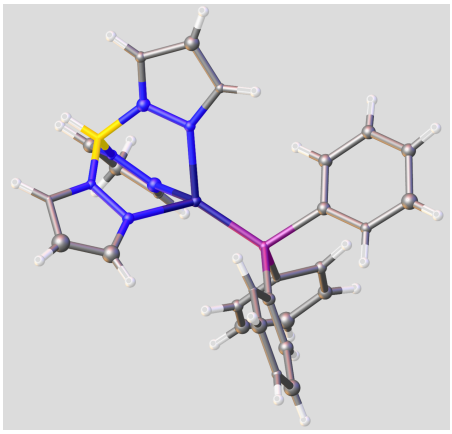

TpCuPPh$_3$

Figure 4.18 Solid state structures for TpCuDMAP and TpCuPPh$_3$.

Isonitriles were also observed to displace maleic anhydride, but we were unable to obtain suitable crystals for X-ray diffraction. Ligands unable to displace maleic anhydride included alcohols, nitriles, and alkynes.

4.6 Conclusions

Herein we present the first intermolecular 2+2 photocycloaddition of aliphatic imines and alkenes to form azetidines. The use of

hydrotris(pyrazolyl)borate copper(I) as a pre-catalyst allows for coordination of the olefin component and selective absorption of light 280-300 nm, enabling remarkable chemoselectivity and functional group tolerance. A combination of solution ^{1}H NMR and electronic absorption spectroscopies with DFT calculations from solid-state structural information supports that Cu(*d*) to olefin(π^*) MLCT leads to azetidine formation. This work highlights a catalyst controlled 2+2 imine-olefin photocycloaddition strategy that selectively activates π-components at red-shifted wavelengths compared to uncoordinated substrates and produce synthetically challenging azetidines.

4.7 Acknowledgements

Permission to include unpublished results are reported here in, and are currently in preparation as manuscript by Flores, D. M., Neville, M. L., Schmidt, V. A. The dissertation author is the primary author of this manuscript.

4.8 Synthetic Procedures and Characterization Data

General Considerations. All air- and moisture-sensitive manipulations were carried out using standard high vacuum line, Schlenk or cannula techniques or in an M. Braun inert atmosphere drybox containing an atmosphere of purified nitrogen. Solvents for air- and moisture-sensitive manipulations were dried and deoxygenated using literature procedures.[24]

^{1}H and ^{13}C NMR were recorded on Bruker 300 MHz or Varian 500 MHz spectrometers at 300 and 126 MHz, respectively. All chemical shifts are reported relative to $SiMe_4$ using ^{1}H (residual) chemical shifts of the solvent as a secondary standard. GC analyses were performed using an Agilent Technologies 7890B gas chromatograph equipped with an Agilent 7693 autosampler and Agilent HP-5 capillary column (30 m x 0.320mm x 250μm). Standard method parameters: 1.2 mL/min flow rate with oven program 80 – 250 °C with a ramp rate of 25 °C/min and hold time of 8.7 minutes at 250 °C. High-resolution mass spectra were measured using a Thermo LCQdeca APCI-MS.

Photophysical Methods. Electronic absorption and fluorescence experiments were conducted using sealable 1-cm path length fused quartz cuvettes (Starna Cells, catalog number 3-Q-10-GL14-C, 3.5 mL volume) using a Shimadzu UV-2450 UV-Vis spectrometer and a HORIBA Scientific Fluoromax-4 fluorometer. Samples were prepared in a dry nitrogen glove box. Filter experiments were conducted using a long pass UV filter with a cut-on wavelength of 300 nm (Asahi Spectra XUL0300).

Photochemical Reactions. Photochemical reactions were carried out using two 100-W Blak-Ray Long Wave Ultraviolet Lamps (Hg) in a fume hood. The light sources was placed approximately 20 cm from the sample and the reaction mixture was stirred vigorously using a magnetic stir bar. All reactions were performed in

VWR 13 x 100 mm borosilicate culture tubes that were capped and sealed with electrical tape.

Preparation of TpCu

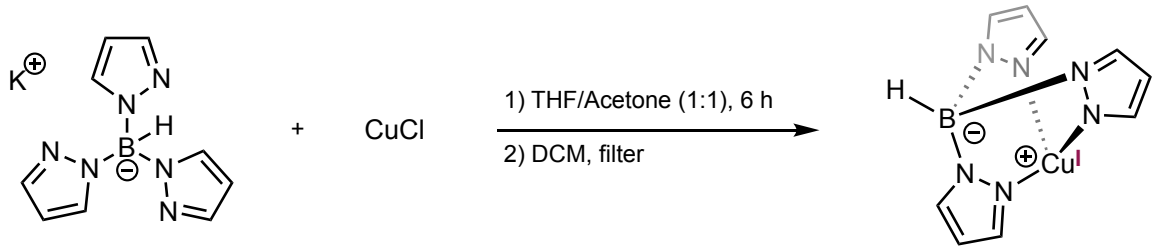

In a nitrogen filled glovebox, a 20 mL vial was charged with CuCl (0.125g, 1 equiv), potassium trispyrazolylborate (0.318 g, 1 equiv) and a magnetic stir bar. A mixture of THF (4 mL) and dried, degassed acetone (4 mL) was added and the mixture was stirred vigorously for 6 h. The solvent was removed under reduced pressure, the resultant solid extracted with dichloromethane (5 mL), and the suspension filtered through a thin pad of celite on a fritted funnel. Removal of the solvent under reduced pressure provided **TpCu** (0.349 g, 98% yield) as a faint blue solid. Analytical data for **TpCu**:

^{1}H-NMR (500 MHz; C_6D_6): δ 7.58 (d, J=1.8 Hz, 3H), 7.09 (d, J=1.2 Hz 3H), 5.96 (t, J=1.8 Hz, 3H).

^{13}C-NMR (126 MHz; C_6D_6): δ 141.8, 135.9, 104.9.

HRMS (ESI-TOFMS): Calc. for $[C_9H_{10}BCuN_6]^+$ =276.0352, Found = 276.0354.

Preparation of Substrates

General Procedure A: To a round bottom flask charged with a magnetic stir bar was added isobutryaldehyde (1.2 equiv), sodium sulfate (2.0 equiv), DCM (0.50 M) and placed under a nitrogen atmosphere. A solution of amine (1.0 equiv) in DCM (10 mL) was added via syringe over the course of 5 min and the reaction mixture was allowed to stir for 12 h. The reaction was then filtered, and solvent was removed under reduced pressure to provide the desired imine as an oil. Imines were then freeze-pump-thawed, and vacuum transferred before being brought into a dry nitrogen filled glovebox and stored in the freezer.

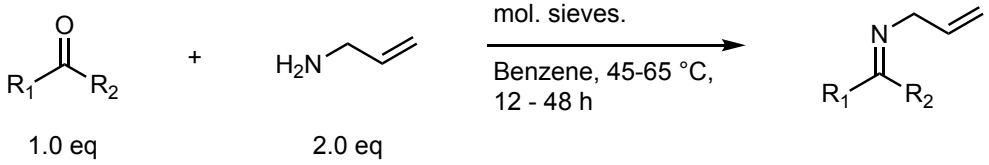

General Procedure B: To a round bottom flask charged with a magnetic stir bar was added carbonyl (1.0 equiv), allyl amine (2.0 equiv), crushed molecular sieves (1.0 g), benzene (0.50 M) and placed under a nitrogen atmosphere. The reaction mixture was heated to 45-65 °C and allowed to stir vigorously for at least 12 h. Upon consumption of the carbonyl as monitored by NMR the reaction was then filtered through a medium frit funnel, and solvent was removed under reduced pressure to provide the desired imine as an oil. Imines were then freeze-pump-

thawed and vacuum transferred before being brought into a dry nitrogen filled glovebox and stored in the freezer.

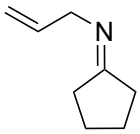

N-Allylcyclopentylideneamine was synthesized by general procedure B. Physical and spectral data was in accordance with literature data.[21]

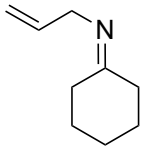

N-Allylcyclohexylideneamine was synthesized by general procedure B. Physical and spectral data was in accordance with literature data.

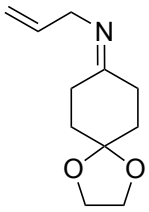

N-Allylcyclohexylideneamine-4-monoethylene acetal was synthesized by general procedure B. Physical and spectral data was in accordance with literature data.[25]

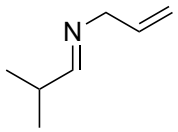

N-allyl-2-methylpropan-1-imine was synthesized by general procedure A. Physical and spectral data was in accordance with literature data.[26]

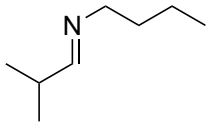

N-isobutylidenebutylamine was synthesized by general procedure A. Physical and spectral data was in accordance with literature data.[27]

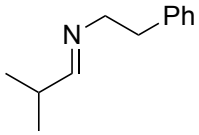

N-(2-methylpropylidene)-2-phenethylamine was synthesized by general procedure A. Physical and spectral data was in accordance with literature data.[28]

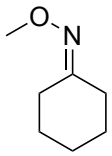

Cyclohexanone O-methyl oxime was synthesized by general procedure A. Physical and spectral data was in accordance with literature data.[29]

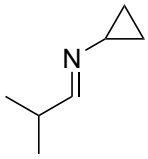

N-isobutylidenecyclopropylamine was synthesized by general procedure A. Physical and spectral data was in accordance with literature data.[30]

exo-(bicyclo[2.2.1]hept-5-en-2-yl) tert-butyldimethylsilyl ether was synthesized according to a known procedure. Physical and spectral data was in accordance with literature data.[31]

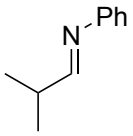

N-(2-methylpropylidene)aniline was synthesized by general procedure A. Physical and spectral data was in accordance with literature data.[32]

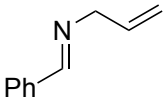

Benzylidene allylamine was synthesized by general procedure A. Physical and spectral data was in accordance with literature data.[33]

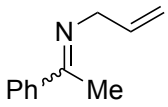

N-(1-phenylethylidene)prop-2-en-1-amine was synthesized by general procedure B. Physical and spectral data was in accordance with literature data.[34]

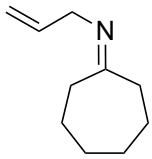

N-Allylcycloheptylideneamine was synthesized by general procedure B in 87% yield as a colorless oil. Analytical data:

^{1}H NMR (300 MHz; C_6D_6): δ 6.16 (m, 1H), 5.35 (dq, *J* = 17.2, 2.0 Hz, 1H), 5.11 (dq, *J* = 10.3, 2.0 Hz, 1H), 3.78 (d, *J* = 5.3 Hz, 2H), 2.49-2.45 (m, 2H), 2.17 (d, *J* = 9.0 Hz, 2H), 1.92 (d, *J* = 6.0 Hz, 2H), 1.46 (m, 2H), 1.37-1.23 (m, 11H).

^{13}C-NMR (126 MHz; C_6D_6): δ 174.9, 137.7, 114.3, 52.8, 43.3, 40.9, 31.4, 30.1, 26.9, 24.8, 24.0

HRMS (ESI-TOFMS) Calc. for $[C_{10}H_{17}N+H^+]^+$ = 152.1434 Found = 152.1434

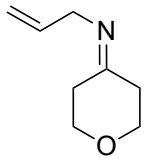

4-N-allyl-tetrahydro-4H-pyran was synthesized by general procedure B in 92% yield as a colorless oil. Analytical data:

^{1}H NMR (300 MHz; C_6D_6): δ 6.60-5.939 (m, 1H), 5.244-5.023 (m, 2H), 3.82-3.79 (m, 2H), 3.54 (t, J=6 Hz, 2H), 3.36 (t, J=6 Hz, 2H), 2.28 (t, J=6 Hz, 2H), 1.87 (t, J=6 Hz, 2H).

^{13}C-NMR (126 MHz; C_6D_6): δ 167.2, 136.8, 114.1, 68.6, 67.0, 42.5, 39.9, 30.1

HRMS (ESI-TOFMS) Calc. for $[C_8H_{13}NO+H^+]^+$ = 140.1070 Found = 140.1070

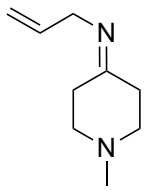

N-allyl-1-methyl-4-piperidinylidene was synthesized by general procedure B in 89% yield as a colorless oil. Analytical data:

^{1}H NMR (300 MHz; C_6D_6): δ 5.91-5.78 (m, 1H), 5.03-4.94 (m, 2H), 3.86 (d, *J* = 5.6 Hz, 2H), 2.58 (t, *J* = 5.9 Hz, 1H), 2.46 (t, *J* = 6.1 Hz, 2H), 2.40-2.27 (m, 9H), 2.20 (s, 4H), 2.17-2.14 (m, 1H).

^{13}C-NMR (126 MHz; C_6D_6): δ 168.9, 136.9, 114.0, 56.4, 55.3, 55.0, 45.5, 40.9, 28.3

HRMS (ESI-TOFMS) Calc. for $[C_9H_{16}N_2+H]^+$ = 153.1386 Found = 153.1388

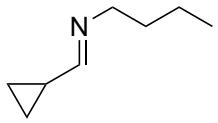

N-cyclopropylidenebutylamine was synthesized by general procedure A in 93% yield as a colorless oil. Analytical data:

^{1}H NMR (300 MHz; $CDCl_3$): δ 6.87 (d, *J* = 6.8 Hz, 1H), 3.27 (td, *J* = 6.8, 1.3 Hz, 2H), 1.61-1.47 (m, 3H), 1.39-1.26 (m, 2H), 0.86 (t, *J* = 7.3 Hz, 3H), 0.51-0.45 (m, 4H).

^{13}C-NMR (126 MHz; $CDCl_3$): δ 164.7, 60.8, 33.3, 20.4, 15.7, 13.7, 5.7

HRMS (ESI-TOFMS) Calc. for $[C_8H_{15}N+H^+]^+$ = 126.1282 Found = 126.1284

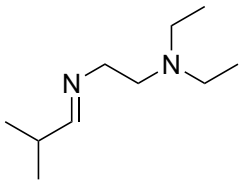

N'-isobutylidene-N,N-diethyl-1,2-ethanediamine was synthesized by general procedure A in 92% yield as a colorless oil. Analytical data:

^{1}H NMR (300 MHz; $CDCl_3$): δ 7.36 (dt, *J* = 4.1, 1.3 Hz, 1H), 3.47-3.42 (m, 2H), 2.67 (t, *J* = 6.8 Hz, 2H), 2.44 (q, *J* = 7.1 Hz, 4H), 2.34-2.23 (m, 1H), 1.00-0.92 (m, 12H).

^{13}C-NMR (126 MHz; $CDCl_3$): δ 168.3, 60.0, 53.8, 47.4, 33.7, 18.9, 12.2

HRMS (ESI-TOFMS) Calc. for $[C_{10}H_{22}N_2+H^+]^+$ = 171.1856 Found = 171.1856

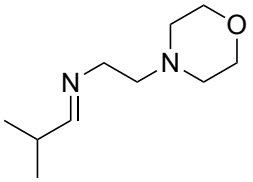

N-isobutylidene-1,2-ethanemorpholine was synthesized by general procedure A in 95% yield as a colorless oil. Analytical data:

^{1}H NMR (300 MHz; $CDCl_3$): δ 7.30 (dt, *J* = 4.2, 1.3 Hz, 1H), 3.58-3.55 (m, 4H), 3.42-3.37 (m, 2H), 2.46 (t, *J* = 6.8 Hz, 2H), 2.26-2.22 (m, 5H), 0.97 (d, *J* = 6.9 Hz, 6H)

^{13}C-NMR (126 MHz; $CDCl_3$): δ 168.9, 66.7, 59.3, 58.7, 54.0, 33.7, 18.9

HRMS (ESI-TOFMS) Calc. for $[C_{10}H_{20}N_2O+H^+]^+$ = 185.1648 Found = 185.1649

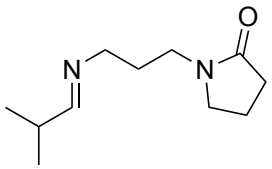

N-isobutylidene-1,3-propanepyrrolidone was synthesized by general procedure A in 93% yield as a colorless oil. Analytical data:

^{1}H NMR (300 MHz; $CDCl_3$): δ 7.34 (d, *J* = 2.9 Hz, 1H), 3.20 (q, *J* = 7.2 Hz, 4H), 2.67 (t, *J* = 7.0 Hz, 2H), 2.33-2.22 (m, 1H), 1.98 (t, *J* = 8.1 Hz, 2H), 1.65 (quintet, *J* = 6.9 Hz, 2H), 1.28 (dt, *J* = 15.2, 7.5 Hz, 3H), 0.98 (d, *J* = 6.9 Hz, 6H)

^{13}C-NMR (126 MHz; $CDCl_3$): δ 173.2, 168.8, 58.4, 46.0, 40.0, 33.7, 30.5, 28.5, 19.0, 17.6

HRMS (ESI-TOFMS) Calc. for $[C_{11}H_{20}N_2O+H^+]^+$ = 197.1648 Found = 197.1649

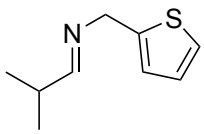

N-isobutylidene-methylenethiophene was synthesized by general procedure A in 88% yield as a colorless oil. Analytical data:

^{1}H NMR (300 MHz; $CDCl_3$): δ 7.23 (m, 1H), 6.85-6.73 (m, 3H), 4.49 (s, 2H), 2.21 (m, 1H), 0.90 (d, *J* = 6.8 Hz, 6H).

^{13}C-NMR (126 MHz; $CDCl_3$): δ 170.0, 143.4, 126.8, 124.53, 124.43, 59.5, 34.1, 19.1

HRMS (ESI-TOFMS) Calc. for $[C_9H_{13}NS+H]^+$ = 168.0841 Found = 168.0839

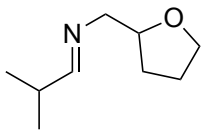

N-isobutylidene-methylenefuran was synthesized by general procedure A in 88% yield as a colorless oil. Analytical data:

^{1}H NMR (300 MHz; $CDCl_3$): δ 7.38 (dt, *J* = 4.1, 1.3 Hz, 1H), 4.13-4.05 (m, 1H), 3.74-3.67 (m, 1H), 3.59-3.39 (m, 4H), 2.27 (m, 1H), 1.73-1.65 (m, 1H), 1.60-1.50 (m, 3H), 0.96 (dd, *J* = 6.9, 2.0 Hz, 6H).

^{13}C-NMR (126 MHz; $CDCl_3$): δ 169.6, 78.3, 67.7, 65.6, 33.8, 29.2, 25.7, 18.95, 18.92

HRMS (ESI-TOFMS) Calc. for $[C_9H_{17}NO+H]^+$ = 156.1388 Found = 156.1387

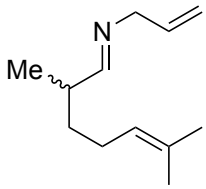

N-isobutylidene-melonal was synthesized by general procedure A in 92% yield as a colorless oil. Analytical data:

^{1}H NMR (300 MHz; $CDCl_3$): δ 7.27 (d, *J* = 4.8 Hz, 1H), 6.00-5.93 (m, 1H), 5.19-5.12 (m, 2H), 5.01 (dt, *J* = 10.3, 1.6 Hz, 1H), 3.87 (d, *J* = 5.3 Hz, 2H), 2.27 (dt, *J* = 12.6, 6.4 Hz, 1H), 2.00 (m, 2H), 1.64 (s, 3H), 1.52 (s, 3H), 1.28 (m, 1H), 0.97 (d, *J* = 6.9 Hz, 3H).

^{13}C-NMR (126 MHz; $CDCl_3$): δ 168.8, 136.7, 131.1, 124.5, 114.6, 63.3, 38.7, 34.0, 25.64, 25.51, 17.4, 17.0

HRMS (ESI-TOFMS) Calc. for $[C_{12}H_{21}N+H]^+$ = 180.1752 Found = 180.1753

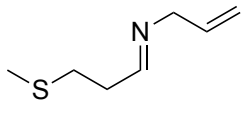

N-isobutylidene-methional was synthesized by general procedure A in 89% yield as a colorless oil. Analytical data:

^{1}H NMR (300 MHz; $CDCl_3$): δ 7.25 (d, *J* = 1.1 Hz, 1H), 5.94-5.86 (m, 1H), 5.12 (m, 1H), 4.98 (m, 1H), 3.81 (d, *J* = 5.4 Hz, 2H), 2.44 (t, *J* = 7.3 Hz, 3H), 2.24 (m, 2H), 1.73 (d, *J* = 1.8 Hz, 3H).

^{13}C-NMR (126 MHz; $CDCl_3$): δ 162.7, 136.3, 114.8, 63.2, 35.2, 29.9, 14.8

HRMS (ESI-TOFMS) Calc. for $[C_7H_{13}NS+H]^+$ = 144.0846. Found = 144.0845

D. General IOPC Procedures.

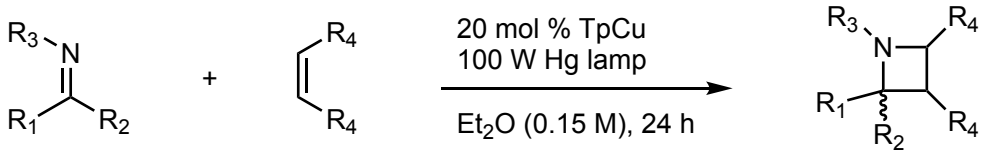

In a glovebox to a borosilicate culture tube charged with a magnetic stir bar was added imine (30 mg, 1.1 equiv), TpCu (0.2 equiv), alkene (1.0 equiv), and diethyl ether (0.15 M). The vial was capped, sealed with electrical tape, and irradiated with a UVP Blak-Ray B-100A UV lamp in a fume hood. After 24 h, or otherwise indicated, the reaction mixture was opened to air for 15 min, then concentrated under reduced pressure. The residue was taken up in methanol and purified by a short plug of basic alumina. If the paramagnetic byproduct Tp_2Cu still remains (indicated by a dark blue coloring), the azetidine product can be extracted with methanol.

E. Characterization of IOPC Products.

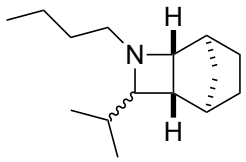

1 was synthesized via general IOPC procedure (24 h reaction time) in 79% yield (55:45 diastereomeric mixture at C2, >95:5 exo:endo as determined by analogy to **2** and **13**) as a colorless oil. Analytical data for **1**:

^{1}H-NMR (300 MzHz; C_6D_6): δ 3.44 (d, *J* = 4.4 Hz, 1H), 2.83 (d, *J* = 11.2 Hz, 1H), 2.71 (d, *J* = 5.4 Hz, 1H), 2.58-2.46 (m, 3H), 2.34 (m, 3H), 2.06 (s, 1H), 1.95 (m, 4H), 1.78 (d, *J* = 9.6 Hz, 1H), 1.69 (m, 1H), 1.36 (m, 12H), 1.13 (m, 2H), 0.90 (m, 18H), 0.72 (d, *J* = 6.3 Hz, 2H).

^{13}C-NMR (126 MHz; C_6D_6): δ 73.9, 73.5, 69.0, 64.5, 59.0, 48.3, 42.6, 39.9, 38.6, 37.9, 37.0, 34.89, 34.85, 34.6, 34.0, 31.9, 30.6, 29.3, 28.7, 27.7, 25.5, 24.1, 20.66, 20.52, 19.2, 19.0, 18.4, 17.3, 14.11, 14.09

HRMS (ESI-TOFMS) Calc. for $[C_{15}H_{27}N + H]^+$ = 222.2216 Found = 222.2216

R_f (3 % MeOH in DCM): 0.2

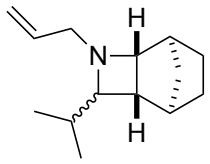

2 was synthesized via general IOPC procedure (24 h reaction time) in 92% yield (55:45 diastereomeric mixture at C2, >95:5 exo:endo, as determined by a series of multidimensional NMR experiments) as a colorless oil. Analytical data for **2**:

^{1}H-NMR (300 MHz; C_6D_6): δ 5.83 (m, 1H), 5.21 (dd, *J* = 28.5, 13.7 Hz, 1H), 5.00 (t, *J* = 7.0 Hz, 1H), 3.45 (d, *J* = 3.3 Hz, 1H), 3.37 (dd, *J* = 11.6, 4.5 Hz, 1H), 3.24 (d, *J* = 10.8 Hz, 1H), 2.94-2.85 (m, 1H), 2.76 (d, *J* = 4.7 Hz, 1H), 2.53 (t, *J* = 7.2 Hz, 1H), 2.46 (s, 1H), 2.26 (s, 1H), 2.02 (s, 1H), 1.93 (m, 1H), 1.85 (m, 1H), 1.68 (m, 1H), 1.37-1.22 (m, 3H), 1.09 (m, 2H), 0.82 (dd, *J* = 16.4, 3.8 Hz, 6H), 0.66 (d, *J* = 4.3 Hz, 1H).

^{13}C-NMR (126 MHz; C_6D_6): δ 137.9, 136.9, 116.1, 114.9, 74.03, 73.96, 69.1, 65.2, 62.6, 52.0, 43.3, 40.0, 39.0, 38.2, 37.4, 35.27, 35.11, 34.96, 34.3, 29.6, 29.0, 27.9, 25.7, 24.4, 19.45, 19.30, 18.7, 17.7

HRMS (ESI-TOFMS) Calc. for $[C_{14}H_{23}N + H]^+$ = 206.1903 Found = 206.1905

R_f (3 % MeOH in DCM): 0.2

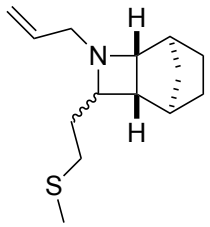

3 was synthesized via general IOPC procedure (24 h reaction time) in 59% yield (51:49 diastereomeric mixture at C2, >95:5 exo:endo as determined by analogy to **2** and **13**) as colorless oil. Analytical data for **3**:

^{1}H-NMR (300 MzHz; C_6D_6): δ 5.86-5.74 (m, 1H), 5.17 (m, 1H), 4.97 (dd, *J* = 9.0, 5.7 Hz, 1H), 3.38 (d, *J* = 5.1 Hz, 1H), 3.27 (dd, *J* = 14.5, 4.9 Hz, 1H), 3.11 (td, *J* = 16.4, 6.2 Hz, 1H), 2.96 (d, *J* = 13.5 Hz, 1H), 2.79 (d, *J* = 6.0 Hz,), 2.45 (d, *J* = 8.9 Hz,), 2.36-2.19 (m, 3H), 1.98 (d, *J* = 12.4 Hz, 1H), 1.88 (s, 1H), 1.80-1.70 (m, 6H), 1.36-1.25 (m, 3H), 1.10 (dd, *J* = 12.7, 8.2 Hz, 1H), 0.79 (m, 2H).

^{13}C-NMR (126 MHz; C_6D_6): δ 137.4, 136.5, 115.9, 114.9, 69.3, 66.10, 66.06, 65.8, 61.2, 51.5, 44.5, 39.2, 39.0, 37.6, 37.4, 36.1, 34.57, 34.49, 33.8, 31.0, 30.0, 29.8, 29.1, 27.5, 25.0, 23.9, 15.12, 15.07

HRMS (ESI-TOFMS) Calc. for $[C_{14}H_{23}NS + H]^+$ = 238.1629 Found = 238.1630

R_f (3 % MeOH in DCM): 0.25

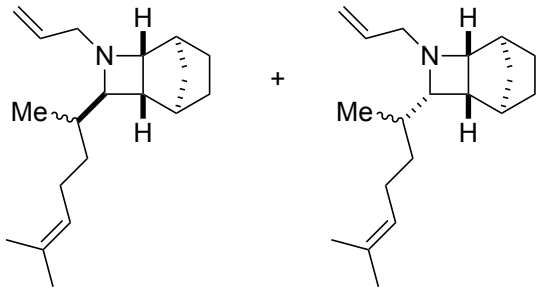

4 was synthesized via general IOPC procedure (24 h reaction time) in 73% yield (61:39 diastereomeric mixture at C2, >95:5 exo:endo as determined by analogy to **2** and **13**) as colorless oil. Analytical data for **4**:

^{1}H-NMR (300 MzHz; C_6D_6): δ 5.83 (ddt, *J* = 21.7, 10.7, 5.3 Hz, 1H), 5.27-5.15 (m, 2H), 5.00 (q, *J* = 9.6 Hz, 1H), 3.46 (d, *J* = 4.8 Hz, 1H), 3.38 (dt, *J* = 14.4, 7.4 Hz, 1H), 3.27 (t, *J* = 14.0 Hz,), 2.95 (t, *J* = 12.8 Hz, 1H), 2.89 (d, *J* = 8.7 Hz,), 2.78 (d, *J* = 6.1 Hz,), 2.66 (t, *J* = 8.5 Hz, 1H), 2.58 (t, *J* = 3.3 Hz,), 2.48 (d, *J* = 8.8 Hz,), 2.27 (s, 1H), 2.12 (d, *J* = 10.3 Hz, 1H), 2.00 (dt, *J* = 23.7, 11.2 Hz, 2H), 1.90 (dd, *J* = 24.2, 4.7 Hz, 2H), 1.70 (d, *J* = 9.2 Hz, 1H), 1.66 (d, *J* = 9.8 Hz, 3H), 1.56 (d, *J* = 6.7 Hz, 3H), 1.33-1.27 (m, 2H), 1.12 (dd, *J* = 21.7, 7.9 Hz, 1H), 1.06-1.01 (m, 1H), 0.90-0.80 (m, 4H), 0.70 (d, *J* = 6.4 Hz, 1H).

^{13}C-NMR (126 MHz; C_6D_6): δ 137.5, 136.50, 136.38, 130.70, 130.57, 130.46, 125.32, 125.30, 125.15, 115.71, 115.64, 114.54, 114.46, 72.72, 72.54, 72.41, 72.34, 68.87, 68.72, 65.08, 65.00, 62.36, 62.31, 51.60, 51.56, 43.3, 42.6, 39.80, 39.60, 39.09, 38.95, 38.7, 37.92, 37.87, 37.13, 37.06, 34.91, 34.76, 34.62,

34.60, 34.00, 33.95, 33.75, 33.4, 33.16, 33.01, 32.7, 32.2, 29.21, 29.17, 27.60, 27.57, 25.89, 25.73, 25.58, 25.53, 25.51, 25.45, 25.36, 25.33, 24.1, 17.46, 17.43, 17.38, 15.4, 14.1

HRMS (ESI-TOFMS) Calc. for $[C_{19}H_{31}N + H]^+$

R_f (3 % MeOH in DCM): 0.25

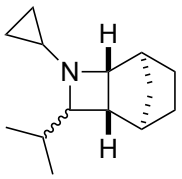

5 was synthesized via general IOPC procedure in 95% yield (55:45 diastereomeric mixture at C2, >95:5 exo:endo as determined by analogy to **2** and **13**) as a colorless oil. Analytical data for **5**:

^{1}H-NMR (300 MzHz; C_6D_6): δ 3.34 (d, *J* = 4.2 Hz, 1H), 3.04 (d, *J* = 5.1 Hz, 1H), 2.78-2.71 (m, 2H), 2.42 (s, 1H), 2.29 (d, *J* = 7.4 Hz, 1H), 2.01 (m, 2H), 1.96 (t, *J* = 5.8 Hz, 1H), 1.88 (m, 5H), 1.78 (m, 1H), 1.66 (m, 1H), 1.29 (m, 6H), 1.16 (d, *J* = 8.1 Hz, 2H), 1.06 (d, *J* = 7.6 Hz, 1H), 0.94-0.80 (m, 14H), 0.72 (d, *J* = 5.2 Hz, 2H), 0.40-0.25 (m, 7H).

^{13}C-NMR (126 MHz; C_6D_6): δ 75.6, 74.3, 68.4, 65.8, 42.0, 39.6, 39.08, 38.89, 38.3, 38.1, 34.6, 34.4, 34.1, 33.5, 29.5, 29.3, 28.3, 27.7, 25.3, 24.0, 20.4, 19.09, 18.99, 17.5, 8.64, 8.47, 4.7, 4.0

HRMS (ESI-TOFMS) Calc. for $[C_{14}H_{24}N + H]^+$ = 206.1904 Found = 206.1903

R_f (3 % MeOH in DCM): 0.2

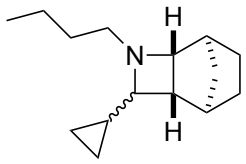

6 was synthesized via general IOPC procedure (24 h reaction time) in 94% yield (55:45 diastereomeric mixture at C2, >95:5 exo:endo as determined by analogy to **2** and **13**) as a colorless oil. Analytical data for **6**:

^{1}H-NMR (300 MzHz; C_6D_6): δ 3.29 (d, *J* = 5.4 Hz, 1H), 2.75 (d, *J* = 5.5 Hz, 2H), 2.70-2.59 (m, 1H), 2.48-2.41 (m, 3H), 2.23 (m, 2H), 2.06-1.94 (m, 4H), 1.37-1.31 (m, 10H), 1.24-1.12 (m, 3H), 0.93-0.86 (m, 10H), 0.42-0.40 (m, 2H), 0.28-0.24 (m, 3H), 0.06-0.05 (m, 2H), -0.13 (m, 1H).

^{13}C-NMR (126 MHz; C_6D_6): δ 73.7, 70.3, 68.8, 66.6, 57.5, 48.4, 44.6, 39.96, 39.77, 38.4, 37.3, 35.0, 34.6, 33.6, 31.7, 30.9, 29.3, 27.8, 24.8, 24.0, 20.58, 20.57, 15.0, 14.08, 14.01, 10.7, 4.2, 3.2, 1.2, 0.7

HRMS (ESI-TOFMS) Calc. for $[C_{15}H_{25}N + H]^+$ = 220.2060 Found = 220.2060

R_f (3 % MeOH in DCM): 0.2

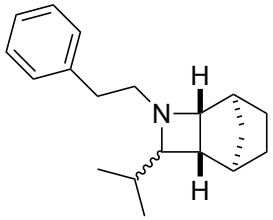

7 was synthesized via general IOPC procedure (72 h reaction time) in 51% yield (51:49 diastereomeric mixture at C2, >95:5 exo:endo as determined by analogy to **2** and **13**) as colorless oil. Analytical data for **7**:

^{1}H-NMR (300 MzHz; C_6D_6): δ 7.19-7.18 (m, 1H), 7.12-7.02 (m, 4H), 3.51 (t, *J* = 6.8 Hz, 1H), 3.43 (d, *J* = 5.5 Hz, 1H), 3.09-3.01 (m, 1H), 2.85 (t, *J* = 7.1 Hz, 1H), 2.78-2.75 (m, 1H), 2.67-2.56 (m, 4H), 2.53-2.44 (m, 3H), 2.25-2.24 (m, 1H), 2.05-2.04 (m, 1H), 2.01-1.97 (m, 1H), 1.96 (s, 1H), 1.88 (d, *J* = 9.1 Hz, 2H), 1.71 (m, 1H), 1.64 (m, 1H), 1.36-1.27 (m, 3H), 1.17-1.07 (m, 2H), 0.92 (d, *J* = 6.9 Hz, 3H), 0.81 (q, *J* = 7.0 Hz, 9H), 0.68 (d, *J* = 6.6 Hz, 2H).

^{13}C-NMR (126 MHz; C_6D_6): δ 141.32, 141.12, 128.84, 128.79, 125.86, 125.75, 73.74, 73.51, 69.27, 64.46, 61.24, 50.85, 42.65, 39.87, 38.59, 37. 85, 36.92, 36.50, 35.24, 34.86, 34.83, 34.59, 33.91, 29.25, 28.63, 27.60, 25.41, 24.07, 18.91, 18.89, 18.28, 17.24

HRMS (ESI-TOFMS) Calc. for $[C_{14}H_{24}N + H]^+$ = 270.2216 Found = 270.2217

R_f (3 % MeOH in DCM): 0.2

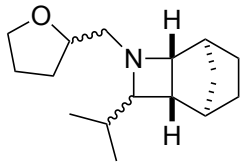

8 was synthesized via general IOPC procedure (24 h reaction time) in 73% yield (55:45 diastereomeric mixture at C2, >95:5 exo:endo as determined by analogy to **2** and **13**) as colorless oil. Analytical data for **8**:

^{1}H-NMR (300 MzHz; C_6D_6): δ 3.85 (d, *J* = 5.4 Hz, 1H), 3.75 (dt, *J* = 10.9, 5.7 Hz, 2H), 3.58-3.49 (m, 2H), 3.12 (dd, *J* = 12.5, 5.6 Hz,), 2.98 (ddd, *J* = 17.9, 12.7, 5.5 Hz, 1H), 2.73 (dd, *J* = 12.6, 4.4 Hz, 1H), 2.66-2.60 (m, 1H), 2.53-2.43 (m, 2H), 2.22 (dd, *J* = 12.5, 5.9 Hz,), 2.12 (s, 1H), 2.04 (d, *J* = 7.5 Hz,), 1.97 (td, *J* = 12.5, 5.6 Hz, 1H), 1.90 (s, 1H), 1.85 (s, 1H), 1.75-1.67 (m, 3H), 1.60-1.55 (m, 2H), 1.48 (dd, *J* = 13.7, 6.5 Hz, 2H), 1.38-1.27 (m, 3H), 1.16-1.08 (m, 1H), 0.86 (qd, *J* = 14.2, 6.7 Hz, 9H), 0.68 (dd, *J* = 6.3, 3.5 Hz, 1H).

^{13}C-NMR (126 MHz; C_6D_6): δ 79.3, 79.0, 78.8, 78.1, 74.4, 74.0, 73.7, 71.6, 70.1, 67.61, 67.60, 67.50, 66.3, 65.6, 63.7, 62.5, 53.4, 52.5, 43.1, 42.5, 39.63, 39.55, 39.24, 39.06, 38.04, 37.99, 36.87, 36.85, 34.77, 34.75, 34.74, 34.72, 34.69, 34.2, 33.6, 33.3, 30.3, 29.8, 29.33, 29.24, 29.17, 29.0, 28.74, 28.68, 27.61, 27.54, 25.90, 25.82, 25.39, 25.26, 25.11, 24.05, 24.04, 19.11, 18.96, 18.90, 18.86, 18.28, 18.16, 17.25, 17.05

HRMS (ESI-TOFMS) Calc. for $[C_9H_{17}NO + H]^+$ = 156.1388 Found = 156.1387

R_f (3 % MeOH in DCM): 0.23

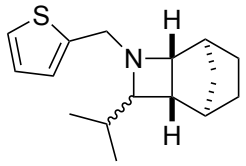

9 was synthesized via general IOPC procedure (48 h reaction time) in 59% yield (51:49 diastereomeric mixture at C2, >95:5 exo:endo as determined by analogy to **2** and **13**) as colorless oil. Analytical data for **9**:

^{1}H-NMR (300 MzHz; C_6D_6): δ 6.89-6.73 (m, 10H), 4.11 (d, *J* = 11.7 Hz, 2H), 3.77 (d, *J* = 11.1 Hz, 1H), 3.57 (d, *J* = 11.1 Hz, 1H), 3.48 (m, 3H), 2.80 (d, *J* = 5.0 Hz, 1H), 2.59 (t, *J* = 7.5 Hz, 1H), 2.53-2.47 (m, 3H), 2.22-2.18 (m, 2H), 1.99 (m, 3H), 1.90 (t, *J* = 5.9 Hz, 1H), 1.85 (s, 2H), 1.82 (s, 1H), 1.66 (m, 3H), 1.24 (m, 2H), 1.19 (m, 4H), 1.08 (m, 4H), 0.91 (dd, *J* = 5.5, 1.2 Hz, 5H), 0.85 (dd, *J* = 5.3, 1.3 Hz, 5H), 0.81-0.79 (m, 10H), 0.67 (m, 5H), 0.57 (s, 1H).

^{13}C-NMR (126 MHz; C_6D_6): δ 146.43, 144.40, 126.64, 126.51, 124.67, 124.36, 124.20, 123.33, 73.89, 73.75, 69.79, 64.77, 59.60, 57.92, 48.14, 43.04, 39.85, 39.05, 38.19, 37.13, 35.06, 35.03, 34.98, 34.17, 29.59, 28.94, 27.80, 25.60, 24.31, 19.26, 19.22, 19.13, 18.45, 17.65

HRMS (ESI-TOFMS) Calc. for $[C_{16}H_{23}NS + H]^+$ = 262.1624 Found = 262.1623

R_f (3 % MeOH in DCM): 0.2

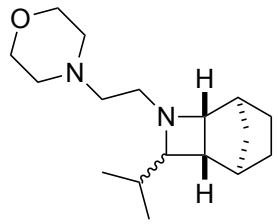

10 was synthesized via general IOPC procedure (24 h reaction time) in 51% yield (64:36 diastereomeric mixture at C2, >95:5 exo:endo as determined by analogy to **2** and **13**) as a colorless oil. Analytical data for **10**:

^{1}H-NMR (300 MzHz; C_6D_6): δ 3.57 (s, 8H), 3.39 (s, 1H), 2.92 (s, 1H), 2.71 (m, 1H), 2.54 (s, 1H), 2.47-2.38 (m, 4H), 2.24 (m, 11H), 2.01 (d, *J* = 11.6 Hz, 1H), 1.86 (m, 3H), 1.72 (s, 1H), 1.64 (s, 1H), 1.30 (d, *J* = 8.1 Hz, 3H), 1.12 (m, 2H), 0.94 (s, 1H), 0.83 (m, 8H), 0.67 (s, 2H).

^{13}C-NMR (126 MHz; C_6D_6): δ 73.9, 73.7, 69.72, 66.88, 64.66, 58.54, 57.66, 56.90, 54.33, 46.61, 4282, 39.96, 38.84, 37.88, 36.96, 34.89, 34.79, 34.65, 33.89, 29.22, 28.66, 27.58, 25.33, 24.02, 19.12, 18.90, 18.31, 17.23

HRMS (ESI-TOFMS) Calc. for $[C_{17}H_{30}N_2O + H]^+$ = 279.2431 Found = 279.2431

R_f (3 % MeOH in DCM): 0.2

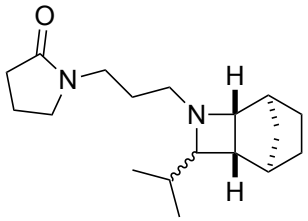

11 was synthesized via general IOPC procedure (48 h reaction time) in 60% yield (59:41 diastereomeric mixture at C2, >95:5 exo:endo as determined by analogy to **2** and **13**) as a colorless oil. Analytical data for **11**:

^{1}H-NMR (300 MzHz; C_6D_6): δ 3.41 (d, *J* = 5.4 Hz, 1H), 3.24 (m, 3H), 2.72 (m, 6H), 2.52-2.42 (m, 3H), 2.31 (m, 1H), 2.25-2.16 (m, 2H), 2.02 (m, 5H), 1.90 (m, 3H), 1.66 (m, 2H), 1.45 (m, 4H), 1.28 (m, 8H), 1.12 (dd, *J* = 17.7, 10.0 Hz, 2H), 0.83 (m, 12H), 0.69 (d, *J* = 6.5 Hz, 2H).

^{13}C-NMR (126 MHz; C_6D_6): δ 173.23, 173.16, 73.8, 73.4, 68.9, 64.4, 56.5, 46.15, 46.05, 42.5, 40.6, 39.8, 38.5, 37.8, 36.9, 34.80, 34.61, 34.58, 34.0, 30.54, 30.52, 29.2, 28.6, 27.5, 27.3, 26.1, 25.4, 24.1, 19.1, 18.9, 18.4, 17.6, 17.2

HRMS (ESI-TOFMS) Calc. for $[C_{18}H_{30}N_2O + H]^+$ = 291.2431 Found = 291.2430

R_f (3 % MeOH in DCM): 0.15

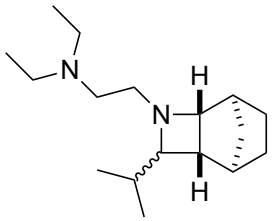

12 was synthesized via general IOPC procedure (24 h reaction time) in 37% yield (54:46 diastereomeric mixture at C2, >95:5 exo:endo as determined by analogy to **2** and **13**) as a colorless oil. Analytical data for **12**:

^{1}H-NMR (300 MzHz; C_6D_6): δ 3.46 (d, *J* = 5.3 Hz, 1H), 3.02 (m, 1H), 2.75 (m, 1H), 2.59-2.39 (m, 15H), 2.35 (d, *J* = 3.0 Hz, 1H), 2.03 (s, 1H), 1.96 (t, *J* = 7.0 Hz, 1H), 1.90 (d, *J* = 4.3 Hz, 1H), 1.86 (s, 1H), 1.77 (d, *J* = 10.2 Hz, 1H), 1.69 (m, 1H), 1.30 (m, 4H), 1.12 (t, *J* = 9.0 Hz, 2H), 0.98 (m, 10H), 0.90 (d, *J* = 6.5 Hz, 3H), 0.86 (d, *J* = 6.5 Hz, 2H), 0.82 (d, *J* = 6.5 Hz, 3H), 0.68 (d, *J* = 6.5 Hz, 2H).

^{13}C-NMR (126 MHz; C_6D_6): δ 73.88, 73.84, 69.9, 64.7, 58.2, 53.2, 52.2, 47.87, 47.71, 47.62, 42.9, 40.0, 38.9, 37.9, 37.0, 35.0, 34.83, 34.63, 33.9, 29.2, 28.7, 27.6, 25.4, 19.05, 18.91, 18.3, 17.3, 12.37, 12.26

HRMS (ESI-TOFMS) Calc. for $[C_{17}H_{32}N_2 + H]^+$ = 265.2638 Found = 265.2637

R_f (5 % MeOH in DCM): 0.25

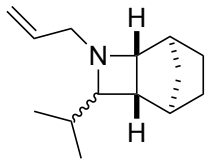

13 was synthesized via general IOPC procedure (24 h reaction time) in 95% yield (>95:5 exo:endo as determinded by a series of multidimensional NMR experiments) as a colorless oil. Analytical data for **13**:

^{1}H-NMR (300 MHz; C_6D_6): δ 5.82 (m, 1H), 5.18 (d, *J* = 16.5 Hz, 1H), 4.98 (d, *J* = 8.6 Hz, 1H), 3.18 (d, *J* = 11.0 Hz, 1H), 2.96 (d, *J* = 7.0 Hz, 1H), 2.91 (d, *J* = 3.5 Hz, 1H), 2.55 (d, *J* = 7.0 Hz, 1H), 2.05 (s, 1H), 1.98 (s, 1H), 1.89 (s, 1H), 1.77 (s, 1H), 1.53 (d, *J* = 3.5 Hz, 1H), 1.46-1.35 (m, 8H), 1.16 (d, *J* = 7.0 Hz, 1H), 0.85 (m, 2H).

^{13}C-NMR (126 MHz; C_6D_6): δ 137.7, 115.2, 74.1, 67.7, 53.3, 48.3, 39.4, 35.4, 33.8, 32.7, 31.9, 28.9, 24.1, 22.4, 22.1.

HRMS (ESI-TOFMS) Calc. for $[C_{15}H_{23}N + H]^+$ = 218.1903 Found = 218.1905.

R_f (3 % MeOH in DCM): 0.2

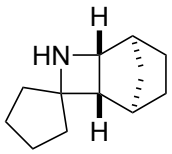

13a was synthesized from **13** according to a known procedure in 82% yield (>95:5 exo:endo).[34]

^{1}H-NMR (300 MzHz; C_6D_6): δ 3.77 (d, *J* = 4.2 Hz, 1H), 2.40 (d, *J* = 8.8 Hz, 1H), 2.32 (t, *J* = 4.3 Hz, 2H), 2.17 (s, 2H), 2.11 (dd, *J* = 10.6, 6.1 Hz, 1H), 1.75 (d, *J* = 2.4 Hz, 1H), 1.65-1.58 (m, 3H), 1.45-1.32 (m, 4H), 1.28-1.23 (m, 1H), 1.13-1.06 (m, 3H), 0.59-0.54 (m, 2H)

^{13}C-NMR (126 MHz; C_6D_6): δ 74.2, 59.3, 48.9, 40.7, 37.5, 36.0, 33.4, 30.8, 27.2, 24.1, 23.2, 22.5

HRMS (ESI-TOFMS) Calc. for $[C_{12}H_{19}N + H]^+$ = 178.1595 Found = 178.1596

R_f (5 % MeOH in DCM): 0.3

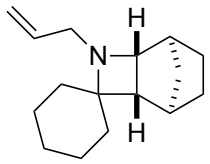

14 was synthesized via general IOPC procedure (24 h reaction time) in 78% yield (>95:5 exo:endo as determined by analogy to **13**) as a colorless oil. Analytical data for **14**:

^{1}H-NMR (300 MHz; C_6D_6): δ 5.85 (m, 1H), 5.19 (d, *J* = 18.0 Hz, 1H), 4.98 (d, *J* = 9.3 Hz, 1H), 3.27 (dd, *J* = 4.5 Hz, *J* = 4.5 Hz , 1H), 2.93 (d, *J* = 6 Hz, 1H), 2.63 (d, *J* = 3.5 Hz, 1H), 2.07-1.94 (m, 3H), 1.66 (d, *J* = 12.0 Hz, 1H), 1.52-0.789 (m, 15H).

^{13}C-NMR (126 MHz; C_6D_6): δ 138.2, 114.9, 67.6, 66.0, 51.7, 45.7, 38.8, 34.9, 34.6, 32.8, 32.4, 29.6, 25.8, 24.3, 23.9, 22.5

HRMS (ESI-TOFMS) Calc. for $[C_{16}H_{25}N+H]^+$ = 232.2060 Found = 232.2062.

R_f (3 % MeOH in DCM): 0.2

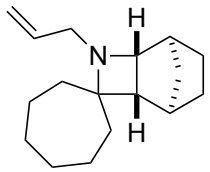

15 was synthesized via general IOPC procedure (24 h reaction time) in 58% yield (>95:5 exo:endo as determined by analogy to **13**) as a colorless oil. Analytical data for **15**:

^{1}H-NMR (300 MHz; C_6D_6): δ 5.72 (m, 1H), 5.12 (d, *J* = 23.1 Hz, 1H), 4.96 (d, *J* = 13.2 Hz, 1H), 3.25 (dd, *J* = 17.7, 6.1 Hz, 1H), 3.01-2.92 (m, 2H), 2.33 (d, *J* = 11.5 Hz, 1H), 2.24 (s, 1H), 2.12 (s, 1H), 2.00 (dd, *J* = 18.7, 10.2 Hz, 2H), 1.91 (s, 1H), 1.84-1.72 (m, 3H), 1.63 (d, *J* = 8.5 Hz, 1H), 1.50-1.26 (m, 15H), 1.12 (d, *J* = 12.1 Hz, 1H), 0.88 (td, *J* = 25.8, 15.7 Hz, 3H).

^{13}C-NMR (126 MHz; C_6D_6): δ 138.2, 115.0, 88.5, 81.0, 68.9, 67.4, 52.3, 47.6, 38.7, 35.7, 35.4, 35.2, 34.5, 29.5, 29.2, 24.0, 22.5

HRMS (ESI-TOFMS) Calc. for $[C_{17}H_{27}N+H\ ]^+$ = 246.2216 Found = 246.2218

R_f (3 % MeOH in DCM): 0.2

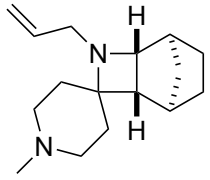

16 was synthesized via general IOPC procedure (24 h reaction time, 3 equiv. of imine) in 91% yield (>95:5 exo:endo as determined by analogy to **13**) as a colorless oil. Analytical data for **16**:

^{1}H-NMR (300 MHz; C_6D_6): δ 5.77 (m, 1H), 5.13 (d, *J* = 17.0 Hz, 1H), 4.93 (d, *J* = 9.9 Hz, 1H), 3.19 (dd, *J* = 13.1, 4.8 Hz, 1H), 2.88 (m, 2H), 2.54 (m, 3H), 2.07 (s, 3H), 2.02 (d, *J* = 21.6 Hz, 2H), 1.89 (d, *J* = 12.3 Hz, 1H), 1.82 (m, 2H), 1.70 (m, 1H), 1.55 (m, 1H), 1.49 (d, *J* = 6.2 Hz, 1H), 1.45 (d, *J* = 8.6 Hz, 1H), 1.32 (m, 3H), 1.12 (d, *J* = 9.2 Hz, 1H), 0.87-0.75 (m, 2H).

^{13}C-NMR (126 MHz; C_6D_6): δ 137.8, 115.2, 67.5, 63.9, 54.0, 52.1, 51.8, 46.1, 45.6, 38.7, 34.6, 34.4, 32.3, 31.8, 29.5, 23.9.

HRMS (ESI-TOFMS) Calc. for [$C_{16}H_{26}N_2$ +H]$^{+}$ = 247.2169 Found = 247.2171

R_f (3 % MeOH in DCM): 0.15

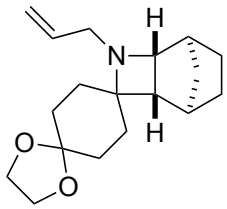

17 was synthesized via general IOPC procedure (72 h reaction time) in 52% yield (>95:5 exo:endo as determined by analogy to **13**) as a colorless oil. Analytical data for **17**:

^{1}H-NMR (300 MHz; C_6D_6): δ 5.99 (m, 1H), 5.21-4.99 (m, 2H), 3.85 (d, *J* = 6.5 Hz, 1H), 3.56 (m, 1H), 3.49 (s, 3H), 3.43 (s, 1H), 2.58 (t, *J* = 8.9 Hz, 2H), 2.29 (t, *J* = 9.3 Hz, 1H), 2.15 (dd, *J* = 20.0, 10.7 Hz, 2H), 2.06 (s, 1H), 1.76 (t, *J* = 8.9 Hz, 2H), 1.68-1.60 (m, 3H).

^{13}C-NMR (126 MHz; C_6D_6): δ 137.7, 115.1, 108.2, 106.9, 67.5, 64.0, 63.8, 51.8, 44.9, 38.7, 35.1, 34.5, 33.7, 32.8, 31.1, 29.5, 29.4, 29.0, 23.8

HRMS (ESI-TOFMS) Calc. for $[C_{18}H_{27}NO_2 + H]^+$ = 290.2115 Found = 290.2113

R_f (3 % MeOH in DCM): 0.2

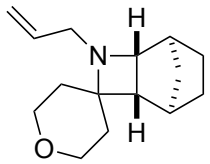

18 was synthesized via general IOPC procedure (48 h reaction time) in 66% yield (>95:5 exo:endo as determined by analogy to **13**) as a colorless oil. Analytical data for **18**:

^{1}H-NMR (300 MHz; C_6D_6): δ 5.76 (m, 1H), 5.13 (d, *J* = 18.0, 1H), 4.95 (d, *J* = 12.0, 1H), 3.73 (m, 2H), 3.16 (m, 3H), 2.84 (m, 2H), 2.45 (d, *J* = 9.0, 1H), 1.99 (s, 1H), 1.90 (s, 1H), 1.70 (m, 2H), 1.46 (d, *J* = 6.0, 1H), 1.43-1.22 (m, 5H), 1.10 (d, *J* = 6.0, 1H), 0.96-0.75 (m, 3H)

^{13}C-NMR (126 MHz; C_6D_6): δ 137.6, 115.3, 67.4, 65.8, 63.8, 51.6, 45.2, 38.6, 34.7, 34.3, 33.5, 32.9, 29.3, 23.8, 14.0

HRMS (ESI-TOFMS) Calc. for $[C_{15}H_{23}NO + H]^+$ = 234.1852 Found = 234.1853

R_f (3 % MeOH in DCM): 0.25

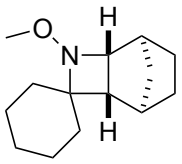

19 was synthesized via general IOPC procedure (48 h reaction time) in 90% yield (>95:5 exo:endo as determined by analogy to **13**) as a colorless oil. Analytical data for **19**:

^{1}H-NMR (300 MHz; C_6D_6): δ 3.53 (d, *J* = 7.5 Hz, 1H), 3.42 (s, 3H), 2.28 (d, *J* = 9.3 Hz, 1H), 2.21 (s, 1H), 1.97-1.85 (m, 4H), 1.64 (d, *J* = 13.3 Hz, 1H), 1.55 (d, *J* = 7.6 Hz, 1H), 1.46 (m, 2H), 1.37-1.22 (m, 5H), 1.10 (m, 3H), 0.86-0.73 (m, 2H).

^{13}C-NMR (126 MHz; C_6D_6): δ 72.1, 71.2, 61.9, 44.3, 38.4, 34.9, 34.2, 29.4, 25.9, 23.9, 23.7, 22.3

HRMS (ESI-TOFMS) Calc. for $[C_{14}H_{23}NO + H]^+$ = 221.852 Found = 221.854

R_f (3 % MeOH in DCM): 0.25

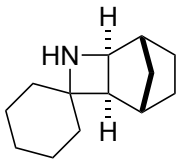

19a was synthesized from **19** according to a known procedure in 93% yield (>95:5 exo:endo)**.**[35]

^{1}H-NMR (300 MzHz; C_6D_6): δ 3.50 (d, *J* = 3.1 Hz, 1H), 3.50 (br s, 1H), 2.57 (d, *J* = 7.6 Hz, 1H), 2.12 (s, 1H), 1.98 (s, 1H), 1.65 (s, 1H), 1.54 (m, 2H), 1.40 (s, 4H), 1.29-1.24 (m, 5H), 1.14 (m, 3H), 0.76 (dd, *J* = 19.9, 8.0 Hz, 2H).

^{13}C-NMR (126 MHz; C_6D_6): δ 63.86, 60.0, 49.0, 41.0, 39.1, 35.4, 34.2, 32.5, 29.1, 25.9, 24.5, 23.3, 22.8

HRMS (ESI-TOFMS) Calc. for $[C_{13}H_{21}N + H]^+$ = 192.1752 Found = 192.1751

R_f (5 % MeOH in DCM): 0.3

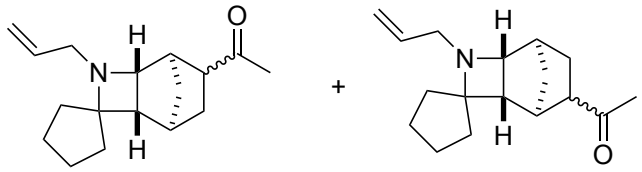

20 was synthesized via general IOPC procedure (48 h reaction time) in 95% yield (65:35 regiomeric mixture, >95:5 exo:endo as determined by analogy to **2**) as a colorless oil. Analytical data for **20**:

^{1}H-NMR (300 MzHz; C_6D_6): δ 5.72 (m, 1H), 5.17-4.89 (m, 2H), 3.14-2.74 (m, 3H), 2.58 (d, *J* = 9.0 Hz, 1H), 2.23 (m, 1H), 2.17 (m, 1H), 2.08 (s, 1H), 1.99 (d, 1H), 1.93 (d, *J* = 3.2 Hz, 1H), 1.85 (d, *J* = 12.1 Hz, 1H), 1.76 (s, 2H), 1.67 (s, 1H), 1.63-1.57 (m, 2H), 1.44-1.20 (m, 8H), 1.14 (m, 1H).

^{13}C-NMR (126 MHz; C_6D_6): δ 206.44, 206.40, 137.3, 115.55, 115.49, 74.6, 73.9, 66.9, 63.6, 54.1, 53.08, 53.06, 51.5, 47.5, 43.04, 42.88, 40.2, 39.1, 36.3, 35.94, 35.81, 32.70, 32.64, 31.82, 31.62, 28.62, 28.57, 28.43, 24.4, 22.31, 22.30, 22.09, 22.05

HRMS (ESI-TOFMS) Calc. for $[C_{17}H_{25}NO + H]^+$ = 260.2009 Found = 260.2010

R_f (3 % MeOH in DCM): 0.2

21 was synthesized via general IOPC procedure (48 h reaction time) in 85% yield (56:44 regiomeric mixture, 75:25 diastereomeric ratio, >95:5 exo:endo as determined by analogy to **2**) as a colorless oil. Analytical data for **21**:

^{1}H-NMR (300 MzHz; C_6D_6): δ 5.73 (m, 2H), 5.13 (t, *J* = 15.5 Hz, 1H), 4.93 (m, 3H), 3.33 (d, 1H), 3.14 (m, 1H), 2.94-2.86 (m, 1H), 2.60 (t, *J* = 9.4 Hz, 1H), 2.40 (m, 1H), 2.10 (s, 1H), 2.01-1.90 (m, 2H), 1.82 (m, 1H), 1.74 (m, 1H), 1.65-1.49 (m, 2H), 1.36-1.15 (m, 9H), 1.10 (m, 1H), 0.76 (d, *J* = 11.0 Hz,), 0.63 (d, *J* = 7.2 Hz,).

^{13}C-NMR (126 MHz; C_6D_6): δ 143.58, 143.46, 140.94, 140.82, 137.63, 137.53, 115.32, 115.27, 114.2, 113.6, 111.9, 111.6, 74.5, 73.98, 73.85, 73.67, 67.6, 67.33, 67.20, 63.7, 53.38, 53.24, 53.23, 53.18, 48.60, 48.54, 48.1, 45.5, 45.13, 44.97, 44.3, 42.09, 42.04, 41.4, 41.1, 40.4, 39.8, 36.66, 36.52, 36.0, 35.53, 35.43, 34.3, 32.99, 32.88, 32.68, 32.63, 31.82, 31.73, 31.55, 31.43, 30.9, 29.9, 29.5, 22.49, 22.39, 22.34, 22.21, 22.17, 22.13, 22.07

HRMS (ESI-TOFMS) Calc. for $[C_{17}H_{25}N + H]^+$ = 244.2060 Found = 244.2062

R_f (3 % MeOH in DCM): 0.25

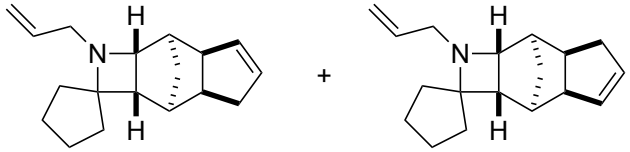

22 was synthesized via general IOPC procedure (60 h reaction time) in 82% yield (53:47 diastereomeric ratio, >95:5 exo:endo at azetidine juncture as determined by X-ray crystallography) as a colorless oil. Azetidine was reacted with excess methyl iodide, upon standing and slow evaporation from THF colorless crystals were obtained, identified as the HI salt. Analytical data for **22**:

^{1}H-NMR (300 MzHz; C_6D_6): δ 5.79 (m, 1H), 5.46 (m, 2H), 5.14 (dd, *J* = 17.1, 6.4 Hz, 1H), 4.95 (d, *J* = 7.1 Hz, 1H), 3.18 (m, 2H), 3.03 (m, 1H), 2.92 (m, 2H), 2.71-2.69 (m, 1H), 2.45 (m, 1H), 2.18-2.00 (m, 4H), 1.91-1.77 (m, 4H), 1.35 (m, 8H).

^{13}C-NMR (126 MHz; C_6D_6): δ 137.77, 137.72, 131.4, 131.10, 131.03, 130.2, 115.20, 115.11, 74.53, 74.38, 65.1, 63.0, 53.49, 53.41, 53.31, 51.3, 44.4, 43.9, 42.22, 42.08, 41.1, 40.4, 39.9, 38.15, 38.04, 37.1, 33.16, 33.00, 32.12, 32.07, 31.3, 31.0, 22.57, 22.45, 22.38, 22.1

HRMS (ESI-TOFMS) Calc. for $[C_{18}H_{25}N + H]^+$ = 256.2060 Found = 256.2061

R_f (3 % MeOH in DCM): 0.3

23 was synthesized via general IOPC procedure (48 h reaction time) in 47% yield (50:50 regiomeric mixture, 60:40 diastereomeric ratio, >95:5 exo:endo as determined by analogy to **2**) as a colorless oil. Analytical data for **23**:

^{1}H-NMR (300 MzHz; C_6D_6): δ 5.63 (m 1H), 5.07 (m, 1H), 4.92 (m, 1H), 3.61 (d, 1H), 2.99 (m, 1H), 2.76 (m, 1H),

^{13}C-NMR (126 MHz; C_6D_6): δ 137.05, 137.04, 136.89, 136.82, 122.74, 122.66, 121.5, 121.2, 115.91, 115.79, 115.63, 115.60, 74.4, 74.02, 73.93, 73.7, 66.1, 65.8, 65.5, 63.7, 52.87, 52.83, 52.71, 47.1, 46.7, 44.4, 43.3, 41.7, 40.7, 39.3, 38.8, 35.5, 35.12, 35.05, 34.3, 33.94, 33.92, 32.75, 32.60, 32.56, 32.53, 32.48, 32.43, 32.1, 31.85, 31.71, 31.67, 31.59, 30.3, 29.93, 29.87, 29.6, 29.16, 29.12, 25.9, 25.6, 22.45, 22.25, 22.21, 22.19, 22.14, 21.99, 21.96, 21.91

HRMS (ESI-TOFMS) Calc. for $[C_{16}H_{23}N + H]^+$ = 243.1856 Found = 243.1858

R_f (3 % MeOH in DCM): 0.2

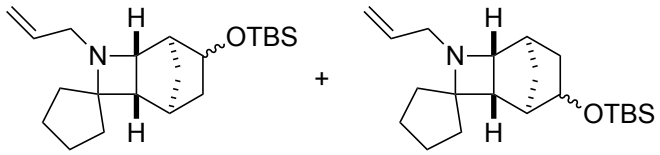

24 was synthesized via general IOPC procedure (192 h reaction time) in 82% yield (50:50 regiomeric mixture, 90:10 diastereomeric ratio, >95:5 exo:endo as determined by analogy to **2**) as a colorless oil. Analytical data for **24**:

^{1}H-NMR (300 MzHz; C_6D_6): δ 5.79 (m, 1H), 5.46 (m, 2H), 5.14 (dd, *J* = 17.1, 6.4 Hz, 1H), 4.95 (d, *J* = 7.1 Hz, 1H), 3.18 (m, 2H), 3.03 (m, 1H), 2.92 (m, 2H), 2.71-2.69 (m, 1H), 2.45 (m, 1H), 2.18-2.00 (m, 4H), 1.91-1.77 (m, 4H), 1.35 (m, 8H).

^{13}C-NMR (126 MHz; C_6D_6): δ 137.77, 137.72, 131.4, 131.10, 131.03, 130.2, 115.20, 115.11, 74.53, 74.38, 65.1, 63.0, 53.49, 53.41, 53.31, 51.3, 44.4, 43.9, 42.22, 42.08, 41.1, 40.4, 39.9, 38.15, 38.04, 37.1, 33.16, 33.00, 32.12, 32.07, 31.3, 31.0, 22.57, 22.45, 22.38, 22.1

HRMS (ESI-TOFMS) Calc. for $[C_{18}H_{25}N + H]^+$ = 256.2060 Found = 256.2061

R_f (2 % MeOH in DCM): 0.25

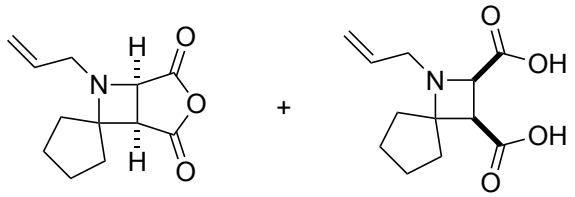

25 was synthesized via general IOPC procedure (24 h reaction time) in 98% yield (>95:5 exo:endo) as a colorless oil. Without TpCu 51% yield. Analytical data for **25**:

^{1}H-NMR (300 MzHz; C_6D_6): δ 8.48 (s, 1H), 5.76 (m, 1H), 5.17-5.07 (m, 2H), 4.96 (s, 1H), 4.33-4.24 (m, 1H), 4.04 (m, 1H), 3.31 (s, 1H), 2.96 (m, 1H), 2.86 (m, 1H), 2.75 (m, 1H), 2.63-2.54 (m, 2H), 2.39 (m, 2H), 2.29 (t, *J* = 8.6 Hz, 1H), 1.98 (m, 1H), 1.65 (quintet, *J* = 10.4 Hz, 1H).

^{13}C-NMR (126 MHz; C_6D_6): δ 168.8, 167.9, 141.0, 139.0, 133.2, 131.8, 117.0, 115.7, 111.4, 105.7, 46.0, 45.2, 44.0, 34.6, 33.5, 32.1, 30.8, 29.7, 29.2, 21.3

HRMS (ESI-TOFMS) Calc. for $[C_{12}H_{15}NO_3 - H]^-$ = 220.0979 Found = 220.0981

Calc. for $[C_{12}H_{16}NO_4 - H]^-$ = 238.1082 Found = 238.1085

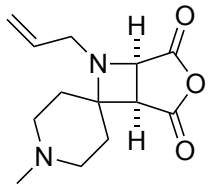

26 was synthesized via general IOPC procedure (24 h reaction time) in 98% yield (>95:5 exo:endo) as a colorless oil. Without TpCu 13% yield. Analytical data for **27**:

^{1}H-NMR (300 MzHz; C_6D_6): δ 6.04 (d, *J* = 9.6 Hz, 1H), 5.78 (d, *J* = 9.8 Hz, 2H), 5.29 (br s, 3H), 4.56 (s, 1H), 3.84 (m, 1H), 3.13 (m, 1H), 2.77-2.73 (m, 1H), 1.43 (s, 2H), 1.32 (s, 1H), 1.22-1.02 (m, 5H), 0.78-0.63 (m, 7H), 0.38 (s, 1H), 0.26 (m, 1H), 0.17-0.10 (m, 2H), -0.13 (m, 1H).

^{13}C-NMR (126 MHz; C_6D_6): δ 165.1, 164.4, 152.8, 139.8, 135.2, 105.1, 89.4, 41.8, 32.3, 20.5, 13.9, 11.9, 4.5, 2.7

HRMS (ESI-TOFMS) Calc. for $[C_{13}H_{18}N_2O_3 + H]^+$ = 251.1395 Found = 251.1393

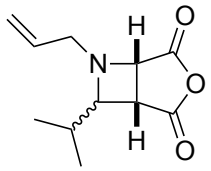

27 was synthesized via general IOPC procedure (24 h reaction time) in 98% yield (75:25 diastereomeric mixture at C2, >95:5 exo:endo) as a colorless oil. Without TpCu 47% yield. Analytical data for **28**:

^{1}H-NMR (300 MzHz; C_6D_6): δ δ 5.76-5.63 (m, 1H), 5.30-5.22 (m, 2H), 4.99 (d, *J* = 1.7 Hz, 1H), 4.28 (dd, *J* = 15.1, 5.6 Hz,), 4.18 (dd, *J* = 15.1, 5.2 Hz, 1H), 3.84 (dd, *J* = 15.0, 7.3 Hz,), 3.69 (dd, *J* = 15.0, 7.8 Hz, 1H), 2.88 (dd, *J* = 19.2, 5.1 Hz, 1H), 2.80 (d, *J* = 1.3 Hz, 1H), 2.74-2.67 (m,), 2.61 (d, *J* = 1.4 Hz,), 2.51 (d, *J* = 1.8 Hz,), 2.36-2.35 (m, 1H), 1.23-1.14 (m, 6H).

^{13}C-NMR (126 MHz; C_6D_6): δ 176.3, 175.6, 166.5, 166.0, 132.6, 132.1, 118.7, 117.5, 93.4, 48.2, 46.7, 45.9, 43.0, 41.3, 39.2, 33.4, 32.9, 23.7, 23.1, 17.42, 17.28

HRMS (ESI-TOFMS) Calc. for $[C_{11}H_{15}N + H]^+$ = 162.1282 Found = 162.1283

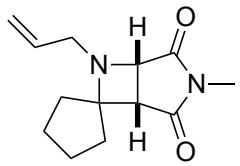

28 was synthesized via general IOPC procedure (24 h reaction time) in 50% yield (95:5 exo:endo) as a colorless oil. Without TpCu 25% yield. Analytical data for **29**:

^{1}H-NMR (300 MzHz; C_6D_6): 5.88 (m, 1H), 5.18-5.02 (m, 2H), 3.56-3.43 (m, 2H), 2.86 (m, 3H), 2.72 (s, 1H), 2.63 (m, 1H), 2.45 (m, 1H), 2.38 (s, 1H), 2.29 (m, 1H), 2.03 (m, 1H), 1.71-1.59 (m, 1H), 1.37 (m, 4H), 1.05 (m, 1H), 0.76 (m, 1H).

^{13}C-NMR (126 MHz; C_6D_6): δ 179.3, 179.1, 178.1, 176.60, 176.52, 176.33, 136.62, 136.58, 114.69, 114.62, 55.70, 55.65, 47.4, 47.2, 40.4, 40.1, 33.0, 31.4, 28.88, 28.82, 28.5, 27.0, 24.6, 24.3, 22.43, 22.33

HRMS (ESI-Orbitrap) Calc. for $[C_{13}H_{21}N + H]^+$ = 221.1441 Found = 235.1443

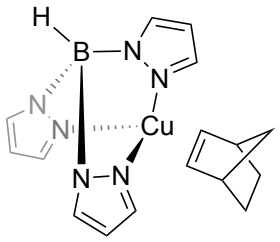

TpCu-NB was synthesized via the equimolar combination of **TpCu** and norbornene in THF. After allowing the solution to stir for 15 min the solution was filtered solvent was removed and the title compound was obtained in 87% yield as a white solid. Recrystallization from DCM/pentane via vapor diffusion at -30 °C led to crystals suitable for X-ray diffraction. Analytical data for **TpCu-NB**:

^{1}H-NMR (300 MzHz; C_6D_6): 7.54 (s, 3H), 7.41 (s, 3H), 5.97 (s, 3H), 4.97 (brs, 2H), 2.81 (s, 2H), 1.64 (brs, 1H), 1.39 (d, *J* = 7.4 Hz, 2H), 0.90-0.85 (m, 3H), 0.69 (d, *J* = 9.0 Hz, 1H).

^{13}C-NMR (126 MHz; C_6D_6): δ 139.4, 134.2, 104.0, 42.3, 25.0

EA (C,H,N) Calc. : C = 51.84%, H = 5.44%, N = 22.67% Found: C = 47.36%, H = 4.62%, N = 20.53%

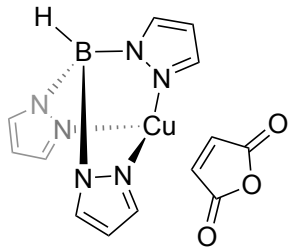

TpCu-MA was synthesized synthesized via the equimolar combination of **TpCu** and maleic anhydride in THF. After allowing the solution to stir for 15 min the solution was filtered and solvent was removed and the title compound was obtained in 93% yield as a yellow-orange solid. Recrystallization from DCM/pentane via vapor diffusion at -30 °C led to crystals suitable for X-ray diffraction Analytical data for **TpCu-MA**:

^{1}H-NMR (300 MzHz; C_6D_6): 7.39 (s, 3H), 7.33 (s, 3H), 5.81 (s, 3H), 4.90 (s, 2H).

^{13}C-NMR (126 MHz; C_6D_6): δ 165.4, 140.2, 135.4, 105.3

EA (C,H,N) Calc. : C = 41.68%, H = 3.23%, N = 22.43% Found: C = 42.41%, H = 3.35%, N = 21

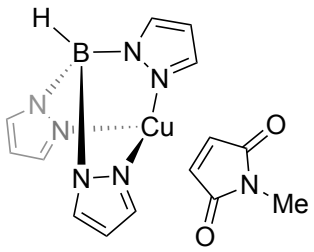

TpCu-MI was synthesized via the equimolar combination of **TpCu** and maleimide in THF. After allowing the solution to stir for 15 min the solution was filtered and solvent was removed and the title compound was obtained in in 91% yield as a yellow-orange solid. Analytical data for **TpCu-MI**:

^{1}H-NMR (300 MzHz; C_6D_6): 7.55 (s, 3H), 7.34 (s, 3H), 5.84 (s, 3H), 5.02 (s, 2H), 2.53 (s, 3H).

^{13}C-NMR (126 MHz; C_6D_6): δ 171.0, 139.6, 134.8, 104.6

EA (C,H,N) Calc. : C = 41.79%, H = 3.51%, N = 26.24% Found: C = 40.52%, H = 3.36%, N = 22.57%

4.8 Details of Crystallographic Structure Determinations

General Information. Single crystal X-ray structure determinations were carried out at low temperature on Bruker Kappa diffractometers equipped with a Mo sealed tube or rotating anode or Cu rotating anode radiation source and a Bruker APEX-II, or Proteum Pt135 detector. All structures were solved via intrinsic methods with SHELXT and refined by full-matrix least squares procedures using SHELXL within the Olex2 small-molecule solution, refinement and analysis software package. Crystallographic data collection and refinement information are listed below.

Synthesis of TpCuDMAP: To 20 mL vial containing **TpCuMA** (100 mg) in THF (5 mL) was added DMAP (mg, 1.0 equiv) and the solution was allowed to stir vigorously for 5 min. Immediately upon addition of DMAP a noticeable color change from yellow to dark orange/red was observed. The solution was then filtered through a glass filter and solvent was removed under reduced pressure. The resulting dark solid was taken up in THF (2 mL) and filtered a second time into a 1-dram vial. Recrystallization was achieved through vapor diffusion with pentane to produce orange crystals.

Synthesis of TpCuPPh$_3$: To 20 mL vial containing **TpCuMA** (100 mg) in THF (5 mL) was added PPh$_3$ (mg, 1.0 equiv) and the solution was allowed to stir vigorously for 5 min. Immediately upon addition of PPh$_3$ a noticeable color change

from yellow to clear was observed. The solution was then filtered through a glass filter and solvent was removed under reduced pressure. The resulting dark solid was taken up in THF (2 mL) and filtered a second time into a 1-dram vial. Recrystallization was achieved through vapor diffusion with pentane to produce orange crystals.

Name	**TpCuNB**	**TpCuMA**	**25-HI**
Formula	$C_{16}H_{20}BCuN_6$	$C_{13}H_{12}BCuN_6O_3$	$C_{18}H_{26}NI$
Crystal System	Monoclinic	Monoclinic	Monoclinic
Space Group	P 1 2_1/c 1	P 1 2_1/c 1	P 1 2_1/n 1
a, Å	7.6331(10)	8.1689(12)	8.5711(7)
b, Å	19.237(3)	9.7468(16)	13.9176(13)
c, Å	11.6490(16)	19.047(3)	14.4476(11)
a, deg	90	90	90
b, deg	103.118(4)	92.700(3)	104.176(5)
g, deg	90	90	90
V, $Å^3$	1665.9(4)	1514.9(4)	1671.0(2)
Z	4	4	4
Radiation (l, Å)	0.71073	0.71073	0.71073
ρ (calcd.), g/cm^3	1.478	1.643	1.520
m (Mo Ka), mm^{-1}	1.320	1.468	14.963
Temp, K	100 K	100 K	100 K
q max, deg	25.422	25.362	69.345
data/parameters			
R_1	0.0254	.0243	0.0774
wR_2	0.0603	0.0624	0.2425
GOF	1.052	1.042	1.154

Figure 4.19 Crystallographic data collection and refinement information for **TpCuNB**, **TpCuMA**, and **25-HI**.

Name	**TpCuDMAP**	**$TpCuPPh_3$**
Formula	$C_{16}H_20BCuN_8$	$C_{27}H_{25}BCuN_6P$
Crystal System	Orthorhombic	Triclinic
Space Group	P b c a	P -1
a, Å	12.7539(10)	9.3317(10)
b, Å	15.2221(18)	10.6681(9)
c, Å	18.583(2)	14.5103(16)
a, deg	90	88.195(3)
b, deg	90	85.660(4)
g, deg	90	89.651(4)
V, $Å^3$	3607.7(6)	1439.7(3)
Z	8	2
Radiation (l, Å)	0.71073	0.71073
r (calcd.), g/cm^3	1.469	1.439
m (Mo Ka), mm^{-1}	1.229	1.029
Temp, K	100 K	100 K
q max, deg	25.757	26.515
data/parameters		
R_1	0.0285	0.0238
wR_2	0.0761	0.0618
GOF	0.74	1.045

Figure 4.20 Crystallographic data collection and refinement information for **TpCuDMAP** and **$TpCuPPh_3$**.

4.10 Results of Computational Studies

Computational Details: Geometry optimizations for TpCuNorb and TpCuMA were done starting from the crystallographic atomic coordinates obtained from the respective crystal structures. All ground state geometry optimizations and frequency calculations were performed using the M11 density functional[36,37] with Ahlrichs' def2-tzvpp basis set.[38] using the Gaussian09 software package. This research was supported in part by the W. M. Keck Foundation through computing resources at the W. M. Keck Laboratory for Integrated Biology II.

TpCuNB and its excited states were analyzed via Tam-Dancoff approximation density functional theory (TDA-DFT) calculations (first ten excited states). This provided a theoretical UV-vis spectrum that most closely resembled the experimental spectra (see **Figure S14-S15**). From this an absorption band at 255 nm, which corresponds to an excitation from the HOMO - 2 (MO 94) to the LUMO + 1 (MO 98) could be computed. Further absorption bands were detected at 243.9 nm, and 200 nm. MO 94 was chosen to visualize because it contributes (49.8%) the most significantly in the excitation at 255 nm. While there are various HOMOs contributing to the possible transitions to the excited state each is primarily metal based (see below images). Therefore, the observed excitation can be interpreted as a metal to ligand charge transfer (MLCT). The HOMO shows

significant contributions from the Cu dyz orbital, and the LUMO shows contribution from the Cu dxy orbital and norbornene pi* orbital.

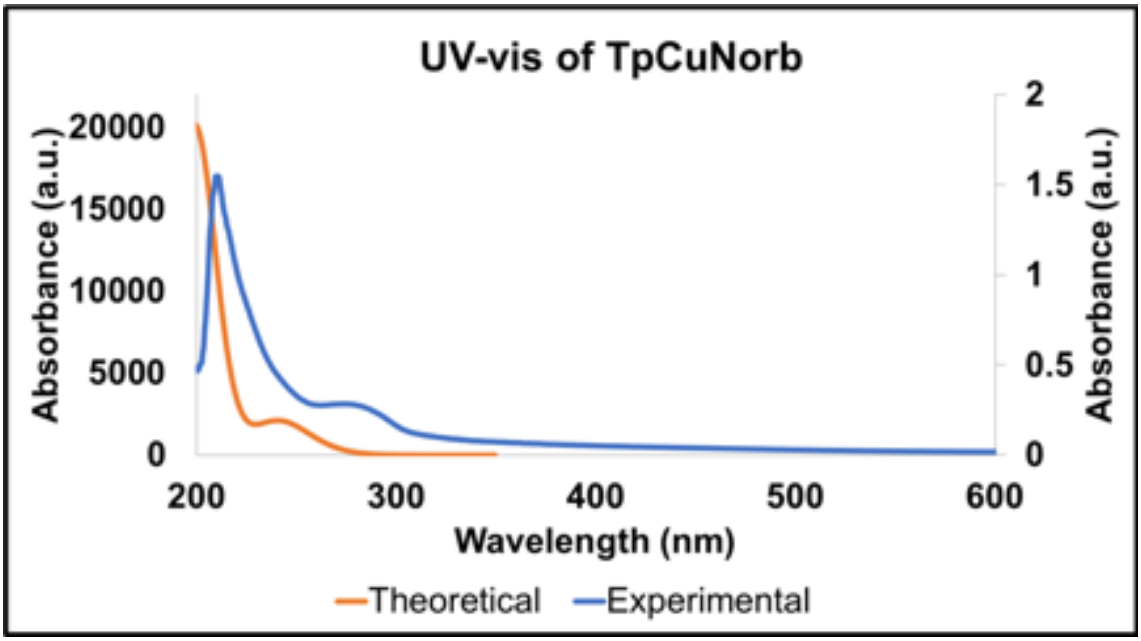

Figure 4.21 Theoretical and experimental electronic absorption spectra of TpCuNorb. The theoretical spectrum was calculated using TDA-DFT approach using the M11 functional with Alhdrichs' def2-tzvpp basis set.

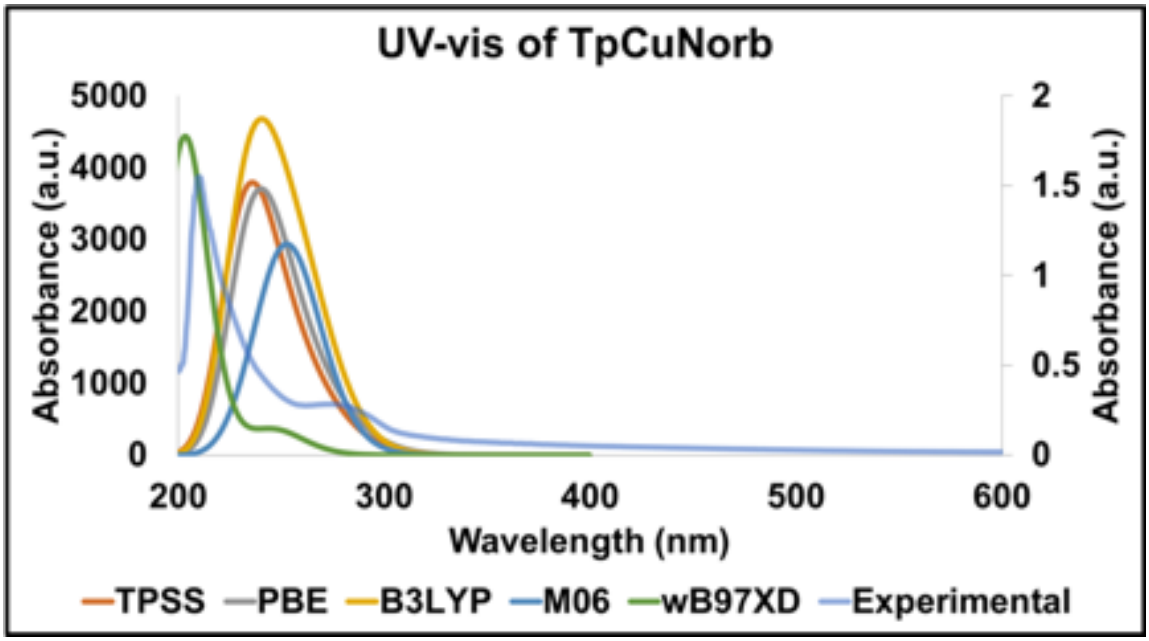

Figure 4.22 Theoretical electronic absorption spectra of TpCuNorb using various functionals with Ahldrichs' def2-tzvpp basis set.

Performing the analogous TDA-DFT calculations utilizing other functionals such as B3LYP, PBEPBE, Wb97x-D, TPSSTPSS, and M06 with various basis sets including 6-311+g(2d,p), def2-svp, and def2-tzvp gave theoretical UV-vis spectra that were not similar to the experimental data.

```
%mem=20GB
%nprocshared=8
%chk=TpCuNorb-M11.chk
# opt freq m11/def2tzvpp scrf=(solvent=diethylether) integral=ultrafinegrid
pop=full

Title Card Required

0 1
xyz
```

Figure 4.23 Input file for geometry optimization and frequency calculations.

```
%mem=20GB
%nprocshared=8
%chk=TpCuNorb-TDA-M11.chk
# tda=nstates=10 m11/def2tzvpp scrf=(solvent=diethylether)
integral=ultrafinegrid

Title Card Required

0 1
xyz
```

Figure 4.24 Input file for TDA-DFT calculations.

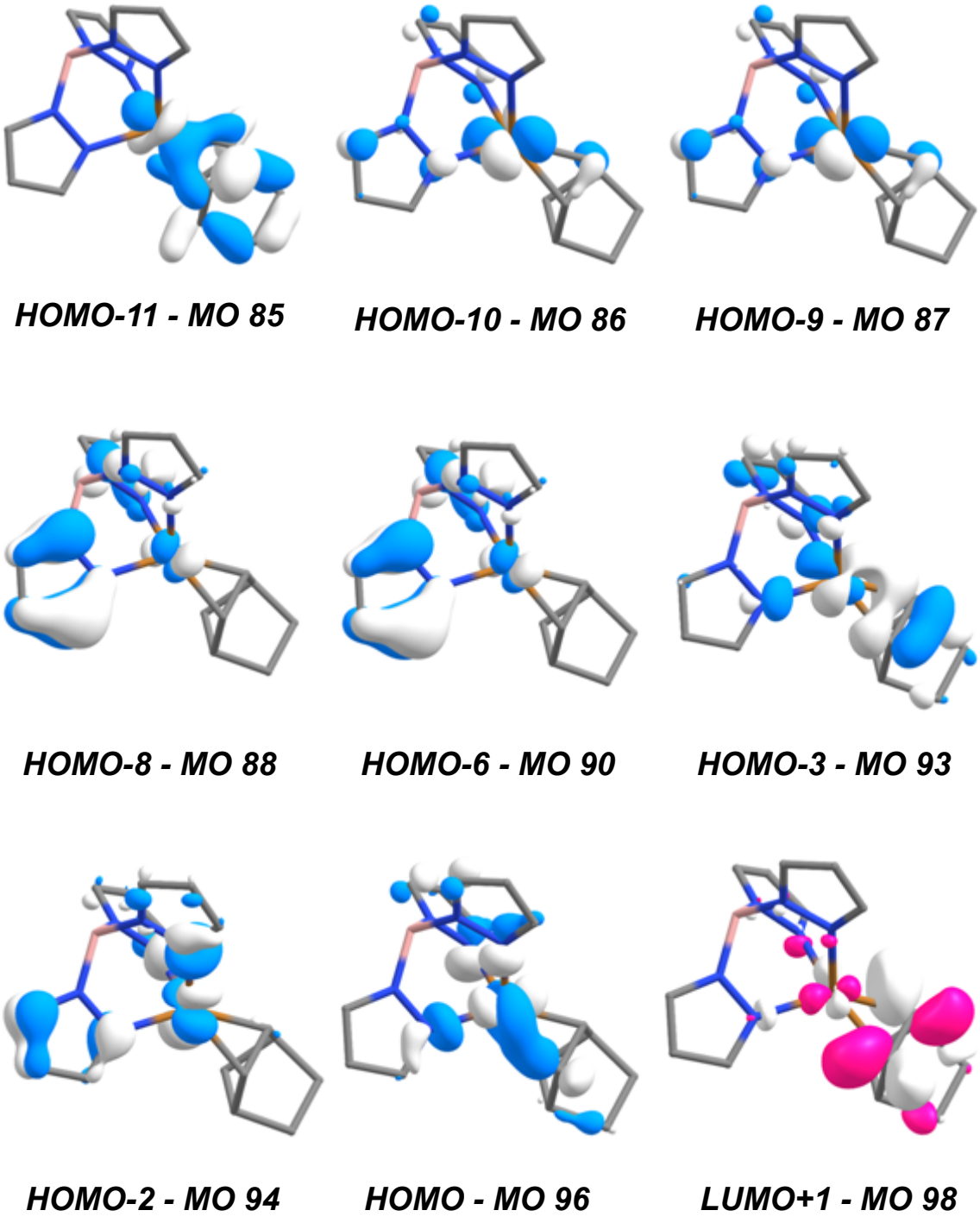

Figure 4.25 Frontier bonding molecular orbitals for **TpCuNB**.

Excited State 1: 4.8525 eV,
255.51 nm f=0.0055
80 -> 98 -0.18415
88 -> 98 -0.20707
90 -> 98 -0.32933
94 -> 98 0.49866
96 -> 98 -0.10063

Excited State 2: 5.0822 eV,
243.96 nm f=0.0298
85 -> 98 0.33925
86 -> 98 0.11018
90 -> 98 0.11157
93 -> 98 0.42799
96 -> 98 -0.32348

Excited State 3: 5.2697 eV,
235.28 nm f=0.0189
86 -> 98 0.24132
87 -> 98 0.44226
93 -> 98 0.21481
96 -> 98 0.34039

Excited State 4: 5.3399 eV,
232.18 nm f=0.0029
84 -> 98 -0.11371
85 -> 98 -0.11158
86 -> 98 0.46131
87 -> 98 -0.19323
88 -> 98 -0.21389
90 -> 98 -0.26130
94 -> 98 -0.24180

Excited State 5: 6.1830 eV,
200.52 nm f=0.4611
87 -> 98 0.22185
89 -> 98 0.23278
91 -> 98 0.35237
92 -> 98 -0.14788
94 -> 99 0.18026
96 -> 98 -0.32325

Excited State 6: 6.5356 eV,
189.70 nm f=0.0050
90 -> 100 0.19282
91 -> 99 -0.10624
94 -> 99 0.11863
94 -> 100 -0.28128
96 -> 99 0.48280

Excited State 7: 6.6926 eV,
185.26 nm f=0.0286
90 -> 104 0.18349
91 -> 99 -0.11900
93 -> 100 0.10890
94 -> 99 -0.23895
94 -> 100 -0.20069
95 -> 99 0.31710
96 -> 97 0.17555
96 -> 99 -0.11861
96 -> 100 0.27251

Excited State 8: 6.7216 eV,
184.46 nm f=0.0096
91 -> 104 0.17563
93 -> 99 0.13494
94 -> 99 -0.13370
94 -> 100 0.29948
95 -> 98 0.15715
95 -> 100 0.34976
96 -> 97 0.12104
96 -> 99 0.15263
96 -> 100 0.10690

Excited State 9: 6.8071 eV,
182.14 nm f=0.1081
88 -> 104 -0.12511
90 -> 99 -0.19764
90 -> 100 -0.18753
91 -> 99 -0.13794
91 -> 100 0.10152
92 -> 99 0.17293
94 -> 99 0.15543
94 -> 100 0.12556
94 -> 104 0.18399
95 -> 99 0.31418
96 -> 99 0.12056
96 -> 100 -0.21366

Excited State 10: 6.8250 eV,
181.66 nm f=0.1592
89 -> 104 -0.12170
90 -> 99 -0.23099
90 -> 100 0.16674
91 -> 99 0.14895
91 -> 100 0.13487
94 -> 100 -0.21593
95 -> 98 0.10523
95 -> 100 0.28672
96 -> 99 -0.20542
96 -> 100 -0.17522
96 -> 104 0.17499

Figure 4.26 First ten electronic transitions calculated for **TpCuNB**.

TpCuMA and its excited states were analyzed via Tam-Dancoff approximation density functional theory (TDA-DFT) calculations (first ten excited states). This provided a theoretical UV-vis spectrum that most closely resembled the experimental spectra (see **Figure S16**). From this an absorption band at 341.9 nm, which corresponds to an excitation from the HOMO - 7 (MO 88) to the LUMO (MO 96) could be computed. Further absorption bands were detected at 308.2 nm, and 224 nm. While there are various HOMOs contributing to the possible

transitions to the excited state each is primarily metal based (see images below). Therefore, the observed excitation can be interpreted as a metal to ligand charge transfer (MLCT). The HOMO shows significant contributions from the Cu dz^2 orbital, and the LUMO shows contribution from the Cu dxy orbital and maleic anhydride pi* orbital.

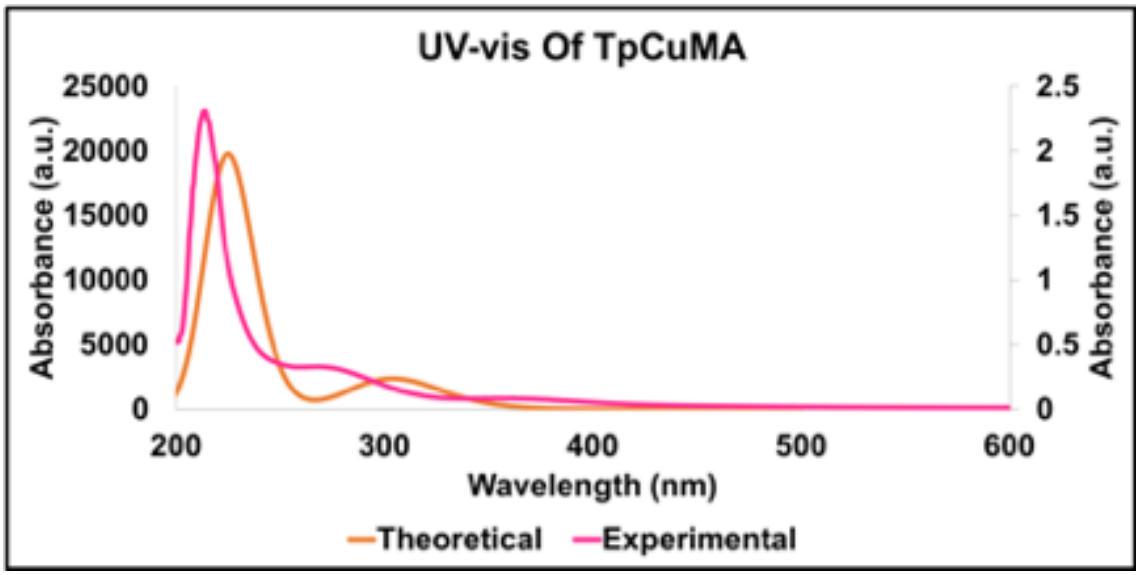

Figure 4.27 Theoretical and experimental electronic absorption spectra of TpCuMA. The theoretical spectrum was calculated using TDA-DFT approach using the M11 functional with Alhdrichs' def2-tzvpp basis set.

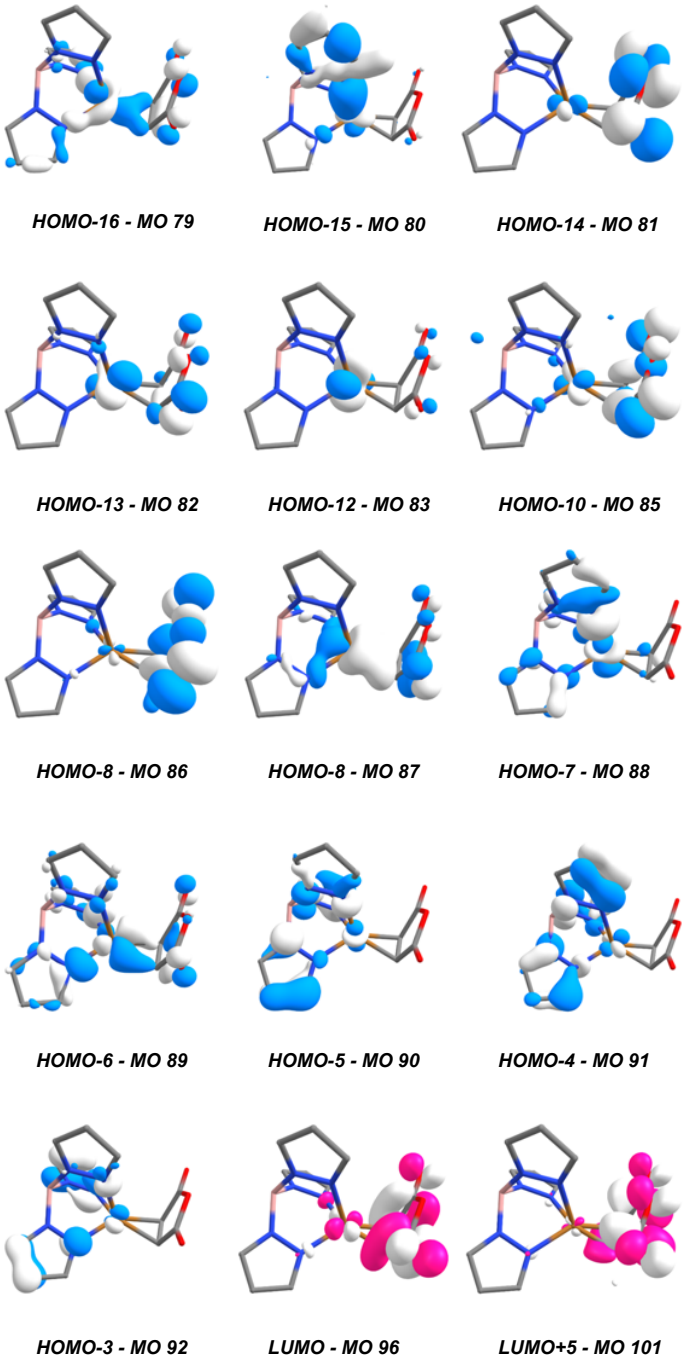

Figure 4.28 Frontier bonding molecular orbitals for **TpCuMA**.

Excited State 1: 3.6255 eV,
341.97 nm f=0.0016
79 -> 96 -0.10830
80 -> 96 0.19795
88 -> 96 0.47863
90 -> 96 0.30710
92 -> 96 0.24187

Excited State 2: 4.0229 eV,
308.20 nm f=0.0280
79 -> 96 0.22606
80 -> 96 0.11565
81 -> 96 0.12023
82 -> 96 -0.12166
87 -> 96 0.55614
88 -> 96 0.12809

Excited State 3: 4.1218 eV,
300.80 nm f=0.0298
83 -> 96 0.48127
83 ->104 -0.10970
86 -> 96 -0.14972
89 -> 96 -0.13427
91 -> 96 0.20555
93 -> 96 -0.19785
94 -> 96 -0.27229

Excited State 4: 4.2248 eV,
293.47 nm f=0.0003
82 -> 96 0.42312
82 ->104 -0.10128
85 -> 96 -0.31625
86 -> 96 0.13088
87 -> 96 0.17622
88 -> 96 -0.16593
92 -> 96 0.27629

Excited State 5: 4.5501 eV,
272.49 nm f=0.0045
83 -> 96 0.18695
85 ->101 0.12456
86 -> 96 0.57533
86 ->104 0.11288
89 -> 96 0.19876

Excited State 6: 5.2446 eV,
236.40 nm f=0.0042
79 -> 96 0.19264
82 -> 96 0.33533
85 -> 96 0.46184
85 ->104 0.10529
86 ->101 0.23047

Excited State 7: 5.3037 eV,
233.77 nm f=0.0020
93 -> 96 0.12953
94 -> 96 -0.19401
95 -> 96 0.65438

Excited State 8: 5.3307 eV,
232.59 nm f=0.0248
83 -> 96 0.14102
91 -> 96 -0.11250
92 -> 96 -0.10250
93 -> 96 -0.41000
94 -> 96 0.45831
95 -> 96 0.24788

Excited State 9: 5.5199 eV,
224.61 nm f=0.4618
83 -> 96 0.22462
86 -> 96 -0.22512
89 -> 96 0.44330
91 -> 96 -0.31997
93 -> 96 0.15464

Excited State 10: 5.9332 eV,
208.97 nm f=0.0060
83 -> 96 0.24290
89 -> 96 -0.15101
91 -> 96 0.14825
92 -> 96 0.16978
93 -> 96 0.44283
94 -> 96 0.36904

Figure 4.29 First ten electronic transitions calculated for **TpCuMA**

4.11 References

(1) Vitaku, E.; Smith, D. T.; Njardarson, J. T. Analysis of the Structural Diversity, Substitution Patterns, and Frequency of Nitrogen Heterocycles among U.S. FDA Approved Pharmaceuticals. *J. Med. Chem.* **2014**, *57* (24), 10257–10274. https://doi.org/10.1021/jm501100b.

(2) Brandi, A.; Cicchi, S.; Cordero, F. M. Novel Syntheses of Azetidines and Azetidinones. *Chem. Rev.* **2008**, *108* (9), 3988–4035. https://doi.org/10.1021/cr800325e.

(3) Mehra, V.; Lumb, I.; Anand, A.; Kumar, V. Recent Advances in Synthetic Facets of Immensely Reactive Azetidines. *RSC Adv.* **2017**, *7* (72), 45763–45783. https://doi.org/10.1039/c7ra08884a.

(4) Antermite, D.; Degennaro, L.; Luisi, R. Recent Advances in the Chemistry of Metallated Azetidines. *Org. Biomol. Chem.* **2017**, *15* (1), 34–50. https://doi.org/10.1039/C6OB01665K.

(5) Behnke, N. E.; Lovato, K.; Yousufuddin, M.; Kürti, L. Titanium-Mediated Synthesis of Spirocyclic NH-Azetidines from Oxime Ethers. *Angew. Chemie Int. Ed.* **2019**, *58* (40), 14219–14223. https://doi.org/10.1002/anie.201909151.

(6) Bondada, L.; Rondla, R.; Pradere, U.; Liu, P.; Li, C.; Bobeck, D.; McBrayer, T.; Tharnish, P.; Courcambeck, J.; Halfon, P.; et al. Azetidines and Spiro Azetidines as Novel P2 Units in Hepatitis C Virus NS3 Protease Inhibitors. *Bioorg. Med. Chem. Lett.* **2013**, *23* (23), 6325–6330. https://doi.org/https://doi.org/10.1016/j.bmcl.2013.09.068.

(7) Kirichok, A. A.; Shton, I. O.; Pishel, I. M.; Zozulya, S. A.; Borysko, P. O.; Kubyshkin, V.; Zaporozhets, O. A.; Tolmachev, A. A.; Mykhailiuk, P. K. Synthesis of Multifunctional Spirocyclic Azetidines and Their Application in Drug Discovery. *Chemistry* **2018**, *24* (21), 5444–5449. https://doi.org/10.1002/chem.201800193.

(8) Reckenthäler, M.; Griesbeck, A. G. Photoredox Catalysis for Organic Syntheses. *Adv. Synth. Catal.* **2013**, *355* (14–15), 2727–2744. https://doi.org/10.1002/adsc.201300751.

(9) Mallory, F. B. Synthetic Organic Photochemistry. Molecular and Supramolecular Photochemistry, Volume 12 Edited by Axel G. Griesbeck (Universität Zu Köln, Germany) and Jochen Mattay (Universität Bielefeld, Germany). Series Edited by V. Ramamurthy and K. S. Schanze. Marce. *J.*

Am. Chem. Soc. **2005**, *127* (32), 11531. https://doi.org/10.1021/ja0410441.

(10) Scharf, D.; Korte, F. Photosensibilisierte Cyclodimerisierung von Norbornen. *Tetrahedron Lett.* **1963**, *4* (13), 821–823. https://doi.org/https://doi.org/10.1016/S0040-4039(01)90722-1.

(11) Arnold, D. R.; Hinman, R. L.; Glick, A. H. Chemical Properties of the Carbonyl n, π State. The Photochemical Preparation of Oxetanes. *Tetrahedron Lett.* **1964**, *5* (22), 1425–1430. https://doi.org/https://doi.org/10.1016/S0040-4039(00)90493-3.

(12) Michon, C.; Medina, F.; Capet, F.; Roussel, P.; Agbossou-Niedercorn, F. Inter- and Intramolecular Hydroamination of Unactivated Alkenes Catalysed by a Combination of Copper and Silver Salts: The Unveiling of a Brønstedt Acid Catalysis. *Adv. Synth. Catal.* **2010**, *352* (18), 3293–3305. https://doi.org/10.1002/adsc.201000536.

(13) Fallis, A. G.; Brinza, I. M. Free Radical Cyclizations Involving Nitrogen. *Tetrahedron* **1997**, *53* (52), 17543–17594. https://doi.org/https://doi.org/10.1016/S0040-4020(97)10060-6.

(14) Hernvann, F.; Rasore, G.; Declerck, V.; Aitken, D. J. Stereoselective Intermolecular [2 + 2]-Photocycloaddition Reactions of Maleic Anhydride: Stereocontrolled and Regiocontrolled Access to 1{,}2{,}3-Trifunctionalized Cyclobutanes. *Org. Biomol. Chem.* **2014**, *12* (41), 8212–8222. https://doi.org/10.1039/C4OB01383B.

(15) Xiaohua, B.; Holt, E. M. Copper(I) Halide Complexation to Norbornene: (CuCl)5(Norbornene)4: A Complex of Novel Structure. *J. Crystallogr. Spectrosc. Res.* **1990**, *20* (4), 339–345. https://doi.org/10.1007/BF01274141.

(16) Pasquali, M.; Floriani, C.; Gaetani-Manfredotti, A.; Chiesi-Villa, A. Interaction of an Aliphatic Carbon-Hydrogen Bond with Copper in a Norbornene(Diethylenetriamine)Copper(I) Cation Complex. *J. Am. Chem. Soc.* **1978**, *100* (15), 4918–4919. https://doi.org/10.1021/ja00483a061.

(17) F. Straub, B.; Eisenträger, F.; Hofmann, P. A Remarkably Stable Copper(I) Ethylene Complex: Synthesis{,} Spectroscopy and Structure. *Chem. Commun.* **1999**, No. 24, 2507–2508. https://doi.org/10.1039/A907928I.

(18) Marsh, R. E.; Ubell, E.; Wilcox, H. E. The Crystal Structure of Maleic Anhydride. *Acta Crystallogr.* **1962**, *15* (1), 35–41. https://doi.org/10.1107/S0365110X62000080.

(19) Straub, B. F.; Gleiter, R.; Meier, C.; Gade, L. H. Organometallic Chemistry. *Beilstein J. Org. Chem.* **2016**, *12*, 2216–2221. https://doi.org/10.3762/bjoc.12.213.

(20) Budzellar, P. H. M.; Timmermans, P. J. J. A.; Mackor, A.; Baerends, E. J. Bonding in the Ground State and Excited States of Copper-Alkene Complexes. *J. Organomet. Chem.* **1987**, *331* (3), 397–407. https://doi.org/10.1016/0022-328X(87)80011-6.

(21) Wright, D. L.; Schulte, J. P.; Page, M. A. An Imine Addition/Ring-Closing Metathesis Approach to the Spirocyclic Core of Halichlorine and Pinnaic Acid. *Org. Lett.* **2000**, *2* (13), 1847–1850. https://doi.org/10.1021/ol005903b.

(22) Friestad, G. K. Addition of Carbon-Centered Radicals to Imines and Related Compounds. *Tetrahedron* **2001**, *57* (26), 5461–5496. https://doi.org/10.1016/S0040-4020(01)00384-2.

(23) Friestad, G. K. Addition of Carbon-Centered Radicals to Imines and Related Compounds. *Tetrahedron* **2001**, *57* (26), 5461–5496.

(24) Salvi, L.; Davis, N. R.; Ali, S. Z.; Buchwald, S. L. A New Biarylphosphine Ligand for the Pd-Catalyzed Synthesis of Diaryl Ethers under Mild Conditions. *Org. Lett.* **2012**, *14* (1), 170–173. https://doi.org/10.1021/ol202955h.

(25) Diaba, F.; Montiel, J. A.; Serban, G.; Bonjoch, J. Synthesis of Normorphans through an Efficient Intramolecular Carbamoylation of Ketones. *Org. Lett.* **2015**, *17* (15), 3860–3863. https://doi.org/10.1021/acs.orglett.5b01832.

(26) Cook, G. R.; Barta, N. S.; Stille, J. R. Lewis Acid-Promoted 3-Aza-Cope Rearrangement of N-Alkyl-N-Allyl Enamines. *J. Org. Chem.* **1992**, *57* (2), 461–467. https://doi.org/10.1021/jo00028a016.

(27) Dar'in, D.; Bakulina, O.; Chizhova, M.; Krasavin, M. New Heterocyclic Product Space for the Castagnoli–Cushman Three-Component Reaction. *Org. Lett.* **2015**, *17* (15), 3930–3933. https://doi.org/10.1021/acs.orglett.5b02014.

(28) Katritzky, A. R.; Hong, Q.; Yang, Z. Preparations of Secondary Amines and .Beta.-Amino Esters via Additions of Grignard and Reformatsky Reagents to Imines and by One-Pot Reactions of Primary Amines, Aldehydes, and Grignards. *J. Org. Chem.* **1995**, *60* (11), 3405–3408. https://doi.org/10.1021/jo00116a027.

(29) Barton, V.; Ward, S. A.; Chadwick, J.; Hill, A.; O'Neill, P. M. Rationale Design of Biotinylated Antimalarial Endoperoxide Carbon Centered Radical Prodrugs for Applications in Proteomics. *J. Med. Chem.* **2010**, *53* (11), 4555–4559. https://doi.org/10.1021/jm100201j.

(30) Pirrung, M. C.; Ghorai, S. Versatile, Fragrant, Convertible Isonitriles. *J. Am. Chem. Soc.* **2006**, *128* (36), 11772–11773. https://doi.org/10.1021/ja0644374.

(31) Mayo, P.; Tam, W. Ring-Opening Metathesis–Cross-Metathesis Reactions (ROM–CM) of Substituted Norbornadienes and Norbornenes. *Tetrahedron* **2002**, *58* (47), 9513–9525. https://doi.org/https://doi.org/10.1016/S0040-4020(02)01276-0.

(32) Capon, B.; Wu, Z. P. Comparison of the Tautomerization and Hydrolysis of Some Secondary and Tertiary Enamines. *J. Org. Chem.* **1990**, *55* (8), 2317–2324. https://doi.org/10.1021/jo00295a017.

(33) Poplata, S.; Tröster, A.; Zou, Y. Q.; Bach, T. Recent Advances in the Synthesis of Cyclobutanes by Olefin [2 +2] Photocycloaddition Reactions. *Chem. Rev.* **2016**, *116* (17), 9748–9815. https://doi.org/10.1021/acs.chemrev.5b00723.

(34) Lemaire-Audoire, S.; Savignac, M.; Genêt, J. P.; Bernard, J.-M. Selective Deprotection of Allyl Amines Using Palladium. *Tetrahedron Lett.* **1995**, *36* (8), 1267–1270. https://doi.org/https://doi.org/10.1016/0040-4039(95)00003-U.

(35) Shirokane, K.; Wada, T.; Yoritate, M.; Minamikawa, R.; Takayama, N.; Sato, T.; Chida, N. Total Synthesis of (±)-Gephyrotoxin by Amide-Selective Reductive Nucleophilic Addition. *Angew. Chemie Int. Ed.* **2014**, *53* (2), 512–516. https://doi.org/10.1002/anie.201308905.

(36) Zhao, Y.; Truhlar, D. G. The M06 Suite of Density Functionals for Main Group Thermochemistry, Thermochemical Kinetics, Noncovalent Interactions, Excited States, and Transition Elements: Two New Functionals and Systematic Testing of Four M06-Class Functionals and 12 Other Function. *Theor. Chem. Acc.* **2008**, *120* (1–3), 215–241. https://doi.org/10.1007/s00214-007-0310-x.

(37) Peverati, R.; Truhlar, D. G. M11-L: A Local Density Functional That Provides Improved Accuracy for Electronic Structure Calculations in Chemistry and Physics. *J. Phys. Chem. Lett.* **2012**, *3* (1), 117–124.

https://doi.org/10.1021/jz201525m.

(38) Weigend, F.; Ahlrichs, R. Balanced Basis Sets of Split Valence{,} Triple Zeta Valence and Quadruple Zeta Valence Quality for H to Rn: Design and Assessment of Accuracy. *Phys. Chem. Chem. Phys.* **2005**, *7* (18), 3297–3305. https://doi.org/10.1039/B508541A.

Chapter 5

Density Functional Theory as a Guide for Rational Ligand Design

5.1 Introduction

The development of the 2+2 COPC and IOPC is a novel approach towards activating electronically unbiased olefins for a concise synthesis of oxetanes and azetidines. The current limitation to it being widely applied by synthetic chemists is the lack of alkene scope; attributed to the inability of simple olefins to coordinate to the photocatalyst **TpCu** (see Chapters 3.4 and 4.4). To address this shortcoming, efforts were focused on ligand design in the hopes of synthesizing a catalyst that promotes coordination to simple alkenes.

The design of a photocatalyst can be particularly challenging due to the inherent major risks. Small changes to the structure, particularly the incorporation of additional chromophores, can have pronounced effects on the photophysical properties of the catalyst. This makes predicting the photophysical properties and catalytic activity of these complexes particularly difficult. Synthesizing a large library of derivatives is an enormous use of resources (e.g. chemicals, time, and personnel) with no guarantee of discovering a superior catalyst. Due to this we sought to use our previous experience with Density Functional Theory (DFT) as a guide to help identify promising ligand scaffolds to synthesize (see Chapter 4.4).

Tp ligands have been extensively researched with hundreds of derivatives reported in the literature, but the photophysical properties of these ligands coordinated to Cu is not well documented. Instead of arbitrarily picking ligands to

synthesize we wanted to use Time-dependent Density Functional Theory (TD-DFT) calculations to predict how the incorporation of substituents on the ligand would affect the theoretical electronic absorption spectra of the Cu-olefin complex. If there are a number of electronic transitions possible near the desired MLCT this could result in dramatically reduced reaction efficiency and overall yield. Additionally, this enabled us to visualize these complexes and recognize possible steric inhibition of olefin coordination.

Furthermore, we were curious how altering the coordinating atom would affect the Cu-olefin MLCT. There are a number of tridentate scorpionate ligand scaffolds that utilize various heteroatoms as the point of coordination to the metal center. We wanted to determine if the desired MLCT still occurred with these ligands and if it did establish if the desired electronic transition could be shifted to longer wavelengths.

With these questions in mind a series of DFT calculations were conducted with the goal of identifying potential ligands that could expand the olefin scope in the 2+2 IOPC and COPC. Based on our optimized computational parameters (see Chapter 4) we began our studies using the M11 density functional with Aldrich's def2-tzvpp basis set.

5.2 The Influence of Tp Substituents on Theoretical Electronic Absorption

A survey of the literature reveals that a variety of **Tp^{x}Cu** derivatives readily form complexes with CH_3CN,[1,2] CO,[3] phosphines,[4] alkynes,[5] amines,[6] arenes,[7]

and ethylene.[8–10] These structures have been unambiguously determined via single X-ray diffraction, and in many instances are bench top stable. Interestingly, **Tp^{mes}Cu** is the only derivative that has been clearly demonstrated to coordinate simple olefins other than ethylene, such as 1-hexene, cyclohexene, and allyl ethyl ether (**Figure 5.1**).[11] It is postulated that the mesityl groups form a pocket around the L ligand, trapping it and enforcing coordination to the metal center. Due to this precedent we began our computational studies with this complex.

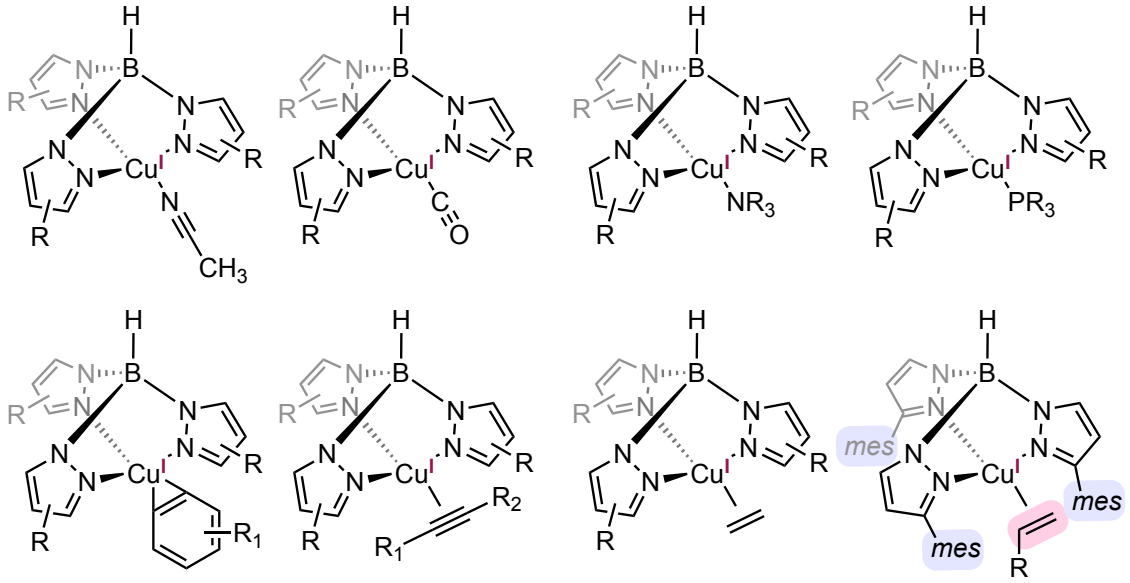

Figure 5.1 Previously reported Tp^{X}CuL complexes.

TD-DFT calculations on **Tp^{Mes}CuNB** revealed that the desired MLCT is the lowest energy transition, however there are multiple electronic transitions on the mesityl rings close in energy (**Figure 5.2**). This indicates that using our Hg-lamp as an irradiation source would induce several undesired electronic transitions, lowering reaction efficiency and likely yield. Therefore, the incorporation of highly

conjugated substituents that strongly absorb in the 260-310 nm range (i.e. arenes) should be avoided.

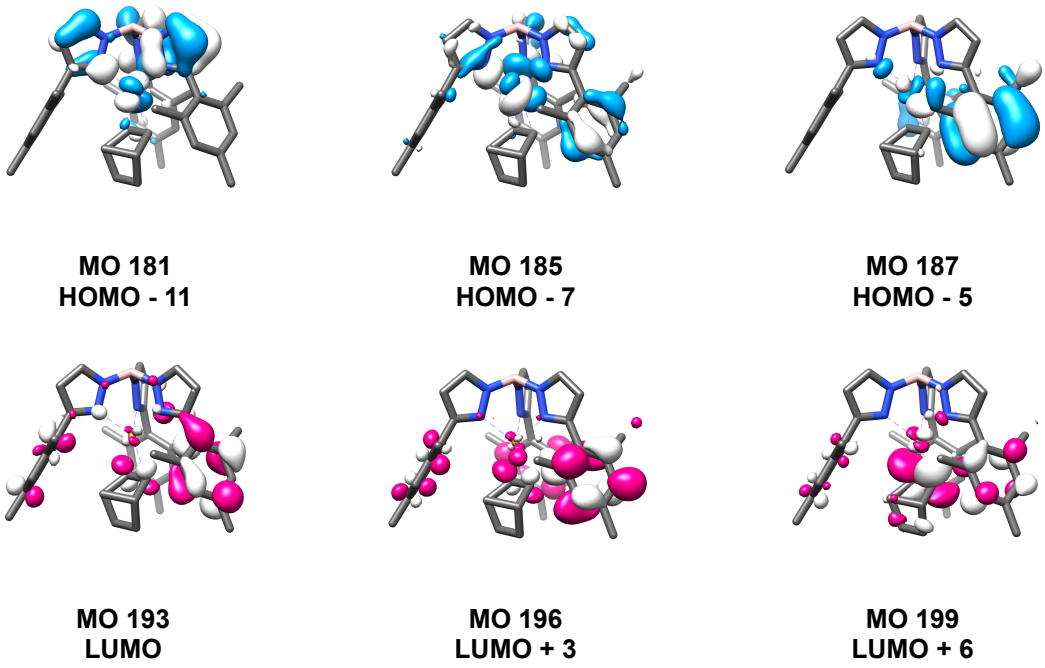

Figure 5.2 Molecular orbitals of Tp^{mes}CuNB involved in the lowest energy transition as predicted by TD-DFT calculations

This led to the substituent at the pyrazole C-3 position being changed to a methyl group as it is nonconjugated and could potentially form the desired pocket/cone around the incoming ligand. Geometry optimizations reveal that these methyl groups are positioned almost perpendicular to the incoming alkene and are expected to sterically inhibit coordination. Due to the commercial availability of potassium tris(3 5-dimethyl-1-pyrazolyl)borate (Tp*) the copper complex was readily synthesized and exposed to equimolar norbornene in solution. Indeed, ^{1}H-NMR of this sample revealed incomplete ligation of norbornene by **Tp*Cu** as the two species give distinct spectra (**Figure 5.3**). Unsurprisingly, no coordination was

observed when the alkene was altered indicating/suggesting/implying that the substituents at the C-3 position of the pyrazole should be planar so as to not

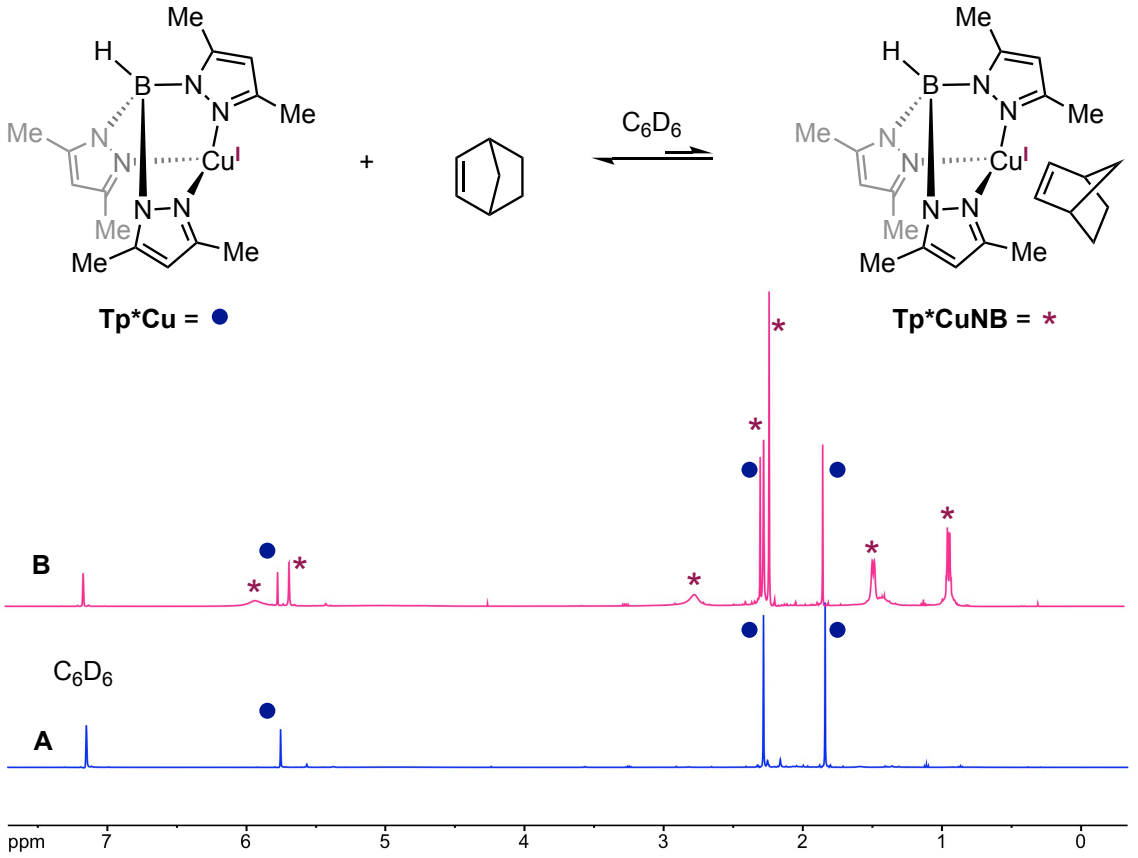

Figure 5.3. **A** ^{1}H-NMR spectrum of **TpCu***. **B** is **TpCu*** and one equivalent of norbornene.

sterically congest the metal center.

With these modifications in mind several ligands were proposed where the substituent was either a furan (**Tp^{Fur}**), thiophene (**TpTh**) or a cyclopropyl ring (**Tp^{cy}**). The analogous calculations produced theoretical electronic absorption spectra which can be seen below (**Figure 5.4**). Visually, the spectra of **Tp^{Fur}CuNB** and **TpThCuNB** do not resemble **TpCuNB** and is attributed to the limitation of the computational method accurately predicting extinction coefficients of each transition. Despite this, the desired MLCT from Cu to norbornene remains the

lowest energy transition (**Figure 5.5**). Combined with the fact that furan and

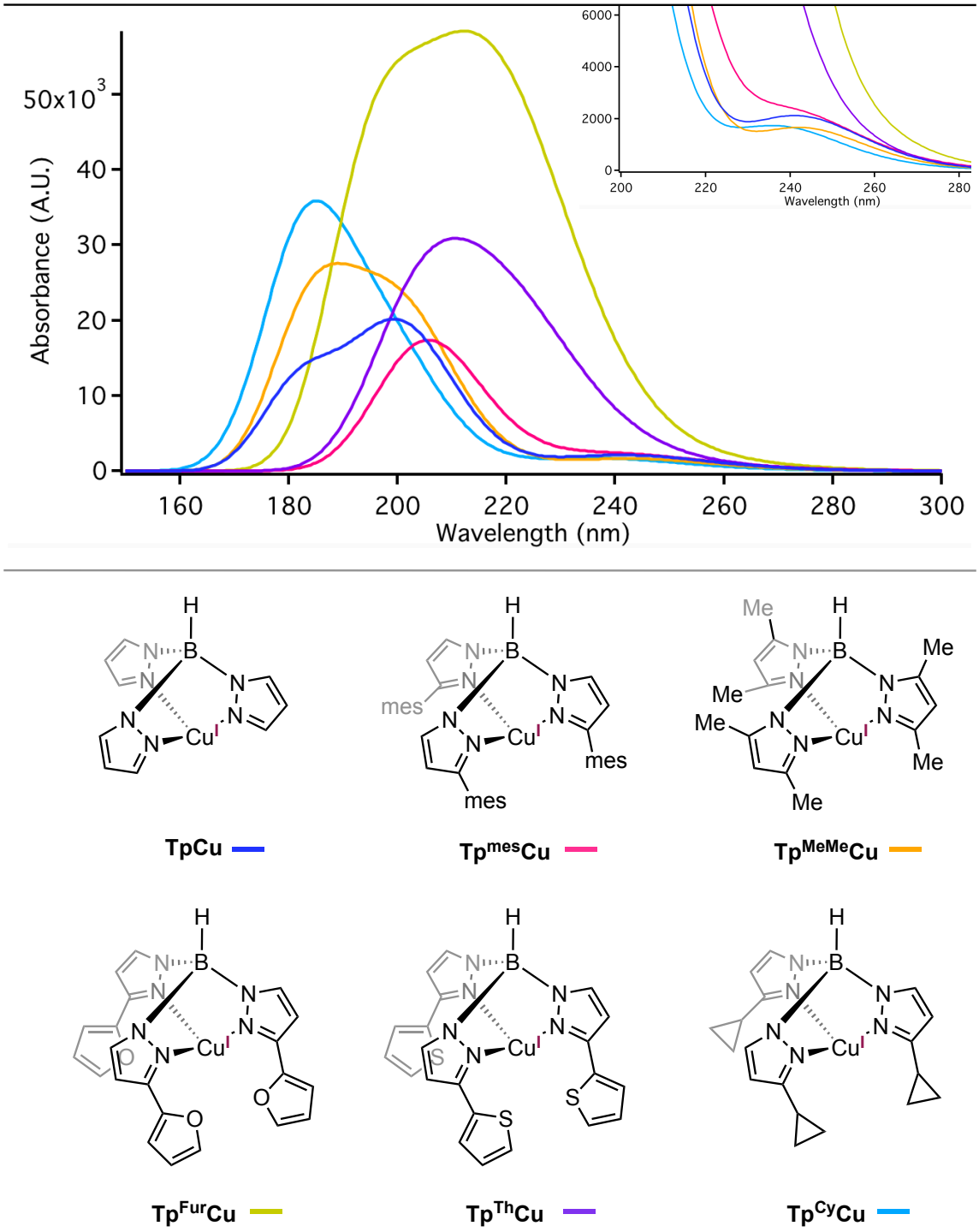

Figure 5.4 Theoretical electronic absorption spectra produced by TD-DFT calculations perfomed on complexes when coordinated to norbornene.

thiophene should absorb at shorter wavelengths than a mesityl group there should be fewer competing electronic transitions. **Tp^{cy}CuNB** displays nearly an identical theoretical spectrum as the parent complex, with no competing electronic transitions near the MLCT (**Figure 5.4**). Based on this data these three ligands are promising and should be synthesized, their photophysical properties characterized, and ability to coordinate to simple alkenes evaluated.

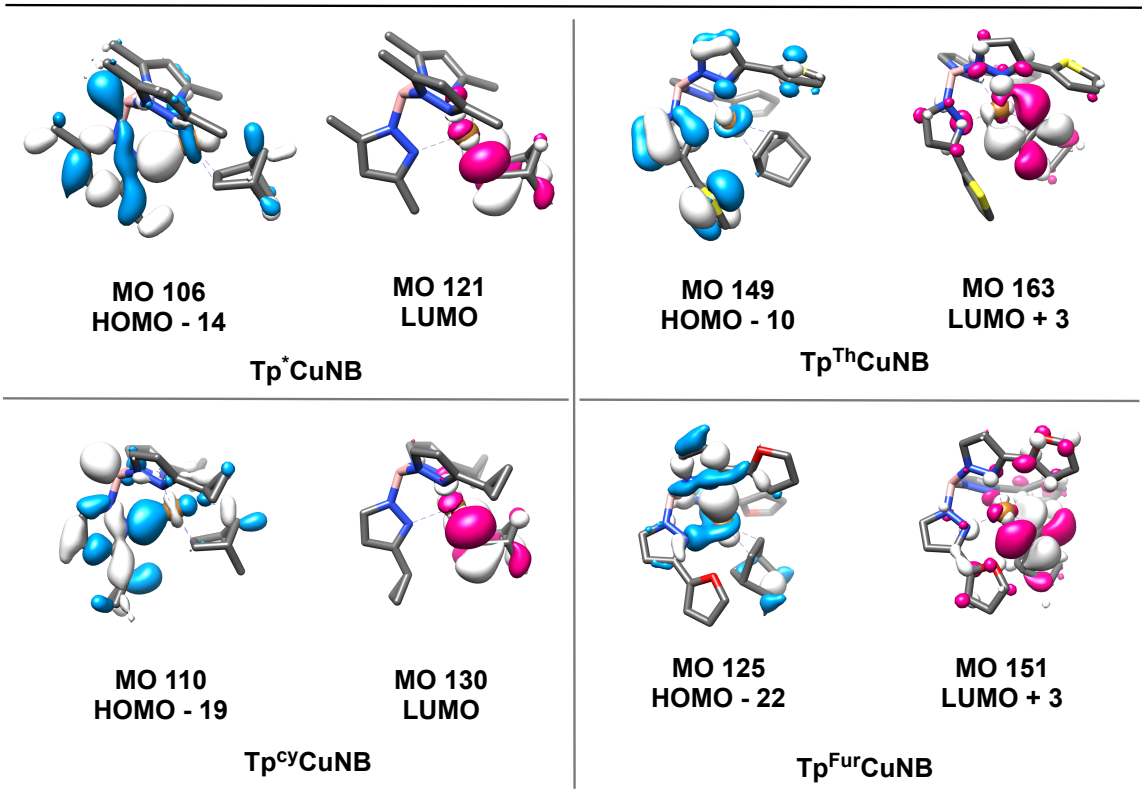

Figure 5.5 Molecular orbitals of various Tp^{x}CuNB complexes involved in the lowest energy transition as predicted by TD-DFT calculations

Designing ligands with substituents that satisfy the proposed modifications of being minimally conjugated and planar is challenging as these two attributes are generally contradictory within organic chemistry. This led us to consider other

tridentate ligands analogous to Tp that could induce olefin coordination.

5.3 The Influence of Coordinating Atoms on MLCT in Cu(I) Complexes

Tris(pyrazolyl)borates are a versatile class of ligands with widespread application stemming from their ability to be tuned sterically, but to a much lesser degree electronically.[12–14] The success of Tp ligands inspired the development of analogous scorpionate ligands that either replace the bridgehead boron atom or utilize different atoms at the point of coordination. These include trispyrazolyl methane ($Tp^{methane}$)[15,16] or borate ligands with tris-thioimidazolyl (Tm),[17] tris-selenoimidazolyl (TSe),[18] tris-phosphino (TP^{iPr}),[19] tris-N-heterocyclic carbene (Tc)[20], and tris-benzimidazole donors (**Figure 5.6**).[21] These variants are

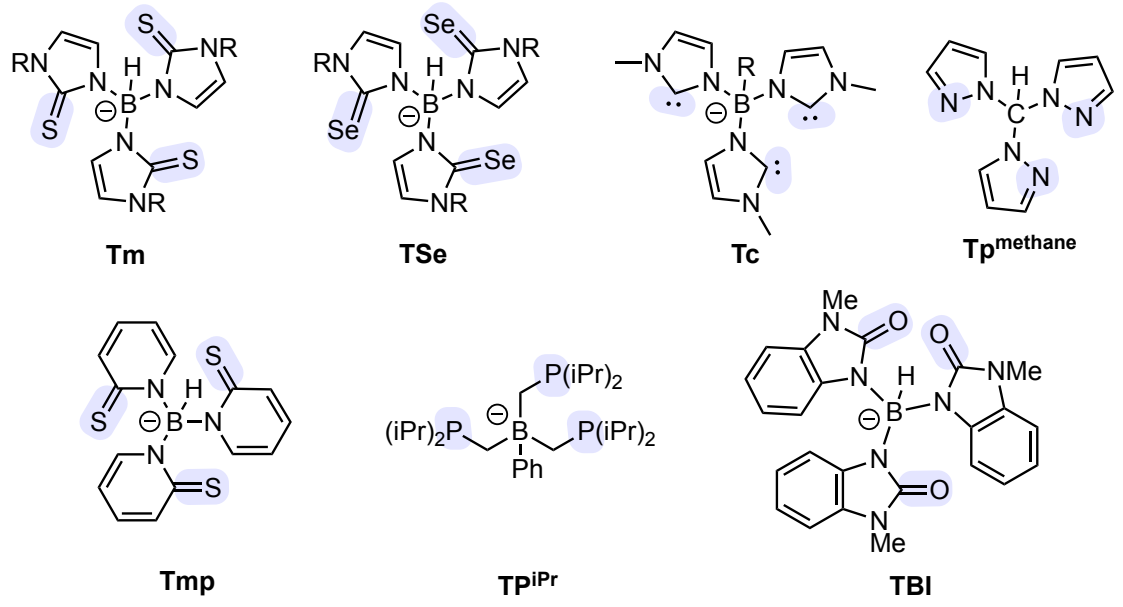

Figure 5.6 Tridentate scorpionate ligands derived from Tp.

particularly appealing because they offer a wider diversity in ligand electronic

properties with the relative donor strength of these ligands being Tc > TP^{iPr}> Tm > Tp = TSe.[22]

Due to the significant difference in electronic properties TD-DFT calculations were run on various copper complexes when coordinated with norbornene. Visually the theoretical electronic absorption spectra for these complexes lacks distinct maxima for each transition (**Figure 5.7**). This is attributed to the computational method used was optimized specifically for **TpCuNB**. Slight changes to the complex, such as the incorporation of several heteroatoms, could alter the spectra significantly. What is more important are the electronic transitions occurring and at what wavelength they are the induced.

In each complex, except for **TBICuNB**, the lowest energy transition is a MLCT from a primarily Cu-based orbital to the norbornene π^* orbital (**Figure 5.8**). In **TBICuNB** the lowest energy transition is a π-π^* transition on the ligand, further enforcing the idea that the incorporation of chromophores should be avoided. This demonstrates that this electronic transition is characteristic of a Cu(I)-olefin complex and is not inhibited by a change in ligand. The noticeable difference between these different complexes is where this electronic transition took place. **TmCuNB**, **TmpCuNB**, **TSeCuNB**, **TBICuNB**, and **TP^{iPr}CuNB** all displayed this transition between 257-272 nm, which is a 2-17 nm bathochromic shift from **TpCuNB** (see **Chapter 5.6**). **TcCuNB** displayed the most notable shift in the desired MLCT predicting it to occur at 282 nm. It is worth noting that the theoretical

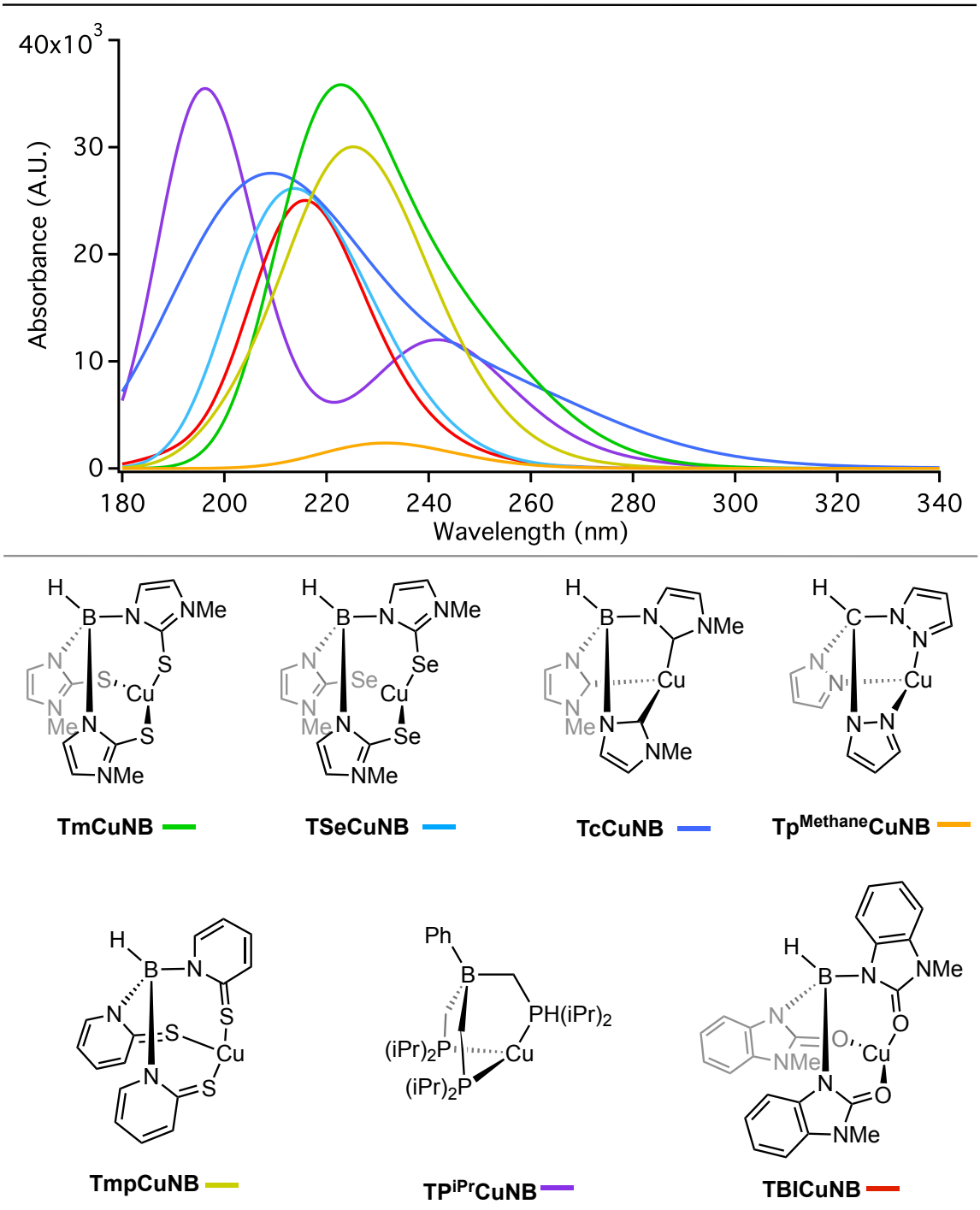

Figure 5.7 Theoretical electronic absorption spectra produced by TD-DFT calculations perfomed on complexes when coordinated to norbornene.

approximations for this transition in **TpCuNb** is ~30 nm lower than the experimental

data. If this underapproximation is assumed to be consistent while changing the scorpionate ligand then these complexes can potentially absorb light at wavelengths greater than 300 nm. This is of great significance as it would enable more readily accessible light sources to be used in our experimental setup.

Perhaps even more attractive is the fact that Tm, TSe, and phosphino ligands incorporate extra atoms between the boron and donor atoms. This enables them to form more flexible bicyclo [3.3.3] cages upon coordination to a metal center. As a consequence, the Cu atom sits deeper in the pocket of the ligand and more in plane with the coordinating atoms than it does with Tp. This also results in less steric interaction of the incoming alkene and the ligand, which should enable a wider scope of olefins to readily coordinate. These results indicate **TmCu**, **TSeCu**, **TP^{iPr}Cu**, **TcCu** and are photocatalysts that should be synthesized and evaluated.

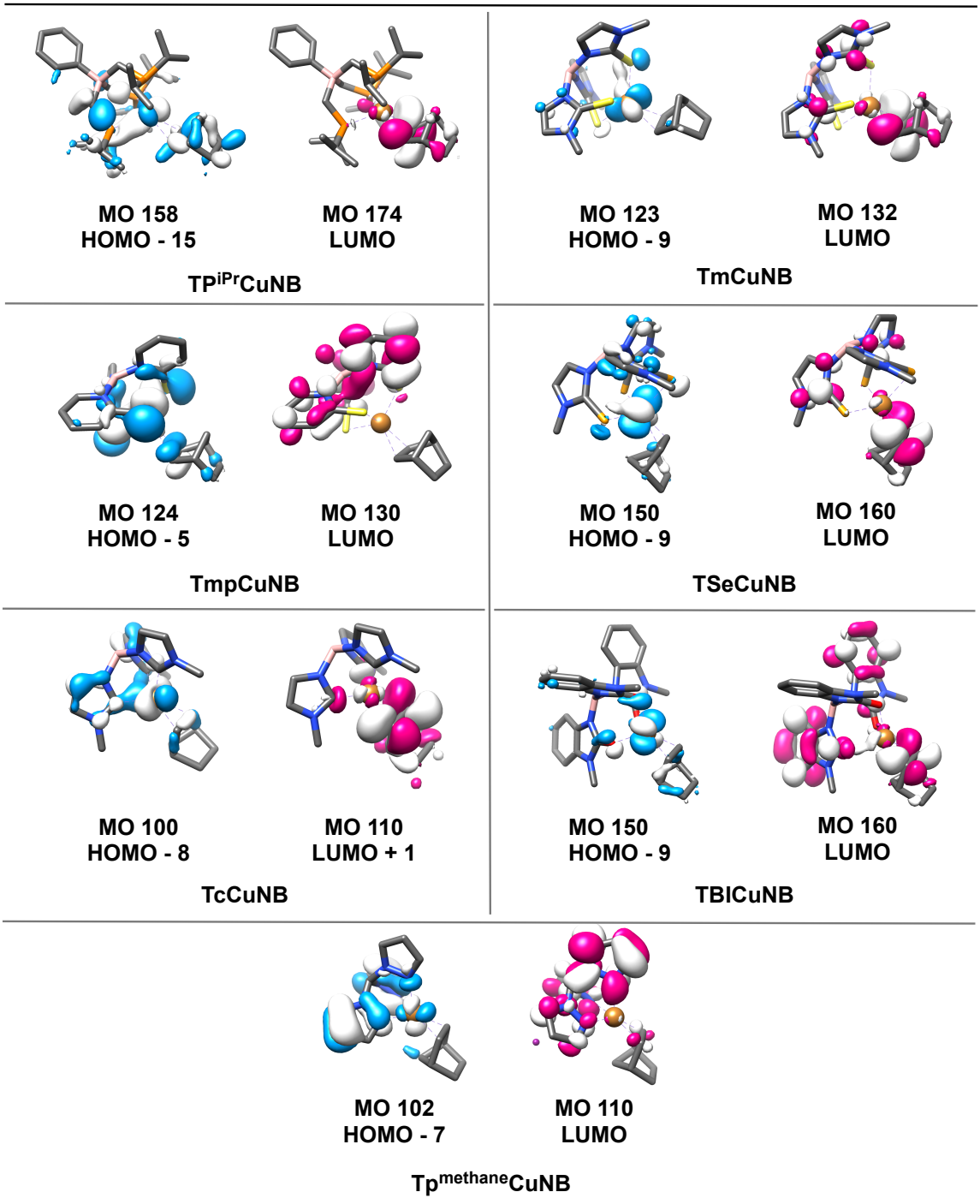

Figure 5.8 Various Cu complexes and the respective MOs involved in the lowest energy transition as predicted by TD-DFT calculations

5.4 Conclusions

A computational high through put screening method has been developed for evaluating the photophysical properties of various tridentate ligands bound to copper. While there are discrepancies with experimental data this enables a quick evaluation of the electronic transitions and an approximation of where they will occur. This has led to the rational design of several Tp derivatives as well as identifying Tm, Tmp, Tc, and trisphosphino as promising ligands. Moving forward these scorpionates will be synthesized and their corresponding Cu complexes evaluated as catalysts for the 2+2 COPC and 2+2 IOPC.

5.5 Synthetic Procedures and Characterization Data

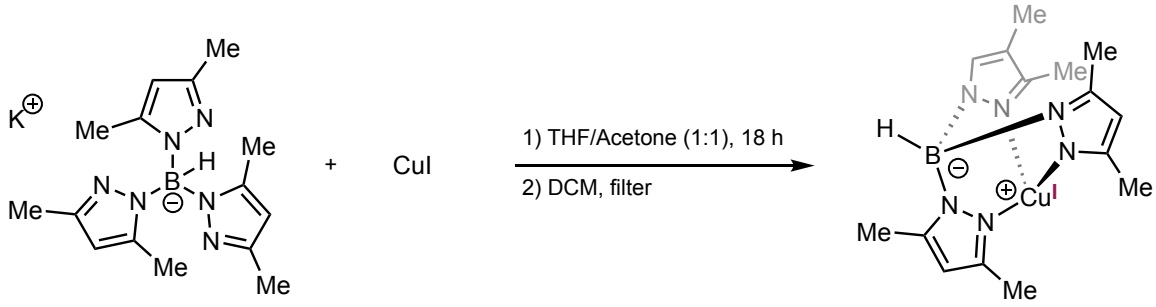

In a nitrogen filled glovebox, a 20 mL vial was charged with CuI (0.125g, 1 equiv), potassium tri(3,5-dimethyl-1-pyrazolyl)borohydride (0.253 g, 1 equiv) and a magnetic stir bar. A mixture of THF (4 mL) and dried, degassed acetone (4 mL) was added and the mixture was stirred vigorously for 18 h. The solvent was removed under reduced pressure, the resultant solid extracted with

dichloromethane (5 mL), and the suspension filtered through a thin pad of celite on a fritted funnel. Removal of the solvent under reduced pressure provided **Tp*Cu** (0.338 g, 92% yield) as a faint blue solid. Analytical data for **Tp*Cu**:

^{1}H-NMR (500 MHz; C_6D_6): δ 5.75 (s, 3H), 2.28 (s, 9H), 1.84 (s, 9H).

^{13}C-NMR (126 MHz; C_6D_6): δ 148.6, 144.9, 105.4, 13.79, 13.66

HRMS (ESI-TOFMS): Calc. for $[C_9H_{10}BCuN_6]^+$ = 360.1294, Found = 360.1292

5.6 Computational Details

Geometry optimizations for all $Tp^xCu(Norb)$ complexes were done starting from the crystallographic atomic coordinates obtained from TpCuNorb. Substituents were then built off of the pyrazole rings. For Tm, Tmp, Tc, TBI, tris-phsophino ligands crystallographic atomic coordinates were obtained for the respective Cu complex. If the data was unavailable coordinates were obtained when the ligand was bound to a first-row transition metal, and subsequently changed to Cu. All ground state geometry optimizations and frequency calculations were performed using the M11 density functional with Ahlrichs' def2-tzvpp basis set**.** using the Gaussian09 software package. This research was supported in part by the W. M. Keck Foundation through computing resources at the W. M. Keck Laboratory for Integrated Biology II.

All complexes and their excited states were analyzed via Tam-Dancoff approximation density functional theory (TDA-DFT) calculations (first ten excited states) providing a theoretical UV-vis spectrum.

```
%mem=20GB
%nprocshared=8
%chk=TpCuNorb-M11.chk
# opt freq m11/def2tzvpp scrf=(solvent=diethylether) integral=ultrafinegrid
pop=full

Title Card Required

0 1
xyz
```

Figure 5.9 Input file for geometry optimization and frequency calculations.

```
%mem=20GB
%nprocshared=8
%chk=TpCuNorb-TDA-M11.chk
# tda=nstates=10 m11/def2tzvpp scrf=(solvent=diethylether)
integral=ultrafinegrid

Title Card Required

0 1
xyz
```

Figure 5.10 Input file for TDA-DFT calculations.

Excited State 1: 4.8037 eV,
258.10 nm f=0.0095
181 ->193 0.10834
181 ->199 -0.17066
185 ->193 0.25341
185 ->196 0.16279
185 ->197 -0.14178
185 ->199 -0.38610
187 ->199 0.13050
188 ->199 -0.10950
191 ->199 -0.12104

Excited State 2: 5.1182 eV,
242.24 nm f=0.0221
175 ->193 0.15995
175 ->196 0.10608
175 ->199 -0.25403
180 ->199 -0.12763
183 ->193 0.19747
183 ->196 0.12617
183 ->197 -0.10800
183 ->199 -0.29372
188 ->199 0.13005
189 ->193 -0.12235
189 ->199 0.17124
190 ->199 0.11700

Excited State 3: 5.2091 eV,
238.01 nm f=0.0227
177 ->193 0.21512
177 ->196 0.14657
177 ->197 -0.12846
177 ->199 -0.34367
183 ->199 -0.13892
186 ->199 -0.12829
188 ->193 0.13667
188 ->199 -0.21035
190 ->199 -0.11811

Excited State 4: 5.3371 eV,
232.31 nm f=0.0050
176 ->193 0.24718
176 ->196 0.16219
176 ->197 -0.14161
176 ->199 -0.38723
178 ->199 0.14136
181 ->193 0.13719
181 ->199 -0.19866

Excited State 5: 5.3835 eV,
230.30 nm f=0.0014
187 ->193 0.31184
187 ->195 -0.18483
188 ->195 0.10988
189 ->193 -0.12989
190 ->196 -0.13324
191 ->196 0.22944
191 ->198 0.11102
191 ->199 0.12984
192 ->196 -0.14935
192 ->197 0.12899
192 ->198 0.14688

Excited State 6: 5.3837 eV,
230.29 nm f=0.0010
186 ->193 -0.11062
187 ->193 -0.14830
187 ->195 0.11241
188 ->193 0.11446
189 ->193 -0.14519
189 ->194 0.20923
189 ->195 -0.23434
191 ->197 0.13534
191 ->198 0.26647
192 ->196 0.13968
192 ->198 0.23569

Excited State 7: 5.4232 eV,
228.62 nm f=0.0016
183 ->194 0.10402
184 ->197 0.10064
186 ->194 -0.29728
186 ->195 -0.24792
187 ->194 0.13530
187 ->195 0.10962
188 ->197 -0.12436
189 ->194 0.12648
190 ->196 0.16141
190 ->197 0.28685
190 ->198 -0.12259
192 ->197 -0.11748

Excited State 8: 5.9311 eV,
209.04 nm f=0.0472
177 ->193 0.11530
177 ->199 -0.16928
179 ->199 -0.11309
182 ->193 -0.16342
182 ->199 0.21714
185 ->200 0.11607
188 ->193 -0.10585
188 ->199 0.16640
190 ->193 -0.18574
191 ->193 0.19435
192 ->195 0.13239

Excited State 9: 6.0209 eV,
205.92 nm f=0.2214
189 ->198 0.13146
190 ->193 0.12760
191 ->194 -0.26154
191 ->195 0.29967
192 ->193 0.37441
192 ->194 -0.13174
192 ->196 -0.12508

Excited State 10: 6.0714 eV,
204.21 nm f=0.1641
187 ->196 0.10559
189 ->198 -0.10235
190 ->194 -0.23504
190 ->195 -0.26534
191 ->193 -0.26884
192 ->194 0.30880
192 ->195 -0.11159

Figure 5.11 First ten electronic transitions calculated for $Tp^{mes}CuNB$

Excited State 1: 4.6815 eV, 264.84 nm f=0.0014
106 ->121 0.18289
112 ->121 0.22694
114 ->121 -0.10564
116 ->121 0.42037
117 ->121 -0.17002
118 ->121 0.38279

Excited State 2: 5.0530 eV, 245.37 nm f=0.0221
109 ->121 0.30033
110 ->121 0.40341
112 ->121 0.28198
114 ->121 0.12005
116 ->121 -0.26469
118 ->121 0.18436

Excited State 3: 5.1892 eV, 238.93 nm f=0.0147
110 ->121 0.11602
111 ->121 0.53898
112 ->121 -0.11448
118 ->121 0.11372
119 ->121 0.32867

Excited State 4: 5.2394 eV, 236.64 nm f=0.0050
109 ->121 0.28095
110 ->121 -0.40420
111 ->121 0.17904
112 ->121 0.37922
118 ->121 -0.15152

Excited State 5: 6.1650 eV, 201.11 nm f=0.4795
187 ->193 0.31184
111 ->121 0.19875
113 ->121 0.31799
115 ->121 0.33099
118 ->123 0.19645
119 ->121 -0.29944

Excited State 6: 6.4938 eV, 190.93 nm f=0.0149
112 ->124 -0.10891
113 ->123 -0.16580
115 ->123 -0.11712
116 ->124 -0.14551
117 ->122 -0.10186
117 ->123 0.18151
118 ->123 0.11241
118 ->124 -0.10033
119 ->122 -0.19896
119 ->123 0.42202
120 ->123 -0.16063

Excited State 7: 6.6297 eV, 187.01 nm f=0.0303
112 ->124 -0.10630
114 ->124 0.18667
114 ->126 -0.11600
115 ->122 0.18031
115 ->123 -0.23795
116 ->126 -0.12849
117 ->123 -0.10236
118 ->124 -0.24664
120 ->122 -0.20990
120 ->123 0.28276

Excited State 8: 6.6766 eV, 185.70 nm f=0.1654
113 ->124 -0.10145
113 ->126 -0.10092
114 ->122 -0.12777
114 ->123 0.19486
115 ->126 0.16731
116 ->123 0.10786
119 ->124 0.11768
120 ->121 0.14855
120 ->123 -0.11843
120 ->124 0.44833

Excited State 9: 6.6984 eV, 185.10 nm f=0.2055
106 ->124 -0.10013
115 ->123 -0.11292
116 ->124 0.18419
117 ->123 0.12610
117 ->124 -0.16244
118 ->122 -0.12633
118 ->124 0.34490
119 ->123 0.18819
120 ->122 -0.14213
120 ->123 0.13527
120 ->124 0.12835

Excited State 10: 6.8065 eV, 182.16 nm f=0.1776
112 ->123 -0.11939
113 ->126 0.10853
115 ->126 0.11036
117 ->121 -0.10745
117 ->123 0.11428
117 ->124 -0.15678
118 ->122 0.20706
118 ->123 -0.20983
119 ->122 -0.11391
119 ->124 0.39420
120 ->124 -0.12355

Figure 5.12 First ten electronic transitions calculated for Tp*CuNB.

Excited State 1: 4.8517 eV, 255.55 nm f=0.0286

125 ->151	0.15456
139 ->151	0.12821
142 ->150	0.12326
142 ->151	0.20256
144 ->150	0.29986
144 ->151	0.46503
145 ->151	0.10233

Excited State 2: 5.2422 eV, 236.51 nm f=0.0170

130 ->151	0.13502
131 ->150	0.11496
131 ->151	0.18314
132 ->151	0.11557
133 ->151	0.12502
139 ->150	0.14870
139 ->151	0.23883
142 ->150	0.23230
142 ->151	0.35861
144 ->150	-0.11993
144 ->151	-0.19366

Excited State 3: 5.2760 eV, 235.00 nm f=0.0118

135 ->150	-0.15000
135 ->151	-0.24591
136 ->151	0.10759
137 ->150	-0.11455
137 ->151	-0.18589
138 ->151	-0.10283
143 ->150	0.25831
143 ->151	0.37875
146 ->150	0.11498
146 ->151	0.10364

Excited State 4: 5.4457 eV, 227.68 nm f=0.46634

145 ->149	0.13984
146 ->150	-0.13999
147 ->148	0.58929
147 ->149	-0.11598
147 ->150	-0.15138
147 ->151	0.13009

Excited State 5: 5.4691 eV, 226.70 nm f=0.0021

187 ->193	0.31184
134 ->150	0.20938
134 ->151	0.33416
135 ->151	0.14003
136 ->150	0.19403
136 ->151	0.31139
137 ->151	0.13423
139 ->150	0.13739
139 ->151	0.22058
142 ->151	-0.15779

Excited State 6: 5.7219 eV, 216.68 nm f=0.5685

145 ->148	-0.27071
145 ->150	-0.30996
145 ->151	0.13246
146 ->148	0.16390
146 ->149	0.43430
147 ->149	-0.22609

Excited State 7: 5.8824 eV, 210.77 nm f=0.5122

140 ->151	-0.16695
145 ->149	0.41704
145 ->150	-0.15597
146 ->148	-0.24587
146 ->150	-0.24587
146 ->151	0.10654
147 ->150	0.19625

Excited State 8: 6.0746 eV, 204.10 nm f=0.0151

125 ->148	-0.10556
139 ->148	0.12419
142 ->148	0.30825
143 ->149	0.16314
144 ->148	0.42178
144 ->154	0.11598
145 ->148	0.13252
146 ->149	0.13290

Excited State 9: 6.6984 eV, 185.10 nm f=0.2055

140 ->151	-0.13921
141 ->148	-0.14748
142 ->149	0.26482
143 ->148	0.25637
143 ->151	-0.10790
144 ->149	0.38579
144 ->153	-0.10052
146 ->148	0.12249
146 ->150	0.10090

Excited State 10: 6.3342 eV, 195.74 nm f=0.9264

135 ->151	-0.10248
140 ->148	0.13023
140 ->150	-0.20893
140 ->151	-0.28172
141 ->150	-0.11376
143 ->148	-0.19058
143 ->150	-0.24379
143 ->151	-0.18768
145 ->149	-0.16671

Figure 5.13 First ten electronic transitions calculated for $Tp^{Fur}CuNB$.

Excited State 1: 4.8748 eV, 254.34 nm f=0.0130
139 ->163 0.13149
149 ->163 -0.10701
150 ->163 -0.13286
154 ->163 0.45939
154 ->164 -0.15674
156 ->163 -0.19592
157 ->163 0.20798
158 ->163 0.21121

Excited State 2: 5.1859 eV, 239.08 nm f=0.0330
142 ->163 0.31724
142 ->164 -0.11560
144 ->163 -0.12455
150 ->163 0.20058
155 ->163 0.32137
155 ->164 -0.10844
156 ->163 0.26370
157 ->163 0.21717

Excited State 3: 5.2649 eV, 235.49 nm f=0.0101
142 ->163 0.10408
144 ->163 0.37023
144 ->164 -0.13213
145 ->163 0.14737
154 ->163 -0.10060
155 ->163 0.35663
155 ->164 -0.12720
156 ->163 -0.21080
157 ->163 -0.10787
158 ->163 0.11363
159 ->163 0.10120

Excited State 4: 5.4246 eV, 228.56 nm f=0.0037
143 ->163 0.48175
143 ->164 -0.17180
146 ->163 0.18373
149 ->163 0.28302
150 ->163 0.13382
152 ->163 0.11966

Excited State 5: 5.5662 eV, 222.74 nm f=0.3936
159 ->160 0.61080
159 ->162 0.23781

Excited State 6: 5.9155 eV, 209.59 nm f=0.2676
156 ->161 0.10947
158 ->160 0.15603
158 ->161 0.52023
158 ->162 -0.22211
159 ->161 -0.11226

Excited State 7: 6.0347 eV, 205.45 nm f=0.0794
148 ->162 0.16864
150 ->162 -0.11576
154 ->162 -0.16622
156 ->163 0.14602
157 ->160 -0.20852
157 ->161 0.21580
157 ->162 0.35182

Excited State 8: 6.0673 eV, 204.35 nm f=0.1079
151 ->160 -0.27433
151 ->162 -0.14840
152 ->160 0.40116
152 ->162 0.17949
154 ->160 -0.13888
159 ->174 -0.10136

Excited State 9: 6.1358 eV, 202.07 nm f=0.0241
148 ->161 0.18886
148 ->162 0.10208
149 ->160 -0.10571
149 ->161 -0.21718
149 ->162 0.16348
150 ->161 0.15219
150 ->162 -0.20831
151 ->161 0.22035
152 ->160 0.13772
152 ->161 0.16683
153 ->161 -0.10647
156 ->163 -0.12478
158 ->171 -0.12230

Excited State 10: 6.1556 eV, 201.42 nm f=0.1763
148 ->160 0.12886
148 ->162 -0.25264
149 ->161 -0.23864
150 ->161 0.24371
151 ->160 0.15535
151 ->162 -0.14336
152 ->161 0.12511
152 ->162 -0.14092
153 ->162 0.11633
156 ->162 -0.12052
158 ->171 -0.10355

Figure 5.14 First ten electronic transitions calculated for $Tp^{Th}CuNB$.

Excited State 1: 4.7722 eV, 259.80 nm f=0.0035
110 ->130 0.14115
121 ->130 -0.22145
124 ->130 0.19926
125 ->130 0.43767
127 ->130 -0.36144

Excited State 2: 5.1217 eV, 242.08 nm f=0.0210
116 ->130 0.10150
117 ->130 0.18548
118 ->130 0.15157
119 ->130 -0.42708
121 ->130 0.22524
123 ->130 -0.32992
125 ->130 0.10852
127 ->130 0.17576

Excited State 3: 5.2815 eV, 234.75 nm f=0.0151
114 ->130 -0.10439
120 ->130 0.55048
122 ->130 0.13594
126 ->130 -0.19604
128 ->130 -0.26820

Excited State 4: 5.3176 eV, 233.16 nm f=0.0066
117 ->130 0.18177
118 ->130 0.26679
119 ->130 0.34572
120 ->130 0.13089
121 ->130 0.43255
127 ->130 -0.12206

Excited State 5: 6.1846 eV, 200.47 nm f=0.3587
120 ->130 0.18547
122 ->130 0.38369
126 ->130 0.28564
127 ->131 -0.12285
128 ->130 0.32276

Excited State 6: 6.6302 eV, 187.00 nm f=0.0989
121 ->133 0.10874
122 ->131 -0.12585
122 ->132 0.10991
125 ->133 -0.11587
126 ->131 -0.21584
126 ->132 0.19625
128 ->131 -0.34452
128 ->132 0.36682

Excited State 7: 6.6742 eV, 185.77 nm f=0.2658
123 ->133 -0.15747
123 ->134 0.12149
126 ->131 0.16717
126 ->132 -0.26580
127 ->133 -0.20873
128 ->132 0.13946
129 ->131 -0.20539
129 ->132 0.34948
129 ->133 0.14573

Excited State 8: 6.6898 eV, 185.33 nm f=0.3566
123 ->132 -0.13361
124 ->133 0.13231
125 ->132 -0.10166
126 ->134 0.15980
127 ->132 -0.16104
128 ->134 -0.11391
129 ->130 0.15450
129 ->133 0.47231

Excited State 9: 6.8652 eV, 180.60 nm f=0.0550
110 ->133 0.13158
110 ->134 0.11572
121 ->133 0.16722
121 ->134 0.10467
124 ->133 -0.14415
125 ->133 -0.26750
125 ->134 -0.12327
126 ->131 0.12615
127 ->133 0.37891
127 ->134 0.12501
128 ->131 0.11977

Excited State 10: 7.0104 eV, 176.86 nm f=0.0793
121 ->132 0.15743
122 ->134 -0.13258
124 ->132 -0.10191
124 ->133 0.15401
125 ->132 -0.17322
126 ->133 0.17510
127 ->132 0.20526
128 ->133 0.37365
128 ->134 -0.11620

Figure 5.15 First ten electronic transitions calculated for $Tp^{Cy}CuNB$.

Excited State 1: 4.8165 eV,
257.41 nm f=0.0121

119 ->133	-0.13999
123 ->133	0.17472
124 ->133	-0.14719
125 ->133	-0.10662
126 ->133	-0.12211
128 ->133	0.18463
129 ->133	-0.12483
130 ->133	-0.11995
132 ->133	0.50260
132 ->137	-0.10832

Excited State 2: 4.8901 eV,
253.54 nm f=0.0605

120 ->133	-0.19346
126 ->133	-0.24881
126 ->137	0.13423
130 ->133	0.52023
131 ->133	-0.16194

Excited State 3: 5.0305 eV,
246.46 nm f=0.1853

121 ->133	0.16993
123 ->133	-0.13081
124 ->133	-0.14719
126 ->133	-0.12191
129 ->133	0.17606
130 ->133	0.10828
131 ->133	0.50791
132 ->133	0.13087

Excited State 4: 5.2318 eV,
236.98 nm f=0.0257

124 ->133	0.18497
127 ->134	-0.17120
127 ->136	0.17787
128 ->133	0.28440
128 ->137	0.21149
129 ->133	0.26949
129 ->134	-0.18234
129 ->136	0.11760
129 ->137	0.12829
130 ->134	0.14508
130 ->136	-0.13743
131 ->133	-0.10265
131 ->134	-0.11225

Excited State 5: 5.2749 eV,
235.05 nm f=0.0073

127 ->135	-0.23282
128 ->135	-0.30702
129 ->134	-0.14435
129 ->135	0.41772
130 ->135	0.17387
131 ->135	0.14434

Excited State 6: 5.3026 eV,
233.82 nm f=0.0053

126 ->133	-0.10374
127 ->133	0.22672
127 ->137	0.21293
128 ->133	-0.18904
128 ->134	-0.23518
128 ->136	0.24654
128 ->137	-0.15513
129 ->134	-0.17989
129 ->136	0.15711
129 ->137	0.10095
130 ->134	0.10722
132 ->135	-0.18274
132 ->136	0.14182

Excited State 7: 5.4592 eV,
227.11 nm f=0.2123

121 ->133	-0.16817
129 ->134	-0.12393
129 ->137	0.11192
131 ->134	-0.12400
131 ->137	0.10592
132 ->134	-0.14221
132 ->135	0.50451
132 ->136	-0.13124
132 ->137	-0.13189

Excited State 8: 5.4976 eV,
225.52 nm f=0.0911

121 ->133	0.28210
121 ->137	-0.10546
123 ->133	0.10452
124 ->133	0.24875
124 ->137	-0.11194
125 ->133	-0.17581
126 ->133	-0.12608
128 ->137	-0.11785
129 ->133	0.16972
129 ->137	-0.14692
130 ->137	-0.11912
131 ->134	0.14999
131 ->136	-0.13022
132 ->134	-0.10921
132 ->135	0.23107

Excited State 9: 5.5847 eV,
222.01 nm f=0.1498

120 ->133	-0.11594
121 ->133	-0.16658
123 ->133	-0.13102
125 ->133	0.13620
126 ->133	-0.11666
130 ->134	0.16966
130 ->137	-0.29965
131 ->134	0.32117
131 ->136	-0.27201
132 ->137	0.10900

Excited State 10: 5.6907 eV,
217.87 nm f=0.4342

123 ->133	0.20824
124 ->133	0.21153
125 ->133	0.11797
128 ->133	0.12183
130 ->134	-0.24535
130 ->136	0.22973
131 ->133	0.13242
131 ->137	0.31186
132 ->134	0.10841
132 ->135	-0.14200

Figure 5.16 First ten electronic transitions calculated for TmCuNB.

Excited State 1: 3.7829 eV, 327.75 nm f=0.0022

124 ->130	0.13885
124 ->132	-0.10813
124 ->133	0.12526
125 ->131	0.18593
125 ->132	0.31926
125 ->135	0.11433
126 ->130	0.10610
126 ->131	0.12180
126 ->132	-0.25099
126 ->135	-0.11302
127 ->132	0.23155
129 ->131	-0.14601
129 ->132	-0.19805

Excited State 2: 3.8071 eV, 325.67 nm f=0.0006

124 ->130	0.10284
124 ->132	0.16681
125 ->130	0.31214
125 ->131	0.25332
125 ->133	0.16677
125 ->134	0.11822
126 ->131	0.20280
126 ->132	0.13981
127 ->131	-0.11997
129 ->130	-0.23170
129 ->131	-0.11760
129 ->133	-0.11153

Excited State 3: 3.8469 eV, 322.30 nm f=0.0051

124 ->131	-0.21061
125 ->130	-0.12999
125 ->132	-0.11841
126 ->130	-0.20037
126 ->131	0.34678
126 ->132	-0.15916
126 ->133	-0.17420
127 ->130	0.11099
127 ->131	-0.21854
128 ->131	0.18467

Excited State 4: 4.0111 eV, 309.10 nm f=0.1286

127 ->130	-0.32955
128 ->130	0.22180
128 ->131	0.33168
128 ->132	0.19509
129 ->130	-0.25614
129 ->131	-0.19641
129 ->132	0.13382

Excited State 5: 4.0359 eV, 307.20 nm f=0.1625

125 ->130	-0.10278
125 ->132	0.10250
126 ->131	-0.10442
127 ->130	0.10092
127 ->131	-0.24777
127 ->132	0.21398
128 ->131	-0.15156
128 ->132	0.27955
129 ->130	-0.27703
129 ->131	0.28077
129 ->132	0.20535

Excited State 6: 4.2112 eV, 294.41 nm f=0.4569

127 ->131	-0.35214
128 ->130	0.40222
129 ->132	-0.37997

Excited State 7: 4.5579 eV, 272.02 nm f=0.2123

125 ->131	0.12932
126 ->130	0.13166
127 ->130	-0.25733
128 ->131	0.21275
128 ->132	-0.11694
129 ->131	0.45891
129 ->132	-0.14502
129 ->136	-0.12795

Excited State 8: 4.5985 eV, 269.62 nm f=0.0336

125 ->130	-0.12130
126 ->130	0.17868
127 ->130	0.36231
127 ->131	0.28019
128 ->131	0.19330
129 ->130	-0.31549
129 ->132	-0.15965

Excited State 9: 4.6531 eV, 266.46 nm f=0.0262

124 ->130	-0.10830
124 ->132	-0.12926
125 ->130	0.23551
125 ->131	-0.17306
126 ->130	0.38920
126 ->131	0.22241
127 ->131	-0.10202
127 ->132	-0.13207
128 ->132	0.27187
129 ->130	0.13577

Excited State 10: 4.6884 eV, 264.45 nm f=0.0638

124 ->130	-0.16140
125 ->130	-0.10588
125 ->132	0.22638
126 ->130	0.13159
126 ->131	0.23155
126 ->132	0.24295
127 ->132	0.21313
128 ->130	0.28139
128 ->131	-0.11348
128 ->132	-0.19506
129 ->132	0.19112

Figure 5.17 First ten electronic transitions calculated for TmpCuNB.

Excited State 1: 4.8011 eV, 258.24 nm f=0.0274

147 ->160	0.11080
150 ->160	0.13297
151 ->160	-0.10247
155 ->160	-0.13375
157 ->160	-0.11540
159 ->160	0.55065

Excited State 2: 4.8496 eV, 255.66 nm f=0.0515

153 ->160	0.15646
153 ->164	-0.10105
155 ->160	0.10255
156 ->161	-0.14851
156 ->163	0.17009
157 ->160	-0.31799
158 ->160	0.46470

Excited State 3: 4.9538 eV, 250.28 nm f=0.0535

154 ->161	-0.14845
154 ->163	0.11302
155 ->162	-0.15533
155 ->163	0.10140
156 ->160	0.29760
156 ->164	0.15136
157 ->160	0.32698
158 ->160	0.24082
158 ->161	-0.12578
158 ->163	0.14475
159 ->162	0.11553
159 ->163	-0.13619

Excited State 4: 4.9979 eV, 248.07 nm f=0.0138

154 ->162	-0.16708
155 ->161	-0.15873
155 ->162	0.38390
156 ->160	0.11438
157 ->161	-0.10008
157 ->162	0.30113
158 ->161	-0.15174
158 ->162	0.14991
159 ->162	-0.13369

Excited State 5: 5.0626 eV, 244.90 nm f=0.1529

151 ->160	-0.10947
155 ->160	-0.12681
156 ->160	-0.18365
156 ->161	0.15312
156 ->163	-0.10034
156 ->164	-0.12807
157 ->160	0.16970
157 ->161	-0.18808
157 ->162	0.12159
158 ->160	0.28174
158 ->161	0.22024
158 ->163	-0.20411
159 ->162	0.10133
159 ->163	-0.11378

Excited State 6: 5.1004 eV, 243.09 nm f=0.0335

145 ->160	-0.12553
151 ->160	-0.10461
153 ->160	-0.19275
153 ->164	0.11194
154 ->160	0.23710
154 ->164	0.10412
155 ->164	0.12226
156 ->160	-0.15996
156 ->161	-0.19442
156 ->163	0.18105
157 ->160	0.20245
157 ->164	-0.10913
159 ->160	0.12377
159 ->162	-0.10724
159 ->163	0.14142
159 ->164	-0.19591

Excited State 7: 5.3019 eV, 233.85 nm f=0.2801

157 ->162	0.19151
158 ->160	-0.11466
159 ->161	-0.15344
159 ->162	0.52844
159 ->163	-0.14427
159 ->164	-0.14236

Excited State 8: 5.4286 eV, 228.39 nm f=0.1040

147 ->160	-0.11996
151 ->160	0.12726
153 ->160	-0.14812
155 ->160	0.10083
156 ->160	0.11123
157 ->161	0.25830
157 ->163	-0.11278
157 ->164	-0.23256
158 ->161	0.30878
158 ->163	-0.14393
159 ->161	-0.14767
159 ->164	0.12438

Excited State 9: 5.5164 eV, 224.76 nm f=0.0410

150 ->160	-0.10759
151 ->160	-0.12367
155 ->169	-0.12261
156 ->161	0.10080
156 ->168	0.13584
157 ->161	0.31610
157 ->162	0.16716
157 ->170	0.11154
158 ->161	-0.12038
158 ->162	-0.13945
158 ->164	-0.24095
159 ->162	0.10329
159 ->163	0.12258

Excited State 10: 5.5317 eV, 224.13 nm f=0.0656

149 ->160	-0.22042
152 ->160	0.10505
156 ->160	-0.13267
156 ->164	0.13573
157 ->161	0.10442
158 ->162	0.11664
158 ->164	0.22535
159 ->161	0.34593
159 ->170	0.11044

Figure 5.18 First ten electronic transitions calculated for TSeCuNB.

Excited State 1: 4.3674 eV,
283.89 nm f=0.0014
96 ->110 0.23440
105 ->110 0.11564
107 ->110 0.24943
108 ->110 0.57492

Excited State 2: 5.1142 eV,
242.43 nm f=0.0437
97 ->110 0.34163
100 ->110 -0.23088
101 ->110 0.19055
103 ->110 0.22405
105 ->110 0.38235
107 ->110 -0.21139

Excited State 3: 5.1353 eV,
241.43 nm f=0.1186
94 ->110 0.10357
97 ->110 0.15909
100 ->110 -0.14862
101 ->110 -0.41487
105 ->110 0.18574
107 ->110 0.37845
108 ->110 -0.18382

Excited State 4: 5.3136 eV,
233.34 nm f=0.0064
97 ->110 0.19081
98 ->110 -0.12417
100 ->110 0.39548
103 ->110 0.34892
107 ->111 -0.24306
108 ->111 0.10066
108 ->112 0.17913
108 ->114 0.11443

Excited State 5: 5.4220 eV,
228.67 nm f=0.0003
100 ->110 -0.30062
103 ->110 -0.18800
107 ->111 -0.32326
107 ->112 0.13021
107 ->113 -0.11989
108 ->111 0.12561
108 ->112 0.32523
108 ->114 0.20109

Excited State 6: 5.6954 eV,
217.69 nm f=0.2132
101 ->110 -0.20851
104 ->110 -0.15471
107 ->109 -0.12434
107 ->110 -0.17958
107 ->111 0.37546
107 ->113 0.15082
108 ->111 0.18004
108 ->112 0.25665
108 ->114 0.15792

Excited State 7: 5.7070 eV,
217.25 nm f=0.1950
101 ->110 -0.18427
104 ->110 -0.13539
107 ->110 -0.16574
107 ->111 -0.17054
107 ->112 -0.16527
107 ->114 -0.10333
108 ->109 -0.12411
108 ->111 0.38531
108 ->112 -0.21519
108 ->113 0.15183
108 ->114 -0.13246
108 ->121 -0.11712

Excited State 8: 5.9176 eV,
209.52 nm f=0.0609
101 ->110 0.14377
107 ->109 0.19266
107 ->110 0.10271
107 ->112 -0.19340
107 ->114 -0.11513
108 ->109 0.50266
108 ->111 0.20660

Excited State 9: 5.9602 eV,
208.02 nm f=0.0293
107 ->109 0.56598
107 ->111 0.13600
108 ->109 -0.31423

Excited State 10: 6.0005 eV,
206.62 nm f=0.2625
101 ->110 -0.23780
103 ->111 0.10187
104 ->110 -0.16583
107 ->109 0.28617
107 ->110 -0.21726
107 ->112 0.22851
107 ->114 0.13345
108 ->109 0.30948
108 ->110 0.10505
108 ->111 -0.16302

Figure 5.19 First ten electronic transitions calculated for TcCuNB.

Excited State 1: 4.6953 eV,
264.06 nm f=0.0287
150 ->163 0.11027
151 ->160 -0.28522
151 ->163 0.38398
153 ->160 0.15993
153 ->163 -0.22109
159 ->160 0.18630
159 ->163 -0.18360

Excited State 2: 4.7942 eV,
258.61 nm f=0.0152
143 ->163 -0.10539
147 ->160 0.12673
147 ->163 -0.17086
151 ->160 0.18636
151 ->163 -0.24066
153 ->160 0.30034
153 ->163 -0.39747

Excited State 3: 5.0319 eV,
246.40 nm f=0.0778
149 ->160 -0.10991
149 ->163 0.16466
150 ->160 -0.27991
150 ->163 0.37903
151 ->163 -0.11970
152 ->160 0.12322
152 ->163 -0.18325
158 ->160 0.23622

Excited State 4: 5.1512 eV,
240.69 nm f=0.0471
145 ->163 -0.12872
149 ->160 0.30099
149 ->163 -0.41053
150 ->163 0.14199
157 ->160 0.12059
158 ->161 0.18781
159 ->160 0.10360

Excited State 5: 5.1980 eV,
238.53 nm f=0.1495
155 ->165 0.13965
155 ->167 -0.16854
156 ->167 -0.17640
157 ->162 -0.31242
158 ->160 -0.10851
158 ->163 -0.12149
159 ->161 -0.31373
159 ->162 0.33836

Excited State 6: 5.2084eV,
238.05 nm f=0.1076
149 ->160 -0.15207
149 ->163 0.20208
154 ->165 -0.18193
155 ->166 -0.12359
156 ->166 0.14278
157 ->160 0.25917
157 ->163 0.14586
158 ->161 0.33598
158 ->162 0.17566
159 ->160 0.16294
159 ->163 0.13678

Excited State 7: 5.2458 eV,
236.35 nm f=0.2394
149 ->160 0.10229
154 ->166 -0.20172
155 ->167 -0.16376
156 ->165 0.17645
157 ->161 0.31068
158 ->160 0.28584
158 ->163 0.19529
159 ->162 0.28754

Excited State 8: 5.8973 eV,
210.24 nm f=0.0097
154 ->160 0.16561
154 ->161 0.24047
154 ->162 0.14061
155 ->160 0.17222
156 ->160 -0.21768
156 ->162 -0.10097
157 ->165 0.13604
157 ->166 0.24109
158 ->165 0.27903
158 ->167 0.11843
159 ->165 0.15957
159 ->166 0.16662

Excited State 9: 5..9008 eV,
210.12 nm f=0.0101
154 ->160 0.17812
154 ->161 -0.14614
154 ->163 0.10862
155 ->161 0.23421
156 ->160 0.11034
156 ->161 -0.11415
156 ->162 -0.23835
157 ->166 -0.10807
157 ->167 0.21194
158 ->165 -0.14464
158 ->166 0.27370
159 ->165 0.20353
159 ->166 -0.10138
159 ->167 -0.13652

Excited State 10: 5.9034 eV,
210.02 nm f=0.0112
154 ->160 0.15240
155 ->162 0.30306
156 ->161 -0.27434
156 ->162 0.15306
157 ->165 0.22873
157 ->167 -0.13473
158 ->166 0.18955
159 ->167 0.34836

Figure 5.20 First ten electronic transitions calculated for TBICuNB.

Excited State 1: 4.6953 eV, 264.06 nm f=0.0287
155 ->174 -0.17688
159 ->174 -0.10240
166 ->174 0.10871
173 ->174 0.63614

Excited State 2: 4.7942 eV, 258.61 nm f=0.0152
158 ->174 0.12961
167 ->174 0.10818
172 ->174 0.64661

Excited State 3: 5.0319 eV, 246.40 nm f=0.0778
166 ->175 0.11469
169 ->175 0.21542
169 ->176 -0.35958
171 ->175 0.46138
171 ->176 0.23267

Excited State 4: 5.1512 eV, 240.69 nm f=0.0471
152 ->174 0.12347
157 ->174 0.13280
159 ->174 0.17643
162 ->174 0.27734
168 ->174 0.39757
170 ->174 -0.36736

Excited State 5: 5.1980 eV, 238.53 nm f=0.1495
160 ->174 0.19695
164 ->174 0.20839
172 ->177 -0.11307
172 ->178 0.39398
172 ->182 0.10031
173 ->176 -0.13625
173 ->179 -0.30738

Excited State 6: 5.2084eV, 238.05 nm f=0.1076
157 ->174 0.12429
158 ->174 0.16437
159 ->174 -0.18377
160 ->174 0.34181
163 ->174 0.10103
164 ->174 0.38090
172 ->178 -0.12811
173 ->176 0.10152
173 ->179 0.22802

Excited State 7: 5.2458 eV, 236.35 nm f=0.2394
158 ->174 -0.23017
159 ->174 -0.11628
161 ->174 0.34562
163 ->174 -0.29353
165 ->174 0.32135
173 ->178 0.17830

Excited State 8: 5.8973 eV, 210.24 nm f=0.0097
172 ->178 0.15534
173 ->177 0.44236
173 ->179 0.10406
173 ->180 0.20964
173 ->181 0.15248
173 ->183 -0.23989
173 ->186 -0.10657

Excited State 9: 5..9008 eV, 210.12 nm f=0.0101
172 ->177 0.47216
172 ->179 0.17544
172 ->183 -0.19829
173 ->177 -0.14099
173 ->178 -0.16121

Excited State 10: 5.9034 eV, 210.02 nm f=0.0112
170 ->175 0.10909
172 ->177 -0.17240
172 ->178 0.35312
173 ->175 -0.10903
173 ->176 0.15973
173 ->177 -0.14140
173 ->179 0.32703
173 ->183 0.14275

Excited State 11: 5..9008 eV, 210.12 nm f=0.0101
152 ->175 -0.10710
168 ->175 0.26078
168 ->176 -0.18542
170 ->175 0.37374
170 ->176 -0.28225
171 ->175 0.10633
171 ->176 -0.15864
172 ->177 0.11890

Excited State 12: 5.9034 eV, 210.02 nm f=0.0112
168 ->175 -0.16421
169 ->175 -0.17844
170 ->175 -0.25460
171 ->175 0.15869
171 ->176 -0.29874
172 ->177 0.10171
172 ->178 0.11063
172 ->182 0.10258
173 ->178 0.31944
173 ->182 0.12089

Excited State 13: 5.9008 eV, 210.12 nm f=0.0101
169 ->175 0.22707
171 ->175 -0.20688
171 ->176 0.36093
172 ->178 0.10677
172 ->182 0.10068
173 ->175 -0.11282
173 ->178 0.34442
173 ->182 0.14637

Excited State 14: 5.9034 eV, 210.02 nm f=0.0112
152 ->176 -0.11529
168 ->175 0.18466
168 ->176 0.29545
170 ->175 0.25613
170 ->176 0.43764

Figure 5.21 First fourteen electronic transitions calculated for $TP^{iPr}CuNB$.

Excited State 1: 5.1276 eV, 241.80 nm f=0.0007
88 ->112 0.16635
99 ->112 0.11984
102 ->112 -0.34088
103 ->110 0.15219
103 ->112 -0.47463
105 ->112 -0.23095

Excited State 2: 5.1628 eV, 240.15 nm f=0.0039
108 ->111 0.68195
109 ->110 0.10583

Excited State 3: 5.2217 eV, 237.44 nm f=0.0009
108 ->110 0.15332
108 ->114 -0.12148
109 ->111 0.66777

Excited State 4: 5.3157 eV, 233.24 nm f=0.0321
89 ->112 0.10674
95 ->112 0.19155
96 ->110 0.10057
96 ->112 -0.36905
103 ->112 -0.21671
105 ->110 -0.13497
105 ->112 0.45345

Excited State 5: 5.3638 eV, 231.15 nm f=0.0064
107 ->111 0.69149

Excited State 6: 5.4666 eV, 226.80 nm f=0.0157
93 ->112 0.11688
94 ->112 0.28492
97 ->112 0.19359
98 ->112 0.29409
100 ->112 0.15567
101 ->112 0.24309
106 ->112 -0.37528

Excited State 7: 5.5245 eV, 224.42 nm f=0.0001
149 ->160 0.10229
154 ->166 -0.20172
155 ->167 -0.16376
156 ->165 0.17645
157 ->161 0.31068
158 ->160 0.28584
158 ->163 0.19529
159 ->162 0.28754

Excited State 8: 5.5470 eV, 223.52 nm f=0.0000
154 ->160 0.16561
154 ->161 0.24047
154 ->162 0.14061
155 ->160 0.17222
156 ->160 -0.21768
156 ->162 -0.10097
157 ->165 0.13604
157 ->166 0.24109
158 ->165 0.27903
158 ->167 0.11843
159 ->165 0.15957
159 ->166 0.16662

Excited State 9: 5.6175 eV, 220.71 nm f=0.0021
108 ->111 -0.13489
109 ->110 0.57869
109 ->114 -0.37048

Excited State 10: 5.7036 eV, 217.38 nm f=0.0000
107 ->110 0.58958
107 ->114 -0.36771

Figure 5.22 First ten electronic transitions calculated for $TP^{Methane}CuNB$.

5.7 References

(1) Schneider, J. L.; Carrier, S. M.; Ruggiero, C. E.; Young, V. G.; Tolman, W. B. Influences of Ligand Environment on the Spectroscopic Properties and Disproportionation Reactivity of Copper-Nitrosyl Complexes. *J. Am. Chem. Soc.* **1998**, *120* (44), 11408–11418. https://doi.org/10.1021/ja982172q.

(2) Despagnet-Ayoub, E.; Jacob, K.; Vendier, L.; Etienne, M.; Álvarez, E.; Caballero, A.; Díaz-Requejo, M. M.; Pérez, P. J. A New Perfluorinated F21-Tp Scorpionate Ligand: Enhanced Alkane Functionalization by Carbene Insertion with (F21-Tp)M Catalysts (M = Cu, Ag). *Organometallics* **2008**, *27* (18), 4779–4787. https://doi.org/10.1021/om800531a.

(3) Kimblin, C.; Bridgewater, B. M.; Churchill, D. G.; Parkin, G. Mononuclear Tris(2-Mercapto-1-Arylimidazolyl)Hydroborato Complexes of Zinc, [Tm(Ar)]ZnX: Structural Evidence That a Sulfur Rich Coordination Environment Promotes the Formation of a Tetrahedral Alcohol Complex in a Synthetic Analogue of LADH. *Chem. Commun.* **1999**, *993* (22), 2301–2302. https://doi.org/10.1039/a906561j.

(4) Rasika Dias, H. V.; Jin, W.; Kim, H. J.; Lu, H. L. Polyfluorinated Tris(Pyrazolyl)Borates. Syntheses and Spectroscopic and Structural Characterization of Group 1 and Group 11 Metal Complexes of [HB(3,5-(CF3)2Pz)3]- and [HB(3-(CF3)Pz)3]-. *Inorg. Chem.* **1996**, *35* (8), 2317–2328. https://doi.org/10.1021/ic951361w.

(5) Martín, C.; Sierra, M.; Alvarez, E.; Belderrain, T. R.; Pérez, P. J. Hydrotris(3-Mesitylpyrazolyl)Borato-Copper(i) Alkyne Complexes: Synthesis, Structural Characterization and Rationalization of Their Activities as Alkyne Cyclopropenation Catalysts. *Dalt. Trans.* **2012**, *41* (17), 5319–5325. https://doi.org/10.1039/c2dt11951j.

(6) Álvarez, M.; Álvarez, E.; Fructos, M. R.; Urbano, J.; Pérez, P. J. Copper-Induced Ammonia N-H Functionalization. *Dalt. Trans.* **2016**, *45* (37), 14628–14633. https://doi.org/10.1039/c5dt04972e.

(7) Álvarez, M.; Urbano, J.; Fructos, M. R.; Álvarez, E.; Pérez, P. J. Copper(I)-Arene Complexes with a Sterically Hindered Tris(Pyrazolyl)Borate Ligand. *Eur. J. Inorg. Chem.* **2018**, *2018* (19), 2026–2030. https://doi.org/10.1002/ejic.201800176.

(8) Dias, H. V. R.; Richey, S. A.; Diyabalanage, H. V. K.; Thankamani, J. Copper(I) Complexes Supported by a Heavily Fluorinated Bis(Pyrazolyl) Borate: Syntheses and Characterization of [H2B(3,5-(CF 3)2Pz)2]CuL (Where L = PPh3, NCCH3, HCCPh, H2CCHPh) and {[H2B(3,5-(CF 3)2Pz)2]Cu}2(1,5-COD). *J. Organomet. Chem.* **2005**, *690* (8 SPEC. ISS.), 1913–1922. https://doi.org/10.1016/j.jorganchem.2004.10.047.

(9) Rasika Dias, H. V.; Lu, H. L.; Kim, H. J.; Polach, S. A.; Goh, T. K. H. H.; Greg Browning, R.; Lovely, C. J. Copper(I) Ethylene Adducts and Aziridination Catalysts Based on Fluorinated Tris(Pyrazolyl)Borates [HB(3-(CF3),5-(R)Pz)3]- (Where R = CF3, C6H5, H; Pz = Pyrazolyl). *Organometallics* **2002**, *21* (7), 1466–1473. https://doi.org/10.1021/om010886v.

(10) Thompson, J. S.; Harlow, R. L.; Whitney, J. F. Copper(I)-Olefin Complexes.

Support for the Proposed Role of Copper in the Ethylene Effect in Plants. *J. Am. Chem. Soc.* **1983**, *105* (11), 3522–3527. https://doi.org/10.1021/ja00349a026.

(11) Martín, C.; Muñoz-Molina, J. M.; Locati, A.; Alvarez, E.; Maseras, F.; Belderrain, T. R.; Pérez, P. J. Copper(I)-Olefin Complexes: The Effect of the Trispyrazolylborate Ancillary Ligand in Structure and Reactivity. *Organometallics* **2010**, *29* (16), 3481–3489. https://doi.org/10.1021/om1002705.

(12) Trofimenko, S. Recent Advances in Poly(Pyrazolyl)Borate (Scorpionate) Chemistry. *Chem. Rev.* **1993**, *93* (3), 943–980. https://doi.org/10.1021/cr00019a006.

(13) Templeton, J. L. ScorpionatesThe Coordination Chemistry of Polypyrazolylbor-Ate Ligands By Swiatoslaw Trofimenko (University of Delaware). Imperial College Press: London 1999. x + 282 Pp. $48.00. ISBN 1-86094-172-9. *J. Am. Chem. Soc.* **2000**, *122* (23), 5670. https://doi.org/10.1021/ja9957940.

(14) Pettinari, C.; Trofimenko, S. *Scorpionates II: Chelating Borate Ligands*; Imperial College Press, 2008.

(15) Reger, D. L.; Grattan, T. C.; Brown, K. J.; Little, C. A.; Lamba, J. J. S.; Rheingold, A. L.; Sommer, R. D. Syntheses of Tris(Pyrazolyl)Methane Ligands and {[Tris(Pyrazolyl)Methane]Mn(CO)3} SO3CF3 Complexes: Comparison of Ligand Donor Properties. *J. Organomet. Chem.* **2000**, *607* (1–2), 120–128. https://doi.org/10.1016/S0022-328X(00)00290-4.

(16) Haldón, E.; Álvarez, E.; Nicasio, M. C.; Pérez, P. J. Copper(I) Complexes with Trispyrazolylmethane Ligands: Synthesis, Characterization, and Catalytic Activity in Cross-Coupling Reactions. *Inorg. Chem.* **2012**, *51* (15), 8298–8306. https://doi.org/10.1021/ic300843a.

(17) Garner, M.; Reglinski, J.; Cassidy, I.; Spicer, M. D.; Kennedy, A. R. Hydrotris(Methimazolyl)Borate, a Soft Analogue of Hydrotris(Pyrazolyl)Borate. Preparation and Crystal Structure of a Novel Zinc Complex. *Chem. Commun.* **1996**, *355* (16), 1975–1976. https://doi.org/10.1039/cc9960001975.

(18) Minoura, M.; Landry, V. K.; Melnick, J. G.; Pang, K.; Marchiò, L.; Parkin, G. Synthesis and Structural Characterization of Tris(2-Seleno-1-Mesitylimidazolyl) Hydroborato Complexes: A New Type of Strongly Electron Donating Tripodal Selenium Ligand. *Chem. Commun.* **2006**, No.

38, 3990–3992. https://doi.org/10.1039/B608078B.

(19) Betley, T. A.; Peters, J. C. The Strong-Field Tripodal Phosphine Donor, [PhB(CH2P IPr2)3]-, Provides Access to Electronically and Coordinatively Unsaturated Transition Metal Complexes. *Inorg. Chem.* **2003**, *42* (17), 5074–5084. https://doi.org/10.1021/ic0343096.

(20) Fränkel, R.; Kernbach, U.; Bakola-Christianopoulou, M.; Plaia, U.; Suter, M.; Ponikwar, W.; Nöth, H.; Moinet, C.; Fehlhammer, W. P. Homoleptic Carbene Complexes. *J. Organomet. Chem.* **2001**, *617–618*, 530–545. https://doi.org/10.1016/s0022-328x(00)00713-0.

(21) Al-Harbi, A.; Kriegel, B.; Gulati, S.; Hammond, M. J.; Parkin, G. Bis- and Tris(2-Oxobenzimidazolyl)Hydroborato Complexes of Sodium and Thallium: New Classes of Bidentate and Tridentate Oxygen Donor Ligands. *Inorg. Chem.* **2017**, *56* (24), 15271–15284. https://doi.org/10.1021/acs.inorgchem.7b02638.

(22) Smith, J. M. Strongly Donating Scorpionate Ligands. *Comments Inorg. Chem.* **2008**, *29* (5–6), 189–233. https://doi.org/10.1080/02603590802590080.